

UNION INTERNATIONALE DE CHIMIE PURE ET  
APPLIQUEE  
DIVISION DE CHIMIE ORGANIQUE  
et  
L'UNION INTERNATIONALE DE  
CRISTALLOGRAPHIE

# LA CHIMIE ORGANIQUE A L'ETAT SOLIDE—2

*Conférences plénierées présentées au*  
**2<sup>e</sup> SYMPOSIUM INTERNATIONAL DE  
CHIMIE ORGANIQUE A L'ETAT SOLIDE**  
*à Rehovot, Israël*  
*14–18 septembre 1970*

Rédacteur du Symposium  
M. D. COHEN  
*L'Institut des Sciences Weizmann, Rehovot*

LONDRES  
BUTTERWORTHS

INTERNATIONAL UNION OF PURE AND APPLIED  
CHEMISTRY  
ORGANIC CHEMISTRY DIVISION  
in conjunction with  
THE INTERNATIONAL UNION OF  
CRYSTALLOGRAPHY

# ORGANIC SOLID-STATE CHEMISTRY—2

*Plenary lectures presented at the*  
2nd INTERNATIONAL SYMPOSIUM ON  
ORGANIC SOLID-STATE CHEMISTRY  
*held in Rehovot, Israel*  
*14–18 September 1970*

Symposium Editor  
M. D. COHEN  
*Weizmann Institute of Science, Rehovot*

LONDON  
BUTTERWORTHS

**ENGLAND:** BUTTERWORTH & CO. (PUBLISHERS) LTD.  
LONDON: 88 Kingsway, WC2B 6AB

**AUSTRALIA:** BUTTERWORTH & CO. (AUSTRALIA) LTD.  
SYDNEY: 586 Pacific Highway, Chatswood, NSW 2067  
MELBOURNE: 343 Little Collins Street, 3000  
BRISBANE: 240 Queen Street, 4000

**CANADA:** BUTTERWORTH & CO. (CANADA) LTD.  
TORONTO: 14 Curity Avenue, 374

**NEW ZEALAND:** BUTTERWORTH & CO. (NEW ZEALAND) LTD.  
WELLINGTON: 26-28 Waring Taylor Street, 1  
AUCKLAND: 35 High Street, 1

**SOUTH AFRICA:** BUTTERWORTH & CO. (SOUTH AFRICA) (PTY) LTD.  
DURBAN: 152-154 Gale Street

*The contents of this book appear in*

Pure and Applied Chemistry, Vol. 27 No. 3 (1971)

*Suggested U.D.C. number 54-16: 547(063)*

©  
International Union of Pure and Applied Chemistry  
1971

ISBN 0 408 70218 4

Printed in Great Britain by Page Bros. (Norwich) Ltd., Norwich

## **DEDICATION**

This volume is dedicated to the memory of Prof. G. M. J. Schmidt, a pioneer in the field of organic solid-state chemistry and one of the moving spirits behind this series of symposia, who passed away on 12th July, 1971.

## **FOREWORD**

The Second International Symposium on Organic Solid-State Chemistry took place at the Weizmann Institute of Science, Rehovot, Israel on September 14–18, 1970. It was co-sponsored by IUPAC and the International Union of Crystallography. The scientific programme consisted of eleven plenary lectures and twenty eight communications. The latter are not being published in a collected volume; this volume is a collection of the former.

The Organizing Committee consisted of D. P. Craig, F. H. Herbstein, R. M. Hochstrasser, A. Many and G. M. J. Schmidt, with the author of this foreword as Secretary.

The Organizing Committee wishes to acknowledge the financial assistance received from the sponsors and the host institute; from the Hebrew University, Israel Institute of Technology, and Tel Aviv University; and from The Eastman Kodak Company, General Telephone and Electronics Laboratories Inc., Imperial Chemical Industries, and Robert Bosch GmbH.

Some papers of this collection have more than one author; in these cases the lecture was given by the first mentioned.

Unfortunately because of illness Prof. G. M. J. Schmidt was unable to prepare the manuscript of his lecture for this publication.

M. D. COHEN  
Department of Chemistry  
Weizmann Institute of Science

## **DEDICATION**

This volume is dedicated to the memory of Prof. G. M. J. Schmidt, a pioneer in the field of organic solid-state chemistry and one of the moving spirits behind this series of symposia, who passed away on 12th July, 1971.

## **FOREWORD**

The Second International Symposium on Organic Solid-State Chemistry took place at the Weizmann Institute of Science, Rehovot, Israel on September 14–18, 1970. It was co-sponsored by IUPAC and the International Union of Crystallography. The scientific programme consisted of eleven plenary lectures and twenty eight communications. The latter are not being published in a collected volume; this volume is a collection of the former.

The Organizing Committee consisted of D. P. Craig, F. H. Herbstein, R. M. Hochstrasser, A. Many and G. M. J. Schmidt, with the author of this foreword as Secretary.

The Organizing Committee wishes to acknowledge the financial assistance received from the sponsors and the host institute; from the Hebrew University, Israel Institute of Technology, and Tel Aviv University; and from The Eastman Kodak Company, General Telephone and Electronics Laboratories Inc., Imperial Chemical Industries, and Robert Bosch GmbH.

Some papers of this collection have more than one author; in these cases the lecture was given by the first mentioned.

Unfortunately because of illness Prof. G. M. J. Schmidt was unable to prepare the manuscript of his lecture for this publication.

M. D. COHEN  
Department of Chemistry  
Weizmann Institute of Science

# X-RAY STUDIES OF REACTIONS IN ORGANIC SOLIDS

J. Z. GOUGOUTAS

*12 Oxford Street, Department of Chemistry, Harvard University,  
Cambridge, Massachusetts 02138, USA*

## ABSTRACT

Correlations of the chemical structures of products from organic solid state reactions with the molecular packing in the reactant crystal structures define the extent of lattice restraints on molecular motion before and during reaction. The molecular behaviour after the chemical transition state can be inferred from comparisons of the molecular orientations in the initial and final phases. The formation of preferentially oriented product phases suggests that highly specific geometrical mechanisms are operative but additional criteria are needed to establish a direct correspondence between specific reactant and product molecules. Observable intermediate mesomorphic phases are particularly useful in defining the directions in which crystallographic order is not preserved.

Several studies of hydrolysis, isomerization and polymerization reactions suggest surprisingly large molecular migrations and conformational changes may occur without randomizing the total distribution of product molecules. Competing and consecutive transformations often give rise to several simultaneously present and mutually oriented product phases and, in some cases, large molecular moieties of the initial structure do not appear in any of the final ordered phases. Novel twinning frequently is observed when degenerate transformation mechanisms give rise to several preferred orientations of product structures which cannot reorganize to form a single phase of long-range order. While the short-range molecular arrangement in the oriented product phase usually is identical with that produced during conventional crystallizations, exceptions may be found in the formation of chemically unstable molecular structures or metastable polymorphs of the product phase.

## INTRODUCTION

In most reported examples of solid state reactions in molecular crystals, the products are structurally incompatible with the reactant lattice and eventually appear in a separate phase. The product phase usually is amorphous or polycrystalline and therefore has not retained the three-dimensional periodicity of the reactant structure. The chemical reaction, nevertheless, may be quite specific. A wide variation in product states was observed in the extensive studies of solid state photochemical dimerization<sup>1</sup> and no strong correlations are evident between the chemical specificity of the reaction and the overall crystallographic order of the final solid phase.

In these cases, it appears that the initial lattice may restrict selectively the modes of molecular motion before, but not after, the chemical transition state.

Topotactic reactions are notable exceptions<sup>†</sup>. The product molecules assume preferred orientations relative to crystallographic directions of the reactant structure and it seems not unreasonable to suppose that the molecular motions at all stages of topotactic transformations are subject to the restraining effects of the continuously ordered reactant-product matrix. Even in these remarkable transformations, the product molecules virtually always crystallize during the reaction as a separate phase of characteristic cell dimensions and symmetry. The structure of the product phase can be determined and compared with the original phase according to the experimentally observed topotactic angular relationship. Although the topotaxy strictly defines only a reticular correspondence between the initial and final crystal structures, it is often meaningful to consider the phase transformation on a molecular level with the aim of establishing the geometrical mechanism by which the reactant molecules are displaced to their final lattice positions as product molecules of the chemical reaction.

The examples considered below illustrate the wide range of molecular motions which can occur without randomizing the final distribution of product molecules. In the extreme, a direct molecular correspondence is indicated between the initial and final phases. Initially adjacent reactant molecules are transformed to adjacent product molecules which 'crystallize' without further redistribution. The topotaxy reflects a chemical change and reorientation of only a small fraction of the total molecular bulk.

At the other extreme, an initially homogeneous reactant may undergo several different, competing and consecutive chemical reactions which result in many different, simultaneously present and mutually oriented crystal structures. Very extensive solid state redistribution occurs and, in some cases, large molecular moieties of the reactant structure do not appear in any of the final ordered phases. Product molecules which are adjacent or near neighbours in the final phase were relatively distant neighbours in the initial reactant structure. In view of the large displacements, it is not possible to identify particular product molecules with specific reactant molecules and therefore no information can be obtained on the intervening motions of the chemical reaction. The topotaxy clearly is not related simply to the chemical reaction but rather arises from a subsequent oriented growth of initially disoriented product molecules on one or several of the ordered phases.

## TOPOTAXY IN MOLECULAR CRYSTALS

### Solid state polymerization

The current scientific interest in topotactic processes in molecular crystals in no small way stems from their potential practical importance to the production of synthetic polymer fibres without recourse to mechanical orientation processes. The relatively brief history and development of

---

<sup>†</sup> For a review of topotactic processes in inorganic solid state reactions, see reference 2.

## X-RAY STUDIES OF REACTIONS IN ORGANIC SOLIDS

topotactic polymerizations and polycondensations<sup>3</sup> includes most reported cases of topotaxy in the organic solid state. Only some of the general crystallographic aspects of the transformations will be considered here with reference to two examples which raise interesting questions concerning the geometrical reaction mechanism.

The long polymer chains usually grow in several preferred directions of the monomer single crystal and multiple twinning is very common. Although the product phase frequently is fibrous and only unidimensionally oriented, several examples of three-dimensionally oriented polymers have been reported. The geometrical relationship between the end phases is determined from x-ray diffraction measurements of partially polymerized samples. The importance of lattice imperfections and surface effects, more correctly associated with epitactic reactions, is well recognized. General considerations of the crystallographic mechanism of growth are focused on correlations of polymer identity period with intermolecular spacings in growth directions of the monomer phase<sup>4</sup>.

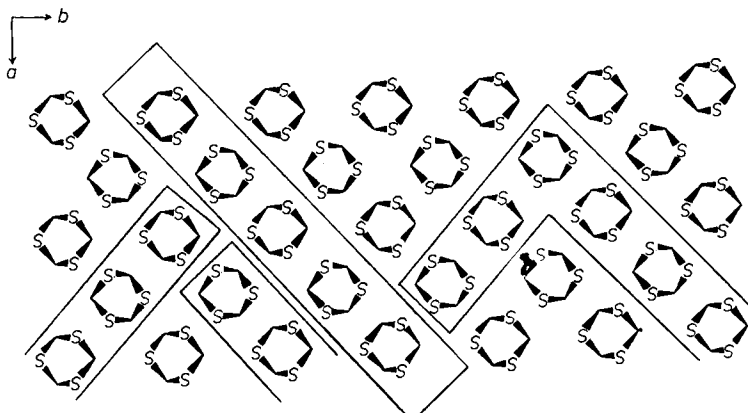


*Figure 1.* The molecular packing of trithiane in projection down [001]. The enclosed monomers indicate possible molecular combinations leading to the observed orientations of polymer chains

The origin of the ubiquitous twinning of product phase is evident in the study of three-dimensionally oriented polythiomethylene from single crystals of trithiane<sup>5</sup>. Two major and four minor preferred orientations of the helical polymer chains are indicated. The polymer crystal structure has a hexagonal cell with the polymer chain axis coincident with the sixfold axis†. Polymerization of the orthorhombic monomer phase (space group  $Pmn2_1$ ) presumably is propagated most favourably through the molecular contacts along the [110] diagonal since, after reaction, this direction defines the chain axis of the polymer structure (*Figure 1*). This direction is structurally unique in the polymer whereas, in the monomer, it is degenerate with [110]. Chain propagation accordingly occurs along both diagonals resulting in two orientations of polymer chains which together are incompatible with the known crystal structure of the polymer. Similarly, the four minor orientations

---

† A hexagonal cell was chosen for the assigned triclinic space group  $P1^\circ$ .

of polymer chains are consistent with the fourfold multiplicity of a general line in the orthorhombic system. It is interesting to note that this type of twinning reflects the unique origin of the polymer crystal structure and apparently has not been observed in other preparations of the crystalline polymer.

The intermolecular distances in trithiane along the directions of preferred growth are less than necessary to accommodate the corresponding atoms of the polymer helix. It has been suggested that when this discrepancy becomes too severe from increasing strain, twinning occurs with growth in an alternative direction. The twinning may represent a geometrical relationship between individual crystallites comprised of straight polymer chains or, more interestingly, may result in a kink in the continuously growing chain.

Detailed considerations of the specific interactions which lead to reaction between trithiane molecules cannot be justified solely on the basis of the static monomer structure. Even small orientational changes of the highly symmetric structure during reaction may lead to several different modes of chain propagation. Such ambiguities were partially avoided in a study of the polymerization of vinyl stearate<sup>7</sup>. The reactive vinyl groups lie in planes separated by approximately 25 Å (*Figure 2*) and it is reasonable to assume

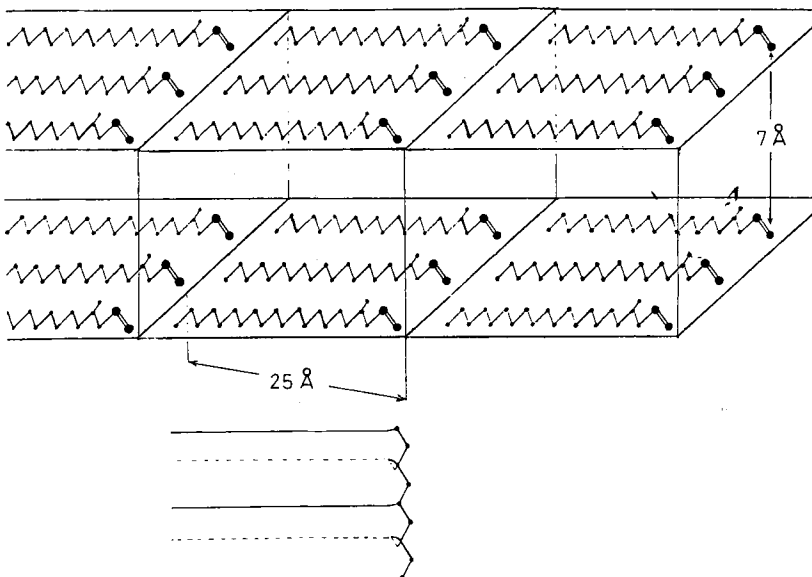


*Figure 2.* A schematic drawing of the crystal structure of vinyl stearate showing the initial separation of vinyl groups. The geometry of a syndiotactic polymer with side chains (lines) parallel to those in the monomer is shown in the lower portion of the drawing

that chain propagation will occur within, rather than between, these planes. In that case, the problem of determining the geometrical mechanism of chain propagation, effectively, is reduced to two dimensions. It is also reasonable to assume that polymerization can occur without appreciably disrupting the parallel arrangement of the large stearate side chains. The polymers generated

## X-RAY STUDIES OF REACTIONS IN ORGANIC SOLIDS

in this manner should have a syndiotactic geometry with side chains extending to the same side of the planes containing the polymer backbones.

Diffraction measurements indicated that a parallel and extended arrangement of the aliphatic side chains indeed was present in the polymer phase. However, a dilemma arose when it was discovered that the polymer was less syndiotactic than polymers obtained from the liquid state. Moreover, an isotactic geometry with side chains extending to both sides of the planes containing the polymer backbones was consistent with some observed crystallographic spacings. It is very difficult to conceive of any way in which the long stearate side chains can move through the very large distances required to produce a polymer of this geometry.

Similar conceptual difficulties in interpreting the molecular motions during transformation arise in our studies of peroxide rearrangements (*vide infra*), where it is clear that 'before and after photographs' of the terminal ordered phases are inadequate measures of the transformation. However, the molecular relationships are clarified considerably when the transformation occurs in discrete steps.

### Solid state rearrangements

An elegant study by Dame Kathleen Lonsdale and her associates illustrates the manner in which the intermediate stages in a transformation can be

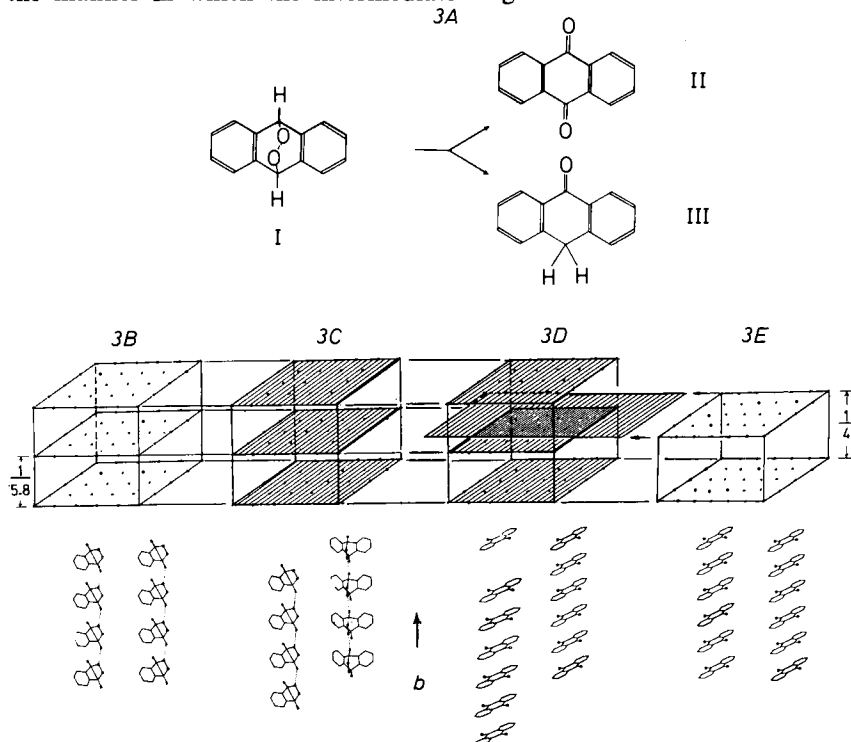
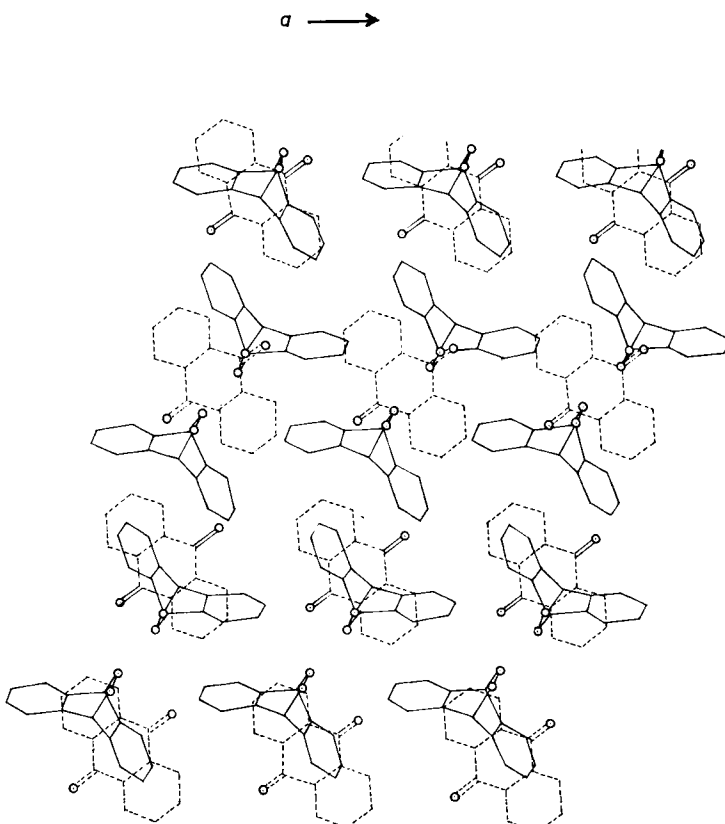


Figure 3. The successive stages in the decomposition of anthracene peroxide. A schematic representation of the behaviour of the molecular chains parallel to [010] is shown below the corresponding changes—*B*, *C*, *D*, *E*—in the reciprocal lattice

followed by x-ray diffraction methods. Single crystals of anthracene peroxide, I, (*Figure 3*), upon moderate heating or continued exposure to x-irradiation at room temperature, are transformed, without change in external shape, into mixed single crystals of anthraquinone, II and anthrone, III<sup>8</sup>. Before reaction, the Bragg and Laue spots which correspond to structure I are well-shaped and apparently normal (*Figure 3B*). After a relatively brief period, there appear thin continuous sheets of diffraction passing through existing *k*-constant points of the peroxide reciprocal lattice (*Figure 3C*). These diffraction effects correspond to a mesomorphic phase consisting of chains of molecules parallel to the original *b* lattice repeat. The molecular interval along each chain is constant and identical with the original peroxide spacing in this direction (5.8 Å). However, there is no ordered relationship between individual chains; they may have rotated about the chain axis, moved sideways or shifted in the *b* direction relative to one another. Upon further irradiation, new diffraction sheets appear in reciprocal space, parallel to and between the original sheets (*Figure 3D*). This second mesomorphic phase is similar to the first but the molecular interval along the chains has



*Figure 4.* A possible superposition of the initial and final crystal structures in the decomposition of I. The invariant direction of the molecular chains, [010], is normal to the drawing.  
(Courtesy of Prof. K. Lonsdale)

## X-RAY STUDIES OF REACTIONS IN ORGANIC SOLIDS

contracted to 4 Å. It was suggested that this change corresponds to chemical reaction. The chains of flat product molecules are formed within the mesomorphic peroxide chains and remain parallel to *b*. Finally, the continuous reciprocal lattice sheets which characterize the product chains are replaced by relatively sharp diffraction spots corresponding to the known II-III mixed crystal diffraction pattern (*Figure 3E*). In this stage, the chains of product molecules have crystallized to form the three-dimensionally ordered structure. The product phase is twinned in modes not previously observed in mixed crystals grown during solution crystallizations.

It is instructive to compare the initial and final structures. The possible superposition shown in *Figure 4* was presented together with the comment that the reaction clearly requires large movements of the chains. In comparisons of this type, the experimentally observed angular orientation of the two structures must be retained. The superposition, however, is not uniquely defined and the two structures may be shifted in an infinite number of ways while preserving the angular orientation. The loss of crystallographic order normal to the chain axes suggests that no particular correspondence can be expected between reactant and product molecules in different chains. Nevertheless, the *a* lattice repeats are nearly equal in length and essentially coincident. The molecular correspondence in other directions between the

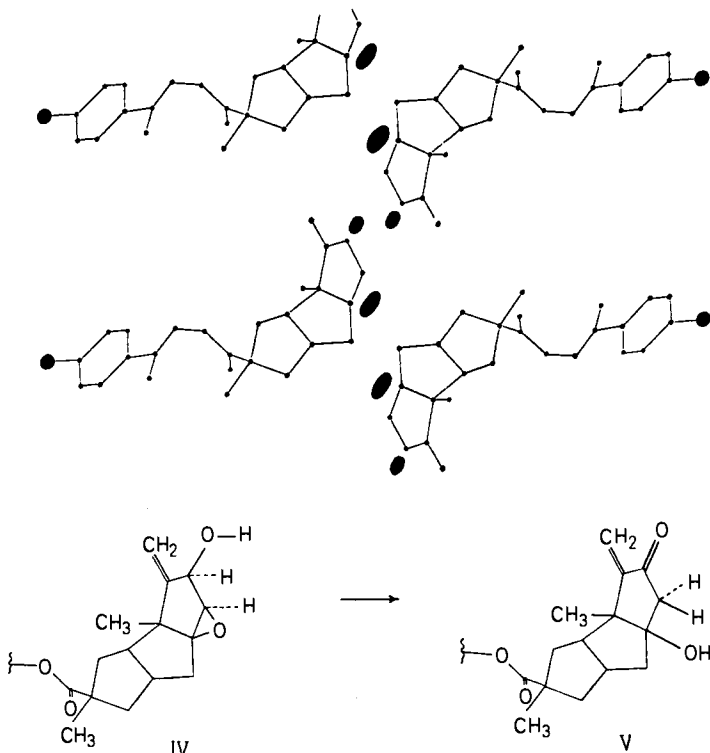


*Figure 5.* The molecular changes in the crystal structure of the *p*-bromophenacyl ester of hirsutic acid. 'Partial' oxygen atoms were found in the shaded regions

chains obviously is not simple. The product molecules along the chains may be identified with corresponding reactant molecules in the [010] direction. Even there, however, the chain contraction allows for an exact correspondence over only relatively short distances.

This method of assessing the significance of any apparent molecular correspondence between the initial and final structures, primarily, is one of elimination. It is thus possible to define the directions in which crystallographic order is *not* preserved. In the absence of experimentally observable disorder, however, the transformations appear three-dimensionally ordered throughout and the interesting possibility of direct transitions leading to an exact molecular correspondence should not be discounted.

A remarkably smooth isomerization was discovered during the crystal structure analysis of the *p*-bromophenyl ester (IV) of hirsutic acid, a metabolite from *stereum hirsutum*<sup>9</sup>. This molecular rearrangement is a rare example of a topotactic reaction in which the product is not structurally incompatible with the reactant lattice and does not eventually appear in a separate phase. Indeed, a chemical reaction was not suspected until most of

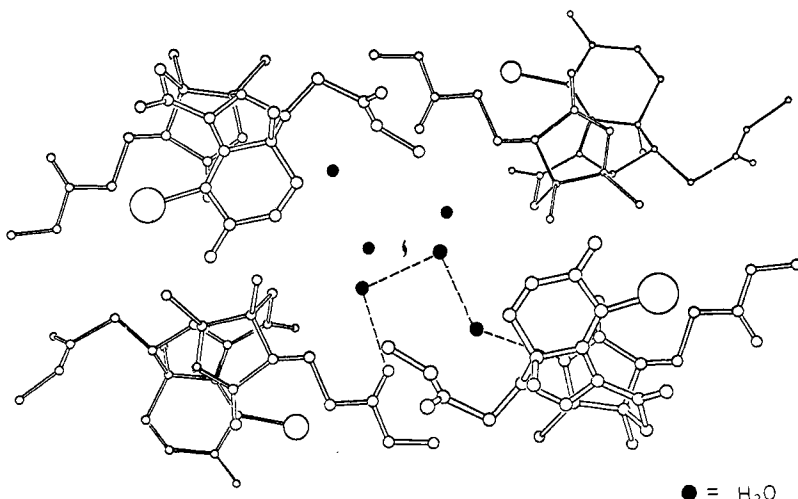


Figure 6. The crystal packing showing the unobstructed channels of water molecules; the molecular arrangement is repeated by simple translation along the normal to the drawing, [001]

the crystal structure had been revealed. The unsatisfactory progress of least squares refinements assuming structure IV was clarified when it was discovered that the final crystal structure was a solid solution of the isomers IV and V in the approximate ratio 2:3 respectively. Although the cell parameters changed by *ca* 1 per cent during the transformation, presumably no significant changes in reflection intensities were observed. The solid state isomerization (Figure 5) requires the rupture and formation of three covalent bonds and the migration of at least two hydrogen atoms. The oxygen atoms involved in the reaction must move slightly from their initial positions.

## X-RAY STUDIES OF REACTIONS IN ORGANIC SOLIDS

The initial homogeneity of crystalline IV and the unique radiation-induced isomerization were verified by independent chemical and spectroscopic methods. Walker later determined a lower limit of  $G(\text{isomerization}) \geq 57$  and suggested that this high value indicates either a chain reaction involving a chemically active propagating species or a highly efficient transfer process<sup>10</sup>.

It seems highly likely, in this case, that the large molecules remain at their original lattice positions throughout the transformation and a direct correspondence exists between the initial and final crystal structures. The terminal isomer ratio in the final pseudomorph supports this conclusion. Although hydrogen bonding is not possible in pure crystals of IV, it can occur between IV and V and between two molecules of V. The former hydrogen bonding accounts for the incomplete conversion of IV while the latter accounts for the predominance of V. In view of this unexpected isomerization, the investigators recommend chromatographic analysis of samples after every crystal structure determination.

Miss Barbara Kaski in our laboratory observed a comparable transformation during the crystal structure analysis of a synthetic intermediate<sup>11</sup>. The initial crystal structure (*Figure 6*) contains water of crystallization which appears to be hydrogen bonded to the organic structure. The water molecules, originally contained within approximately cylindrical channels running throughout the crystal in the *c* direction, may diffuse out of the crystal without appreciably disrupting the molecular packing of the large organic molecules. The small changes in cell parameters observed during the transformation suggest that a slight molecular reorganization occurs in order to fill the vacated channels.

### Reactions of 2-iodobenzoylperoxide derivatives†

A report that the isomerization of bis-(orthoiodobenzoyl) peroxide, VI, to the benziodoxole structure VII (*Figure 7*) occurs in the solid state<sup>12</sup>

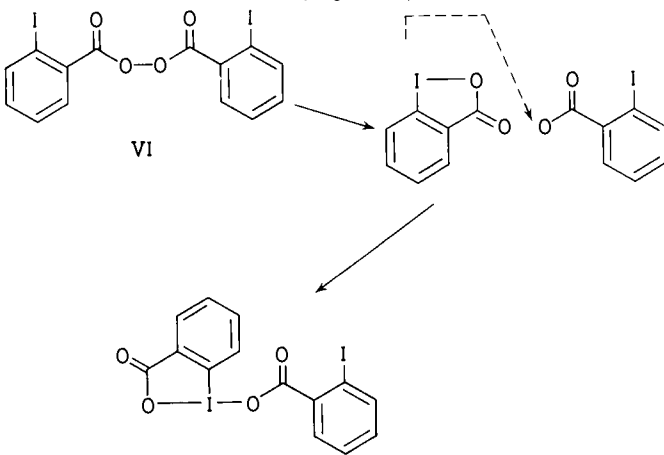


*Figure 7.* The structural changes in the isomerization of bis-(orthoiodobenzoyl) peroxide

† Financial support by the U.S. Air Force Office of Scientific Research (Grant No. AFOSR-69-1769) is gratefully acknowledged.

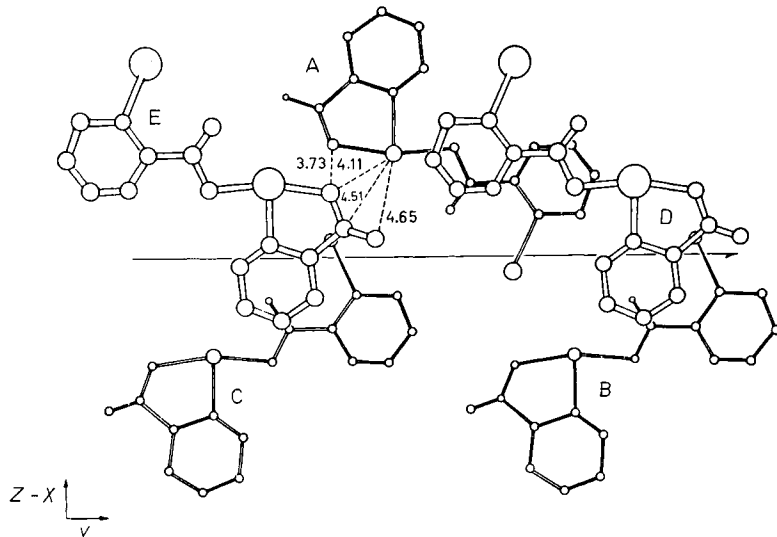
prompted us to investigate the reaction for possible topotaxy. Although the solid peroxide explodes when heated rapidly to 80°, rearrangement occurs smoothly during storage at room temperature for several weeks. The morphologically unchanged crystals are found to be twinned single crystals of the expected product, VII<sup>13</sup>. The same transformation also can be effected by heating overnight at 110°, after first maintaining the temperature at 50° for several hours in order to prevent explosive decomposition. When the temperature is raised to 120°, the initially-formed crystal structure undergoes a polymorphic transformation to a polycrystalline pseudomorph.

VII, synthesized by an independent chemical route<sup>14</sup>, crystallizes from a variety of solvents in two polymorphic modifications ( $\alpha$  and  $\beta$ ) (Table I).

Table 1. Crystal data

Structure	<i>a</i> (Å)	<i>b</i> (Å)	<i>c</i> (Å)	$\beta$ (deg)	<i>z</i>	Space group
VI	13.05	4.21	15.47	121.1	2	<i>Pc</i>
VII $\alpha$	4.21	30.86	22.52	93.3	8	<i>Cc</i>
VII $\beta$	8.03	12.58	13.74	91.6	4	<i>P2<sub>1</sub>/c</i>
VIII	4.32	15.08	11.29	91.5	4	<i>P2<sub>1</sub>/c</i>
IX	12.89	4.10	14.05	96.7	4	<i>P2<sub>1</sub>/c</i>
X	20.81	4.09	15.41	94.7	4	<i>P2<sub>1</sub>/c</i>
XI	12.96	4.12	15.38	121.2	2	<i>Pc</i>
XII	13.00	4.08	15.38	120.9	2	<i>Pc</i>
XIV	22.28	4.06	15.38	94.5	4	<i>P2<sub>1</sub>/c</i>
XV	4.28	24.34	6.89	91.3	2	<i>P2<sub>1</sub></i>
XVI	14.82	4.10	25.90	118.3	8	<i>C2/c</i>

The structural assignment as VII and the polymorphic relationship was verified through three-dimensional crystal structure analysis of both forms<sup>15</sup>. The dimorphs easily can be identified and separated: VII $\alpha$  is acicular with a

Figure 8. The molecular conformation and crystal packing of VII $\beta$

X-RAY STUDIES OF REACTIONS IN ORGANIC SOLIDS

4 Å cell repeat parallel to the needle axis while crystals of VII $\beta$  are stout polyhedra. VII $\alpha$  (see *Figure 12*) is identical to the initial product phase from peroxide decomposition while VII $\beta$  (*Figure 8*) is the modification which results from the high temperature transition. The molecular conformation is markedly different in the two forms. The monovalent iodine atom and carboxyl oxygen atom of the iodobenzoate group adopt a *cisoid* relationship in VII $\beta$  while the presumably less stable *transoid* conformer<sup>16</sup> occurs in VII $\alpha$ .

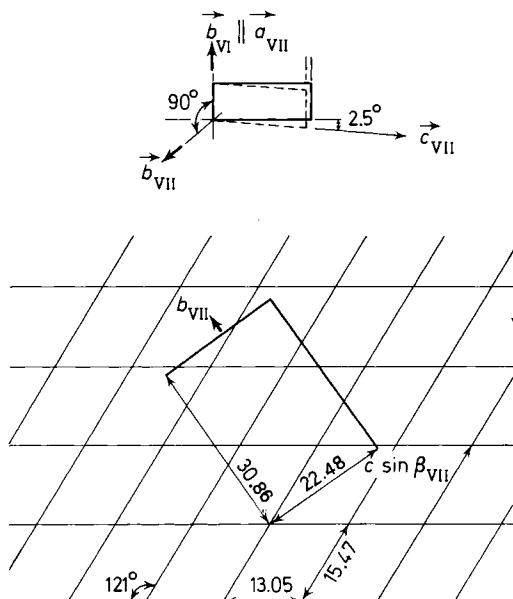


*Figure 9.* The geometrical phase relationship observed in the isomerization of VI. The lower drawing is a projection down [010] of VI and [100] of VII $\alpha$

The approximately flat peroxide molecules are stacked on top of one another in the initial layered crystal structure<sup>17</sup> (see *Figure 12* and *Table I*). Although solid state isomerization is complete within a few days in the x-ray beam at room temperature, the accelerating effect of x-irradiation does not alter the course of the reaction. The geometric relationship:  $[010]_{VI} \parallel [100]_{VII}$  and  $(001)_{VI} \parallel (021)_{VII}$  (*Figure 9*) was determined from x-ray photographs of intermediate states (*Figures 10* and *11*). The remarkably well-ordered product phase appears to be formed directly, without the intermediacy of mesomorphic phases. The relative orientation of the initial and final structures is shown in projection down the common short lattice repeat in *Figure 12*. Surprisingly large molecular displacements are indicated. All considerations of the geometrical mechanism of transformation must confront the unavoidable conclusion that half of the phenyl rings flip through *ca* 180° about an axis parallel to the layers of peroxide molecules. It is difficult to imagine how

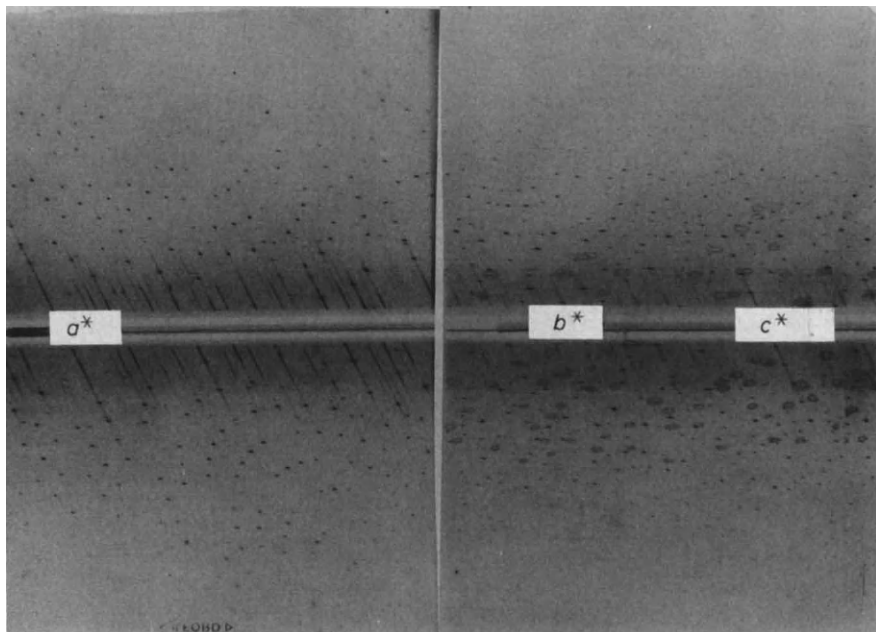


*Figure 10.* (Left)  $h0l$  Weissenberg photograph ( $\text{Cu K}\alpha$ ) of a fresh crystal of VI after *ca* 20 hrs exposure to x-rays at room temperature ( $\pm a^*$  are at the film extremes). Four successive  $00l$  reflections of  $\text{VII}\alpha$  are clearly evident in the right half of the film. (Right) The same crystal after *ca* 100 hrs in the x-ray beam. (Crystal and camera settings have not been changed.) The discrete pattern is  $0kl$  of  $\text{VII}\alpha$ . The extra circled reflections are due to newly-formed VIII

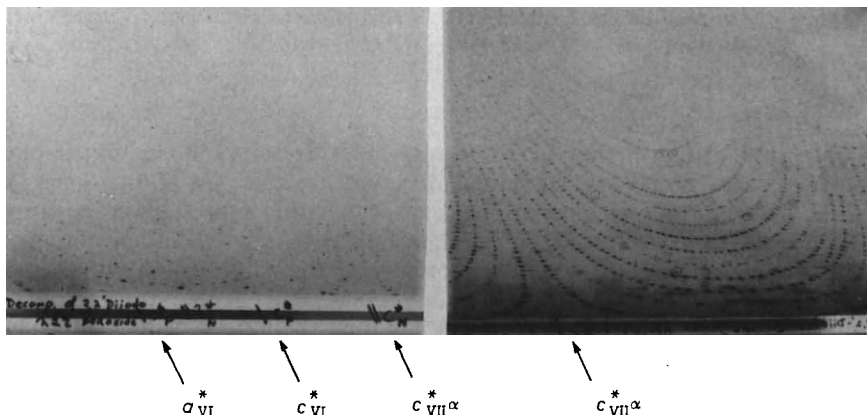


*Figure 11.* (Left)  $hll$  Weissenberg photograph ( $\text{Cu K}\alpha$ ) of VI (slightly mis-set) after *ca* 40 hrs total exposure to x-rays at room temperature. The coplanar  $1kl$  net of  $\text{VII}\alpha$  is clearly evident. (Right) The original  $hll$  net of VI has been replaced by the  $1kl$  net of  $\text{VII}\alpha$ . Equal twinning across  $(00l)$  of  $\text{VII}\alpha$  results in  $mm$  symmetry and an apparent doubling of  $c^*$

## X-RAY STUDIES OF REACTIONS IN ORGANIC SOLIDS

such rotations within the inadequate space between the layers can occur with retention of the interlayer spacing†.

*Figure 13* shows the product phase partitioned into regions of 'flipped' and 'unflipped' iodobenzoate groups and it is clear that every molecule of

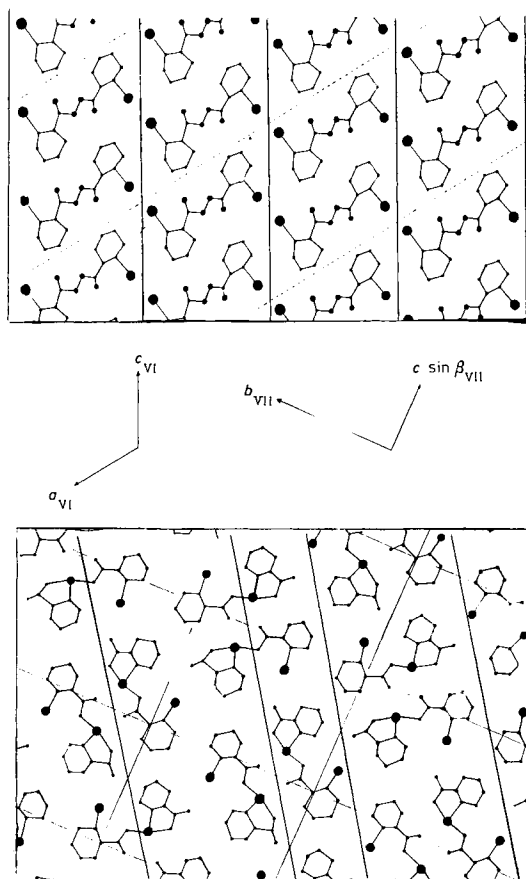


*Figure 12.* The molecular arrangements in the crystal structures of VI and VII $\alpha$ . The structures, shown in projection down their common short lattice repeat, are oriented according to the observed geometrical relationship (see *Figure 9*)

product contains one of each. The dimensions, orientation and molecular distribution of this chequerboard pattern are reminiscent of the original peroxide structure and it is tempting to assume a simple correspondence. If a peroxide molecule originally lay wholly within one of these regions, the chemical mechanism is one of separation and *intermolecular recombination*. This being the case, either both or none of the phenyl rings in a given peroxide

† Similar rotations are necessary to interconvert the conformers of VII $\alpha$  and VII $\beta$ . As mentioned above, the solid state transformation in that case completely disrupts the initial single crystal matrix.

molecule flip during the transformation. Alternatively, if the boundaries of the chequerboard pattern divide rather than contain original peroxide molecules, a mixed mechanism is operative. Half of the peroxide molecules rearrange *intramolecularly* while the others separate and recombine *intermolecularly*. Several chemical and crystallographic rationales for these and other mechanisms have been considered but none seem entirely satisfactory.

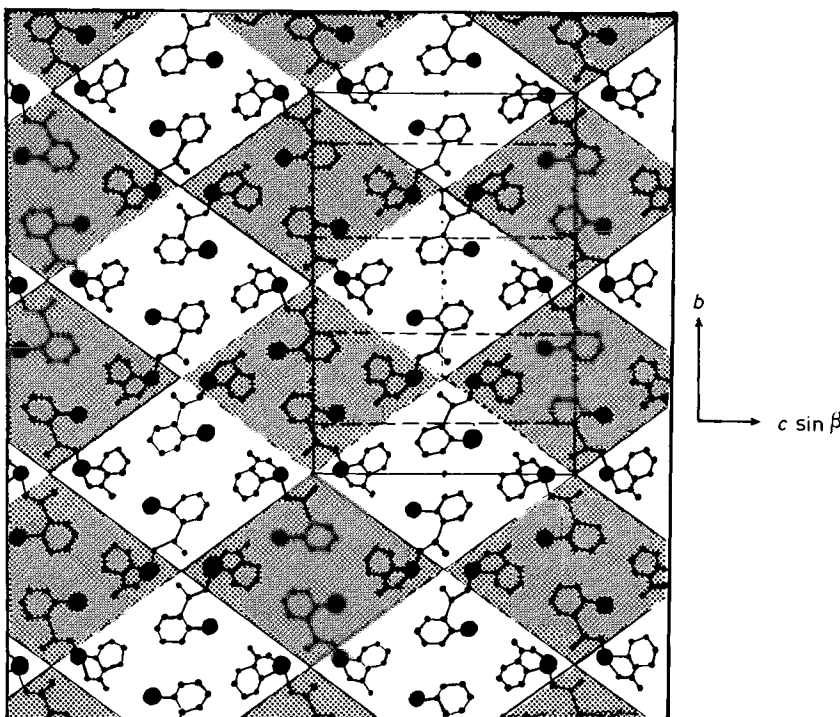
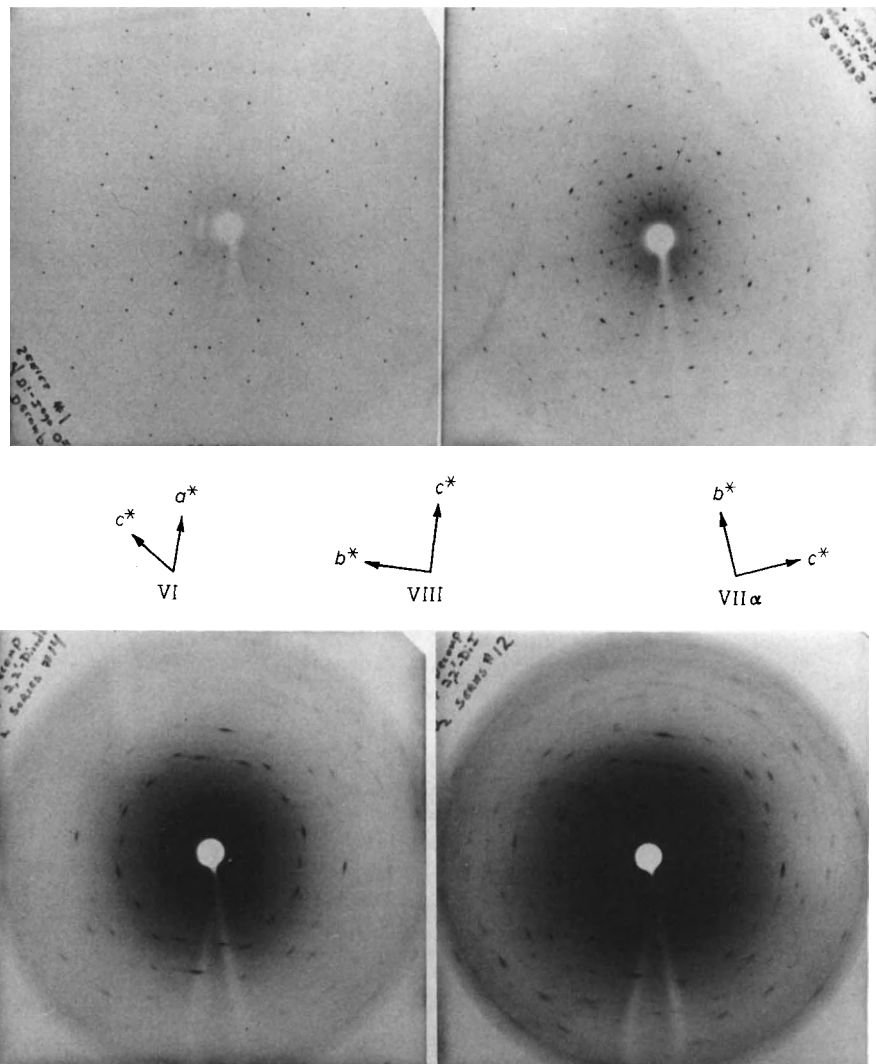


Figure 13. The crystal structure of VII $\alpha$  partitioned into regions of 'flipped' and 'unflipped' iodobenzoate groups

Further study of the initial pseudomorph revealed a second, consecutive topotactic reaction. The initial diffraction spectrum of VII $\alpha$  is slowly replaced by the single crystal spectrum of *o*-iodobenzoic acid<sup>15</sup>, VIII (*Figure 14*). The increased background level and rather streaked reflections suggest a somewhat fibrous crystal with considerable amorphous structure. Again, the external shape of the crystal is unchanged. The crystal structure of VIII also contains a 4 Å lattice repeat which, in the solid state reaction, is generated parallel to the short repeats of VI and VII $\alpha$ . The mutual orientations of VI, VII $\alpha$ , and VIII are shown in *Figure 15*. No obvious correlation exists between VII $\alpha$  and VIII even though it is not necessary to invoke 'flipping' during the second transformation. Striking similarities are evident between the initial peroxide structure and the twice-removed acid structure. It appears that half of the original halobenzoate groups have remained virtually stationary while

X-RAY STUDIES OF REACTIONS IN ORGANIC SOLIDS



*Figure 14.* A series of precession photographs ( $\text{Cu K}\alpha$ ) of successive stages in the transformations  $\text{VI} \rightarrow \text{VII}\alpha \rightarrow \text{VIII}$  of one crystal. (Identical experimental settings.) (Top Left)  $h0l$  of freshly crystallized VI. (Top Right)  $0kl$  of  $\text{VII}\alpha$ . A few discrete reflections from VI are still visible. (Bottom Right) (ca three weeks after stage two.) Reflections of the  $0kl$  zones of both  $\text{VII}\alpha$  and VIII are present. (Bottom Left) (ca three weeks after stage three)  $0kl$  reflections of VIII. A few intense reflections of  $\text{VII}\alpha$  have not yet disappeared

the others have separated and 'flipped'. This relationship probably is fortuitous since the acid appears well after the disappearance of a discrete peroxide phase. The direct solid state conversion VI → VIII has never been observed.

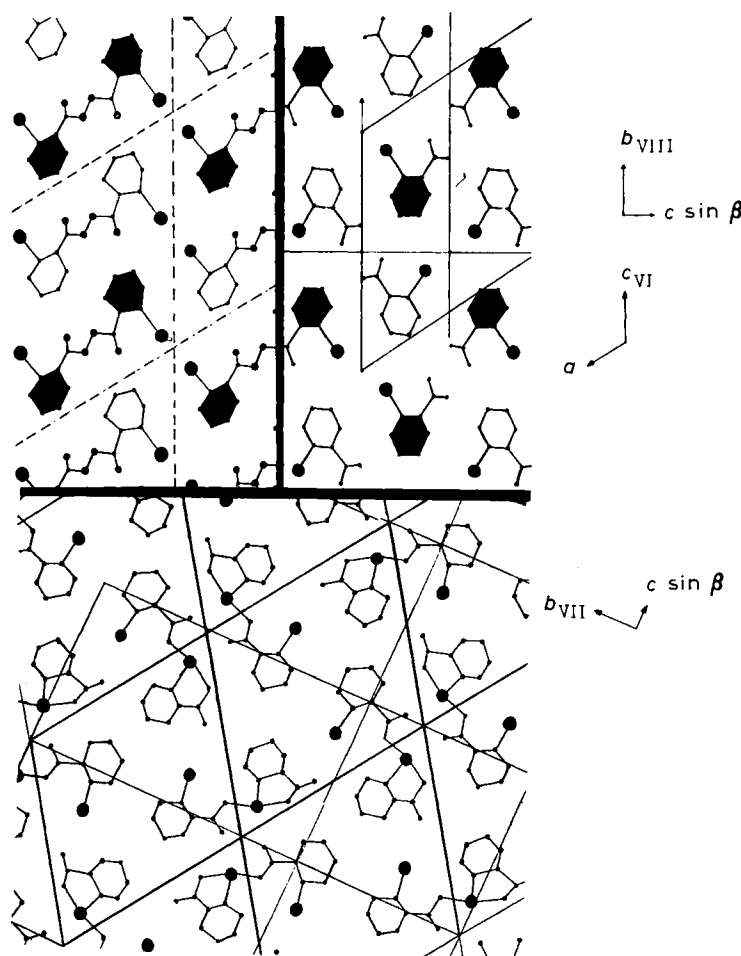
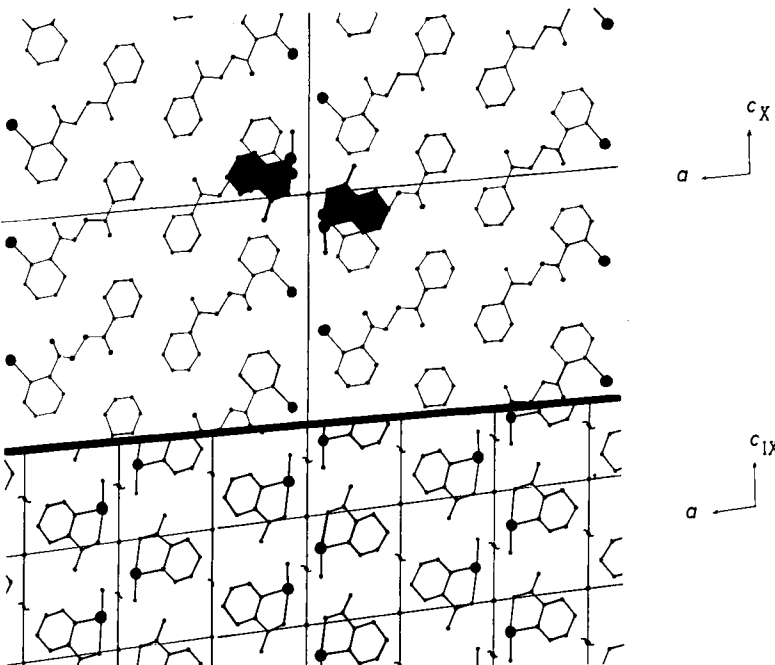


Figure 15. The experimentally observed mutual orientations of VI, VII $\alpha$  and VIII are shown in projection down their common short lattice repeat. Heavy lines separate the structures. Lighter lines within each structure are traces of several different planes which are qualitatively useful in comparing the molecular distributions

The initially-formed opaque pseudomorph contains numerous defects and readily admits atmospheric moisture for the subsequent hydrolysis reaction. By contrast, crystals of VII $\alpha$  from solution crystallizations do not undergo the transformation VII $\alpha$  → VIII at any appreciable rate. Hydrolysis of VII in various solvents gives an equal mixture of VIII and *o*-iodosobenzoic acid, IX.

## X-RAY STUDIES OF REACTIONS IN ORGANIC SOLIDS

Although an ordered structure of IX often is observed in topotactic reactions of other related peroxides (*vide infra*), in this case it presumably occupies the amorphous regions of the pseudomorph. Solid state recrystallization after hydrolysis necessitates major molecular reorganization which nullifies any molecular correlations involving VIII. After several months, well-formed transparent needles of VIII grow out of the pseudomorph strictly parallel to [010] of the original peroxide crystal.



**Figure 16.** The experimentally observed orientation of initial and final crystal structures in the transformation  $X \rightarrow IX$ . [010] of both structures is normal to the drawing. The solid structures in  $X$  are oriented molecules of  $IX$ .

The solid state chemistry of several other related peroxides was explored in order to examine the generality of the above transformations: X, 2-iodobenzoyl peroxide; XI, 2-iodo-2'-bromobenzoyl peroxide; XII, 2-iodo-2'-chlorobenzoyl peroxide; XIII, 2-iodo-2'-fluorobenzoyl peroxide; XIV, 2-iodo-3'-chlorobenzoyl peroxide; XV, 2-iodo-4'-nitrobenzoyl peroxide. These peroxides have layered crystal structures with a short cell dimension of 4 Å (Table I). With the interesting exception of XV, the molecular packing within the layers is similar to that in VI. Although all of the peroxides decompose in the solid state, no topotaxy has been observed in the case of XV.

The others undergo several competing and consecutive topotactic transformations which cannot be fully described in this presentation. Some typical processes are exemplified by the extraordinary behaviour of XI, which is isostructural with VI. The corresponding benziodoxole isomer is dimorphic

but neither form is isostructural with either VII $\alpha$  or VII $\beta$ . During reaction, an interphase perpendicular to the crystal needle axis (*b*) often can be observed to progress along the length of the crystal. X-ray studies of crystals cleaved at the boundary demonstrate that one part is product and the other, unchanged peroxide. Either one, or the other, and often both crystal structures of the isomeric product are formed directly as single crystal phases. Once again, half of the phenyl rings of the peroxide phase 'flip' during the transformation<sup>†</sup> and no clear molecular correspondence is indicated between the initial and final structures<sup>‡</sup>. This product is hydrolyzed by atmospheric moisture to *o*-iodosobenzoic acid, IX and *o*-bromobenzoic acid, XVI. Unlike the hydrolysis of VII $\alpha$ , however, both of the acidic products crystallize in the pseudomorph as discrete oriented phases of known crystal structure<sup>18, 19</sup>.

The direct topotactic formation of IX from a peroxide crystal structure has been observed in decompositions of X and XIV. In the case of the former peroxide, it is also the only crystalline product. Benzoic acid, the major product from the other half of the peroxide molecule, is contained in amorphous regions of the pseudomorph. The extensive molecular reorganization which must ensue can be inferred from the experimentally observed phase relationship (Figure 16). If hydrolysis of X occurs through the addition of water to the more electrophilic and less hindered carboxyl group, benzoic acid and 2-iodoperbenzoic acid, XVII, should be formed. The latter appears to be unstable with respect to its cyclic isomer, IX<sup>¶</sup>. In this connection, the direct hydrolysis of XI (and XII) is highly interesting.

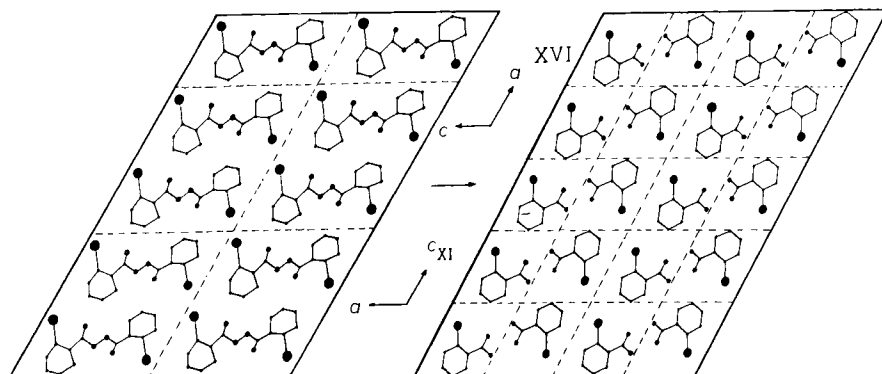


Figure 17. The experimentally observed orientation of the initial and final crystal structures in the transformation XI → XVI. [010] of both structures is normal to the drawing

The specific behaviour of XI is variable and depends on the ambient temperature and humidity as well as the history of the particular crystal specimen. Direct hydrolysis competes with molecular isomerization and

<sup>†</sup> The molecular conformation is *transoid* (*vide supra*) in both dimorphs. In this case, 'flipping' is necessary for the formation of both product crystal structures.

<sup>‡</sup> Indeed, the single crystal spectrum of VII $\alpha$  has been observed in some decomposing crystals of XII! Peroxides XI and XII are isostructural, as are their corresponding benziodoxole isomers.

<sup>¶</sup> Attempted syntheses of XVII by conventional methods<sup>20, 21</sup> yield IX.

## X-RAY STUDIES OF REACTIONS IN ORGANIC SOLIDS

often the formation of the oriented structure of XVI precedes the appearance of single crystal reflections from the benziodoxole phase. The striking geometrical correspondence in the direct topotactic transformation XI → XVI (Figure 17) is not relevant to the chemical reaction since only the bromobenzoate groups of the peroxide appear in the acid phase†. Frequently, a second, relatively unstable single crystal phase appears in conjunction with XVI. The diffraction spectrum of the former, as yet unidentified phase is similar to that of IX, and VII $\alpha$  and may represent either the elusive crystal structure of XVII or a third, metastable modification of the benziodoxole product. Both alternatives are particularly noteworthy since the other topotactic transformations simply duplicate crystal structures which are obtained from conventional crystallizations. The significant possibility that topotaxy is instrumental in the formation of a unique crystal structure cannot be excluded‡.

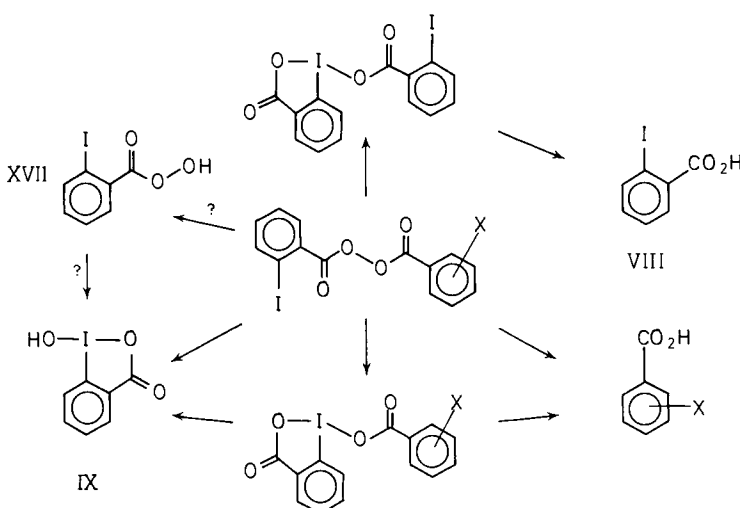


Figure 18. Solid state chemical reactions of 2-iodobenzoyl peroxide derivatives. (For a review of polyvalent iodine compounds, see reference 24)

The vicissitudes of these transformations (Figure 18) can be appreciated in the x-ray photograph of a decomposing crystal of XI (Figure 19). At least seven discrete single crystal phases have been identified. The elucidation of the individual crystal structures and the complicated topotactic reactions of these peroxides reflects the unusual skill of my collaborators in this work—J. C. Clardy, A. M. Glazer, L. Lessinger, S. Singh and R. Weiss.

---

† 2-Iodobenzoic acid has an entirely different crystal structure and a solid solution seems unlikely<sup>22</sup>.

‡ Uncommon crystal structures frequently are formed in reactions which yield  $\beta$ -truxinic acids<sup>23</sup>. It is not clear, however, whether these phases are unique to the solid state process or simply solvent free modifications which also could be obtained by other methods.

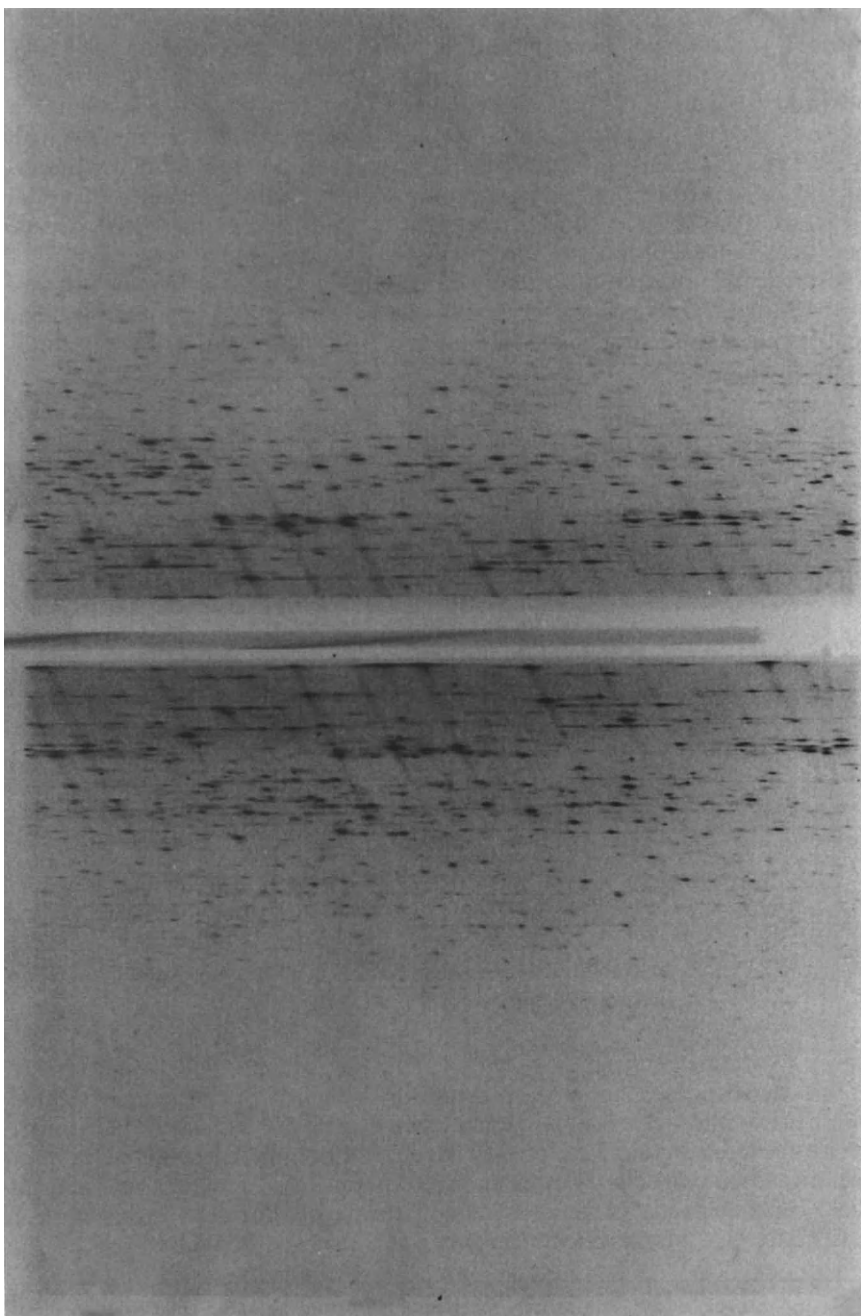


**Figure 19.** Weissenberg photograph ( $\text{Cu K}\alpha$ ) of a decomposing single crystal of XI mounted along [010]. Sharp, discrete  $h0l$  reflections from XI are easily identified in the centre of the film at low angles of diffraction. The diffraction spectrum initially resembled that in *Figure 10* (left)

## CONCLUSION

Finally, I must apologize for oversimplifying both the positive and negative results of the above investigations. A discussion of the quantitative reticular correspondence was postponed in order to concentrate on the molecular aspects of the transformations. The interdependence of the two, however, appears to be quite subtle. The topotaxy and epitaxy between the various phases presumably defines a unique assembly of crystal structures and interphases. Crystallographic ordering is obvious but minimal motion is by no means a critical requirement. This seems less to be the case in the equally novel twinned product structures where selective restrictions of the different types of molecular reorientation, necessary to form the individual members, are indicated<sup>25</sup>. In virtually all cases, however, the short-range molecular arrangement simply duplicates that formed in an unrestricted milieu.

The study of the molecular motions during transformation is crucial to an understanding of these interrelationships. Additional evidence is necessary when only the initial and final structures are available for study by x-ray methods. Where possible, identical or different types of topotaxy and, in some cases its conspicuous absence, should be considered for the same chemical reaction in polymorphic forms of the molecular reactant. The behaviour of crystallographically isostructural reactants of inherently different chemical reactivity is also relevant to this problem.

## REFERENCES

- <sup>1</sup> M. D. Cohen, G. M. J. Schmidt *et al.* *J. Chem. Soc.* 1966 (1964).
- <sup>2</sup> L. S. Dent Glasser, F. P. Glasser and H. F. W. Taylor. *Quart. Rev. (London)* **16**, 343 (1962).
- <sup>3</sup> H. Morawetz. *Pure and Appl. Chem.* **12**, 201 (1966).
- <sup>4</sup> See, for example: S. Okamura, K. Hayashi and Y. Kitanishi. *J. Polymer Sci.* **58**, 925 (1962); G. Carazzolo, S. Leghissa and M. Mammi. *Makromol. Chem.* **60**, 171 (1963); N. Morosoff, D. Lim and H. Morawetz. *J. Am. Chem. Soc.* **86**, 3167 (1964).
- <sup>5</sup> J. B. Lando and V. Stannett. *J. Polymer Sci. Part A* **3**, 2369 (1965).
- <sup>6</sup> G. Carazzolo and G. Valle. *Makromol. Chem.* **90**, 66 (1966).
- <sup>7</sup> N. Morosoff, B. Post and H. Morawetz. *J. Am. Chem. Soc.* **87**, 3035 (1965).
- <sup>8</sup> K. Lonsdale, E. Nave and J. F. Stephens. *Phil. Trans. Roy. Soc. London A* **261**, 1 (1966).
- <sup>9</sup> F. W. Comer and J. Trotter. *J. Chem. Soc. B*, 13 (1966).
- <sup>10</sup> D. C. Walker. *Chem. Commun.* 1050 (1967).
- <sup>11</sup> B. Kaski. Ph.D. Thesis. Harvard University (1970).
- <sup>12</sup> J. E. Leffler, R. D. Faulkner and C. C. Petropoulos. *J. Am. Chem. Soc.* **80**, 5435 (1958).
- <sup>13</sup> J. Z. Gougoutas, J. C. Clardy, A. M. Glazer, L. Lessinger and S. Singh. *Acta Cryst. A* **25**, S 232 (1969).
- <sup>14</sup> W. Honsberg and J. E. Leffler. *J. Org. Chem.* **26**, 733 (1961).
- <sup>15</sup> J. C. Clardy. Ph.D. Thesis. Harvard University (1969).
- <sup>16</sup> G. Eglinton, G. Ferguson, K. M. S. Islam and J. S. Glasby. *J. Chem. Soc. B* 1141 (1967).
- <sup>17</sup> J. Z. Gougoutas and J. C. Clardy. *Acta Cryst. B* **26**, 1999 (1970).
- <sup>18</sup> E. Shefter and W. Wolf. *J. Pharm. Sci.* **54**, 104 (1965).
- <sup>19</sup> G. Ferguson and G. A. Sim. *Acta Cryst.* **15**, 346 (1962).
- <sup>20</sup> L. S. Silbert, E. Siegel and D. Swern. *J. Org. Chem.* **27**, 1336 (1962).
- <sup>21</sup> J. R. Moyer and N. C. Manley. *J. Org. Chem.* **29**, 2099 (1964).
- <sup>22</sup> A. I. Kitaigorodskii, *Kristallografiya* **2**, 456 (1957); also *Dokl. Akad. Nauk. SSSR* **113**, 604 (1957).
- <sup>23</sup> G. M. J. Schmidt. *J. Chem. Soc.* 2014 (1966).
- <sup>24</sup> D. F. Banks. *Chem. Rev.* **66**, 243 (1966).
- <sup>25</sup> K. Lonsdale. *Acta Cryst.* **21**, 5 (1966).

# ELECTRON PARAMAGNETIC RESONANCE AND ELECTRON NUCLEAR DOUBLE RESONANCE OF CHEMICALLY REACTING TRIPLET STATE SPECIES IN SINGLE ORGANIC CRYSTALS<sup>†</sup>

CLYDE A. HUTCHISON JR.

*Department of Chemistry and the Enrico Fermi Institute,  
University of Chicago, Ill. 60637, USA*

## ABSTRACT

In this lecture I review a series of both published and unpublished investigations made together with my colleagues and students who are named in *Table 1*. We have studied the organic single crystal system consisting of 1,1-diphenylethylene (DPE) which contained small amounts of diphenyldiazomethane (DPDAM). I describe the ways in which we use electron paramagnetic resonance (EPR), electron nuclear double resonance (ENDOR), optical spectroscopy with polarized light, and x-ray crystallography, to study the photolysis of the DPDAM and the reaction of diphenylmethylene (DPM) with DPE at crystal sites, without serious disruption of the structure of the host crystal. All of the methods and techniques nicely supplement each other to give a detailed picture of this single crystal system. The magnetic resonance methods serve to give a most detailed account of the local structure at the reaction sites in the vicinity of the chemical impurity, DPM.

## 1. INTRODUCTION

Electron paramagnetic resonance (EPR) methods offer many attractive features in connection with the study of chemical reactions in which a paramagnetic species is a reactant or a product. The intensity of EPR absorption may be used to follow the course of the reaction and measure the rate, and to give the actual number of paramagnetic molecules present at any given time. In the case of a reaction in a crystal, a very convenient method of determining the kinetics is thus afforded by EPR and the microwave information carrier offers almost the ideal perturbationless probe. Moreover, if the reactant or product is a relatively dilute triplet state paramagnetic species in a diamagnetic host crystal, the fine structure of the EPR spectrum gives considerable information on the orientation of the species in its crystal environment. In addition, this spectral fine structure gives much information on internal molecular structure and electron spin distribution in the reactant or product. The interactions between the electrons of the paramagnetic molecule and the magnetic nuclei in it offer an additional very powerful means of determining

CLYDE A. HUTCHISON JR.

its geometry, orientation, and spin distribution. Knowledge of such interactions is obtainable in great detail from the hyperfine structure of the EPR spectra and from electron nuclear double resonance (ENDOR) spectra. Furthermore, the so called distant ENDOR spectra, i.e. the ENDOR spectra originating with magnetic nuclei outside a reactive paramagnetic molecule, offer a very important source of information for our purposes of study of chemical reactions in crystals, in that they give detailed knowledge of the structural situation in the environment of a dilute reactive species.

In this lecture I will review a series of studies made by a variety of EPR, ENDOR, optical spectroscopic and x-ray crystallographic methods in our laboratory, at the University of Chicago, which bear on the matters just mentioned, for a particular case. I will be discussing a variety of published and unpublished work<sup>1-9</sup> which is the result of the efforts of quite a number of my colleagues and students. In *Table 1* I summarize their contributions.

*Table 1.* List of contributors to this work

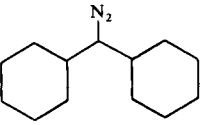
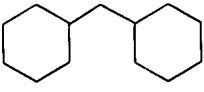
<u>Kinetics</u>	<u>EPR</u>	<u>ENDOR</u>
D. C. Doetschman	R. W. Brandon Professor G. L. Closs C. E. Davoust	B. E. Kohler
X-ray	D. C. Doetschman	<u>Optical</u>
D. C. Doetschman Professor E. Fleischer	B. E. Kohler R. Silbey	Professor G. L. Closs B. E. Kohler

## 2. PRELIMINARY EXPERIMENTS

### 2.1 The molecules

In *Table 2* are listed three molecules with which we will be concerned at the beginning, and their code names which will be used throughout this lecture.

*Table 2.* Molecules

	diphenyldiazomethane <b>DPDAM</b>
	diphenylmethylene <b>DPM</b>

## 2.2 Some preliminary EPR observations<sup>1, 2, 6</sup>

When a single crystal of DPE, at a temperature  $\sim 77^{\circ}\text{K}$ , and containing from 0.0015 to 0.036 mole fraction DPDAM, was irradiated in an EPR spectrometer with the light from a high pressure mercury arc, an intense, very anisotropic, persistent, narrow line (8G width), triplet state spectrum appeared<sup>1, 2</sup>. When such a crystal was irradiated at any temperature down to the boiling point of He, we obtained the same results.

When the irradiation was terminated and the crystal was maintained at  $\sim 77^{\circ}\text{K}$  the EPR signal would remain sensibly constant in intensity for at least several hours. If warmed to  $100^{\circ}\text{K}$  the signal would decay, exponentially with time, to half the initial intensity in 2 min, and at  $110^{\circ}\text{K}$  to half initial intensity in 3.5 sec<sup>6</sup>.

When such a DPE crystal containing 0.3 per cent DPDAM was irradiated at  $\sim 96^{\circ}\text{K}$  with a high pressure mercury arc the initial rate of signal growth gradually decreased until in  $\sim 15$  sec a maximum saturation value would be reached and no further signal increase would occur<sup>6</sup>. If irradiation was then terminated the signal would decay exponentially with a half life,  $\sim 10$  min, or, if the temperature was raised, with a shorter half life as described previously. In either case if the irradiation was begun again at  $96^{\circ}\text{K}$  or any lower temperature after the decay of the signal, the signal would return.

Our interpretation of such results was as follows<sup>1, 2, 6</sup>. The long persistence of the triplet state spectrum after termination of irradiation at low temperatures (down to  $< 4.2^{\circ}\text{K}$ ) was taken to mean that a ground state triplet species was being observed. The very large anisotropy of the EPR spectra, with respect to the direction of  $\mathbf{H}_0$ , the laboratory dc field, in the crystallographic axis system, together with the sharpness of the spectral lines, showed clearly that the paramagnetic species was well oriented in the DPE crystal<sup>1, 2, 4, 6, 7</sup>. The fine structure of the EPR spectrum was describable within the errors of the measurements by the conventional triplet state spin hamiltonian<sup>5</sup>,

$$\mathcal{H}_s = + |\beta_e| \mathbf{S} \cdot \mathbf{g}_e \cdot \mathbf{H}_0 + DS_z^2 + E(S_x^2 - S_y^2), \quad S = 1. \quad (1)$$

shown in *Table 3*, with the values<sup>4</sup> of the parameters given in *Table 3*. The magnitude of the value of  $D$  is an expression of the amount of anisotropy of the EPR spectrum. Since the anisotropy arises from the magnetic dipole-dipole interaction<sup>5</sup> which varies inversely as the cube of the distance between the two electrons, the fact that our  $|D|$  is, in this case, about 4 times as large as for a photoexcited triplet state of an aromatic molecule indicated that these two electrons in the triplet state species in DPE spent considerable time together on the same C atom in a pair of orthogonal  $p$  orbitals. In the photo-excited aromatic molecules, considered in the  $\pi$  electron approximation, the Pauli principle keeps the two electrons 1 C-C distance away from each other and this holds down the size of  $D$ .

All of these facts, together with many others, to be discussed subsequently, showed that the DPM molecule with its divalent C atom, often assumed as an intermediate in the photochemical reactions of DPDAM in fluid phase, was responsible for the EPR signals<sup>1</sup>. This divalent C molecule was presumed to

Table 3. Spin hamiltonian parameters at ~ 77°K

(1) $\mathcal{H}_s = +  \beta_e  \mathbf{S} \cdot \mathbf{g}_e \cdot \mathbf{H}_0 + \mathbf{S} \cdot \mathbf{T} \cdot \mathbf{S} = 1$ , for diphenylmethylene	
$D/hc(\text{cm}^{-1})$	+ 0.39644 (0.00045)
$E/hc(\text{cm}^{-1})$	- 0.01516 (0.00020)
$g_{zz}$	2.0010 (0.0013)
$g_{xx}$	2.0030 (0.0008)
$g_{yy}$	2.0028 (0.0014)

have been generated by the absorption of light by a DPDAM molecule which had been substitutionally incorporated in the host DPE crystal as it was grown. The absorption of light removed N<sub>2</sub> leaving the DPM molecule substitutionally incorporated and oriented in the host. The decay of the signal from DPM in dilute crystal solutions, when the irradiation was terminated and the temperature was sufficiently high, was interpreted as the result of chemical reaction with the host DPE to form diamagnetic products. The series of events in which (a) the EPR signal attained a maximum value with continued irradiation, then (b) was removed by chemical reaction of the formed paramagnetic species, and then (c) was regenerated by further irradiation was explained as follows. The growth of the signal was assumed to be terminated by light filtering action of the formed DPM which absorbed all the light necessary for its formation from DPDAM. Warming of the crystal in the dark removed the filter because of the chemical reaction, in the dark, of the DPM with the host crystal, forming products which did not absorb the required light. With the filter removed, further irradiation could generate more DPM. These last suppositions were confirmed by (a) quantitative measurements of all the absorption spectra involved<sup>3,7</sup>; by (b) absolute EPR intensity measurements which showed that the number of divalent C molecules formed at maximum signal intensity corresponded to a small fraction of the number of DPDAM molecules in the light beam and available for DPM production, in the absence of filtering action; and (c) the demonstration that the possible number of signal regenerations was a small finite number, predictable from (a) and (b), which exhausted the supply of DPDAM.

### 2.3 Some preliminary x-ray studies<sup>9</sup>

At the time that the first EPR spectra, which I have just been describing, were obtained, the crystal structure of DPE was unknown. Professor Closs had suggested DPE to us as a suitable host in which we might produce DPM from DPDAM for optical spectroscopic studies. Three reasons for its selection for such purposes were: (1) The probable geometrical similarity of DPE, DPDAM and DPM; (2) the expected chemical inertness of DPE toward divalent C compounds; and (3) the optical transmission of DPE very far into the ultraviolet. Professor Fleischer<sup>9</sup> made some preliminary x-ray diffraction studies of DPE crystals which showed that these crystals had the

## EPR AND ENDOR OF REACTING TRIPLETS IN ORGANIC CRYSTALS

properties shown in *Table 4*. These observations, of course, made it possible for us to know the orientations in our EPR spectrometer of our DPE crystals containing DPDAM.

*Table 4.* Preliminary x-ray studies on 1,1-diphenylethylene crystals

- 
1. Orthorhombic
  2. Preliminary space group assignment, *Pnc2* or *Pncm*
  3. Unit cell, 2 molecules,  
 $a = 19.919/2 \text{ \AA}$   
 $b = 7.876 \text{ \AA}$   
 $c = 6.759 \text{ \AA}$
  4. 2-fold axis along *c*
  5. Cleavage plane, *bc*
  6. Optical extinction directions, polarized visible light transmitted normal to cleavage plane, *b* and *c*
  7. Polarization direction for visible absorption by DPDAM in DPE, *c*
- 

### 2.4 Some preliminary optical studies<sup>3, 7</sup>

The optical absorptions of polarized light in some DPE crystals containing 0.002 to 0.010 mole fraction DPDAM were studied<sup>3, 7</sup>. The spectra were obtained at 20°K both before and after irradiation with light from a high pressure mercury arc. The results are described in *Figure 1* and in *Figure 2*. The cleavage plane of DPE was known from x-ray studies to be the *bc* plane. The polarization of the DPDAM spectrum along the *c* axis made it possible to know directions in this cleavage plane by visual inspection in DPE crystals containing DPDAM, because they were magenta in colour when viewed against light polarized along *c* and colourless when it was polarized along *b*. The strong polarization of the spectra showed that the guest DPDAM molecules were well oriented. These spectra also showed that DPDAM was disappearing as the paramagnetic species was formed. The amount of paramagnetic species formed was proportional to the amount of DPDAM destroyed. They also explained the termination of growth of EPR signals because of the very intense optical absorptions by the species produced by the photolysis of the DPDAM, which produced the filtering effects mentioned previously.

### 3. EPR EXPERIMENTS<sup>1, 2, 4, 5, 6</sup>

In *Figure 3* are shown the values<sup>6</sup> of the magnetic field strengths at which EPR lines were observed in a light irradiated DPE crystal containing DPDAM, as a function of angle of rotation of the laboratory dc field,  $\mathbf{H}_0$ , when the field was rotated in the planes of the orthorhombic DPE crystallographic axis system. (The field strengths are given as proton fluxmeter frequencies.) When  $\mathbf{H}_0$  was rotated in the *bc* plane (the *bc* plane) only the three lines of a single triplet state spectrum were observed. When  $\mathbf{H}_0$  was rotated in the *ac* plane, only a single spectrum was observed. When  $\mathbf{H}_0$  was rotated in the *ab* plane, two magnetically distinguishable molecules were observed. However, the two spectra were only very slightly displaced from each other ( $0.0306\pi(5.5^\circ)$ ). The rotations in the *ab* plane caused  $\mathbf{H}_0$  to pass through the principal *x* and *z* axes of the spin hamiltonian (1), within experimental error. The *a* axis bisected the angle between the two *z* axes of the two

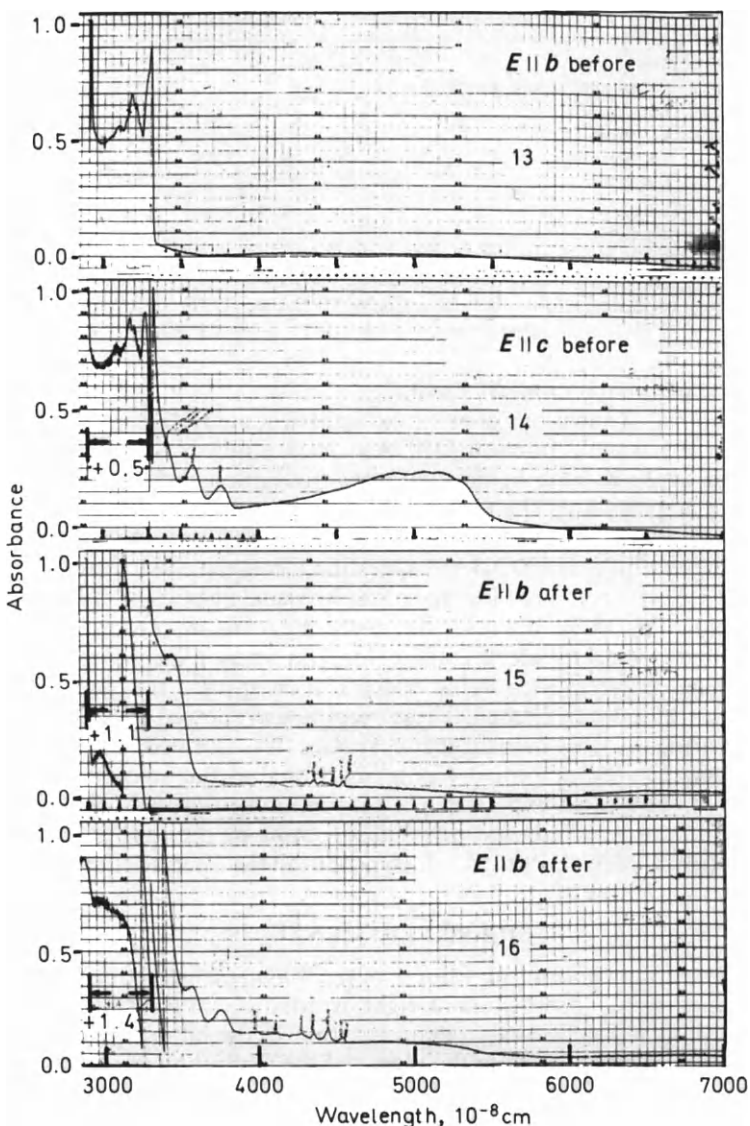
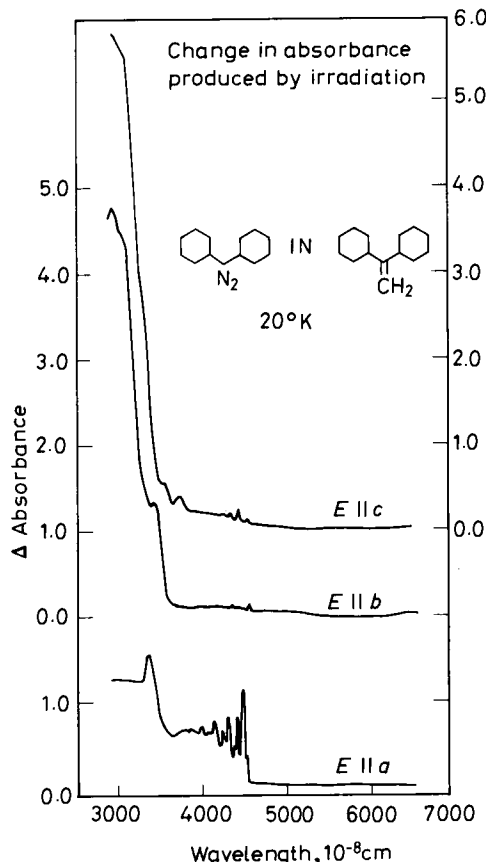


Figure 1. Polarized light optical spectra of 1,1-diphenylethylene (DPE) crystals containing  $\sim 0.002$  mole fraction diphenyldiazomethane (DPDAM) at  $20^\circ\text{K}$ , before and after irradiation with unpolarized light.  $E \times H \parallel a$ .

## EPR AND ENDOR OF REACTING TRIPLETS IN ORGANIC CRYSTALS

magnetically distinguishable molecules and the *b* axis bisected the angle between the two *x* axes. When  $\mathbf{H}_0$  was rotated in the other two planes (*ac* plane and *bc* plane)  $\mathbf{H}_0$  passed, within experimental error, through the *y* axes (of course, of both molecules, there being only a single spectrum) but missed the *x* or *z* axes by just a little bit. It thus became very clear that the principal axes, *x,y,z*, of the fine structure tensor of (1) were oriented as shown in *Figure 4*.



*Figure 2.* Change produced in the polarized light optical spectrum of 1,1-diphenylethylene (DPE) crystals containing diphenyldiazomethane (DPDAM) by irradiation at 20°K with unpolarized light.

We also noted that the anisotropy of the EPR spectrum was very small for the rotation of  $\mathbf{H}_0$  in the cleavage plane (*bc* plane) whereas there was an extremely large anisotropy in the other two crystallographic planes. We should now take a look at the DPM molecule<sup>4</sup> described in *Figure 5*. We believed, for the reasons explained previously, that most of the electron spin density was on the central C atom in an approximately toroidal distribution in two orthogonal *p* orbitals. The small anisotropy of the EPR spectrum in the *bc* crystallographic plane showed that this *bc* plane was in the plane of

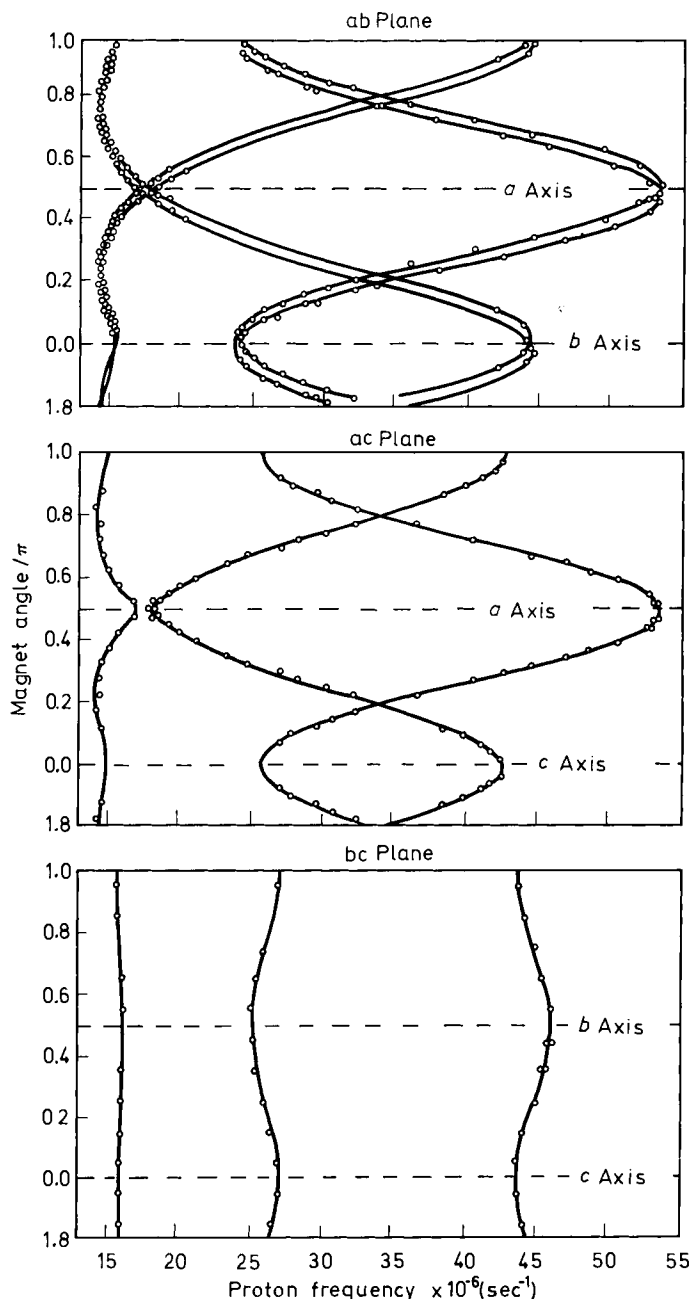


Figure 3. Magnetic field strengths (proton gaussmeter frequencies) for electron magnetic resonance at  $\sim 77^\circ\text{K}$  and at fixed frequency,  $\sim 2.4 \times 10^{10} \text{ Hz}$ , in single crystals of 1,1-diphenyl-ethylene (DPE) containing diphenyldiazomethane after irradiation with light from Hg-Xe arc. (The circles represent experimental points and the solid lines are calculated using the spin hamiltonian and parameters given in Table 3.)

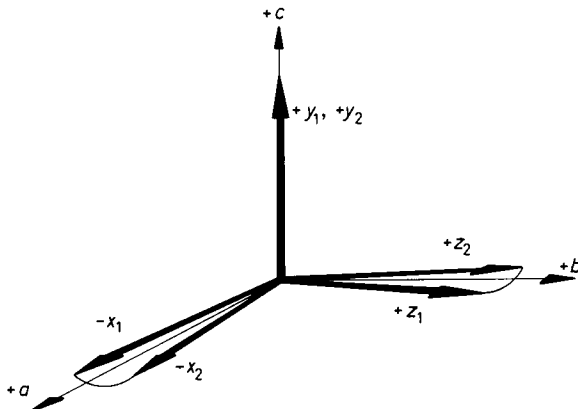


Figure 4. Orientation of the principal axes,  $x$ ,  $y$ ,  $z$ , of the fine structure tensor (in the spin hamiltonian, (1), given in Table 3) in the crystallographic,  $a$ ,  $b$ ,  $c$ , axis system, for diphenylmethylene (DPM) in 1,1-diphenylethylene (DPE).

the toroidal spin distribution. In fact, if the central  $\overset{2'}{\text{C}}-\overset{1}{\text{C}}-\overset{2}{\text{C}}$  bonding were linear and the two phenyl ring planes were perpendicular to each other, symmetry would demand that  $E$  in the spin hamiltonian, (1), be zero, i.e. that there would be no magnetic anisotropy in the  $xy$  fine structure plane of either of the magnetically distinguishable molecules. Each of the  $p$  orbitals on the central C would be  $\pi$  to one plane and  $\sigma$  to the other. They would give a toroidal spin distribution with axial symmetry. So we pictured<sup>4</sup> the DPM molecule as being a little bent, through angle,  $\theta$ , and a little twisted, through angle,  $\phi - \pi/4$ , from this idealized symmetrical structure which we just mentioned. This distortion introduced the anisotropy in the  $xy$  plane of the molecule. We also saw that the  $y$  fine structure axis, which we found to lie exactly along the  $c$  axis of the crystal for both magnetically distinguishable

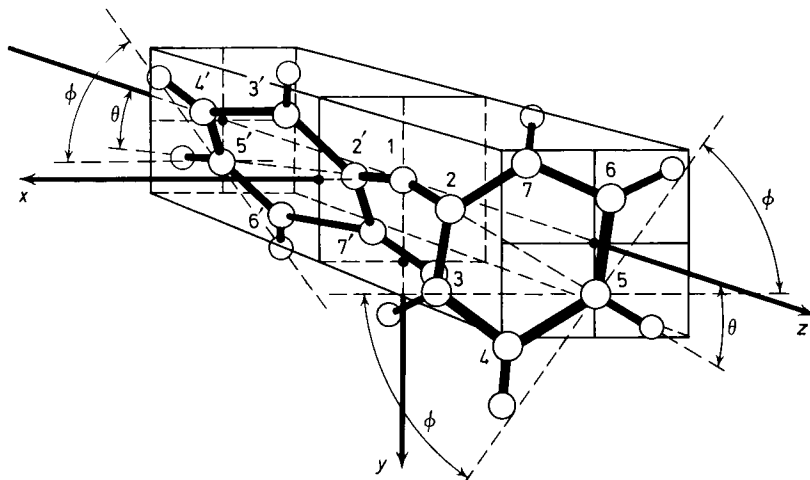


Figure 5. Schematic diagram of the diphenylmethylene (DPM) molecule.

DPM molecules, was therefore a 2-fold axis of the DPM molecule. Thus the molecule was actually describable as a bent and twisted molecule<sup>4</sup> as shown in *Figure 5*, with the 2-fold symmetry axis along the crystal's *c* axis and the molecule's *y* axis. The + value of *D* in the spin hamiltonian, (1), meant an oblate spin distribution with respect to the *z* axis in agreement with our notion concerning its arising from *p* orbitals on the central C atom. The *x* and *z* principal axes of the fine structure tensor were seen to lie in the crystal's *ab* plane, their directions being only very slightly different for the two molecules.

We of course realized<sup>7</sup> at this point what an ideal host the DPE crystal was for polarized light optical studies of the DPM molecule, because of the fact that all molecular axes of all DPM molecules are so nearly coincident in directions.

There was seen to be such a small amount of electron spin on the phenyl rings that their interactions with the protons did not produce a resolvable EPR hyperfine structure. However, substitution of <sup>13</sup>C in the central C position gave large <sup>13</sup>C hyperfine interactions with the triplet state electrons.

Measurements<sup>4</sup> of <sup>13</sup>C hyperfine splitting of each EPR line into two lines afforded a very detailed view of the spin distribution about the central C atom. Both the isotropic and anisotropic components of this tensor interaction, which is described by the spin hamiltonian,

$$\mathcal{H}_C = \mathbf{I} \cdot \mathbf{A} \cdot \mathbf{S}, S = 1, I = \frac{1}{2}. \quad (2)$$

*Table 5.* <sup>13</sup>C hyperfine interactions of diphenylmethylen (DPM) in 1,1-diphenylethylene (DPE)

(2)	$\mathcal{H}_C = \mathbf{I} \cdot \mathbf{A} \cdot \mathbf{S}$
	$\rho_{2p_x} = 0.565$
	$\rho_{2p_y} = 0.646$
	$\rho_{2s} = 0.0867$

shown in *Table 5*, were measured. If we described the spatial distribution of the electron spin on the central C atom by means of a  $2p_x$  atomic orbital, a  $2p_y$  orbital, and a  $2s$  orbital, the anisotropic components of the <sup>13</sup>C hyperfine interaction gave the spin densities in the *p* orbitals and the isotropic component gave the the spin density in the *s* orbital. The results are given in *Table 5*.

#### 4. ENDOR EXPERIMENTS<sup>4,5,6</sup>

Our most powerful tool for investigating the local structure in the vicinity of a DPM molecule, which had been generated in a DPE crystal, was ENDOR. In the proton ENDOR experiment we determined the nuclear resonance frequencies of the protons in the paramagnetic molecule by sweeping the frequency of an rf field with time. The frequency of this rf field was swept through values in the vicinity of those required for normal proton resonance for the  $|\mathbf{H}_0|$  used in the EPR experiment. When proton resonance occurred at the resonance value of the rf frequency, the EPR line intensity changed. This was a very convenient method for measuring proton resonance frequencies in our paramagnetic molecule. The differences between these

## EPR AND ENDOR OF REACTING TRIPLETS IN ORGANIC CRYSTALS

proton ENDOR frequencies and the frequency of the EPR lab. magnet's proton gaussmeter, in which the protons occur in diamagnetic water, measured the local magnetic fields which the protons experienced in the paramagnetic molecule, DPM.

As I have already said, the electron spin was mostly on the central C. The rest of it was distributed over 12 C's. The hyperfine interactions of a proton on a C with the electron spin in its vicinity were thus very small. Moreover, with 10 protons, there were  $2^{10}$  lines in the hyperfine pattern of the EPR line for a general direction of  $\mathbf{H}_0$ . With so many lines and such small interactions, the result was a single line of 8 G width.

In the case of the ENDOR spectrum, when one watched the EPR intensity as the rf field was swept in frequency, there was just one line for each proton, i.e. for a general orientation of  $\mathbf{H}_0$ , 10 lines. Moreover, ENDOR lines were very much narrower than the EPR lines on an energy or frequency scale. The inhomogeneous broadening by local fields, which accounted for a large fraction of the broadening of the lines in these systems, was reduced, on a frequency scale, in the ENDOR spectrum from that in the EPR spectrum by a factor of the ratio of the Bohr magneton to the nuclear magneton. Inasmuch as we scanned frequency and had so many fewer lines than in the unresolved hyperfine pattern of the EPR spectrum, we found<sup>4</sup>, instead of the single 8 G wide line of the EPR spectrum, an ENDOR spectrum of 10 extremely widely spaced, 5 to 10 kHz wide lines as shown in *Figure 6*<sup>4</sup>. The line widths shown in this figure are larger than their true values.  $\sim$  5–10 kHz. for very small modulation fields and sweep rates.

In addition, the signs of the hyperfine interactions were directly observable from the ENDOR spectrum because the oppositely signed interactions displaced the proton ENDOR lines in opposite frequency directions from the gaussmeter frequency, marked G in *Figure 6*. Moreover, if we plotted all the ENDOR shifts versus angle of  $\mathbf{H}_0$  in the x,y,z, axis system of the diphenyl-methylene molecule<sup>4</sup>, as in *Figure 7* and in *Figure 8*, the anisotropic component of the hyperfine interaction, combined with our semiquantitative knowledge of the DPM structure and orientation, was sufficient to identify the particular proton of DPM which was responsible for a given ENDOR line. These assignments are given in *Figure 7* and *8* using the numbering system which is used in *Figure 5*.

The interactions of the protons in DPM with the triplet state electrons and with the laboratory dc field,  $\mathbf{H}_0$ , were described by the spin hamiltonian,

$$\mathcal{H}_H = - |\beta_n| g_n \mathbf{H}_0 \cdot \sum_{k=1}^{10} \mathbf{I}_k + \mathbf{S} \cdot \sum_{k=1}^{10} \mathbf{A}_k \cdot \mathbf{I}_k, \quad S = 1, I_k = \frac{1}{2} \quad (3)$$

*(k indexes the protons)*

shown in *Table 6*<sup>4</sup>.

The resulting shifts,  $\Delta\nu_k$ , of proton ENDOR frequency of the  $k$ th proton in DPM from the free proton frequency in the same external field were given by this spin hamiltonian. They are also shown in *Table 6*. The expectation values,  $\langle S_x \rangle$ ,  $\langle S_y \rangle$ , and  $\langle S_z \rangle$ , of the electron spin components in the fine structure axis system of *Table 3*, and the direction cosines,  $l$ ,  $m$ , and  $n$ , of  $\mathbf{H}_0$ , in the

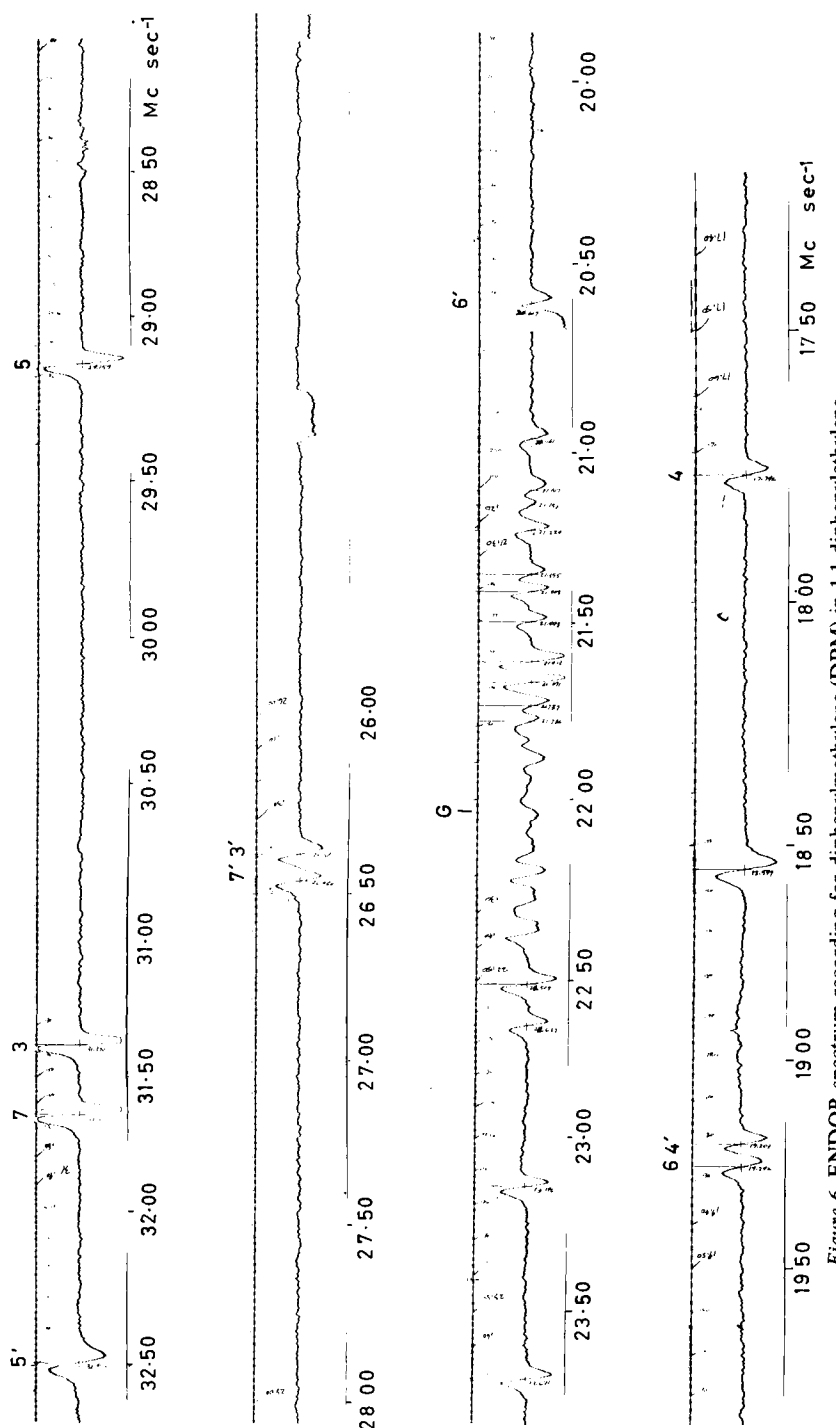


Figure 6. ENDOR spectrum recording for diphenylmethylenediphenylmethane (DPM) in 1,1-diphenylethylene

# EPR AND ENDOR OF REACTING TRIPLETS IN ORGANIC CRYSTALS

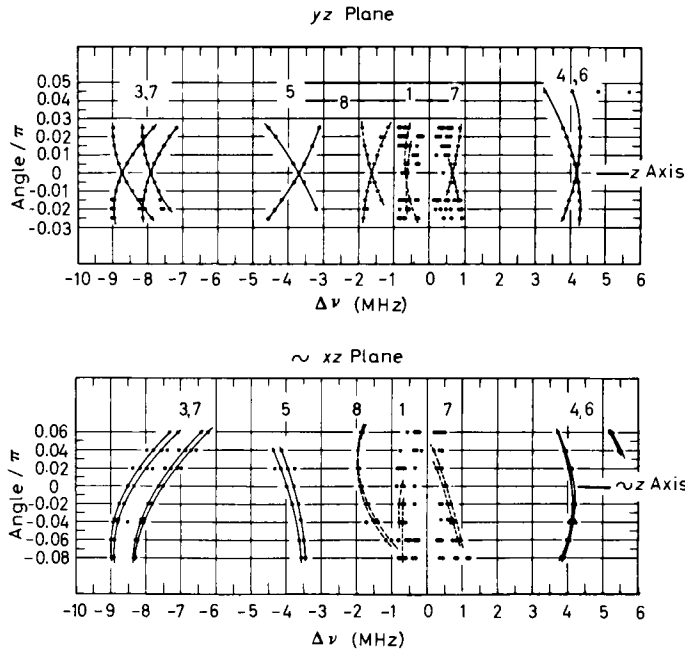


Figure 7. Proton ENDOR shifts vs angle of  $H_0$  for diphenylmethylene (DPM) in 1,1-diphenylethylene (DPE).

same system, were obtained from the EPR data. Then the measured ENDOR shifts of Figures 7 and 8 were fitted with (4) in Table 6 by adjustment of the components,  $A_{rsk}$ , of the tensor  $\mathbf{A}_k$ , in (3), for the  $k$ th proton. The resulting values<sup>4</sup> of the  $\mathbf{A}_k$  components are shown in Table 7. These 30 numbers describe the measured interactions of the protons with the triplet state electrons. The precision with which these values are fixed by the experiments is to be noted.

We then considered the model of DPM shown in Figure 5. We fixed<sup>4</sup> the following properties of the model.

- (a) Regular plane hexagon phenyl rings.
- (b) C—C ring bonds  $1.390 \times 10^{-8}$  cm long.
- (c) 1, 2, C—C distance,  $1.425 \times 10^{-8}$  cm.
- (d) C—H bonds,  $1.084 \times 10^{-8}$  cm long, bisecting the hexagon angles.

Table 6. Spin hamiltonian for proton electron hyperfine interaction and proton Zeeman interaction. ENDOR shifts for  $k$ th proton

$$(3) \quad \mathcal{H}_H = -|\beta_n|g_n\mathbf{H}_0 \cdot \sum_{k=1}^{10} \mathbf{I}_k + \mathbf{S} \cdot \sum_{k=1}^{10} \mathbf{A}_k \cdot \mathbf{I}_k$$

$S = 1, I_k = \frac{1}{2}, k$  indexes protons

$$(4) \quad \Delta\nu_k = h^{-1} [(\langle S_x \rangle A_{xxk} + \langle S_y \rangle A_{xyk} + \langle S_z \rangle A_{xzk} - lv_p)^2 \\ + (\langle S_x \rangle A_{xyk} + \langle S_y \rangle A_{yyk} + \langle S_z \rangle A_{yzk} - mv_p)^2 \\ + (\langle S_x \rangle A_{xzk} + \langle S_y \rangle A_{yzk} + \langle S_z \rangle A_{zzk} - nv_p)^2]^{\frac{1}{2}} \\ - v_p$$

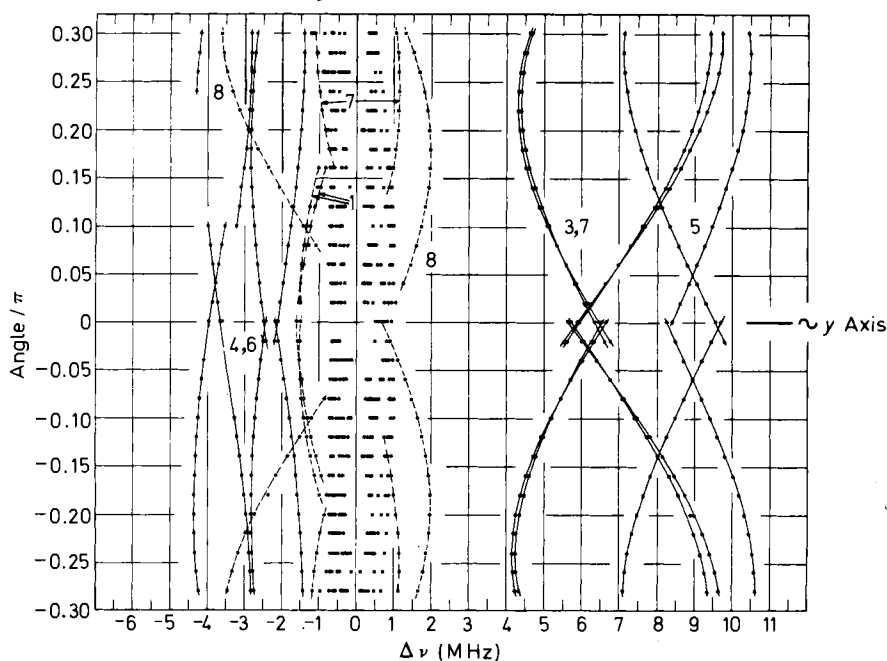
$\sim xy$  Plane of both molecules

Figure 8. Proton ENDOR shifts vs angle of  $H_0$  for diphenylmethane (DPM) in 1,1-diphenylethylene (DPE).

- (e) Spin distribution on the central C determined by the  $^{13}\text{C}$  EPR data.
- (f) Anisotropic hyperfine interaction components for interaction of the proton with electron spin on adjacent C, value given by previous measurements on photoexcited aromatic molecules in triplet states.
- (g) Spin distribution on ring C's not adjacent to  $k$ th proton, 2 point spins, 0.7665 Å above and below the hexagon plane.

Table 7. Best values of the element of the  $\mathbf{A}_k$  for diphenylmethane in 1,1'-diphenylethylene (DPE). (Standard deviations are given in parentheses.)

Proton Position $k$	3	4	5	6	7
$A_{xxk}/h$ (MHz)	-7.6336 (0.0042)	+2.0808 (0.0072)	-9.4227 (0.0031)	+3.5157 (0.0065)	-7.9418 (0.0036)
$A_{yyk}/h$ (MHz)	-6.5061 (0.0212)	+2.5141 (0.0025)	-9.9857 (0.0087)	+4.1849 (0.0022)	-6.5422 (0.0169)
$A_{zzk}/h$ (MHz)	-7.9720 (0.0031)	+4.1687 (0.0013)	-3.8070 (0.0026)	+5.8278 (0.0034)	-8.7763 (0.0023)
$A_{xyk}/h$ (MHz)	+2.8889 (0.0070)	+0.6828 (0.0024)	-2.1519 (0.0031)	+0.7412 (0.0020)	+3.1182 (0.0056)
$A_{xzk}/h$ (MHz)	-1.4376 (0.0109)	-0.0706 (0.0043)	+0.9089 (0.0105)	+0.0020 (0.0078)	-1.1519 (0.0083)
$A_{yzk}/h$ (MHz)	-0.9560 (0.0146)	+0.4939 (0.0036)	+1.9088 (0.0158)	+0.5535 (0.0036)	-1.1587 (0.0107)

## EPR AND ENDOR OF REACTING TRIPLETS IN ORGANIC CRYSTALS

We allowed the following properties to vary:

( $\alpha$ ) Angle of bend,  $\theta$ .

( $\beta$ ) Angle of twist,  $\phi$ .

( $\gamma$ ) 7 distinguishable spin densities,  $\rho_i$ , on the C atoms, C = 1 to 7.

For a given value of the pair,  $\theta, \phi$ , we adjusted the 7  $\rho_i$  to give a best fit. We did this for numerous  $\theta, \phi$ , pairs in the range  $0.060\pi \leq \theta \leq 0.110\pi$ ,  $0.250\pi \leq \phi \leq 0.400\pi$ . The best fit gave us the values of  $\theta$  and  $\phi$  and the spin densities. The spin density values are given in *Table 8*. The angle values will be given in a subsequent table.

*Table 8.* Best values of spin densities of diphenylethylene in 1,1'-diphenylethylene (DPE) and their standard deviations  $\sigma$

$i$	1	2	3	4	5	6	7	Total
$\rho_i$	+0.590	-0.022	+0.101	-0.0392	+0.1108	-0.0381	+0.1215	1.060
$\sigma\{\rho_i\}$	0.062	0.037	0.012	0.0051	0.0044	0.0043	0.0090	

If we now look again at *Figures 7* and *8*, we see that there are many ENDOR lines not assignable to protons in the DPM molecule. These lines were very important<sup>6</sup> for our purposes. They originate with the protons of the DPE host crystal molecules. Some of these lines, which come from protons of DPE which are relatively close to the DPM molecule, show relatively large anisotropies of ENDOR shift,  $\Delta v$ . There are many from greater distances which lie very near the proton gaussmeter frequency and have  $\Delta v \cong 0$ . Six of these plots of ENDOR shift versus angle of  $\mathbf{H}_0$  were fitted<sup>6</sup> by least squares adjustment of values of components of  $\mathbf{A}_k$ , in the same manner as we have described for the proton in the DPM molecule. Values of these components are given in *Table 9*<sup>6</sup>. Values of the isotropic parts,  ${}^1A_k$ , of these tensors are given in the last row of this table. Only half the tensors are given since, because

*Table 9.* Best values of the elements of the  $\mathbf{A}_k$  and the values of  ${}^1A_k$  of 1,1-diphenylethylene protons near diphenylmethylene molecules in crystals of 1,1-diphenylethylene. (Standard deviations are given in parentheses.)

Proton Position $k$	$1(0, 0, 1)$	$7(0, -\frac{1}{2}, -\frac{1}{2})$	$8(0, -\frac{1}{2}, -\frac{1}{2})$
$A_{xxk}/h$ (MHz)	-1.172 (0.039)	+0.115 (0.016)	+1.998 (0.014)
$A_{xrk}/h$ (MHz)	+0.180 (0.007)	+1.251 (0.006)	+2.724 (0.006)
$A_{xck}/h$ (MHz)	-0.102 (0.032)	+0.787 (0.020)	+1.011 (0.010)
$A_{yyk}/h$ (MHz)	+1.790 (0.005)	-0.396 (0.008)	-0.344 (0.006)
$A_{yck}/h$ (MHz)	+0.175 (0.009)	+0.673 (0.014)	+0.701 (0.012)
$A_{zzk}/h$ (MHz)	-0.661 (0.003)	+0.627 (0.004)	-1.694 (0.003)
${}^1A_k/h$ (MHz)	-0.014 (0.013)	+0.115 (0.006)	-0.013 (0.005)

of the 2-fold axis. the others are different from the given ones only with respect to algebraic signs of the values. It is to be noted that the isotropic components, which measure the electron nucleus contact interaction, have values larger than their standard deviation and thus we see that there is actually a small amount of triplet electron spin on the host DPE molecules.

Having arrived at  $\mathbf{A}_k$  values for host DPE proton interactions with electron spin on DPM molecules, we extracted the values of the anisotropic parts of these interactions, which arose from magnetic dipole-dipole interactions between DPE protons and electron spin on DPM. These anisotropic interactions depended on the positions,  $\mathbf{r}_k$ , of the DPE protons, the positions,  $\mathbf{r}_i$ , of the point electron spins in our DPM model, and the spin density  $\rho_i$ , at each C of the DPM. We used the values of  $\rho_i$  and  $\mathbf{r}_i$  given previously, as determined by ENDOR, and adjusted the  $\mathbf{r}_k$  to give a least squares best fit to the  $\mathbf{A}_k$ . In Table 10<sup>6</sup> are given the values of the  $\mathbf{r}_k$  components, for DPE protons, in the DPM  $x$ ,  $y$ ,  $z$ , axis system with the origin fixed at the central C of DPM.

Table 10. Coordinates of 1,1-diphenylethylene protons near diphenylmethylenes molecules in 1,1-diphenylethylene crystals. (Standard deviations are given in parentheses.)

Proton Position <i>k</i>	1,(0, 0, 1)	7,(0, - $\frac{1}{2}$ , - $\frac{1}{2}$ )	8,(0, - $\frac{1}{2}$ , - $\frac{1}{2}$ )
<i>x</i> ( $\text{\AA}$ )	+0.163 (0.053)	-1.838 (0.025)	-2.495 (0.005)
<i>y</i> ( $\text{\AA}$ )	+4.100 (0.044)	-0.623 (0.020)	-1.707 (0.006)
<i>z</i> ( $\text{\AA}$ )	+0.382 (0.072)	+3.874 (0.013)	+0.578 (0.010)

Before proceeding with an assignment of these proton positions to particular protons of particular DPE molecules, we must further consider the optical spectroscopic and x-ray diffraction studies.

## 5. OPTICAL EXPERIMENTS<sup>3, 7</sup>

As I mentioned before, the DPE crystal was an excellent host for the study of the polarized light, optical absorptions by DPM molecules because they were held in this crystal with  $x$ ,  $y$ , and  $z$  axes of all four molecules per unit cell nearly parallel or anti-parallel.

The most striking feature<sup>3, 7</sup> of the visible ( $\sim 4500 \text{ \AA}$ ) spectrum of the DPM molecule, at both  $\sim 20^\circ\text{K}$  and  $\sim 77^\circ\text{K}$ , was a structured absorption band of medium intensity ( $f \sim 0.2$ ) which appeared only in polarization along the crystallographic *a* axis. All structure is accounted for by assuming a 0-0 transition at  $22174 \text{ cm}^{-1}$  and vibronic additions of 192, 520 and  $956 \text{ cm}^{-1}$ . For *b* and *c* axis polarization there was an absorption band of approximately  $\frac{1}{10}$  the intensity of the *a* polarized band. This band had its origin at  $22022 \text{ cm}^{-1}$ . It was sensibly the same in intensity and position for all polarization directions in the *bc* plane but there were small differences at shorter wavelengths for the *b* polarized and the *c* polarized spectra.

## EPR AND ENDOR OF REACTING TRIPLETS IN ORGANIC CRYSTALS

Careful analysis showed that the  $a$  polarized band and the  $bc$  polarized band were actually different electronic transitions and not the same transition with electronically forbidden, vibronically allowed components in one of the orientations of the polarization.

It was very clear<sup>3, 7</sup>, before the availability of ENDOR data, that the optical spectrum showed that the optically absorbing species generated by the irradiation of DPE crystals containing DPDAM was cylindrically symmetrical with respect to electric dipole absorption. The optical information thus showed that if this species were the DPM molecule of *Table 2* and *Figure 5*, its geometry might be expected to approximate the situation in which the 5',2'-1-2,5 C's lay in a straight line near the  $a$  axis and the planes of the two phenyl rings were more nearly normal to each other than parallel to each other.

We made relatively simple calculations of the energies of the possible electronic states of a DPM molecule which resulted from assigning the 14 electrons ( $\pi$  electrons of phenyl rings and 2 electrons on the divalent C) to Hückel orbitals of lowest energy, assigning spins, taking properly anti-symmetrized products of these spin orbitals and introducing electron repulsion in a manner similar to that of Longuet-Higgins and Pople<sup>29</sup> for free radicals. The approximation of neglect of differential overlap was employed<sup>30</sup>. The calculated electric dipole transitions for such a model with the phenyl rings parallel (i.e.,  $\phi = 0, \theta = 0$ , in *Figure 5*) are in disagreement with experiment for the  $xy$  polarizations as far as relative frequencies and positions are concerned, as expected. Such calculations for a DPM molecule with phenyl rings perpendicular (i.e.  $\phi = \pi/4, \theta = 0$  in *Figure 5*) gave much better agreement. The small disagreements that remained may be interpreted in terms of a small bend by angle,  $\theta$ , and a small change in  $\phi$ , from that just mentioned, by means of more accurate configuration interaction calculations which are currently in progress.

There was thus seen to be a striking consistency between the results of EPR, ENDOR and optical absorption investigations of the DPM molecule oriented in the DPE crystal host, with respect to the conformation of the divalent C molecule and to its angles of orientation in the DPE structure.

## 6. X-RAY STUDIES<sup>6, 8, 9</sup>

As I stated earlier in this lecture, the x-ray diffraction patterns of the DPE crystal were consistent only with space groups *Pnc2* or *Pncm*. The density of the crystal showed that there must be two molecules per unit cell. Thus *Pncm* required  $2/m$  symmetry for the molecule, DPE, and was rejected. A consideration of the *Pnc2* revealed that when packing energies and proton-proton internuclear distances were computed, any arrangement corresponding to this space group was impossible. The conclusion was therefore reached that some type of disordering existed in these crystals.

We knew that the DPM molecules were well oriented in the DPE crystals and that there were only two magnetically distinguishable molecules. We knew that the symmetry of the host crystal determines the orientation of the guest molecules. Thus whatever the disordering was, it must preserve the observed orientation of both the EPR fine structure and ENDOR hyperfine

structure principal axis systems of the substitutionally incorporated DPM molecules. Therefore we considered a disordering in which different domains are translationally coherent with cell edges exactly parallel or antiparallel. The basic domains were required to have a structure which, when averaged over all domains, gave *Pnc*2 or *Pncm*. A space group was sought which

- (a) was a subgroup of *Pnc*2 or *Pncm*;
- (b) would allow the long axis of DPE to be nearly parallel to the *a* axis (EPR of DPM); and
- (c) would have a 2-fold axis at molecule sites which were along the *c* axis.

*Pnca* satisfied these requirements. *Pnca* comes from *Pncm* by removing the mirror in the *ab* plane and by expanding the *a* length to twice the value which I gave in *Table 4*. The structure of DPE was thus one in which the domains have space group symmetry, *Pnca*, the *a* length is 19.918 Å, there are four molecules per unit cell, two of the molecules are related to the other two by an inversion (which cannot be detected by EPR of DPM oriented in DPE), there is a 2-fold axis along the *c* axis at each molecule site, the long axes of the DPE molecules lie only slightly off from being parallel to the *a* axis, and the disordering is such that crystallographic axes of all the domains are

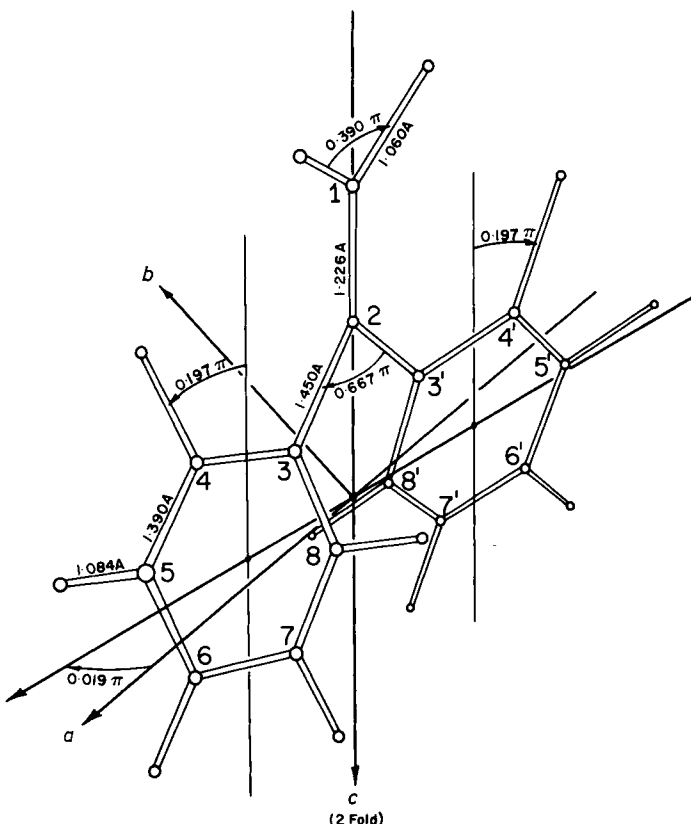
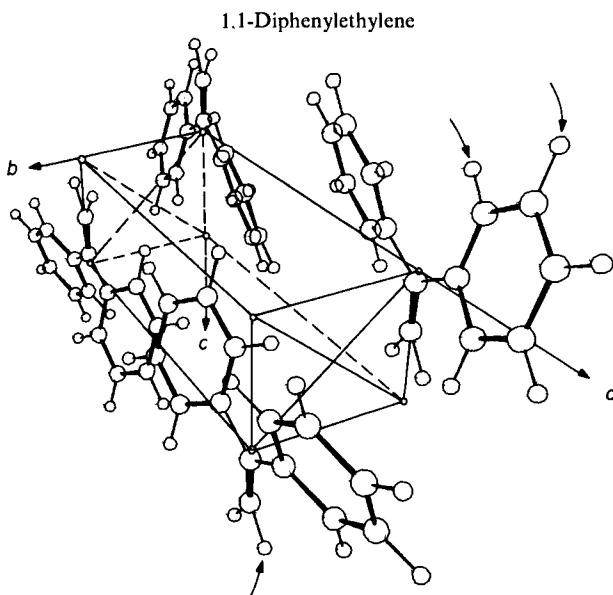


Figure 9. Simplified model of the 1,1-diphenylethylene (DPE) molecule.

## EPR AND ENDOR OF REACTING TRIPLETS IN ORGANIC CRYSTALS

parallel or antiparallel and translational coherence exists between domains such that there is equal probability that any unit cell be displaced along  $a$  by either  $na$  or  $(n + \frac{1}{2})a$ ,  $n$  any integer.



*Figure 10.* View of the 1,1-diphenylethylene (DPE) crystal structure.

We used the values of the C atom coordinates determined by x-ray diffraction for the construction of a model of the DPE molecule which is shown in *Figure 9*. In this DPE model, the phenyl rings were taken to be planar regular hexagons lying in the planes which gave the best fit to the ring C atom coordinates determined by x-rays. Each ring edge was taken to be 1.390 Å.

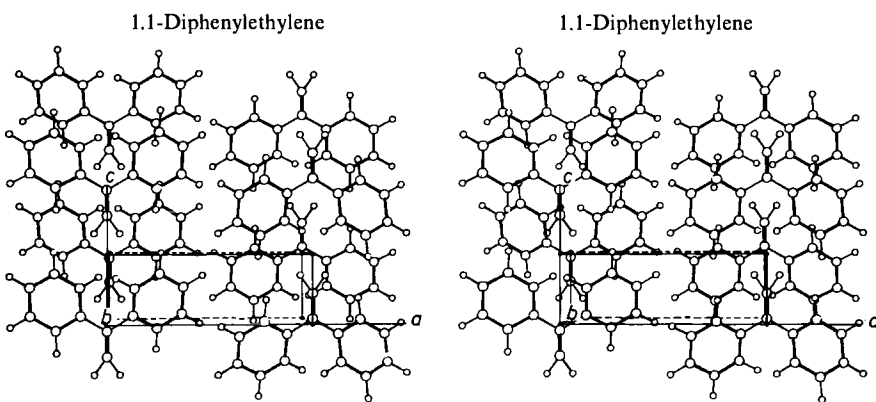


*Figure 11.* View of the 1,1-diphenylethylene (DPE) crystal structure.

The central 1, 2, 3, 3' C's were placed in a common plane which was the best fit plane for all the C atoms of a DPE molecule as determined by x-rays. The 2 H's on the C(1) were placed in this same best plane at the distances shown. The central C distances and angles are those given by x-ray diffraction. Three views of the DPE crystal structure, with such molecules in it, are shown in Figures 10, 11 and 12.

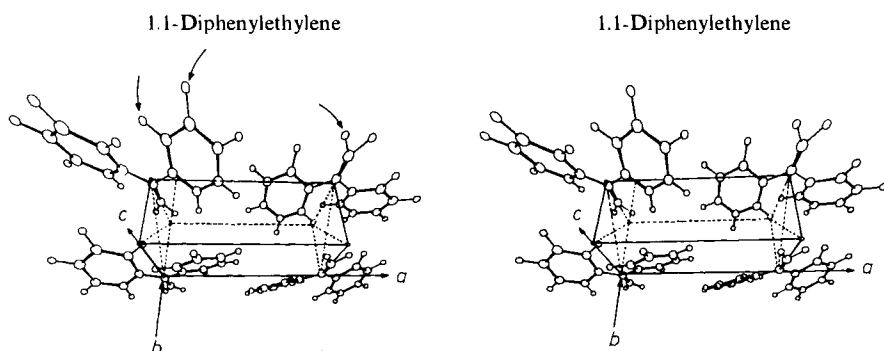


Figure 12. View of the 1,1-diphenylethylene (DPE) crystal structure.

## 7. THE LOCAL STRUCTURE AT GUEST MOLECULE SITES

In Table 11 is given a comparison of the molecular geometry of DPE determined by x-ray diffraction<sup>8</sup> and DPM geometry determined by EPR and ENDOR<sup>4,6</sup>. In this table are presented the values of the dihedral angles (closely related to the  $\phi$  angle of Figure 5) between the planes of the phenyl rings and the planes which give a least squares best fit to the coordinates of all the C atoms, the bend angle (in this table the angle given is  $2\pi - 2\theta$  in which  $\theta$  is the  $\theta$  of Figure 5), and the angle between the long axis of the molecule (which is parallel to a line through the ring centres) and the  $a$  axis of the crystal. The similarity of the values for the DPE host molecule and the DPM guest molecule is striking.

We assigned<sup>6</sup> the sets of coordinates of DPE host protons in the DPM  $x$ ,  $y$ ,  $z$ , axis system, obtained from the ENDOR results, to particular protons on particular host molecules as follows. Eight models of the substitution of DPM molecules into DPE sites were considered. A substituted DPM molecule may be either right handed or left handed with respect to the pitch

Table 11. Structure and orientation angles of 1,1-diphenylethylene and diphenylmethane in equivalent sites in 1,1-diphenylethylene crystals

	DPE	DPM
Phenyl ring twist from best molecular plane	+0.197 $\pi$ (+35°)	+0.20 $\pi$ (+36°)
Central C—C—C bond angle to rings	0.684 $\pi$ (123°)	0.84 $\pi$ (151°)
Angle between long axis and $a$ axis	+0.019 $\pi$ (+3.5°)	-0.015 $\pi$ (2.8°)

## EPR AND ENDOR OF REACTING TRIPLETS IN ORGANIC CRYSTALS

of the propellor blades formed by the phenyl rings. It may have its central C *c* coordinate larger or smaller than the *c* coordinate of the 2 C's to which it is attached. And the line of ring centres may be twisted slightly clockwise or slightly counterclockwise from the *a* axis looking out from the origin along the +*c* axis. This gives eight different kinds of orientation of the guest DPM molecule. The DPM shape determined by EPR and ENDOR was assumed. The 2-fold DPM axis was assumed to lie on the 2-fold axis of the (0,0,0) site of the DPE structure. All DPE molecules were assumed to have the *Figure 9* model structure. The coordinates of all protons of all eight DPE molecules in the nearest neighbour shell (assuming no disruption of DPE structure) about the DPM (0,0,0) site were calculated. The DPE proton coordinates previously given in *Table 10* were transformed to the crystallographic axis system, for each of the eight possible DPM orientations. For every reasonable assignment of the transformed coordinates of *Table 10* to DPE protons, the *c* coordinate of the DPM origin was fixed by making the average of the three measured *c* coordinates of DPE protons equal to the average of the three assigned proton coordinates of the model. The assignment of protons, and orientation of DPM molecules, which gave the smallest sum of the squares of the deviations of the three measured positions from the model positions was taken to be the correct assignment.

*Table 12.* Coordinates of 1,1-diphenylethylene host protons near diphenylmethylene guest molecules, from ENDOR and x-ray diffraction. (Coordinates of the protons in the crystal model are given in parentheses.)

Proton Position <i>k</i>	1(0, 0, 1)	7(0, -½, -½)	8(0, -½, -½)
<i>a</i> (Å)	+0.389 (+ 0.609)	+3.781 (+ 2.728)	+0.458 (+ 0.589)
<i>b</i> (Å)	+0.144 (- 0.037)	-2.022 (- 2.860)	-2.520 (- 2.730)
<i>c</i> (Å)	+4.491 (+ 4.389)	-0.232 (- 0.105)	-1.316 (- 1.342)

In *Table 12*<sup>6</sup> are given the coordinates of these assigned protons as determined by x-rays for the simplified model of the undisturbed DPE structure and as determined by ENDOR. The coordinates in parentheses are those obtained from the model, and the others are the coordinates of the same protons obtained from ENDOR. The differences in these pairs of values may be taken to be measures of the local disruption of the DPE structure because of the presence of the DPM at that site. Of course, it was difficult to assess what part of these disagreements came from such local structure disruption and what part came from inadequacies of the DPM model.

## 8. CHEMICAL KINETICS<sup>6</sup>

### 8.1 Methods and conditions

EPR was used for quantitative studies<sup>6</sup> of the rates of (a) formation by irradiation and (b) decay of DPM in crystals of DPE containing DPDAM.

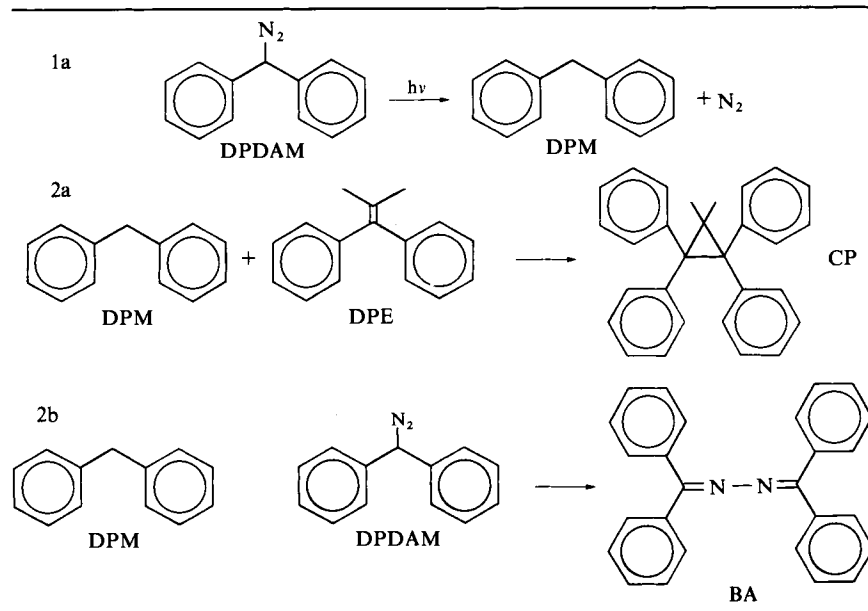
The temperature of the crystal could be controlled and measured to better than 2°K by means of thermocouples attached to the crystals during the EPR measurements. The intensity of the EPR signals was determined by means of a standard Mn<sup>+2</sup> sample which was always present in the microwave cavity during the EPR measurements. The light intensity was determined by standard actinometric methods under conditions which simulated actual experiments.

Experiments were performed under a wide variety of conditions. The ranges of variables investigated are summarized in *Table 13*<sup>6</sup>.

*Table 13.* Experimental conditions for study of kinetics

1.	Light. Hg-Xe arc with 3 filters.	
1.1	UV light, ~ 2900–3200 Å	
1.2	Visible light, ~ 4800–5800 Å	
1.3	Both UV and visible	
2.	Concentration of DPDAM in DPE	
2.1	Dilute, < 0.005 mole fraction	
2.2	Concentrated, 0.023 to 0.036 mole fraction	
3.	Temperature	
3.1	Low, ~ 77°K	
3.2	High, 90–117°K	
4.	Deuteration	Code
4.1	DPDAM-h <sub>10</sub> in DPE-h <sub>2</sub>	HH
4.2	DPDAM-d <sub>10</sub> in DPE-h <sub>2</sub>	DH
4.3	DPDAM-h <sub>10</sub> in DPE-d <sub>2</sub>	HD

*Table 14.* Chemical reactions.



## EPR AND ENDOR OF REACTING TRIPLETS IN ORGANIC CRYSTALS

Experiments in which large samples of DPE crystals containing DPDAM were irradiated at  $\sim 77^{\circ}\text{K}$ , warmed to room temperature, and analyzed by various means, showed two and only two reaction products, tetraphenylcyclopropane (CP) and benzophenone azine (BA). The only paramagnetic species ever observed under any of the experimental conditions was DPM. Thus the chemical reactions which we observed were assumed to be the three reactions described in *Table 14<sup>6</sup>*.

### 8.2 Photolysis<sup>6</sup>

Some experimentally measured values at the beginning of the irradiation, at  $\sim 77^{\circ}\text{K}$ , of previously unirradiated DPE crystals dilute in DPDAM are given in *Table 15<sup>6</sup>*. The spectral information for determining these values came from our optical studies<sup>7</sup> of this system.

*Table 15.* Initial experimental conditions for photolysis at the boiling point of N<sub>2</sub>.

Light	Ultraviolet and visible	Ultraviolet	Visible
DPM production rate (sec <sup>-1</sup> )	$4 \times 10^{14}$	$1 \times 10^{15}$	$2 \times 10^{12}$
Light Incidence rate (quanta sec <sup>-1</sup> )	$3 \times 10^{16}$	$1 \times 10^{16}$	$7 \times 10^{16}$
Number of DPDAM's in the irradiated part of the crystal	$1 \times 10^{16}$	$3 \times 10^{15}$	$2 \times 10^{16}$
Rate of light absorption by DPDAM (quanta sec <sup>-1</sup> )	$4 \times 10^{15}$	$8 \times 10^{15}$	$8 \times 10^{15}$
Fraction of quanta absorbed by DPDAM in the ultraviolet	0.13	0.54	0.00
Fraction of quanta absorbed by DPDAM in the visible	0.04	0.01	0.10

It is to be noted that the initial rate of low temperature production of DPM is much higher for ultraviolet than for visible light. This arises<sup>7</sup> partly from the fact that the DPDAM ultraviolet absorption coefficient is  $\sim 10^3$  mole<sup>-1</sup> 1 cm<sup>-1</sup> and the visible absorption coefficient is  $\sim 10^2$  mole<sup>-1</sup> 1 cm<sup>-1</sup>. The apparent DPM quantum yield is 0.129 in the ultraviolet and is  $1.25 \times 10^{-4}$  in the visible. We had no quantitative information on the amounts of CP formed so that some of the DPM formed could have reacted during the photolysis process to form products, in spite of the fact that when photolysis was terminated, the formed DPM was very stable.

### 8.3 Reactions of DPM<sup>6</sup>

In low concentration crystals of DPE containing DPDAM, the rate of decay of EPR signals from DPM was exponential within the errors of the measurements. In high concentration crystals, the rate of decay was the sum

of two clearly distinguishable exponential decays. In *Figure 13*<sup>6</sup> the intensity of the DPM EPR signal is plotted versus time. Curve A is for a dilute crystal at  $\sim 96^\circ\text{K}$ . Curve B is for a concentrated crystal at  $\sim 112^\circ\text{K}$ .

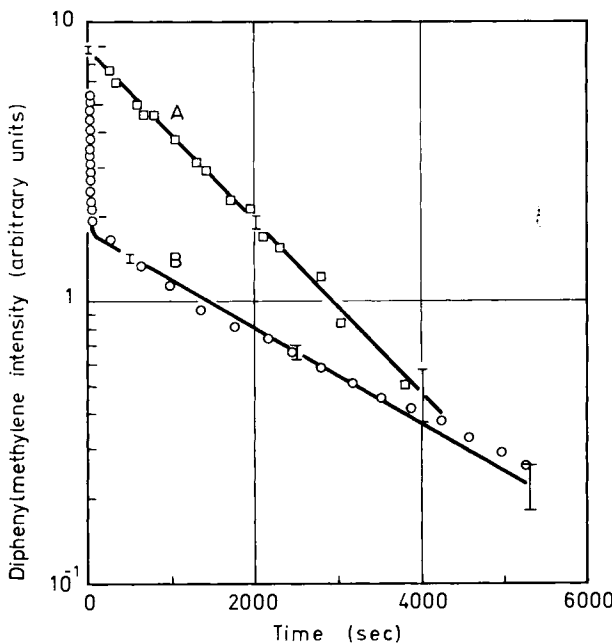


Figure 13. Decay of electron magnetic resonance signal from diphenylmethylene (DPM). Curve A for dilute crystal at  $\sim 96^\circ\text{K}$ . Curve B for concentrated crystal at  $\sim 112^\circ\text{K}$ .

The decays of 36 different low concentration crystals were each least squares fitted by the relation,

$$I = I_0 e^{-kt}, \quad (5)$$

in which  $I$  is the EPR signal intensity and  $t$  is time, by adjustment of the constants,  $I_0$  and  $k$ . Then the variation of the  $k$ 's, found in this manner with

Table 16. Values of parameters for best fit of  $\log_e(k/A) = -B/T$  to the diphenylmethylene decay in 1,1-diphenylethylene crystals. (Standard deviations are shown in parentheses).

Crystal and Decay Component	$\log_e A_n \dagger$	$\log_{10} A_n \dagger$	$B \times R$ $\text{kcal mole}^{-1}$	$(B \times k/hc)$ $(\text{cm}^{-1})$
HH rapid decay	34 (2)	14.8	7.8 (0.3)	$2.73 \times 10^3$
DH rapid decay	28 (5)	12.2	6.7 (1.0)	$2.34 \times 10^3$
HD rapid decay	27 (2)	11.7	6.6 (0.4)	$2.31 \times 10^3$
HD slow decay	13 (3)	5.6	4.6 (0.6)	$1.61 \times 10^3$

<sup>†</sup>  $A_n$  = Numerical value of  $A$  measured in  $\text{sec}^{-1}$

## EPR AND ENDOR OF REACTING TRIPLETS IN ORGANIC CRYSTALS

temperature, were least squares fitted with the relation,

$$\ln(k/A) = B/T, \quad (6)$$

in which  $T$  is the temperature, by adjustment of the constants,  $A$  and  $B$ .

Plots of  $k$ 's versus  $T$ , obtained in this manner, are given in *Figure 14*<sup>6</sup> for all three isotropic systems. In *Figure 15*<sup>6</sup> are presented similar plots for

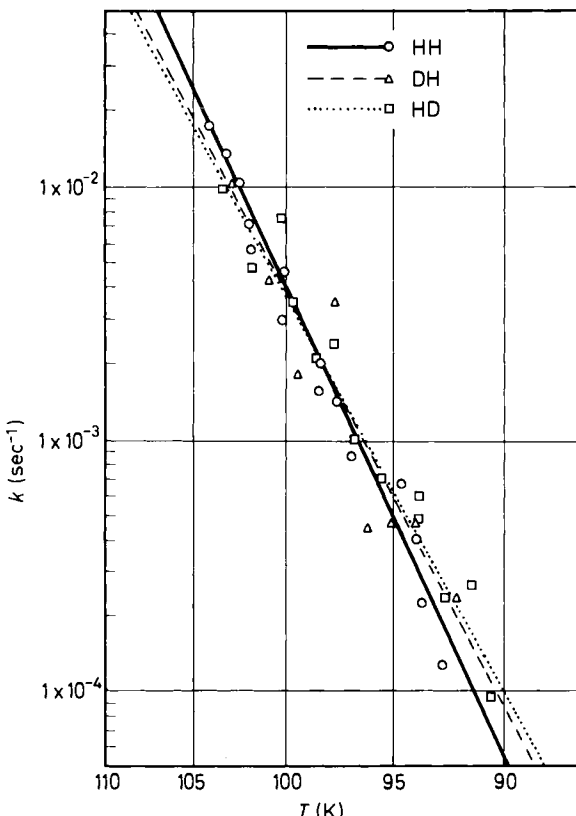


Figure 14.  $k$  (in (5)) vs  $T$  for the fast decay.

the slow decay process in concentrated crystals. The ratio of the  $I_0$  for the slowly decaying component to the  $I_0$  for the fast decay in the same concentrated crystal was always  $< 0.11$ .

The values of the parameters,  $A$  and  $B$ , for best fit are given in *Table 16*<sup>6</sup>.

## 9. REACTION MECHANISMS<sup>6</sup>

All of our experimental results were consistent with the occurrence of the three chemical reactions shown in *Table 14*<sup>6</sup>. We assumed that the appearance of the EPR signal is accounted for by reaction 1 and the decay by reactions 2a and 2b. We assumed that the fast decay was produced by reaction 2a and the slow decay by reaction 2b. It is important to note that the clear

distinguishability of the fast and the slow decays shows that a particular given DPM molecule must decay by a particular one of the processes, 2a or 2b; i.e. it is predestined as to which of the two decay processes is going to produce the decay of a given DPM at a given site in the crystal.

When the large crystal samples were irradiated and warmed the relative amounts of BA and CP were close to the relative values of  $I_0$ 's of (5) for the slow and the fast decay processes. This was the main reason for associating reactions 2a and 2b with CP and BA production, respectively. We thus assumed that the larger fraction of the EPR signal would decay by reaction 2a and a smaller fraction by reaction 2b.

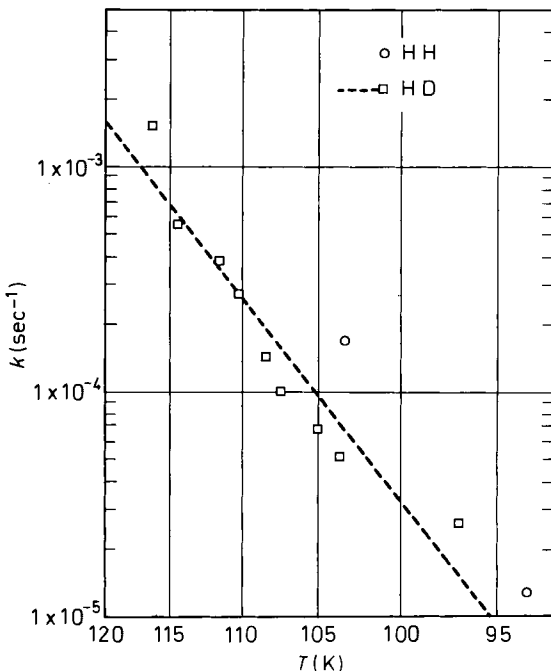


Figure 15.  $k$  (in (5)) vs  $T$  for the slow decay.

The quantum yields of DPM and the initial production rates of DPM are much larger for ultraviolet than for visible light. Our optical studies<sup>7</sup> indicated that the visible absorption of DPDAM was an  $n-\pi^*$  transition and that the ultraviolet absorption was a  $\pi-\pi^*$  transition. The C—N bond may be considerably more weakened by the  $\pi-\pi^*$  transition than by the  $n-\pi^*$  transition.

The strictly exponential decay of the DPM signal when reaction 2a occurs, and the fact that the Arrhenius type relation (6) is well obeyed, suggested to us that a thermally activated first order process was being observed<sup>6</sup>. If we interpreted the  $B$  of (6) as an activation energy, its value, which was  $\sim 7$  kcal mole<sup>-1</sup>, corresponding to  $\sim 2.45 \times 10^3$  cm<sup>-1</sup>, was certainly not nearly large enough to account for a molecular diffusion of such large molecules, if that had been the thermally activated process. It was also much too small

## EPR AND ENDOR OF REACTING TRIPLETS IN ORGANIC CRYSTALS

to account for a complete rotation of the DPE or DPM molecule in its crystal site, or a complete rotation of a phenyl ring in the DPE crystal structure. It was also clear that phase changes and crystal defects of a localized character could not be of great importance, inasmuch as the EPR spectrum showed the existence of a very high degree of molecular orientation during the reaction, and the crystals must have been highly perfect (except for the translationally coherent disordering of the structure mentioned previously). The values of  $B$  were equivalent to a few quanta of molecular vibration or to a few tens of quanta of molecule libration modes or of phonon modes.

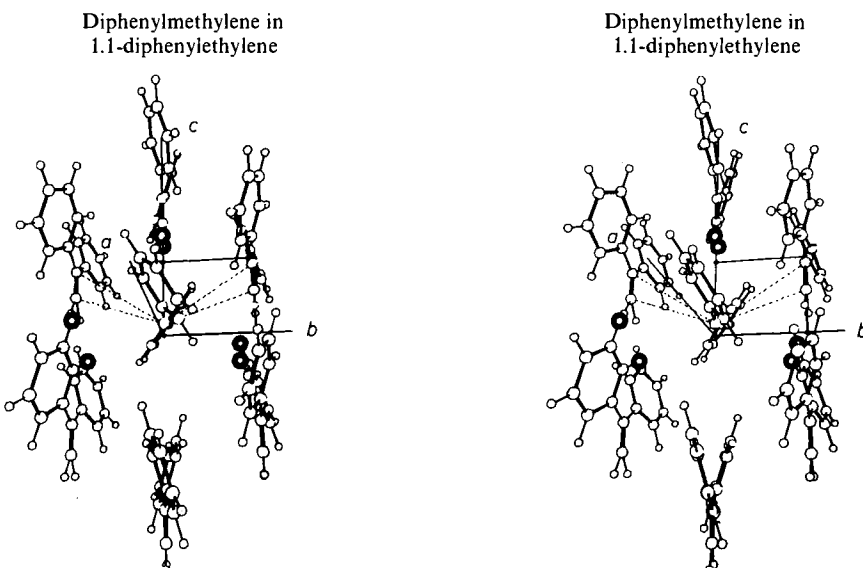


*Figure 16.* View of diphenylmethylene (DPM) molecule in 1,1-diphenylethylene (DPE) crystal.

We now again examine the local structure about a DPM molecules as determined from ENDOR measurements combined with the x-ray diffraction results. In *Figure 16* we see a DPM molecule situated in the DPE crystal in the manner given by the ENDOR results. The three distinguishable protons whose coordinates were determined by ENDOR are represented by heavy circles. The remarkable resemblance in shapes of the DPM molecule as determined by ENDOR and of the DPE molecule as determined by x-ray diffraction is to be noted. We see, by examining this structure, that the DPE molecule which was located at the site  $(0, -\frac{1}{2}, +\frac{1}{2})$ , was ideally situated for reaction with the DPM molecule situated at the site,  $(0, 0, 0)$ . The cyclopropane ring bands that were formed are represented as broken lines in *Figure 16*. The plane of the cyclopropane rings that would be created, would lie nearly parallel to the  $bc$  plane. The three C atoms which would form this ring lay very close to the  $bc$  plane before reaction. The ring closure could be accomplished with only a slight movement of the pair of very bulky molecules which are involved in the chemical reaction. The distance from

the centre of the ethylene bond of the DPE molecule, at site,  $(0, -\frac{1}{2}, +\frac{1}{2})$ , to the central C atom of the DPM molecule, at site,  $(0, 0, 0)$ , was  $\sim 4.5 \text{ \AA}$ . Schmidt<sup>10</sup> has shown that two molecules, each containing ethylene bonds, will commonly react in crystals to form cyclobutane rings when the perpendicular distance between nearly parallel ethylene bonds is  $< 4.2 \text{ \AA}$ .

We proposed<sup>6</sup> that reaction 2a of *Table 14* was accomplished by a relatively very small change in the geometry and orientation of the two molecules which were involved. From data on cyclopropane bond lengths, we estimated that if the central C of the DPM moved and the two DPE C's stayed put, this central C would be required to move  $\sim 3.4 \text{ \AA}$  in order to form the CP. Of course, the actual motion distance would be expected to be less than this. It is clear that relatively low frequency vibrational modes, librational modes, and phonon modes would be involved in such a movement.

For a discussion of details of the mechanism which we have just been discussing, we chose<sup>6</sup> to consider the reaction, 2a of *Table 14*, to be a unimolecular reaction in which the reacting species was the lowest triplet state of the pair, DPE plus DPM, i.e. of the particular singlet state DPE molecule of *Figure 16* which could react with the DPM, and a DPM in its lowest triplet state, taken as a single species, with the nuclei in the positions shown in *Table 14*. The final end product was these same nuclei in their cyclopropane arrangement.

For both reactions 2a and 2b we considered two general types of mechanisms<sup>6</sup>, as follows.

(A) In one mechanism the lowest triplet state of the product lay lower in energy than populated vibrational states of the ground triplet state of the reactant.

(B) In the other mechanism, the lowest triplet state of the product lay higher in energy than any appreciably populated vibrational states of the ground triplet state of the reactant.

*Table 17. Kinetic processes.*

---

(I)	$^3R \xrightleftharpoons[k_1]{k_1} ^3R^*$
(II)	$^3R^* \xrightleftharpoons[k_{ii}]{k_{ii}} ^1P^*$
(III)	$^3R^* \xrightleftharpoons[k_{iii}]{k_{iii}} ^3P^*$
(IV)	$^1P^* \xrightarrow{k_{iv}} ^1P$
(V)	$^3P^* \xrightarrow{k_v} ^3P$
(VI)	$^3P \xrightleftharpoons[k_{vi}]{k_{vi}} ^1P$

---

For mechanism (A) we considered<sup>6</sup> the possible processes, shown in *Table 17*;

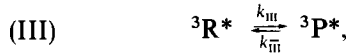


EPR AND ENDOR OF REACTING TRIPLETS IN ORGANIC CRYSTALS

vibrational excitation and deexcitation of the ground triplet state reactant;



radiationless transition from the vibrationally excited triplet state of the reactant to a vibrationally excited singlet state of the product;



radiationless transition from a vibrationally excited triplet state of the reactant to a vibrationally excited triplet state of the product;



a vibrational deexcitation of singlet product to ground state product;



a vibrational deexcitation of triplet state product;



a radiationless transition from triplet state product to singlet state product followed by vibrational relaxation to ground state product.

We were never able to detect any phosphorescence arising from triplet state species during reaction, so processes such as (VI) must have been fast relative to our measured reaction rates. Processes (IV) and (V) must have also been very fast. We considered processes, (I), (II), and (III), in detail.

For the reasons about to be given we believed that the decay of DPM by reaction 2a of *Table 14* to form CP proceeded by mechanism (A) described above. Therefore processes (I), (II), and (III), needed to be considered in the discussion of the fast decay process for DPM.

In *Figure 17* we have summarized information concerning the energies of the various states of the molecules involved in reactions 2a and 2b of *Table 14*. On the left side of *Figure 17*, under A, we have given information for the reactant, DPM plus DPE, and the product, CP. Actually the solid lines are for methylene plus ethylene, as reactants, and cyclopropane as product, because sufficient experimental information on energies was not available for the phenyl substituted compounds. The consideration of the effect of substitution will be delayed for the moment. Measurements of heats of reaction have given values of the energy of ethylene plus methylene (i.e. of the reactant, R) relative to the ground state of cyclopropane<sup>11-13</sup>. This value is approximately the  $30.1 \times 10^3 \text{ cm}^{-1} \times hc$ , given as the difference between  ${}^3R$  and  ${}^1P_G$  (*G* stands for ground state) at the left side of A. On the other hand the best information on the difference in energy between the lowest singlet state of cyclopropane and the ground state of cyclopropane was obtained from the investigation of the thermal isomerization of cyclopropane to propylene by Chambers and Kistiakowsky<sup>14</sup>. This process was found to be a thermally activated unimolecular reaction with activation energy,

$22.7 \times 10^3 \text{ cm}^{-1} \times hc$ . There has been accumulated a very substantial amount of experimental information<sup>15, 16, 18-20</sup> related to (a) the thermal isomerization of cyclopropane to propylene, (b) the thermal *cis-trans* isomerization of deuterated cyclopropanes, and (c) the reactions of methylene with ethylene, which shows that these processes proceed via a lowest excited state of cyclopropane which resembles a trimethylene molecule. It is also clear that for such a state of cyclopropane, the singlet triplet energy difference is relatively very small<sup>17</sup>. We therefore assumed that the data of Chambers

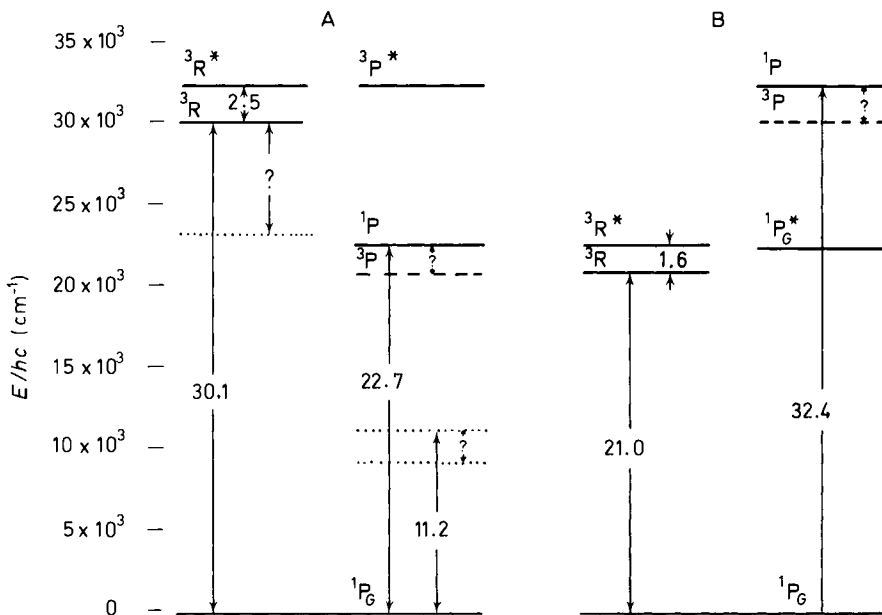


Figure 17. Energy level diagram.

and Kistiakowsky<sup>14</sup>, mentioned above, gave the difference in energy of the lowest excited and ground singlet states of the product, P, of our reaction. We arbitrarily placed the energy of the lowest triplet state of our product very close to this singlet state in energy, i.e.  $\sim 2 \times 10^3 \text{ cm}^{-1} \times hc$  lower. These levels are shown as a solid and a dashed line, respectively, on the right side of our A scheme. It is to be noted that the investigation by Schlag and Rabinovitch<sup>21</sup> of the reversible geometrical isomerization of deuterocyclopropanes showed that this reaction probably proceeded via the same excited state of cyclopropane as did the isomerization to propylene, and also had an activation energy,  $22.7 \times 10^3 \text{ cm}^{-1} \times hc$ . We thus saw that the lowest triplet state of a cyclopropane product would almost certainly be quite far in energy below the lowest triplet state of our reactant, triplet methylene plus ethylene. It was therefore clear that the reaction, 2a of *Table 14*, would be expected to proceed by general mechanism, (A). It was clear that the phenyl substitutions would have the effect of lowering the energies of the states which we have been discussing. There was no information available on phenyl substituted compounds, but Vogel and Sunderman<sup>22</sup> have

studied the thermal isomerization of *trans*-1,2-divinylcyclopropane, and they found an energy of activation,  $11.2 \times 10^3 \text{ cm}^{-1} \times hc$ . The state through which this process proceeded was undoubtedly similar to that mentioned above, and the figure just mentioned indicated that the state was lowered in energy by  $11.5 \times 10^3 \text{ cm}^{-1} \times hc$  from that of the cyclopropane, given previously. A singlet and triplet pair of levels is therefore given as a pair of dotted lines,  $11.5 \times 10^3 \text{ cm}^{-1} \times hc$  lower in energy than those of cyclopropane on the right side of the A diagram of *Figure 17*. The triplet state on the left side would certainly be lowered also, but by a somewhat smaller amount. We have guessed this lowering at  $\sim 7 \times 10^3 \text{ cm}^{-1} \times hc$ , and such a level is indicated on the left side of the A diagram. We thus saw that the effect of substitution would certainly leave intact our conclusion that the reaction 2a proceeded by mechanism (A).

Given that reaction 2a of *Table 14* proceeds by mechanism (A) we needed to consider the processes, (I), (II), and (III), of *Table 17*. In view of the fact that the low frequency vibrational modes, or librational or phonon modes, were probably the active modes for the reaction, the measured values of *B* in (6) which were given in *Table 16* corresponded to excitation of quite a number of such quanta, as previously mentioned. Thus the usual approximation, for unimolecular processes, of the concentration of reacting molecules as a Boltzmann factor times the concentration of ground state reactant species, with a  $\Delta E$  approximately equal to the difference in vibrational energies of the ground and reacting states of the reactant, was appropriate here. The rate of reaction was thus given by the product of this Boltzmann factor and either (a) the rate of the radiationless transition from,  ${}^3R^*$ , the excited triplet state of DPM + DPE, to  ${}^3P^*$ , a vibrationally excited triplet state of CP of the same energy, or (b) the rate of transition of  ${}^3R^*$  to  ${}^1P^*$ , an excited singlet state of CP. The observed preexponential factor, *A*, was shown in *Table 16* to have a value  $\sim 10^{15} \text{ sec}^{-1}$ , for the HH system. This is just the value observed in numerous<sup>14, 21, 23, 24, 25</sup> examples of related processes, e.g. the *cis-trans* isomerizations mentioned above, in which the transition occurs between states of the same multiplicity. The radiationless transition rate, between states of different multiplicity, would be expected to be much smaller<sup>26</sup>, i.e.  $\sim 10^5 \text{ sec}^{-1}$ . Thus process (II) of *Table 17* was neglected in the consideration of reaction 2a.

The foregoing reasons led us to consider that our experiments showed that reaction 2a occurred by general mechanism, (A), with vibrational excitation (process (I) in *Table 17*) of the ground triplet state reactant, DPM + DPE, at a particular crystal site, to a state with  $\sim 2.5 \times 10^3 \text{ cm}^{-1} \times hc$  higher energy (see *B* values in *Table 16*); followed by a radiationless transition (process (III) in *Table 17*) with frequency,  $\sim 10^{15} \text{ sec}^{-1}$  (see *A* value for HH system in *Table 16*), to a vibrationally excited triplet state of the product, CP, followed by rapid deexcitation of the triplet state product. The measured excitation energy,  $\sim 2.5 \times 10^3 \text{ cm}^{-1} \times hc$ , represented the vibrational excitation required in order that the Franck Condon overlap between the vibrational states of the reactant, DPM + DPE, and those of the product, CP, with appreciably different equilibrium nuclear coordinates, be sufficient to permit the radiationless transition at an appreciable rate. The product of the Boltzmann factor,  $\exp(-2.5 \times 10^3(hc/kT))$ , and the *A* value ( $\sim 10^{15}$

$\text{sec}^{-1}$ ) gave  $k$  values such as those found experimentally and plotted in *Figure 14*. The number of DPM + DPE reactant species in the crystal was typically  $\sim 1 \times 10^{15}$ . Thus at  $\sim 97^\circ\text{K}$ , process (III) was taking place at a rate of approximately  $10^{12}$  molecules  $\text{sec}^{-1}$ . A vibrational or librational state lifetime of  $\sim 10^{-11}$  sec would then give vibrational activation and deactivation rates, between the closely spaced adjacent levels of the low frequency vibrational or librational spectrum associated with the thermal activation process, which far exceed the triplet transition rate just mentioned. Thus process (III) was the rate determining process for this mode of decay of the EPR signals.

Inspection of the information contained in *Table 16* revealed that both the  $A$  value and the  $B$  value were measurably smaller for the HD system than for the HH system. If excitation of a given number of vibrational quanta of given type were required in both systems, then the deuterated system would require less energy of excitation to the extent to which the ethylenic protons play a role in the determination of the vibrational frequencies which are important in the thermal excitation. The effect of deuteration on the density of states in the R and P nuclear configurations may be such as to make this approximately the case. The reduction of the frequency of the triplet triplet transition from  $10^{14.8}$  to  $10^{11.7}$  is not surprising in view of the expected effects of deuteration on Franck Condon factors in the vibronic interaction matrix elements and on barrier transmission coefficients, both of which have a negative exponential dependence on the square roots of the nuclear masses.

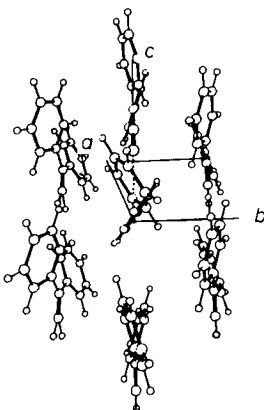
Turning to a consideration of reaction 2b in *Table 14* we look at the  $B$  side of the energy level diagram in *Figure 17*. Consideration of heats of reaction similar to those which led to the figure,  $30.1 \times 10^3 \text{ cm}^{-1} \times hc$ , for the energy difference between  ${}^3\text{R}$  and  ${}^1\text{P}_G$  in the A case, lead here to the value  $21.0 \times 10^3 \text{ cm}^{-1} \times hc$ , where the reactant is DPM + DPDAM and the product is BA. On the other hand the lowest electronically excited singlet state of DPDAM which has been observed spectroscopically<sup>27</sup> is  $32.4 \times 10^3 \text{ cm}^{-1} \times hc$  above the singlet ground state, and we guessed that the triplet state would not be more than  $\sim 2 \times 10^3 \text{ cm}^{-1} hc$  below this for a molecule such as BA. This then made it clear that in the case of reaction 2b, a vibrationally excited state of the ground triplet state of the reactant which lay above it in energy by  $\sim 1.6 \times 10^3 \text{ cm}^{-1} \times hc$ , the measured  $B$  value of *Table 16*, would lie sufficiently far below the lowest triplet state of the product that no appreciably populated vibrational state of the reactant would be higher in energy than the lowest product triplet state. Thus reaction 2b was forced to go by a triplet singlet radiationless transition mechanism. In this case process (III) of *Table 17* could not occur, and the much slower spin forbidden, triplet singlet process (II) was the rate limiting process. Such spin forbidden processes were expected to occur at a frequency very much lower than the  $10^{15} \text{ sec}^{-1}$  which we have been considering; e.g. according to Cundall<sup>28</sup> they would be expected to have preexponential factors,  $\sim 10^5 \text{ sec}^{-1}$ . This is approximately what we found.

In *Figure 18* is shown a probable model of DPDAM substituted in the DPE structure. The molecule of DPAM located at the site  $(0, 0, +1)$ , in the DPE structure, is in a very favourable position for reaction with the DPM molecule at the site  $(0, 0, 0)$ . In *Figure 18* we have indicated, with a broken

## EPR AND ENDOR OF REACTING TRIPLETS IN ORGANIC CRYSTALS

line, the bond that was formed between the terminal N of DPDAM and the central C of DPM such that the linkage  $=\text{C}=\text{N}-\text{N}=\text{C}=$  was nearly parallel to the crystallographic *c* axis. If the DPDAM rings were assumed to be in the same position as the DPE rings in the equivalent site, the distance from the terminal N of DPDAM to the central C of DPM was 3.6 Å. So we believed that, just as in the case of reaction 2a, a vibrational excitation of a reactive species, DPM + DPDAM, would produce the apparently thermally activated first order process. The transition rate or preexponential factor was much smaller than for reaction 2a because process (III) of *Table 17* was not possible and the much slower triplet singlet process (II) was rate determining.

Diphenylmethylene and  
diphenyldiazomethane  
in 1,1-diphenylethylene



Diphenylmethylene and  
diphenyldiazomethane  
in 1,1-diphenylethylene

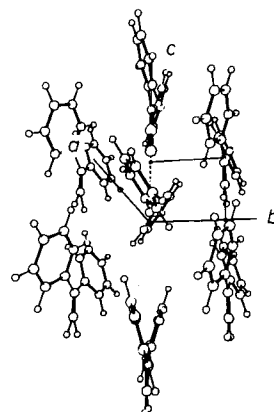


*Figure 18.* View of diphenyldiazomethane (DPDAM) molecule in 1,1-diphenylethylene (DPE) crystal.

It is also to be noted that the occurrence of a DPDAM molecule in such a site next to a DPM molecule must have effectively blocked the reaction of this DPM with DPE, in view of our previous remarks concerning the two distinguishable exponential decays corresponding to the two reactions, 2a and 2b of *Table 14*. The presence of the  $\text{C}=\text{NN}$  group apparently required prohibitively high vibrational excitation of DPM + DPE for process (III). It is, however, a matter of some surprise that such a blockage did not have an observable effect on the EPR spectrum of DPM.

### ACKNOWLEDGEMENT

The author acknowledges the support given by the United States Atomic Energy commission for this work. Acknowledgement is also made to the donors of The Petroleum Research Fund, administered by the American Chemical Society, for partial support of this research.

Electronic equipment used in the experimental work has been supplied by the Advanced Research Projects Agency.

## REFERENCES

- <sup>1</sup> R. W. Brandon, G. L. Closs, and C. A. Hutchison Jr. *J. Chem. Phys.* **37**, 1878 (1962).
- <sup>2</sup> R. W. Brandon, G. L. Closs, C. E. Davoust, C. A. Hutchison Jr., B. E. Kohler, and R. Silbey. *J. Chem. Phys.* **43**, 2006 (1965).
- <sup>3</sup> G. L. Closs, C. A. Hutchison Jr., and B. E. Kohler. *J. Chem. Phys.* **44**, 413 (1966).
- <sup>4</sup> C. A. Hutchison Jr and B. E. Kohler. *J. Chem. Phys.* **51**, 3327 (1969).
- <sup>5</sup> C. A. Hutchison Jr. *The Triplet State*, Ed. A. B. Zahlan, page 63, Cambridge University Press, Cambridge (1967).
- <sup>6</sup> D. C. Doetschman and C. A' Hutchison Jr. Personal communication.
- <sup>7</sup> C. A. Hutchison Jr. and B. E. Kohler. Personal communication.
- <sup>8</sup> D. C. Doetschman and E. Fleischer. Personal communication.
- <sup>9</sup> E. Fleischer. Personal communication.
- <sup>10</sup> G. M. J. Schmidt. "Reactivity of the Photoexcited Organic Molecule" (*Proceedings of the 13th Conference on Chemistry at the University of Brussels*, 1965) page 227, Interscience Publishers, New York (1967).
- <sup>11</sup> H. M. Frey. Chapter 11 in *Carbene Chemistry* by W. Kirmse, page 218, Academic Press, New York and London (1964).
- <sup>12</sup> G. L. Closs. *Topics in Stereochemistry* Ed. E. L. Eliel and N. L. Allinger, page 210, Interscience Publishers, New York (1968).
- <sup>13</sup> H. M. Frey. *Progress in Reaction Kinetics* Ed. G. Porter, Volume 2, page 151, Pergamon Press, New York (1964).
- <sup>14</sup> T. S. Chambers and G. B. Kistiakowsky. *J. Am. Chem. Soc.* **56**, 399 (1934).
- <sup>15</sup> R. B. Cundall. *Progress in Reaction Kinetics* Ed. G. Porter, Volume 2, page 165, Pergamon Press, New York (1964).
- <sup>16</sup> H. M. Frey. *Advances in Physical Organic Chemistry* Ed. V. Gold, Volume 4, page 147, Academic Press London and New York (1966).
- <sup>17</sup> R. Hoffman. *J. Am. Chem. Soc.* **90**, 1475 (1968).
- <sup>18</sup> H. M. Frey. Discussion in Chapter 11, Ref. 11 above.
- <sup>19</sup> G. L. Closs. Discussion in Article. Ref. 12 above.
- <sup>20</sup> H. M. Frey. Discussion in Article, Ref. 13 above.
- <sup>21</sup> E. W. Schlag and B. S. Rabinovitch. *J. Am. Chem. Soc.* **82**, 5996 (1960).
- <sup>22</sup> E. Vogel and R. Sunderman. Referred to on page 163 of article by H. M. Frey in Ref. 16 above.
- <sup>23</sup> H. M. Frey. See *Table 1, Table 2*, page 152. Ref. 16 above.
- <sup>24</sup> R. J. Crawford and A. Misra. *J. Am. Chem. Soc.* **88**, 3963 (1966).
- <sup>25</sup> J. A. Berson and J. M. Balquist. *J. Am. Chem. Soc.* **90**, 7343 (1968).
- <sup>26</sup> See for example, R. B. Cundall, page 178, Ref. 15 above.
- <sup>27</sup> E. R. Blout, V. W. Eager and R. M. Gofstein. *J. Am. Chem. Soc.* **68**, 1983 (1946).
- <sup>28</sup> R. B. Cundall. Page 178 of Ref. 15 above.
- <sup>29</sup> H. C. Longuet-Higgins and J. A. Pople. *Proc. Phys. Soc. (London)* **A68**, 591 (1955).
- <sup>30</sup> R. Pariser and R. G. Parr. *J. Chem. Phys.* **21**, 466, 767 (1953).

# RELAXATION PHENOMENA IN EXCITED MOLECULES

STUART A. RICE and WILLIAM M. GELBART

*Department of Chemistry and The James Franck Institute,  
The University of Chicago, Chicago, Illinois 60637, USA*

## ABSTRACT

This paper reviews the interpretation of radiationless transitions, thermal reactions and photochemical rearrangements and decompositions, developed in the last three years. In each of these cases, the relaxation process involved can be described within a common theoretical framework by simply observing that the system of interest is prepared in a compound (nonstationary) state. We begin (part II) by briefly discussing the role of zero-order properties (e.g. interaction energies and densities of states) in determining the time scales appropriate to the observation of irreversible decay in isolated molecules. We then (part III) identify the various ways in which the usual classification of excited molecular states breaks down. A simple, but quite general, energy level model is shown to represent the essential features of the spectrum of zero-order vibronic manifolds in polyatomic molecules: absorption line shapes, interference effects, and emission lifetimes and quantum yields, are briefly discussed. The experimentally observed dependencies of the nonradiative transition rate on electronic energy gap, molecular geometry and frequency changes, and isotope effects, are shown to follow directly from a many-phonon description of the electronic relaxation process. We discuss further the way in which this theoretical approach provides quantitative predictions of the dependence of the radiationless lifetimes (within a given electronic state) on vibrational excitation.

In part IV we elaborate upon the general theme of this paper, namely that the details of the nuclear and electronic couplings can directly determine the rates of, and products of, reactions in which molecules are prepared with highly non-uniform distributions of internal energy. The models of photo-dissociation and isomerism treated in earlier papers are cast in terms of a resonance scattering formalism in order to emphasize the chemical dynamics common to these diverse decomposition and rearrangement processes. An alternative to the conventional theory of unimolecular reactions is briefly reviewed—the roles of nonuniform internal energy distributions and intramolecular vibrational interactions are shown to be of considerable importance in providing *a priori* predictions of the dissociation kinetics in large molecules. These results are illuminated by reference to recent linear chain calculations and molecular exciton descriptions. Finally, in part V, we discuss several semi-empirical and experimental methods which we feel can complement our theoretical studies by providing unambiguous information on the actual dynamics of intramolecular energy exchange and dissociation.

## I. INTRODUCTION

That part of chemistry which deals with the reactivity of compounds and the possible changes of molecular geometry and bonding is intimately concerned with relaxation phenomena in excited molecules. This sweeping statement is obviously correct in the case when reaction is initiated by the absorption of high energy radiation. Then, as will be argued later, preparation of a molecule in a state with nonuniform distribution of energy requires that we study the various modes of internal energy redistribution before interpretation of the chemical reaction is possible. At the other extreme, namely the case of exothermic reaction without an activation energy barrier, the reaction products are usually generated with a nonequilibrium distribution of internal energy. Hence in this limit also, because the products are in excited states, it is of interest to examine the several possible pathways for molecular relaxation.

It is most common to excite a molecule under conditions such that no chemical reactions occur. For this class of excitation it is possible to observe if, and how, an initial state of the molecule evolves with time. Of the many possible molecule-preserving relaxation processes we shall be particularly interested in those classified as radiationless transitions.

Photochemical reactions, thermal reactions and radiationless transitions appear to be very different phenomena. The apparent differences are, however, more superficial than real. In every case the relaxation process involved can be interpreted within a common theoretical framework; we need only observe that the system under investigation is prepared in a compound (nonstationary) state.

This paper briefly reviews the interpretation of radiationless processes and photochemical reactions developed in the last three years. All details of the mathematical analysis are omitted so that attention can be wholly focused on the important physical ideas.

## II. KEY CONCEPTS

How does a relaxation process take place in a microscopic system? Suppose we describe a system, initially, with some convenient zero-order Hamiltonian, usually chosen to include as many of the system's interactions as possible consistent with mathematical tractability of the corresponding Schroedinger equation. Suppose the spectrum corresponding to the zero-order Hamiltonian can be partitioned into two (or more) sets of states. These states are not eigenstates of the full Hamiltonian of the system, but a true eigenstate of the system can be represented as a time independent linear superposition of the zero-order states.

The coefficients in the linear superposition depend upon the nature and magnitude of the interaction terms omitted from the zero-order Hamiltonian. It often happens that one of the sets of zero-order states (the sparse part) consists of a finite number of discrete energy levels, corresponding to a small subset of the total number of degrees of freedom of the system, while the other set of zero-order states (the dense part) has a continuous or quasi-continuous spectrum and is associated with an infinite, or effectively infinite,

## RELAXATION PHENOMENA IN EXCITED MOLECULES

number of degrees of freedom. A relaxation process takes place when a compound state of the system, consisting of some superposition of zero-order discrete and continuum states, decays into the continuum:<sup>†</sup>

The states corresponding to a specific zero-order Hamiltonian provide a convenient basis for the discussion of quantum relaxation phenomena, but these states have no real physical significance. The two subsets of zero-order levels described above are usually degenerate or quasidegenerate, and therefore extensive configuration mixing is induced by the small interaction which couples the subsets of states. Properties of the total system such as absorption coefficients, relaxation times, etc., must be described in terms of the properties of compound states.

The interpretation of relaxation phenomena requires an understanding of how an initial state of the system is prepared, and of the consequent time evolution of this state. A stationary state of the system will undergo transition to other stationary states only by coupling with the radiation field, so that all transitions between stationary states are radiative in nature. However, if a system is prepared in a nonstationary state of the total molecular Hamiltonian, 'nonradiative transitions' will occur. This follows from the observation that the initial nonstationary state can be represented as a time dependent superposition of the eigenstates of the total molecular Hamiltonian, each of which is a time independent superposition of states which correspond to the sparse and dense subsets of zero-order states. In general, if one of the subsystems of zero-order states is very dense, a compound state of the system with large amplitude of a sparse subsystem component evolves so that the continuum component grows with time. On the other hand, if the densities of states in the two subsystems of zero-order states are comparable and small, the amplitude of a component zero-order state will oscillate with time.

The preceding comment alludes to the importance of the densities of states of the several subsets of states. In a finite system the time for recurrence of an initial state is of the order of magnitude of  $\rho\hbar$ , where  $\rho$  is the density of states<sup>1</sup>. If the time scale of interest is much shorter than  $\rho\hbar$ , irreversible behaviour is observed, i.e. an initial state decays into some other set of states and does not recur. If the time scale of interest is comparable to or longer than  $\rho\hbar$ , reversible behaviour is observed, i.e. the initial states recurs.

The density of states also enters in an important way in the description of the distribution of amplitudes which describes the linear superposition of zero-order states representing an eigenstate of the total Hamiltonian. Let the matrix element coupling the subsets of zero-order states be  $v$ , and consider the case where the zero-order spectrum has one sparse subset and one dense subset of states. Suppose it is possible to create, as an initial nonstationary state, a molecule excited to one level of the sparse subset of states. When  $v\rho > 1$  many states of the dense subset contribute to the linear combination of states representing the eigenstate of the total Hamiltonian. If these states

---

<sup>†</sup> Of course, it is also possible to represent any one (or any combination) of the zero order states as a linear superposition of the exact eigenstates of the system. In this case, however, the coefficients are time dependent. The interplay between the many time rates of change of the terms in the linear superposition defines the overall time rate of change of the nonstationary zero-order state.

are indistinguishable, their phases interfere in a manner such that the probability of radiative decay of the molecule is modulated by an extra exponential decay with reciprocal lifetime  $\tau_{nr}^{-1} = 2\pi v^2 \rho/\hbar$ , and  $\tau_{nr} \ll \rho\hbar$ . In this case the quantum yield of fluorescence is less than unity. On the other hand when  $v\rho < 1$ , usually because the densities of states in the two zero order subsets are sufficiently small that the average level spacing exceeds the interaction energy, only a few zero-order states from the second subset contribute to linear superposition representing an eigenstate of the total Hamiltonian. Then  $\rho\hbar$  is shorter than the radiative lifetime, the probability of radiative decay of the molecule is altered but not exponentially modulated, and the quantum yield of fluorescence is unity.

The extension of the concepts described above to the case of photochemical reactions requires proper identification of the pertinent manifolds of states, and of the nature of their interaction. Although the details are very different, the key ideas are the same.

We now examine, in somewhat more detail, the consequences of exciting a molecule to a nonstationary state.

### III. ASPECTS OF THE THEORY OF RADIATIONLESS PROCESSES

The first successful interpretation of radiationless processes in large aromatic molecules was advanced by Robinson and Frosch<sup>2</sup>. Their analysis included several of the ideas we now recognize as very important, but did not fully exploit the quantum mechanics of compound states. Furthermore, they restricted attention to the case  $v\rho \gg 1$ . Bixon and Jortner<sup>3</sup>, and Rhodes, Henry and Kasha<sup>4</sup> developed, independently and at the same time, the compound state theory sketched in Section II. This theory, which has since been extensively expanded by Jortner, Berry, Freed, Rice and others, is described below.

Almost all quantum mechanical descriptions of molecules are based on the Born–Oppenheimer (BO) approximation. There are many different ways of describing the BO approximation. Perhaps the simplest is to say that, because the mass of the electron is so much smaller than the masses of the nuclei, the electrons may be assumed to move in a static potential field generated by the nuclei distributed over the equilibrium positions characteristic of the molecule. Then, in turn, the nuclei are assumed to oscillate about their equilibrium positions in an effective field generated by the instantaneously responsive electrons. The BO approximation is valid only if the off diagonal matrix elements of the nuclear kinetic energy operator in the basis of BO states are small compared to the separations of the BO states. For large molecules, with many vibrational degrees of freedom, the density of BO states is so large that it is often the case that the energy difference between BO states is very small relative to the off diagonal matrix elements of the nuclear kinetic energy. In these cases the eigenstates of the total Hamiltonian must be very different from BO states for an excited molecule, even when the true ground state is accurately approximated by the BO ground state. In anthracene, for example, the density,  $\rho$ , of  ${}^3B_{2u}$  vibrational levels in the energy region of the  ${}^1B_{2u}$  vibrationless state is as large as  $5 \times 10^{10} \text{ cm}^{-1}$ . The mean interaction energy,  $v$ , is estimated<sup>3</sup> to be roughly  $6 \times 10^{-7} \text{ cm}^{-1}$ , thereby implying

## RELAXATION PHENOMENA IN EXCITED MOLECULES

that  $\rho v \approx 3 \times 10^4 \gg 1$ , i.e.  $v \gg \varepsilon \equiv \rho^{-1}$ , and there is extensive mixing of the zero-order vibronic states. It is also interesting to note<sup>3</sup> that the recurrence time,  $\hbar\rho \approx 0.25$  sec, greatly exceeds the measured radiative lifetime  $\tau \approx 5 \times 10^{-9}$  sec, consistent with the fact that the radiationless transition is observed to take place as an irreversible relaxation process. Other examples of the large molecule limit are given in *Table 1*. It is clear that the study of the photochemistry of these systems, which of necessity concerns itself with the energy region of electronically excited states, depends upon an understanding of the breakdown of the Born-Oppenheimer approximation and the details of the various non-radiative relaxation phenomena.

*Table 1.* Parameters descriptive of radiationless transitions in large molecules

System	$\tau$ (sec)	$v$ ( $\text{cm}^{-1}$ )	$\rho$ (cm)	$v\rho$	$\hbar\rho$ (sec)
Anthracene ${}^1B_{2u} \rightarrow {}^3B_{2u}$ $E = 12000 \text{ cm}^{-1}$	$5 \times 10^{-9}$	$6 \times 10^{-7}$	$5 \times 10^{10}$	$3 \times 10^4$	0.25
Naphthalene ${}^1B_{2u} \rightarrow {}^1B_{3u}$ $E = 3400 \text{ cm}^{-1}$	$10^{-12}$	$6 \times 10^{-2}$	$2 \times 10^3$	$10^2$	$10^{-8}$
Naphthalene ${}^3B_{2u} \rightarrow {}^1A_{1g}$ $E = 20000 \text{ cm}^{-1}$	2	$10^{-14}$	$8 \times 10^{15}$	80	$4 \times 10^4$
Azulene ${}^1B_1 \rightarrow {}^1A_1$ $E = 14000 \text{ cm}^{-1}$	$10^{-11}$	$7 \times 10^{-5}$	$10^{11}$	$7 \times 10^6$	0.5
Benzene ${}^1B_{2u} \rightarrow {}^3B_{1u}$	$10^{-6}$	$1.5 \times 10^{-5}$	$8 \times 10^4$	1.5	$4 \times 10^{-7}$

Experimentally, these large-molecule ( $\rho v \gg 1$ ) processes are manifest in several ways, e.g.

(i) Resonance fluorescence is not observed when, for example, anthracene<sup>5</sup>, naphthalene<sup>6</sup>, and tetracene<sup>7</sup> are optically excited to their second and higher singlet states at low gas pressures (such that the mean time between collisions greatly exceeds the pure radiative lifetime,  $\tau_r$ ). The observed fluorescence resembles the emission which follows direct excitation to the first singlet, but is slightly red-shifted and diffuse.

(ii) The overall lifetime of the first excited singlets, when extrapolated to low gas pressures, are shorter than  $\tau_r$  (calculated from the integrated absorption coefficient) by factors of two<sup>8</sup> to four<sup>9</sup>.

(iii) The fluorescence quantum yield of benzene ( $\phi_f \approx 0.34$ ) is independent of vapour density at sufficiently low pressures, and part of the sample of excited molecules behaves chemically as if it were the lower triplet state<sup>10</sup> (e.g. it isomerizes *cis*-butene).

(iv) In cases where an environment change is not expected to introduce (e.g. through external spin-orbit coupling, or crystal field effects, etc.) any

basic changes in the character of the electronic states, there is no conclusive evidence for believing that the radiationless transitions are sensibly influenced by coupling of the molecule to a dense medium.

Exceptions to the above generalizations, as well as a comprehensive discussion of the experimental background, have been considered by Jortner, Rice and Hochstrasser<sup>1</sup>.

Aside from neglecting the nuclear kinetic energy, the conventional theory of molecular electronic structure also uses, as an additional approximation, a spin independent Hamiltonian. The natural consequence of this approximation is the classification of all the electronic states of the molecule into pure spin manifolds, e.g. singlet, triplet, quintet, etc. Of course, the existence of spin-orbit coupling implies that pure spin states cannot be stationary states of the total Hamiltonian. However, the lifetime of a nonstationary pure spin state can be very long if the spin-orbit coupling matrix element is small and the states to which the initial state is coupled are sparsely distributed; the reverse is true if the density of states is large, or the spin-orbit coupling large. In the case of large molecules, for which the density of zero-order pure spin BO states is very large, the conventional classification of excited states according to spin multiplicity is no longer valid.

More explicitly, we write  $v = v_{mr, ns}$  where  $v_{mr, ns} \equiv \langle \Psi_{mr} | T(Q) | \Psi_{ns} \rangle$ :  $T(Q) = -\sum_k (\hbar^2/2M_k) \partial^2/\partial Q_k^2$  is the nuclear kinetic energy operator and

$\Psi_{mr} = \psi_m(q, Q) \chi_{mr}(Q)$  and  $\Psi_{ns} \equiv \psi_n(q, Q) \chi_{ns}(Q)$  are the wavefunctions corresponding to the  $mr^{\text{th}}$  and  $ns^{\text{th}}$  vibronic states. That is,  $\psi_m(q, Q)$  is the  $m^{\text{th}}$  solution to the electronic Schrodinger equation

$$H_{el}\psi_m(q, Q) \equiv [T(q) + U(q, Q) + H_s] \psi_m(q, Q) \equiv E_m(Q) \psi_m(q, Q) \quad (1)$$

for fixed nuclear configuration  $Q$ : here  $T(q)$  is the kinetic energy of the electrons,  $U(q, Q)$  is the Coulomb potential energy of the nuclei and electrons, and  $H_s$  denotes the electron spin terms including the spin-orbit coupling  $H_{so}$ . The vibrational wavefunction  $\chi_{mr}(Q)$  is the  $r^{\text{th}}$  solution to the equation

$$[E_m(Q) + T(Q)] \chi_{mr}(Q) \equiv W_{mr} \chi_{mr}(Q). \quad (2)$$

Noting that the electronic wavefunctions are orthogonal in  $q$ -space one has that

$$v_{mr, ns} \approx -\sum_k \frac{\hbar^2}{M_k} \int_Q \chi_{mr}^*(Q) \langle \psi_m(q, Q) \left| \frac{\partial}{\partial Q_k} \right| \psi_n(q, Q) \rangle \frac{\partial}{\partial Q_k} \chi_{ns}(Q) dQ \quad (3)$$

where we have simply neglected the second derivatives of the electronic wavefunctions with respect to the nuclear displacements. Differentiating (1) with respect to  $Q_k$ , multiplying by  $\psi_n(q, Q)$  and integrating over all  $q$ , one finds that

$$\begin{aligned} \langle \psi_m(q, Q) \left| \frac{\partial}{\partial Q_k} \right| \psi_n(q, Q) \rangle &= \frac{\langle \psi_m(q, Q) | (\partial U / \partial Q_k) | \psi_n(q, Q) \rangle}{E_m(Q) - E_n(Q)} \\ &\approx \frac{\langle \psi_m(q, 0) | (\partial U / \partial Q_k)_0 | \psi_n(q, 0) \rangle}{E_m(0) - E_n(0)} \end{aligned} \quad (4)$$

## RELAXATION PHENOMENA IN EXCITED MOLECULES

In order to evaluate  $v_{mr,ns}$  we treat the spin-orbit coupling,  $H_{so}$ , as a perturbation to the zero-order electronic Hamiltonian  $H_{el}^0(0)$ , where  $H_{el}^0(0) = T(q) + U(q, Q = 0) + (H_s - H_{so})$  with eigensolutions  $\{\psi_m^0(q, 0)\}$  (the zero superscript denotes pure spin states). Thus we write, to first order,

$$\psi_m(q, 0) \approx \psi_m^0(q, 0) + \sum_{\gamma \neq m} \frac{\langle \psi_m^0(q, 0) | H_{so} | \psi_\gamma^0(q, 0) \rangle}{E_m^0(0) - E_\gamma^0(0)}. \quad (5)$$

Then  $v_{mr,ns}$  becomes

$$v_{mr,ns} \approx \sum_k F_{mr,ns}^k \\ \times \frac{J_{mn}^{k(0)} + \sum_{\gamma \neq m, n} [k_{m\gamma}^{(0)} J_{\gamma n}^{k(0)} / E_m^0(0) - E_\gamma^0(0) + J_{m\gamma}^{k(0)} k_{\gamma n}^{(0)} / E_n^0(0) - E_\gamma^0(0)]}{E_n^0(0) - E_m^0(0)} \quad (6)$$

where

$$J_{mn}^{k(0)} \equiv \langle \psi_m^0(q, 0) | \left( \frac{\partial U}{\partial Q_k} \right) | \psi_n^0(q, 0) \rangle, \quad (6a)$$

$$k_{m\gamma}^{(0)} \equiv \langle \psi_m^0(q, 0) | H_{so} | \psi_\gamma^0(q, 0) \rangle \quad (6b)$$

and

$$F_{mr,ns}^k \equiv \int_Q \chi_{mr}(Q) \frac{\partial}{\partial Q_k} \chi_{ns}(Q) dQ \quad (6c)$$

is the Franck Condon vibrational overlap integral. If  $m$  and  $n$  refer to states with the same spin multiplicity ('internal conversion') then only the leading term  $J_{mn}^{k(0)} / (E_n^0(0) - E_m^0(0))$  need be retained in the electronic factor. When  $J_{mn}^{k(0)}$  vanishes identically ('intersystem crossing') one must determine the terms in the sum over  $\gamma$ , according to appropriate spin orbit-vibronic coupling selection rules.

Having identified two of the possible forms of interaction between the zero-order BO states of a molecule, we turn to an examination of the time evolution of a compound state initially prepared as a pure BO state.

Bixon and Jortner<sup>3</sup> analyzed the simple model energy level spectrum shown in *Figure 1*. This model is intended to represent the essential features of the spectrum of zero-order BO vibronic levels of a large molecule. The BO state  $\phi_s$  will at first be treated as the vibrationless level of a singlet manifold, but this is not a necessary restriction. A transition from the BO ground state  $\phi_o$  to  $\phi_s$  is allowed, with transition dipole moment  $\mu_{os}$ . The manifold  $\{\phi_i\}$  is taken to be the set of vibrational levels belonging to a BO singlet or triplet electronic state just below  $\phi_s$ . In this model transitions between  $\phi_o$  and the  $\{\phi_i\}$  are forbidden. When the  $\{\phi_i\}$  belong to a triplet, spin orthogonality leads to  $\mu_{oi} = 0$ , and this is not much changed by the small spin-orbit coupling typical of aromatic hydrocarbons. When the  $\{\phi_i\}$  belong to a singlet, the Franck-Condon factors for excitation to a level near  $\phi_s$  are so small that again  $\mu_{oi} = 0$ . In general, the density of the levels  $\{\phi_{ij}\}$  degenerate with  $\phi_s$  increases with the energy gap between the vibrationless levels of the two excited states, and with increasing number of vibrational degrees of freedom.

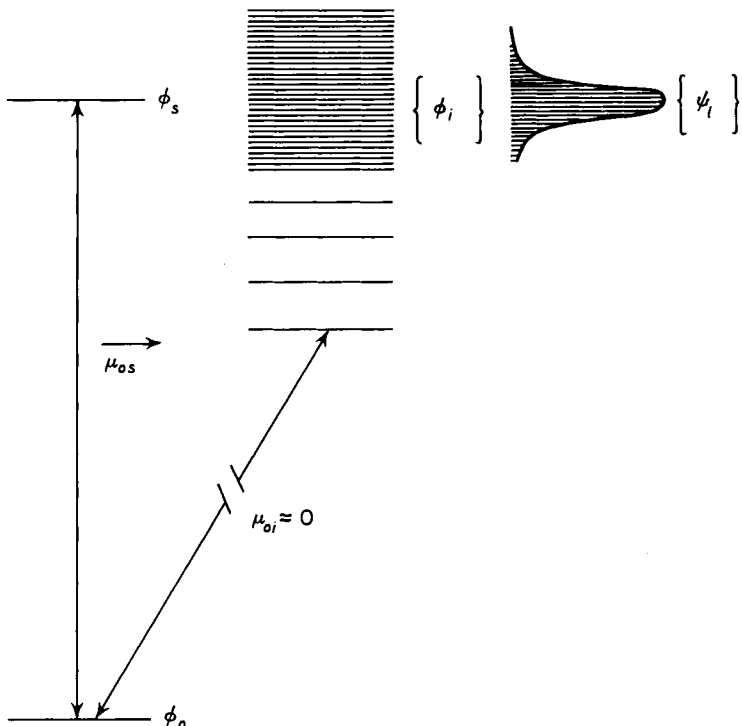


Figure 1. Energy-level scheme for a large molecule.

Because of the degeneracy, or quasi-degeneracy, of  $\phi_s$  with a group of levels from the  $\{\phi_i\}$ , the BO representation of the excited electronic states in the model spectrum shown cannot be valid. Instead, an eigenstate of the total Hamiltonian is of the form

$$\psi_n = a_s^n \phi_s + \sum_i b_i^n \phi_i \quad (7)$$

Bixon and Jortner<sup>3</sup> assumed that the manifold  $\{\phi_i\}$  have uniformly spaced levels with separation  $\varepsilon = \rho^{-1}$ , and that the matrix element which couples  $\phi_s$  to the  $\{\phi_i\}$ ,  $v = \langle \phi_s | H | \phi_i \rangle$ , is the same for all levels (hence independent of energy). It is then found that the expansion coefficients describing the weights of the zero-order state  $\phi_s$  in the eigenstate  $\psi_n$  is of the form

$$|a_s^n|^2 = \frac{v^2}{(E_n - E_s)^2 + (\pi v^2 \rho) + v^2} \quad (8)$$

where  $E_s$  represents the zero-order energy corresponding to  $\phi_s$ , and  $E_n$  the eigenenergy corresponding to  $\psi_n$ . One may immediately draw four conclusions:

(i) Because of the breakdown of the BO approximation in the case of degenerate zero-order levels, the molecular eigenstates contain appreciable contributions from the many degenerate and quasi-degenerate zero-order

## RELAXATION PHENOMENA IN EXCITED MOLECULES

BO states with energy close to the energy of the eigenstate. Thus, if the transition moments are such that the initial nonstationary state prepared by absorption of a photon is a pure BO state, e.g.  $\phi_s$  of *Figure 1*, the absorption profile is inhomogeneously broadened. The inhomogeneous broadening results from a differential distribution of the zero-order BO component among the eigenstates of the total Hamiltonian.

(ii) The absorption line shape is Lorentzian, when  $\rho v \gg 1$ :

$$A(E) \propto \rho |a_s^n|^2 = \frac{v^2 \rho}{(E_s - E_n)^2 + (\pi v^2 \rho)^2} \quad (9)$$

(iii) The line width is given by

$$\Delta = \pi v^2 \rho. \quad (10)$$

(iv) Interference effects between the discrete state and the background states occur only when the transitions to the zero-order background states carry oscillator strength. Hence, for the model spectrum of *Figure 1* no Fano antiresonances<sup>11</sup> are expected to occur.

The state mixing described above is entirely an intramolecular phenomenon; as shown it leads to the distribution of absorption intensity over a moderately large energy region. There is, however, much more that can be learned about the system by considering the mode of preparation and the time evolution of the initial compound state. Let a molecule with model spectrum as in *Figure 1* be coupled to the radiation field. When the band pass of radiation incident on the molecule is such as to coherently excite the molecule (i.e. when the band pass exceeds the inhomogeneously broadened line width), there is interference among the amplitudes of the coherently excited states. Consequently, it is found that the radiationless decay of the probability amplitude of the zero-order state  $\phi_s$  is exponential and characterized by

$$\tau_{nr} = \hbar / 2\pi v^2 \rho. \quad (11)$$

Thus a lifetime appears naturally (as a consequence of interference) in the description of the time evolution of the compound state and need not be introduced by *ad hoc* considerations, or by kinetic arguments. The transition rate is of the form of the Golden Rule of first order time dependent perturbation theory, although it does not arise from a perturbation theory analysis.

Chock, Jortner and Rice<sup>12</sup>, Berry and Jortner<sup>13</sup>, Freed and Jortner<sup>14</sup>, Bixon, Jortner and Dothan<sup>15</sup>, and Freed<sup>16</sup> have significantly generalized the original theory of Bixon and Jortner. It is shown in these papers that a formal theory of radiationless processes, using advanced many-body techniques to describe the time evolution of the compound state and its coupling to the radiation field, leads to the same general conclusions as does the more straightforward analysis of a model spectrum of zero-order levels. These cited studies can be summarized as follows<sup>1</sup>:

(i) A necessary condition for the occurrence of nonradiative decay of a compound state, and concomitantly of inhomogeneous line broadening, is  $v\rho \gg 1$ . The nonradiative decay then occurs on a time scale short compared to  $\hbar\rho$ . For times longer than  $\hbar\rho$ , the amplitude of  $\phi_s$  in the compound state increases towards its initial value. However, for large molecules  $\hbar\rho$  con-

siderably exceeds the time scale on which other interfering processes occur, e.g. collision with the walls or other molecules. The density of states need not be uniform for these conclusions to be valid.

(ii) For  $v\rho \gg 1$ , the observed radiative lifetime, determined on a time scale short relative to  $\hbar\rho$ , consists of independent contributions from the non-radiative and pure radiative components. In large molecules, for which  $\hbar\rho$  is much longer than any other molecular period, this result implies an exponential decay law as already noted. Exponential decay of this particular form (shortened radiative lifetime) does not occur on a time scale longer than  $\hbar\rho$  (see comment (vi) below).

(iii) Let  $n = \rho\Delta$  be the average number of levels within the halfwidth of the inhomogeneously broadened line. Then from  $\tau_{nr} = \hbar/2\Delta$ , we find that  $\tau_{nr} = \hbar\rho/2n$ , and the lifetime against nonradiative decay can be thought of as the recurrence time reduced by the factor  $2n$ .

(iv) The simple additive nonradiative decay rate  $(\hbar/2\Delta)^{-1}$ , in the overall rate of decay of a compound state coupled to the radiation field, is a valid description only if all the molecular eigenstates in an inhomogeneously broadened line correspond to a set of indistinguishable levels<sup>15</sup>. If the levels are distinguishable (e.g. Zeeman levels which emit photons of different polarization) the rate of decay of the compound state can be nonexponential under certain conditions of preparation and observation<sup>14, 15</sup>.

(v) An excited state resulting from intramolecular radiationless transitions in a large molecule decays as follows ( $t \ll \hbar\rho$ ): In the case of internal conversion from the second to the first singlet, the excited state is connected by nonvanishing radiative coupling to high vibronic levels of the ground state. In an isolated molecule, fluorescence radiation will be emitted corresponding to transitions between vibrationally excited levels of the excited and ground electronic states. As a result of this fluorescence, if the molecule stays free, it will eventually emit its excess energy as infra red radiation. However, because of the very long radiative lifetimes for vibrational transitions, relaxation by collision is also likely to take place.

Of course, corresponding to the above described decay mechanism, the quantum yield of fluorescence is less than unity; only a fraction  $Y < 1$  of the absorbed photons can be emitted on the time scale  $t \ll \hbar\rho$ . The fraction  $1 - Y$  will be emitted, as described above, on a time scale long compared to the fluorescence decay time.

(vi) Singlet excited states of small molecules, e.g. triatomics, are quasi-degenerate with only a few vibronic states belonging to the lower triplet state and the ground state. However the coupling matrix element is, in certain cases, sufficiently large that  $v\rho \geq 1$ , so that inhomogeneous broadening of the absorption line can occur. Because the density of levels is small the recurrence time for the compound state is very short, indeed much shorter than the lifetime against fluorescence decay or the time between collisions. Although for a time  $t \ll \hbar\rho$  the overall decay rate has a radiative and non-radiative component, just as for a large molecule, this is unobservable because of the short recurrence time. When  $t \gg \hbar\rho$ , which is a time scale on which experiments can be conducted, the radiative decay consists of a sum of exponential decays, one for each of the separate molecular eigenstates<sup>17</sup>. In this case, when the level spacing exceeds the radiative width  $\Gamma$ , i.e.  $\rho^{-1} > \Gamma$ ,

## RELAXATION PHENOMENA IN EXCITED MOLECULES

the apparent excited state lifetime becomes  $n\hbar/\Gamma$ , and hence is lengthened relative to the radiative lifetime expected on the basis of the integrated oscillator strength<sup>17</sup>. The conditions cited are encountered in the cases of NO<sub>2</sub> and SO<sub>2</sub>, both of which are known to have 'anomalously long' radiative lifetimes<sup>19</sup>.

(vii) The occurrence of inhomogeneous broadening in small molecules implies the spreading out of the  $\phi_s$  oscillator strength, and this redistribution leads to the occurrence of many new lines in the spectrum (corresponding to transitions to all the molecular eigenstates  $\psi_n$ ). This is probably the source of the 'extra' regularly spaced lines in the spectrum of NO<sub>2</sub><sup>18</sup>.

(viii) The Lorentzian absorption line shape, and all the other particulars cited above, represent the description of an isolated resonance degenerate with a single quasi-continuum. When two or more zero-order levels interact with a quasicontinuum, and the widths of the two states exceed their separation, the absorption line shape is not Lorentzian and the nonradiative decay rate is not exponential in form. When one zero-order level interacts with two or more quasicontinua, and both of the continua are sufficiently dense, the absorption line shape is still Lorentzian, but with width determined by the sum  $\sum_i v_i^2 \rho_i$ .

Much of the above information is displayed for convenient comparison in *Table 2*.

*Table 2.* The radiative decay of a manifold of indistinguishable levels

Physical property	Resonance limit	Intermediate case	Statistical limit
$n = \pi v^2 \rho^2$	—	$n \sim 10-100$	$n \gg 1$
Line shape	natural radiative + conventional broadening	inhomogenous broadening, separable lines	$\Delta = \pi v^2 \rho$
Time scale relative to recurrence time ( $\hbar\rho$ )	—	$t \gg \hbar\rho$	$t \ll \hbar\rho$
Form of decay	beat spectrum	non exponential	exponential
Radiative decay time	$\tau_{\text{exp}} = 1/\Gamma$	$\tau_{\text{exp}} \propto n/\Gamma$	$\tau_{\text{exp}} = \Gamma \Delta / \Gamma + \Delta$
Fluorescence quantum yield on time scale $t$	$Y = 1$	$Y = 1$	$Y < 1$
Features of relaxation	external	external	intramolecular
Examples	CN	SO <sub>2</sub> , NO <sub>2</sub> , CS <sub>2</sub>	Benzene Naphthalene Anthracene

Several years ago it was observed, semi-empirically, by Robinson and Frosch<sup>2</sup>, Siebrand<sup>19</sup>, and Ross<sup>20</sup>, and their coworkers, that the efficiencies of nonradiative processes depend directly on the energy gap (0-0 transition energy),  $\Delta E$ , the changes in equilibrium configurations and frequencies of the vibrations, and isotope substitution. It is interesting to note that this situation

is largely analogous to that encountered in cases of localized electronic transitions in solids, e.g. absorption by F-centres (trapped electrons) or isolated impurities in crystals<sup>2</sup>. Using the general line shape formalism developed by Kubo<sup>22</sup> to describe these latter multiphonon processes, Lin and Bersohn<sup>23</sup> and Englman and Jortner<sup>24</sup> have derived all of the experimentally observed dependences of the nonradiative transition probabilities on the electronic energy difference, molecular geometry and frequency changes, and deuterium effects. Gelbart, Freed and Rice<sup>25</sup> have extended these approaches to take into account the necessarily large change in equilibrium configurations accompanying intramolecular rearrangements of the *cis-trans* type. Also, Freed and Jortner<sup>26</sup> have explicitly treated the role of the promoting mode and have shown that, in the case of the aromatic hydrocarbons, it is possible to derive an energy gap law which correlates all the important features of the semi-empirical analyses.

At the same time these extensions of the multiphonon formulation point up the usefulness of keeping the nonradiative rate expression in the form of a constant times a sum over squares of the vibrational overlap integrals between the initial vibrationless state and the nearly degenerate vibronic levels of the lower electronic state. (Contact with the earlier treatments can be made by approximating this sum by the product of a mean Franck-Condon factor ( $v^2$ ) times the number of terms in the sum ( $\rho$ ): in this way one recovers the familiar result that the rate is proportional, through the 'electronic factor' to the product  $v^2 \rho$ ). More explicitly, Freed and Jortner<sup>26</sup> and Gelbart *et al.*<sup>27</sup> show that this sum assumes the form of a microcanonical partition function for 'phonons' which obey Boltzmann statistics and which are distributed amongst states that have 'degeneracies'  $\{x_j \equiv \Delta_j^2/2\}$ , where  $\Delta_j \equiv (M_j \omega_j / \hbar)^{1/2}$ .  $\Delta Q_j^0$  is the reduced displacement between the two electronic states in the equilibrium position of the  $j^{\text{th}}$  normal coordinate (with effective mass  $M_j$  and frequency  $\omega_j$ ). In other words we have that

$$k_{nr} \propto \sum_{\{n_j\}} \prod_j \frac{x_j^{n_j}}{n_j!} \delta[\Delta E - \sum_j n_j \hbar \omega_j], \quad (12)$$

where  $\Delta E_k = \Delta E - \hbar \omega_k$ ,  $k$  denoting the promoting mode. For large enough  $\Gamma E_k$  this sum can be approximated by the corresponding canonical ensemble partition function; viz.  $\sum_{\{n_j\}} (\prod_j x_j^{n_j} / n_j!)$  is evaluated subject to that constraint of conservation of the mean energy. That is, neglecting fluctuations, we have that

$$\Delta E_k = \sum_j n_j \hbar \omega_j \quad (13)$$

is the electronic energy available for distribution over the internal degrees of freedom. As is customary in the statistical mechanical analogue, the canonical ensemble sum, subject to (13), is approximated by its maximum term, using the method of Lagrange multipliers. It is found that  $n_j^0$ , the most probable number of quanta accepted by the  $j^{\text{th}}$  vibration in the non-radiative transition, increases exponentially with the frequency  $\omega_j$  and linearly with the displacement  $x_j$ : this result is consistent with the semi-empirical finding that the best accepting modes are those of maximum frequency, and that among this class the most efficient are those which undergo the largest geometry change between initial and final electronic states. Substituting for  $n_j^0$  in the maximum term,

## RELAXATION PHENOMENA IN EXCITED MOLECULES

$\prod_j (x_j^{n_j} / n_j^0 !)$  and, noting that the  $x_j$ 's are less than unity for the aromatic hydrocarbons, it is found that the most likely distribution of energy  $\Delta E_k$  amongst the internal degrees of freedom is that which allows for the smallest values of  $n_j^0$  and hence  $\sum_j n_j^0$ . This result is simply that which would be expected in an electronic transition (from the vibrationless level of the initial state) for which the Franck-Condon principle was operative. It is also shown<sup>27</sup> that the maximum term can be written in the 'energy gap' form derived by more exact methods by Englman and Jortner.

Most importantly, Gelbart *et al.*<sup>27</sup> use the maximum term method to calculate the energy dependence of the nonradiative rate constant in a molecule under 'collision-free' conditions: they determine the variation of the radiationless lifetimes of resolved vibrational levels in an excited electronic state. Earlier theoretical work had implicitly assumed that the initial state of the optically excited molecule was the vibrationless level resulting from rapid collisional deactivation. Descriptions of this kind had been sufficient to explain the variety of data obtained for molecules in solution, dense gases, and solid hosts. Recently, however, experiments have been carried out at low enough pressures that the optically excited gas molecules decay nonradiatively on a time scale much shorter than the mean time between deactivating collisions. Furthermore, with a bandwidth of, say, an Ångstrom, the initial states of the excited molecule can be meaningfully described in terms of the individual normal modes.

Gelbart *et al.*<sup>27</sup> have calculated the variation in nonradiative lifetime  $\tau_{nr}$  of the benzene  ${}^1B_{2u}$  electronic state, excited with 0, 1, and 2 quanta in the totally symmetric skeletal (breathing) vibration: they find that  $\tau_{nr}$  decreases by factors of 0.83 and 0.70 as one populates the  $v_1$  mode with 1 and 2 quanta. These numerical estimates are shown to be consistent with the corresponding fluorescence lifetimes  $\tau$  measured at  $\approx 0.1$  Torr using nanosecond flash excitation and time correlated photon counting (see Table 3). Agreement between theory and experiment can be sharpened as soon as more accurate quantum yield ( $\phi_f$ ) data become available<sup>28</sup>, thereby allowing us to separate out more cleanly the pure radiative contribution  $\tau_r$  to the observed lifetime [ $\tau \equiv \{\tau_r \tau_{nr} / (\tau_r + \tau_{nr})\} = \tau_{nr}(1 - \phi_f)$ ].

*Table 3.*

Vibrational excitation in ${}^1B_{2u}$	Observed lifetime $\tau$ (nsec)	Standard deviation (nsec)
$1^0$	102.9	2.7
$1^1$	80.5	1.4
$1^2$	61.7	0.9
$6^1 1^0$	81.5	0.4
$6^1 1^1$	73.7	0.4
$6^1 1^2$	57.0	0.4

The states  $1^m$ ,  $m_s = 0, 1, 2$ , correspond to the totally symmetric skeletal vibration excited with 0, 1, and 2 quanta, respectively:  $6^1$  denotes the quantum of  $e_{g}$  C-bending motion on which the CC ( $Q_{1g}$ ) progression is built.  $(1/\tau) = (1/\tau_{nr} + 1/\tau_r)$ , where  $\tau_r$  is the pure radiative lifetime and  $\tau_{nr}$  is the radiationless lifetime discussed in the text.

Further experimental work on benzene is presently in progress and is expected to provide more information on the effect of vibrational excitation

on electronic relaxation processes. The Boltzmann counting method described above can be improved<sup>29</sup> by taking into account the contribution of the vibrational overlaps in the neighbourhood of the maximum term. These corrections give rise to the proper pre-exponential factors in the energy gap form of the rate constant. The theory is also extended<sup>29</sup> to allow for frequency changes, and to include the role of other stretching motions, and out-of-plane bends, as accepting modes. These considerations, in conjunction with the more extensive experimental data, allow for a revealing test of our understanding of the energy dependence of the non-radiative relaxation processes.

#### IV. ASPECTS OF THE THEORY OF PHOTOCHEMICAL REACTIONS

A photochemical reaction differs from a thermal reaction in at least one fundamental way: the absorption of a photon by a molecule 'prepares' the molecule in a well defined nonstationary state with a nonuniform distribution of energy, whereas a thermally excited molecule is almost always in a state in which the distribution of energy over possible modes of motion is uniform, or nearly so. Thus, in the theory of thermal unimolecular reactions the rate of decomposition is relative to two factors:

- (i) The collisional energy transfer leading to activation and,
- (ii) The breaking of a particular bond.

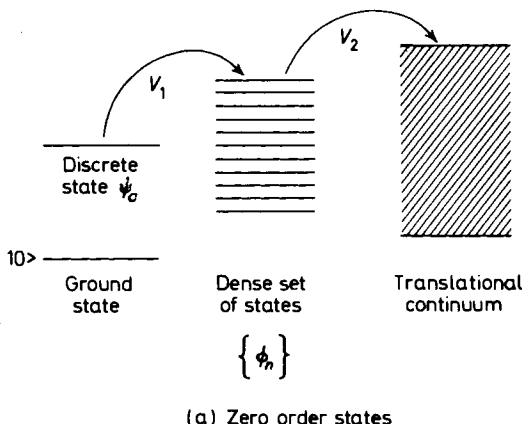
It is usually assumed that the collisions are so 'strong' that the initial and final total energies are uncorrelated so that the probability that a particular molecule will have an energy  $E$  after a collision is determined solely by the Boltzmann factor  $g_E \exp(-E/kT)$ , with  $g_E$  the degeneracy of the state with energy  $E$ . It is also assumed that the coupling between the internal degrees of freedom is so strong that the consequent energy rearrangement can be described statistically, i.e. the probability that a particular molecule, with given total energy, will have a specified configuration after an internal energy exchange is calculated by describing the system in terms of the appropriate microcanonical ensemble. Finally, the bond which breaks is designated *a posteriori*, and is not prescribed by theoretical argumentation.

Our interest in the theory of photochemical reactions started with the observation that in a molecule 'prepared' in a state with nonuniform distribution of the energy, the details of internal nuclear and electron dynamics should influence the rate and the products of the reaction. Now, as argued in earlier sections, in the upper excited states of a molecule it is often found that the vibrational levels corresponding to one Born-Oppenheimer (BO) manifold overlap, the dense set of vibrational levels corresponding to a lower electronic Born-Oppenheimer state. If the energy separation between the overlapping levels is comparable with, or less than, the off-diagonal matrix elements of the nuclear kinetic energy operator in the basis of BO states, the BO representation of the states of the molecule is no longer adequate. In this case the true molecular eigenstates can be thought of as mixtures of BO states. We have referred above to vibrational levels. In a highly excited molecule the harmonic approximation to the description of nuclear motion frequently is not adequate. We shall briefly return to this latter problem later: however, it is important to recognize at the outset that the theories which are familiar and satisfactory

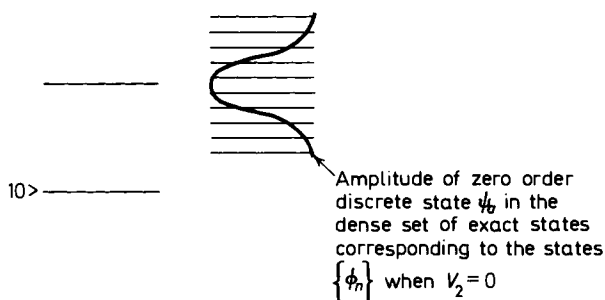
## RELAXATION PHENOMENA IN EXCITED MOLECULES

for the description of the ground state and the lower excited states of a molecule must be extended, or even replaced, when what is sought is a description of the upper excited states of a molecule.

Consider, as a first example, a molecule with an energy spectrum of the type shown in *Figures 2 and 3*. This energy level scheme can be thought of as corresponding to the existence of a localized electronic excitation coupled to electronic ground state vibrations, which in turn are coupled to a fragmentation continuum. Examples of energy spectra resembling this are found in



(a) Zero order states



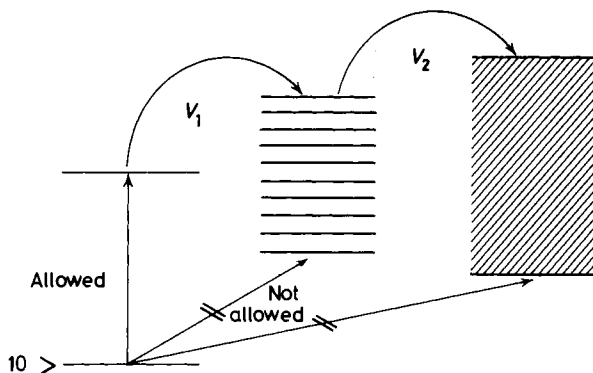
(b) Exact eigenstates in the absence of coupling to the continuum

*Figure 2.* Schematic energy-level diagram of (a) the zero-order states and (b) the exact eigenstates in the absence of coupling to the continuum.

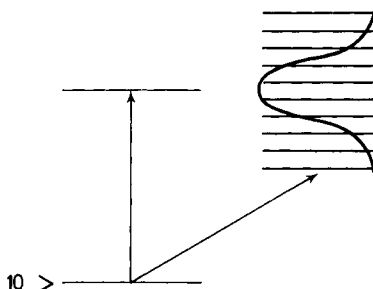
many carbonyl compounds and in methyl substituted benzenes. In both classes of compounds localized excitation of a chromophore may lead to fragmentation at a distant chemical bond.<sup>30</sup>

The properties of the dissociative states of a molecule with the spectrum described above were studied by Rice, McLaughlin and Jortner<sup>31</sup>. They represented the true eigenstates of the molecule in the absence of a radiation

field as a superposition of zero order states (which need not be BO states but which are the eigenstates of a zero order separable Hamiltonian). Suppose that, as shown in *Figure 3*, transitions from the ground state to the dissociative continuum and to the dense manifold of bound zero order vibronic states are forbidden, but that to one discrete zero-order state is



(a) Allowed dipole transitions between zero order states.



(b) Allowed dipole transitions between exact states in the absence of coupling to the translational continuum

*Figure 3.* Schematic diagram showing transitions between the sets of levels of the hypothetical spectrum. (a) Allowed dipole transitions between zero-order states. (b) Allowed dipole transitions between exact states in the absence of coupling to the translational continuum.

allowed. Then absorption of a photon prepares the molecule in a nonstationary state which can be described as a time dependent superposition of exact eigenstates, each of which is itself a time independent superposition of zero order (say BO) states<sup>32</sup>. To study photodecomposition it is imagined that the molecule is illuminated with a pulse of radiation, and the time evolution of the nonstationary state is followed. One of the interesting features of this description is the dependence of the probability of the molecule being in a

## RELAXATION PHENOMENA IN EXCITED MOLECULES

given nonstationary state on the time correlations in the coupled radiation field. Finally, the probability of dissociation of the molecule is related, formally, to the matrix elements coupling the component manifolds of the spectrum, and the densities of states in the dissociative continuum and the manifold to which it is connected.

It is possible, using an approximation relating to the influence of the rate of decomposition on the distribution of amplitude of the discrete zero order state in the dense set of exact vibrational states, to derive a simple expression for the decomposition rate. That expression is

$$k = \frac{2\rho_2 v_2^2}{\hbar} \left[ \frac{\pi}{2} - \tan^{-1} \left( \frac{E_m - E_a}{\pi(\rho_1 v_1^2)} \right) \right] \quad (14)$$

where  $E_m$  is the minimum energy required for fragmentation in the selected bond,  $\rho_1$  and  $\rho_2$  are the densities of states in the vibrational quasicontinuum and the fragmentation continuum, and  $v_1$  and  $v_2$  are the matrix elements connecting the discrete zero order state to the zero order vibrational quasicontinuum, and the zero order vibrational quasicontinuum to the fragmentation continuum, respectively. The limit  $\rho_1 v_1^2 \ll \rho_2 v_2^2$  corresponds to the case where the molecule dissociates as rapidly as the nonstationary wave packet can disperse into the vibrational quasicontinuum. This case is analogous to but not identical with that considered by Peters<sup>33</sup>—direct excitation to a nonbonding state without intermediate intramolecular energy transfer. In the limit  $\rho_1 v_1^2 \gg \rho_2 v_2^2$  the rate of fragmentation is controlled by the rate of internal energy transfer.

Of what use is such a formal description? Can we learn from it anything not already known? We believe the answer to both these questions to be a qualified yes. Perhaps most important is the change in viewpoint put forward from that embodied in the classical theory of unimolecular reactions (thermal or photochemical). In the current theory the excited molecule about to dissociate is regarded as being in a resonant scattering state<sup>34</sup>, and not a bound state. The process by which the molecule decomposes is then just a form of predissociation. Because the exact resonant scattering state is represented as a linear combination of the zero-order localized state, the dense set of zero order vibrational states, and the zero order continuum, and because the zero order state, which can be excited by absorption of a photon, is spread over many exact resonant scattering states, absorption of a photon leads to the population of resonant scattering states spread over a range of energy. Predissociation occurs from this band of states, subject to appropriate selection rules. Thus, it is not necessary to ascribe to the activated molecule the properties of a stable molecule, and the difficulties associated with the concepts of thermodynamic functions of the activated state, and the special role of the reaction coordinate, can be bypassed. Furthermore, by realizing that an excited molecule is in a resonant scattering state, the lifetime against decay into fragments appears naturally in the evaluation of the probability of dissociation—it need not be introduced as an *ad hoc* hypothesis defining irreversibility.

At a more detailed level the analysis raises the possibility that under suit-

able excitation conditions a coherently excited set of resonant scattering states can interfere<sup>34</sup>, perhaps with consequences of chemical interest. Also, depending on the magnitudes of the several coupling matrix elements and densities of states the excited molecule in the resonant scattering state may behave like a long-lived vibrationally hot molecule, like a molecule that decomposes directly to fragments without internal energy transfer, or in an intermediate fashion not like either of the cited classical limits.

The model of the photodissociation reaction described above has been used by Heller<sup>35</sup> to elucidate the nature of hydrogen transfer and hydrogen abstraction reactions. Suppose that, starting from an initial nonuniform distribution of energy in the excited state of the molecule, electronic-vibrational and vibrational-vibrational coupling leads to the excitation of particular vibrations. It is known that high frequency anharmonic stretching vibrations are the preferred energy acceptors in molecule conserving, radiationless process. Then the abundance of hydrogen abstraction and transfer reactions of electronically excited carbonyls and alkanes is explained by preferential energy transfer to high frequency stretching vibrations involving hydrogen. So long as the rate of vibrational deexcitation of such modes is small, relative to the rate of dissociation, the quantum yield of dissociated products should be large. The following rules are natural consequences of the properties built into the model considered<sup>35</sup>:

- (i) The most reactive atoms in a molecule are those that are involved in high frequency molecular motions,
- (ii) Amongst bonds with nearly the same vibrational frequency the more anharmonic the vibration and the lower the bond energy the greater is the bond reactivity, and
- (iii) Amongst bonds with nearly the same vibrational frequency and dissociation energy the closer the bond to the initial concentration of excitation energy the greater is the bond reactivity.

Assuming that there are no changes in relative bond strengths in the excited states of a molecule (as compared to the bond strengths in the ground state) the above model and rules, derived therefrom, correlate the observed intramolecular abstraction of hydrogen by excited carbonyl compounds (in both singlet and triplet states) and the Hg( $^3P_1$ ) sensitized fragmentation of alkanes. Of course in some molecules there are changes in relative bond strengths in the excited state relative to the ground state; the above rules do not apply to the photochemistry of these compounds.

Further evidence of the potential value of representing a unimolecular reaction in terms of the time evolution of a resonant scattering state can be glimpsed from the as yet, incomplete theory of photoisomerization<sup>36, 25</sup>. Taking the *cis-trans* isomerization of stilbene as a prototype reaction Gelbart and Rice<sup>36</sup> studied the properties of a model molecule in which a singlet vibronic level interacts (through spin-orbit coupling) with a nearly degenerate triplet state, which in turn is coupled (by vibronic interactions) to an isoenergetic set of closely spaced vibrational levels belonging to a lower triplet (see *Figure 4*). Unlike the photodissociation reaction, the *cis-trans* isomerization does not involve a true continuum since, even in the limit of free internal rotation, the moments of inertia of the molecular 'ends' may be sufficiently small to lead to internal rotational spacings not grossly different from those

## RELAXATION PHENOMENA IN EXCITED MOLECULES

characteristic of hindered torsional motion. If the molecule is large enough to be in the limit where  $\rho v^2 \gg 1$ , where  $\rho$  is the density of states in some manifold and  $v$  the matrix element coupling that manifold to a discrete state, and this condition holds for all discrete states and dense manifolds of interest, then it is shown that the radiative and nonradiative processes proceed independently of one another. The fluorescence quantum yield and the emis-

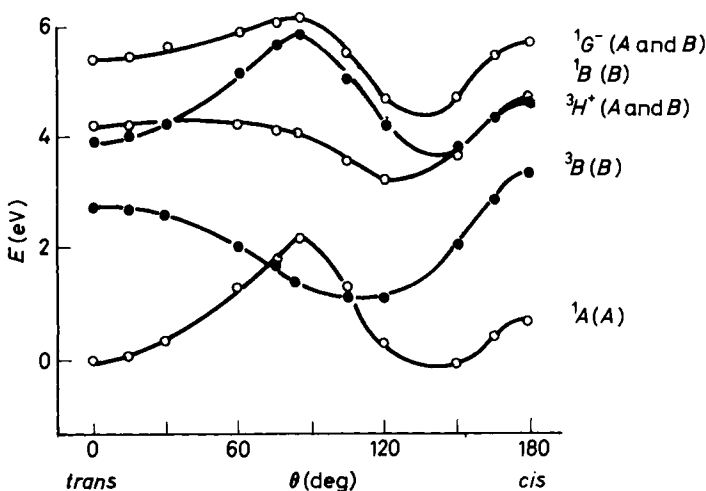


Figure 4. A schematic plot of electronic energy vs. angle of twist (about the double bond) in unsubstituted stilbene [from the SCF-CI calculations of P. Borrell and H. H. Greenwood, *Proc. Roy. Soc. (London)* **A298**, 453 (1967)].

sion lifetime predicted by this model depend explicitly on the (solvent specific) energy difference between the discrete singlet and the triplet, and they may be conveniently parameterized in terms of the level density and coupling matrix elements of the zero-order states.

The role of hindered rotation in the breakdown of the BO approximation can, in fact, be analyzed in considerable detail<sup>25</sup>. It can be shown that the molecular mode whose equilibrium positions differ greatly in the initial and final electronic states (the strongly coupled degree of freedom) may be separated out from the other vibrations in the general expression for the rate of reactions. It is then found that, under conditions appropriate to the description of *cis-trans* isomerization in stilbene-like molecules, most of the electronic energy change should go into the torsional degree of freedom rather than the usual vibrational modes which serve as acceptors if all modes are weakly coupled. The experimentally observable consequence of this conclusion is the lack of (or great diminution of) an isotope effect in the deactivation of the lowest triplet to yield the isomer product. Sufficient experimental data are not now available to test these predictions.

In the classical theory of unimolecular reactions and in the theory of photochemical reactions recently developed the internal transfer of energy

plays an important role. Nevertheless the mechanism of the internal energy transfer and its relationship to specific reaction product selection is not understood. Some insight into the energy transfer process and its coupling to molecular dissociation can be obtained from the study of models. Gelbart, Rice and Freed<sup>37</sup> have examined the properties of a model in which all vibrations are coupled, some weakly and some strongly, to all others, and in which all bonds may break with specified dissociation probabilities. The model is sufficiently general that the nature of the vibrations need not be specified. Thus it is, in principle, possible to account for the breakdown of the normal mode-harmonic oscillator description of a highly excited molecule—harmonic oscillator description of a highly excited molecule—although only in a phenomenological fashion. A stochastic process defined by a set of transition probabilities, which allows one to explicitly include the dynamics of the inter- and intra-molecular energy exchange, replaces the usual micro-canonical ensemble and strong collision assumptions. By providing for the breaking of all bonds at all times and including the competing effects of energy transfer and bond dissociation, information can be obtained about which bond is most likely to break. The following cases of interest have been studied :

(i) If the distribution of energy in the initial state is uniform, corresponding to collisional activation of a gas of polyatomic molecules originally in thermal equilibrium, it is shown that upon ‘heating up’ the gas, all other things being equal (viz. all bond energies the same), the probabilities for the breaking of the individual bonds are equal at all times, regardless of the details of the vibrational interactions. This result is rendered plausible when it is noted that at sufficiently high pressures the rate of collisional excitation exceeds the rate of internal energy transfer. The lack of great specificity in collisional excitation results, in a collection of molecules, in almost equal probability of excitation of all degrees of freedom. Then the details of the vibrational interactions are clearly unimportant and the dissociation probabilities depend on the internal energy distribution. At very low pressures the reaction rate is determined by the rate of collisional activation. Thus, except for a small range of pressure where the rate of collisional excitation is comparable with the rate of internal energy transfer, it is to be expected that individual bond dissociation probabilities will be sensibly independent of the nature of the internal coupling.

The result, just cited, provides a formal justification of the assumption implicit in classical unimolecular reaction rate theory, namely that the reaction rate depends only on the equilibrium internal energy distribution of the activated molecule.

(ii) If the distribution of energy in the initial state is non-uniform, corresponding to certain kinds of photochemical, hot atom, or photosensitization excitation, it is found that, all other things being equal (again, similar dissociation strengths), the more strongly coupled vibrational motions will always be more likely to lead to fragmentation of the molecule than is the case for the weakly coupled vibrations. Furthermore, by virtue of the energy flow into strongly coupled degrees of freedom, a strong bond can break before a weak bond if that weak bond is more weakly coupled to the site where the energy is initially localized.

## RELAXATION PHENOMENA IN EXCITED MOLECULES

The result, just cited, is consistent with the rules deduced by Heller<sup>35</sup>, with the competing fragmentation reactions observed in the mass spectrometric studies of Rosenstock<sup>38</sup> *et al.* and with the chemical activation studies of Rabinovitch and coworkers<sup>39</sup>; in all of these cases there are formed excited molecules, molecular ions and/or radicals with strongly non-uniform internal energy distributions.

(iii) In case (ii) each internal degree of freedom can exchange energy with every other degree of freedom. If, instead, interactions are restricted to 'nearest neighbours', so that a linear chain of interactions exists, different results are obtained. As can be inferred from the work of Magee and co-workers<sup>40</sup>, in a linear chain of bonds, one of which is weakly coupled, it is the weakly coupled bond which breaks because the mean time which the energy spends localized in any of the individual bonds depends inversely on the strength of coupling of that bond to its neighbours. The weakly coupled bond then 'traps' the otherwise delocalized energy for the longest time and is therefore the most likely to break, regardless of the dissociation mechanism. The nature of the competition between energy transfer and fragmentation thus depends in a fundamental way on whether the molecule in question can be regarded as 'effectively linear', is intrinsically nonlinear, or is intermediate between these two limits.

Related to the linear chain calculations of Magee *et al.* is the molecular exciton model which Partridge has recently postulated as an explanation of electronic excitation transfer in alkane polymers<sup>41</sup>. The CH and CC bonds of, say, polyethylene are treated as separate entities (i.e. electron exchange is neglected) which interact through nearest- and next-nearest neighbour transition dipoles during excitation. In this way the principal intramolecular interactions dominate the interchain ones: the theory predicts that there will be sensibly no change in the electronic absorption spectra of these polymers as they pass from the gas to solid phase or as they change their conformation. The lowest edge of the lowest band is found to be a pure CC bond exciton level, but with increasing energy ( $K$ ) some CH bond excitation begins to be mixed in. The narrow upper band is a pure CH exciton band in which there is no excitation at all of the CC bonds. In fact, in the nearest-neighbour approximation the exciton interaction is wholly within pairs of CH bonds attached to the same carbon atom (with no coupling between these pairs and hence degeneracy of the energy levels); in the next-nearest-neighbour description the different pairs interact slightly and there is a small splitting of levels. Thus if a certain CH bond is excited the energy will primarily be shared between this bond and its other CH bond neighbour on the same carbon atom—only occasionally will it migrate to other CH bonds. This exciton mode will consequently give rise to little energy transfer down the polymer chain and, with the excitation essentially localized in just two CH bonds, it is very probable that one or both of them will break. H atom and  $H_2$  molecule elimination from long chain alkanes is in fact observed commonly under vacuum-uv irradiation<sup>41</sup>. The CC exciton band, on the other hand, involves a sharing of excitation between all of the CC bonds. The model therefore predicts that the probability of a main chain (CC bond) scission should be very small since the energy is not localized in any one bond long enough to break that bond. Energy transfer is also possible to chemical defects or to

foreign atoms and molecules lying close by, but not directly attached to, the polymer molecules.

This description of Partridge's certainly constitutes a beginning step in a proper understanding of the radiation chemistry kinetics of long chain saturated molecules. It is important to note, however, that he has not considered at all the effect of electronic-nuclear coupling and the very probable importance of *vibrational* relaxation in determining the excitation energy transfer.

## V. RELEVANT EXPERIMENTS AND EMPIRICAL APPROACHES

We have seen that one must take into explicit account the competing effects of the vibrational interactions in order to properly determine the kinetics of unimolecular reactions. At the same time one is confronted with the fact that hardly anything at all is known about these quantities, i.e. one is almost wholly ignorant of the relevant properties of the nuclear potential energy surface in the region of large displacements from equilibrium. Nevertheless, it is possible to formulate a set of semi-empirical rules which allow one to extrapolate back and forth between the dissociation limit and the limit of small vibrational quantum numbers. It is of interest, then, to consider various schemes of this kind, as well as new experiments, which can provide preliminary information on the actual dynamics of intramolecular energy exchange and dissociation.

A most interesting example of the semi-empirical approach is provided by the work of Bader<sup>42</sup>, Salem<sup>43</sup>, and Pearson<sup>44</sup>, and their coworkers. These investigators have studied the way in which the electron density in a molecule is allowed to follow the nuclear vibrations by taking into account corrections to the crude adiabatic approximation. In this way they are able to formulate certain conditions which relate the most probable unimolecular reaction coordinate to the symmetries of the normal mode motions and the nature of the low-lying electronic states. For, given small enough displacements, one can rigorously show (to second order in perturbation theory) that the electronic energy of a distorted configuration in the  $i^{\text{th}}$  normal coordinate,  $Q_i$ , is given by

$$E(Q_i) = E(0) + \left\{ \langle \psi_0 | \left( \frac{\partial^2 U}{\partial Q_i^2} \right)_0 | \psi_0 \rangle - \sum_{k \neq 0} \frac{|\langle \psi_0 | (\partial U / \partial Q_i)_0 | \psi_k \rangle|^2}{E_k - E_0} \right\} Q_i^2, \quad (15)$$

where  $U$  is the electron-nuclear coulomb energy and  $\{E_k\}$  and  $\{\psi_k\}$  are the energies and wavefunctions corresponding to the zero-order electronic states at the equilibrium configuration. The first term in  $Q_i^2$  gives the increase in energy of the system when the nuclei are displaced by  $Q_i$  and the electron distribution is held fixed according to  $\psi_0$ . The matrix elements in the sum of the second term mix the ground and excited states and thereby allow the electron distribution to relax (follow the motion of the nuclei), hence lowering the energy. Accordingly, the energy is lowered the most for that  $Q_i$  which mixes in the first excited state. It is then assumed that this lowering obtains for larger displacements as well [Salem<sup>43</sup> however, warns of the possible dangers involved here, and argues the importance of the cubic potential

## RELAXATION PHENOMENA IN EXCITED MOLECULES

contributions]. Predictions of the most probable unimolecular reaction coordinate follow immediately: the actual results seem to work surprisingly well even though the rules are implicitly based on an extrapolation from the region of small amplitude vibrations to the dissociation limit. From our present point of view there is still a more important conceptual failing—namely, the nuclear potential energy is taken to be separable with respect to some set of internal coordinates. That is, it is still only the diagonal anharmonicities which are included—the effect of the off-diagonal vibrational interactions is neglected. An extension taking into account these couplings would constitute an important step in developing a new set of correlation rules for the *a priori* prediction of reaction coordinates.

We should mention here the sensitization experiments in which mercury atoms, excited to their metastable singlet and triplet states, are allowed to collide with polyatomic molecules of interest, thereby preparing them in high-lying vibrational levels of the ground electronic state. This class of reactions is of special interest because it provides the cleanest examples of a fragmentation process in which the weakest bonds are not always the most likely to break. Heller<sup>35</sup> has considered in particular the mercury ( ${}^3P_1$ ) sensitized photolysis of alkanes, and observes that the most reactive bonds are not the CC-sigma bonds but the stronger (by as much as 20 kcal/mole) CH bonds. In order to explain this behaviour he assumes that the efficiency of energy transfer from the excited mercury to the internal degrees of freedom of the alkane is directly governed by the appropriate Franck-Condon overlap integrals. It follows immediately that the best accepting vibrations will be those of highest frequency and anharmonicity and therefore that the hydrogen stretching motions will be preferentially excited. It is not at all obvious, however, that the atom-molecule energy transfer can be described by such a simple assumption. Rather it seems likely that more complicated vibrational motions of the alkane are initially excited and that the reactivity of the CH bonds needs to be explained by a different mechanism. Our contention could be investigated by an experiment which measures the lifetime of the sensitized molecule against fragmentation. If this time lag were long, compared with a CH vibrational period, one could infer that the hydrogen atoms are not directly activated by sensitization, but rather are preferentially excited by intramolecular energy transfer according to the stochastic theory of Gelbart, Rice, and Freed<sup>37</sup> described in IV.

A more fruitful class of experiments could be modelled on certain studies of Frey<sup>45</sup> Kistiakowsky<sup>46</sup> and Rabinovitch<sup>47</sup>, which were intended to test, ‘unambiguously’, the fundamental strong coupling assumption of unimolecular reaction theory. In 1960, Frey<sup>45</sup> presented interesting evidence suggesting that the energy exchange between normal mode motions might in fact occur slowly compared with the lifetime of the excited molecule. He studied the addition of methylene to isobutene, and the subsequent isomerization of the vibrationally excited 1, 1-dimethylcyclopropane into 2-methylbut-2-ene (I) and 3-methylbut-1-ene (II). It was found that the ratio of the yields of products I and II is roughly 1.60 whereas the corresponding value obtained in the thermal isomerization of 1, 1-dimethylcyclopropane is as low as 0.96. This result suggests that the initial distribution of vibrational energy in the addition reaction is non-uniform and that the rearrangement

of the 'hot' molecule occurs before the randomization, implied by the strong coupling theories, can take place.

Butler and Kistiakowsky<sup>46</sup> have investigated the validity of these assumptions in a different, and yet related, experiment. They studied the isomerization of vibrationally excited methylcyclopropane prepared by the addition of methylene to cyclopropane, and to propylene. It was found that the yields of the various butene products obtained from the cyclopropane addition are within experimental error of those found from the propylene reaction and that these values are in turn the same as those determined in studies of the direct thermal isomerization of methylcyclopropane. This lack of dependence of the several reaction rates on the initial vibrational energy distributions, in contrast to the earlier conclusions of Frey, was taken to confirm the applicability of the strong coupling assumption. We feel, however, that all these experiments, while properly conceived in spirit, are undermined by the effect of collisions. That is, since the isomerization and dissociation lifetimes are greater than the mean time between encounters in the gas, the internal energy distribution must surely be disturbed by collisions before unimolecular reaction occurs. In order to obtain information on the intramolecular dynamics unambiguously, then, it would be necessary to repeat these experiments at total pressures which are lower by several orders of magnitude. Still better, one can look to chemical lasers and crossed molecular beams for the least ambiguous resolution of these questions.

The relevant chemical laser experiments of special interest are the bimolecular<sup>48</sup> and photo-elimination<sup>49</sup> reactions investigated by Pimentel and his co-workers. In the former case, one studies exothermic exchange processes of the type  $A + BC \xrightarrow{k_v} AB_v^* + C$ : in particular, say, the reaction  $F + H_2(D_2) \rightarrow HF_v^*(DF_v^*) + H$ , which arises in the flash photolysis initiated  $UF_6-H_2(D_2)$  chemical lasers. By measuring the vibrational energy distribution of the diatomic products, and invoking microscopic reversibility arguments, these experiments bear directly on our understanding of the role of internal excitation in simple collision dynamics. At the same time, by studying, say, other  $HF(DF)$  chemical lasers [e.g. those arising from  $H(D)$  atom abstractions in the alkanes] one can begin to learn about the effect of exothermicity of reaction on the distribution of vibrational energy amongst the products.

Perhaps of more interest are the photoelimination<sup>49</sup> chemical lasers developed by Berry and Pimentel. They have studied in detail the  $HCl$  emission following vacuum uv photolysis of the three dichloroethylenes. These experiments point up the way in which the vibrational excitation of the  $HCl$  produced by photoelimination depends upon the structure of the parent molecule. By microscopic reversibility it is inferred that in the reverse (addition) reaction,  $HCl$  vibrational excitation will show a stereospecific preference for the *cis*-1,1- over the 1,2-dichloroethylene product, and further for the *cis*-1,2- over the *trans*-1,2- isomer.

The final, and what we believe to be the most fruitful, class of experiments relevant to this discussion is the crossed molecular beam method which has been developed over the past fifteen years by several groups of investigators. Of special interest are the chemical reactions which proceed through the formation of a collision complex with a lifetime much longer than a rotational

## RELAXATION PHENOMENA IN EXCITED MOLECULES

period. Here the angular distribution of products peaks symmetrically forward and backward in the centre-of-mass system.<sup>50</sup> Several examples of this behaviour have been reported in the recent molecular beam literature, most notably for the alkali-alkali halide<sup>51</sup> and alkali halide-alkali halide exchange reactions<sup>52</sup>. These studies are of importance to us here insofar as they allow for comparisons between the various 'competing' theories of unimolecular dissociation. The distribution of total energy amongst the vibrations and rotations of the products, and the relative motion of the separating fragments, can be estimated experimentally by combining the data from velocity analyses and angular scans. In turn these detailed results can be calculated by a modified RRKM-transition state theory<sup>51, 52</sup> or by the phase space approach of Light<sup>53</sup>. Rough agreement is found<sup>51</sup> in both cases and is taken to confirm the validity of the statistical assumption for these relatively long-lived collision complexes.

These examples, almost by definition, do not lend themselves to a weak coupling stochastic theory of the form considered by Gelbart, Rice and Freed<sup>37</sup>. During the last year, however, work has begun at the University of Chicago on cross-beam experiments which are of a decidedly different nature. It is planned<sup>54</sup> to study the product and energy distributions arising from the addition of fluorine atoms to various ethylene derivatives. Preliminary data from angular scans of the reaction  $F + C_2H_4 \rightarrow C_2H_4F^* \rightarrow C_2H_3F + H$  show a symmetric forward-backward peaking, indicating a long lived ( $\tau_c > 10^{-12}$  sec) collision complex. Rough calculations already suggest that a considerably larger fraction of the available total energy is coupled into the relative motion of the separating fragments than is consistent with the statistical theories. Velocity analysis of the products will allow for more dependable estimates of the most probable distribution of translational and rotational energy in the polyatomic fragment. It will be of interest to run the crossed beam experiment, as well, for addition reactions involving longer chain alkenes, particularly those having weak bonds at the far end of the molecule from the ethylenic linkage. The species of products, their angular distribution and the energy of the relative motion of the separating fragments will indicate the extent of vibrational relaxation which has taken place before dissociation. This kind of information, aside from generally confirming the need for a full stochastic description of the internal energy dynamics, should also provide some preliminary knowledge of the 'off-diagonal' vibrational interactions in highly excited molecules.

## VI. ACKNOWLEDGEMENTS

Our research in photochemistry has been supported by the Directorate of Chemical Sciences, Air Force Office of Scientific Research. We have also benefited from the use of facilities provided by the Advanced Research Projects Agency for materials research at the University of Chicago.

## REFERENCES

<sup>1</sup> The reader is referred to the review article by J. Jortner, S. A. Rice and R. M. Hochstrasser, *Advan. Photochem.* 7, 149 (1969), for a discussion of many of the mathematical details omitted in this paper.

STUART A. RICE AND WILLIAM M. GELBART

- <sup>2</sup> G. W. Robinson and R. P. Frosch. *J. Chem. Phys.* **38**, 1187 (1963); **37**, 1962 (1962).
- <sup>3</sup> M. Bixon and J. Jortner. *J. Chem. Phys.* **48**, 715 (1968).
- <sup>4</sup> W. Rhodes, B. Henry and M. Kasha. *Proc. Nat. Acad. Sci. U.S.* **63**, 31 (1969).
- <sup>5</sup> P. Pringsheim. *Fluorescence and Phosphorescence*, p. 271. Interscience: New York (1949).
- <sup>6</sup> R. J. Watts and S. J. Strickler. *J. Chem. Phys.* **44**, 2423 (1966).
- <sup>7</sup> R. Williams and G. J. Goldsmith. *J. Chem. Phys.* **39**, 2008 (1963).
- <sup>8</sup> Perylene: W. R. Ware and P. T. Cunningham. *J. Chem. Phys.* **44**, 4364 (1966).
- <sup>9</sup> Anthracene: K. H. Hardel and A. Schermann. *Z. Naturforsch.* **12a**, 715 (1957).
- <sup>10</sup> G. B. Kistiakowsky and C. S. Parmenter. *J. Chem. Phys.* **42**, 2942 (1965).
- <sup>11</sup> U. Fano. *Phys. Rev.* **124**, 1866 (1961).
- <sup>12</sup> D. Chock, J. Jortner, and S. A. Rice. *J. Chem. Phys.* **49**, 610 (1968).
- <sup>13</sup> J. Jortner and R. S. Berry. *J. Chem. Phys.* **48**, 2757 (1968).
- <sup>14</sup> K. F. Freed and J. Jortner. *J. Chem. Phys.* **50**, 2916 (1969).
- <sup>15</sup> M. Bixon, J. Jortner and Y. Dothan. *Mol. Phys.* **17**, 109 (1969); see also M. Bixon and J. Jortner. *J. Chem. Phys.* **50**, 4061 (1969).
- <sup>16</sup> K. F. Freed. *J. Chem. Phys.* **52**, 1345 (1970).
- <sup>17</sup> M. Bixon and J. Jortner. *J. Chem. Phys.* **50**, 3284 (1969).
- <sup>18</sup> A. E. Douglas. *J. Chem. Phys.* **45**, 1007 (1966), and references cited therein.
- <sup>19</sup> See W. Siebrand. *J. Chem. Phys.* **47**, 2411 (1967) and earlier papers.
- <sup>20</sup> See J. P. Byrne, E. F. McCoy and I. G. Ross. *Australian J. Chem.* **18**, 1589 (1965) and earlier papers.
- <sup>21</sup> An excellent review of these solid-state problems is given by J. J. Markham. *Rev. Mod. Phys.* **31**, 956 (1959).
- <sup>22</sup> R. Kubo. *Phys. Rev.* **86**, 929 (1952).
- <sup>23</sup> S. H. Lin. *J. Chem. Phys.* **44**, 3759 (1966); S. H. Lin and R. Bersohn, *ibid.* **48**, 2732 (1968).
- <sup>24</sup> R. Englman and J. Jortner. *Mol. Phys.* **18**, 145 (1970).
- <sup>25</sup> W. M. Gelbart, K. F. Freed and S. A. Rice. *J. Chem. Phys.* **52**, 2460 (1970).
- <sup>26</sup> K. F. Freed and J. Jortner. *J. Chem. Phys.* in press.
- <sup>27</sup> W. M. Gelbart, K. G. Spears, K. F. Freed, J. Jortner and S. A. Rice. Submitted to *Chem. Phys. Letters*.
- <sup>28</sup> Fluorescence quantum yields are presently being determined in this laboratory by K. G. Spears and S. A. Rice, as well as by C. S. Parmenter (private communication).
- <sup>29</sup> W. M. Gelbart, Ph.D. thesis, University of Chicago (1970).
- <sup>30</sup> See, for example, J. Calvert and J. Pitts. *Photochemistry*. John Wiley & Sons: New York (1967); also P. Johnson and S. A. Rice. *Chem. Phys. Letters* **1**, 709 (1968).
- <sup>31</sup> S. A. Rice, I. McLaughlin and J. Jortner. *J. Chem. Phys.* **49**, 2756 (1968).
- <sup>32</sup> F. Mies and M. Krauss have used a related method in their elegant theory of unimolecular reactions. They explicitly employ a generalization of the Fano theory of autoionization but they have given less emphasis than we to internal energy redistribution since they study, primarily, thermally excited molecules. F. H. Mies and M. Krauss. *J. Chem. Phys.* **45**, 4455 (1966); F. H. Mies. *J. Chem. Phys.* **51**, 787, 798 (1969).
- <sup>33</sup> D. Peters. *J. Chem. Phys.* **41**, 1046 (1964).
- <sup>34</sup> See also the work cited in reference 33.
- <sup>35</sup> A. Heller. *Mol. Photochem.* **1**, 257 (1969).
- <sup>36</sup> W. Gelbart and S. A. Rice. *J. Chem. Phys.* **50**, 4775 (1969).
- <sup>37</sup> W. Gelbart, S. A. Rice and K. Freed. *J. Chem. Phys.* in press.
- <sup>38</sup> See, for example, H. Rosenstock, M. Wallenstein, A. Wahrhaftig and H. Eyring. *Proc. Nat. Acad. Sci. U.S.* **38**, 667 (1952); also H. Rosenstock and M. Krauss. *Mass Spectrometry of Organic Ions* Ed. F. W. McLafferty (Academic Press, N.Y., 1963), Chapter 1.
- <sup>39</sup> C. W. Larson, B. S. Rabinovitch and D. C. Tardy. *J. Chem. Phys.* **47**, 4570 (1967); **45**, 1163 (1966); M. J. Pearson and B. S. Rabinovitch. *J. Chem. Phys.* **42**, 1624 (1965); B. S. Rabinovitch, R. F. Kubin and R. E. Harrington. *J. Chem. Phys.* **38**, 405 (1963); R. E. Harrington, B. S. Rabinovitch and R. W. Diesen. *J. Chem. Phys.* **32**, 1245 (1960); B. S. Rabinovitch and R. W. Diesen. *J. Chem. Phys.* **30**, 735 (1959).
- <sup>40</sup> J. Magee and K. Funabashi. *J. Chem. Phys.* **34**, 1715 (1961); J. C. Lorquet, S. G. El Komoss and J. Magee. *J. Chem. Phys.* **35**, 1991 (1962).
- <sup>41</sup> R. H. Partridge. *J. Chem. Phys.* **52**, 2485, 2491, 2501 (1970) and earlier papers.
- <sup>42</sup> R. F. W. Bader. *Mol. Phys.* **3**, 137 (1960); *Can. J. Chem.* **40**, 1164 (1962).

## RELAXATION PHENOMENA IN EXCITED MOLECULES

- <sup>43</sup> L. Salem. *Chem. Phys. Letters* **3**, 99 (1969); L. Salem and J. S. Wright. *J. Am. Chem. Soc.* **91**, 5947 (1969).
- <sup>44</sup> R. G. Pearson. *J. Am. Chem. Soc.* **91**, 4947 (1969); *J. Chem. Phys.* **52**, 2167 (1970).
- <sup>45</sup> H. M. Frey. *Trans. Faraday Soc.* **56**, 51 (1960).
- <sup>46</sup> J. N. Butler and G. B. Kistiakowsky. *J. Am. Chem. Soc.* **82**, 759 (1960).
- <sup>47</sup> R. E. Harrington, B. S. Rabinovitch and H. M. Frey. *J. Chem. Phys.* **33**, 1271 (1960).
- <sup>48</sup> J. H. Parker and G. C. Pimental. *J. Chem. Phys.* **51**, 91 (1969); **48**, 5273 (1968);  
K. L. Kompa, J. H. Parker and G. C. Pimental. *ibid.* **49**, 4257 (1968).
- <sup>49</sup> M. J. Berry and G. C. Pimental. *J. Chem. Phys.* in press; also *ibid.* **49**, 5190 (1968) and **51**, 2274 (1969).
- <sup>50</sup> D. R. Herschbach. *Discussions Faraday Soc.* **33**, 149 (1962).
- <sup>51</sup> W. B. Miller, S. A. Safron and D. R. Herschbach. *Discussions Faraday Soc.* **44**, 108 (1967).
- <sup>52</sup> W. B. Miller. Ph.D. Thesis, Harvard University (1969).
- <sup>53</sup> J. C. Light. *Discussions Faraday Soc.* **44**, 14 (1967) and references to earlier papers cited therein.
- <sup>54</sup> Y. T. Lee and J. Parson. Private communication.

# RADIATIONLESS TRANSITIONS

JOSHUA JORTNER

*Department of Chemistry, Tel-Aviv University, Tel-Aviv, Israel*

## ABSTRACT

This review will be concerned with some questions which arise whenever one thinks of analyzing experimental radiative decay times and optical line shape data in polyatomic molecules, and how these quantities are related to fundamental electronic relaxation processes in a large molecule.

## 1. INTRODUCTION

Radiationless processes in excited electronic states of large molecules can be classified as follows:

- (a) Radiationless decomposition<sup>1</sup>:
  - (a1) Molecular predissociation.
  - (a2) Molecular autoionization.
- (b) Intramolecular relaxation<sup>2</sup>:
  - (b1) Electronic relaxation processes which involve internal conversion and intersystem crossing.
  - (b2) Unimolecular photochemical rearrangement reactions in excited electronic states of large molecules such as *cis-trans* isomerization or electrocyclic reactions.

The present review will be concerned mainly with electronic relaxation processes. From the historical point of view it has been known since 1888 that many organic molecules in a dense medium exhibit a strong afterglow (or rather, phosphorescence) when excited by ultraviolet light, this emission invariably being at lower frequencies than the fluorescence (if any) of the compound<sup>3</sup>. These observations were followed in 1933 by the phenomenological description of the three level system by Jablanski<sup>4</sup>. The modern focus on the importance and generality of intramolecular relaxation processes was emphasized by the work of Lewis and coworkers and by Kasha<sup>5</sup>. During the last twenty years extensive studies were performed which elucidated some important features of electronic relaxation processes of polyatomic molecules imbedded in a dense medium (e.g. solutions, rigid glasses, mixed crystals)<sup>2</sup>. These studies resulted in several generalizations:

- (a) The Kasha rules<sup>2</sup>.
- (b) 'Shortening' of the experimental radiative lifetimes of large molecules, accompanied by a reduction of the emission quantum yield<sup>2</sup>.
- (c) The Robinson-Frosch<sup>6</sup> energy gap law.
- (d) The deuterium isotope<sup>6,7</sup>.

In view of the bulk of experimental data concerning radiationless transitions in a dense medium it is not surprising that early theories by Gouterman<sup>8</sup> and by Robinson and Frosch<sup>6</sup> considered the molecule-medium coupling

as an essential ingredient which will provide a pathway for electronic relaxation. An impetus for a drastic revision of theoretical ideas concerning this problem was provided (as usual in theoretical chemistry!) by recent experimental data<sup>9-13</sup> which demonstrate conclusively that radiationless transitions occur in an 'isolated' low density gas phase molecule. About three years ago theoretical studies by Henry and Kasha<sup>24</sup>, Robinson<sup>14</sup> and Bixon and Jortner<sup>15</sup> provided a firm basis for the idea that a radiationless transition in a large molecule involves an intramolecular relaxation process.

I would like to discuss some aspects of recent work on the interpretation of optical line shape data and radiative decay times in large molecules, and how this information relates to intramolecular electronic relaxation processes in large molecules.

## II. COMMENTS ON COMPOUND STATES

How does a relaxation process take place in a microscopic system? Three major points have to be amplified in this context:

- (a) The description of the decaying state.
- (b) The preparation of the metastable nonstationary state.
- (c) The relation between the decay time and the optical line shapes.

Suppose that the system under consideration is described by the Hamiltonian

$$H = H_0 + V \quad (\text{II.1})$$

where  $H_0$  is a 'convenient' zero order Hamiltonian (e.g. independent particles Hamiltonian in the case of autoionization<sup>16</sup>, or the Born-Oppenheimer Hamiltonian in the case of predissociation)<sup>17-19</sup>, while  $V$  is a perturbation term which includes whatever we have left out of  $H_0$ . The zero order eigenstates of  $H_0$  are now partitioned into two sets: a (dynamic) sparse subset which is characterized by a small number of discrete levels  $\phi_1, \phi_2$  and a dissipative part  $\phi_E$  which is characterized by a continuous spectrum. As the zero order states of the two subsystems are degenerate, extensive 'configuration interaction' is induced by the (small) interaction term  $V$  which couples the dynamic and the dissipative part. An atom or molecule in a stationary state cannot make transitions to the other states which are induced by the 'small terms in the molecular Hamiltonian' (i.e.  $V$  in equation (II.1).) Obviously all time dependent transitions between stationary states are radiative in nature. However this conclusion does not apply when the molecular system is prepared by some experiments in a nonstationary state of the system's Hamiltonian. To obtain the physical information concerning the relaxation process it will be convenient to proceed as follows<sup>16, 19</sup>:

(a) The *molecular eigenstates*  $\psi_E$  of the system are constructed (e.g. the eigenstates of  $H$  in the absence of the radiation field) as a time independent superposition of the zero order states. For convenience we shall consider only a single state  $\phi_1$  in the dynamic subset, so that

$$\psi_E = a(E)\phi_1 + \int b_{E'}(E)\phi_{E'}\rho(E')dE' \quad (\text{II.2})$$

where  $\rho(E)$  is the density of states in the zero order continuum, and  $a(E)$  and

## RADIATIONLESS TRANSITIONS

$\{b_E(E)\}$  correspond to expansion coefficients. Note that the eigenstates  $\phi_E$  form a continuous spectrum.

(b) *The resonance width  $\Gamma(E)$*  is given for a single resonance by the Fermi Golden Rule:

$$\Gamma(E) = 2\pi |\langle \phi_1 | V | \psi_E \rangle|^2 \rho(E) \quad (\text{II.3})$$

For the case of a dissipative continuum one expects that it is a slowly varying function of the energy in the vicinity of the  $E = E_1$ , which is the energy of the zero order state  $\phi_1$ .

(c) *The Breit Wigner Formula.* The amplitude square of the zero order state  $\phi_1$  is given by the distribution:

$$|a(E)|^2 = (\Gamma/2)/[(E - E_1 - \gamma_1)^2 + (\Gamma/2)^2] \quad (\text{II.4})$$

where  $\gamma_1$  is a level shift. Thus the effect of configuration interaction is to 'dilute' the discrete state  $\phi_1$  through a manifold of stationary states. The profile of the distribution is a Lorentzian characterized by the width:

$$\Delta = \Gamma \quad (\text{II.5})$$

(d) *The transition matrix element* of the transition operator  $\hat{T}$  for optical (or other type) excitation from the ground state  $\phi_0$  is determined by:

$$\langle \phi_0 | \hat{T} | \psi_E \rangle = a(E) \langle \phi_0 | \hat{T} | \phi_1 \rangle + \int b_E(E) \langle \phi_0 | \hat{T} | \phi_E \rangle \rho(E) dE \quad (\text{II.6})$$

(e) *The line shape  $A(E)$*  for optical excitation will be determined by the square of the transition matrix element:

$$A(E) \propto |\langle \phi_0 | \hat{T} | \psi_E \rangle|^2 \quad (\text{II.7})$$

(f) *Lorentzian line shapes.* The absorption profile will be Lorentzian only, provided that the continuum does not carry oscillator strength, i.e.  $\langle \phi_0 | \hat{T} | \phi_E \rangle = 0$  for all  $\phi_E$ . Then

$$A(E) \propto |a(E)|^2 = (1/(1 + \varepsilon^2)) \quad (\text{II.8})$$

where the reduced energy parameter  $\varepsilon$  is

$$\varepsilon = E - E_1 - \gamma_1/(\Gamma/2) \quad (\text{II.9})$$

(g) *Fano type line shapes.* In the general case, when the continuum does carry oscillator strength from the ground state, interference effects in absorption will be observed arising from the contributions of  $\langle \phi_0 | \hat{T} | \phi_1 \rangle$  and  $\langle \phi_0 | \hat{T} | \phi_E \rangle$  which will interfere with opposite phases on the two sides of the resonance. The line shape function will then be

$$A(E) \propto \frac{(q + \varepsilon)^2}{(1 + \varepsilon^2)} \quad (\text{II.10})$$

where the line profile index  $q$  is determined by the ratio transition moments for the discrete state and for the continuum.

$$q \approx \frac{\langle \phi_0 | \hat{T} | \phi_1 \rangle}{\langle \phi_0 | \hat{T} | \phi_E \rangle \langle \phi_E | V | \phi_1 \rangle \rho(E)} \quad (\text{II.11})$$

Note that equation (II.10) is reduced to the Lorentzian form (II.8) provided that  $q \rightarrow \infty$ . This situation will be realized when:

- (1) the coupling between the zero order states is negligible.
- (2) when the oscillator strength of the background absorption is negligibly small, relative to the intensity carried by  $\phi_1$ .
- (h) A compound state of the system will be described as a time dependent superposition of time independent zero order states. The choice of the basis set is merely a matter of convenience. One possible choice of the basis set involves the stationary states of  $H$  or, alternatively, the basis set of  $H_0$  may be used. Let  $p(E)$  correspond to the excitation amplitude of  $\psi_E$ , then two alternative forms for the time dependent excited state can be immediately written:

$$\Psi(t) = \int p(E) \psi_E \exp(-iEt/\hbar) \rho(E) dE \equiv A(t) \phi_1 + \int B_E(t) \phi_E \rho(E) dE \quad (\text{II.12})$$

It should be noted that the compound state involves an admixture of zero order discrete and continuum states.

- (i) The time evolution of the amplitude of the discrete state can then be given

$$P(t) = |\langle \phi_1 | \Psi(t) \rangle|^2 = |\int \rho(E) a(E) \exp(-iEt/\hbar) \rho(E) dE|^2 \equiv |A(t)|^2 \quad (\text{II.13})$$

Thus the decay law is determined by an energy distribution function. It should be noted that, unlike the line shapes which are definitely experimental observables, the quantity  $P(t)$  may not always be amenable to experimental observation.

- (i). Decay of state 'prepared' initially in  $\phi_1$ .  
The  $|A(0)|^2 = 1$  or  $p(E) = a(E)$ ; provided that  $\Gamma(E)$  is a slowly varying function of the energy an exponential decay law results:

$$P(t) \propto \exp(-\Gamma t/\hbar) \quad (\text{II.14})$$

The half lifetime is just  $\hbar\Gamma^{-1}$  and the simple decay law is related to the width of the amplitude distribution  $|a(E)|^2$ . This is again a 'theoretical exercise' which will not always be realized in a real life experiment.

The foregoing arguments are general, leading to the conclusion that there is a set of features common to all compound states of a wide class of systems. The shapes of resonances encountered in nuclear, atomic, molecular and solid-state physics are nearly the same and the decay rates of many different kinds of metastable states have the same functional form.

For radiationless decomposition processes the dissipative channel is well defined (e.g. a dissociative continuum for the case of predissociation and an ionization continuum for autoionization). The details of the relaxation process (e.g. decay times and line shapes) will be determined by the coupling matrix elements, the transition moments and the line profile index. At first sight it may appear that there is an apparent basic difference between radiationless decomposition and intramolecular relaxation as in the latter case a 'true' dissipative continuum is not involved. In this context several statements have been made concerning non-radiative intramolecular relaxation processes. It was stated by Herzberg<sup>20</sup> in 1966: 'The mechanism of (internal) conversion is not well understood as yet but is presumably connected with

## RADIATIONLESS TRANSITIONS

strong perturbations between the two states involved.' At about the same time Kistiakowsky and Parmenter<sup>13</sup> stated that their experimental observation of a radiationless transition in the isolated benzene molecule 'may be incompatible with the laws of quantum mechanics'. The questions that come up in relation to intramolecular relaxation processes in large molecule can be summarized as follows:

- (a) What is the nature of the intramolecular coupling?
- (b) Do radiationless transitions take place in an isolated large molecule?
- (c) What is the nature of the intramolecular dissipative channel?
- (d) What are the criteria for irreversibility of an intramolecular relaxation process?
- (e) What are the implications of intramolecular coupling and a background quasicontinuum of states concerning intensity distribution in optical absorption?
- (f) Under what conditions can the intramolecular decay be considered as a simple rate process with the rate constant being given by Fermi's 'Golden Rule'?
- (g) What are the consequences of the coupling between radiative and non-radiative decay processes in a large molecule?

### III. INTRAMOLECULAR COUPLING

The nature of the intramolecular coupling responsible for radiationless transitions was elucidated many years ago by Franck and Sponer<sup>21</sup> and by Kubo<sup>22</sup> who pointed out that the nuclear kinetic energy operator provides the major interaction term which is responsible for the occurrence of radiationless processes in large molecules. Naturally, other intramolecular interaction terms may modify the mixing. Thus, for example, spin-orbit interactions have to be included in the case of mixing of quasidegenerate vibronic components which correspond to two electronic states of different multiplicity.

The electronic states of a molecule are conventionally classified within the framework of the Born-Oppenheimer approximation, into separate electronic and nuclear motions. Let us focus our attention on the conventional Born-Oppenheimer (BO) adiabatic approximation for the two level system.

The higher excited electronic state,  $s$ , is characterized by the zero-order BO levels  $\phi_{sa}(\mathbf{r}, \mathbf{Q})$  which are coarsely spaced, each of which is coupled to the dense quasicontinuum of vibronic levels  $\phi_{1\beta}(\mathbf{r}, \mathbf{Q})$ . These functions are usually approximated in the form:

$$\begin{aligned}\phi_{sa}(\mathbf{r}, \mathbf{Q}) &= \Theta_s(\mathbf{r}, \mathbf{Q})\chi_{sa}(\mathbf{Q}) \\ \phi_{1\beta}(\mathbf{r}, \mathbf{Q}) &= \Theta_1(\mathbf{r}, \mathbf{Q})\chi_{1\beta}(\mathbf{Q})\end{aligned}\quad (\text{III.1})$$

where  $r$  represents the electronic coordinates, while  $\mathbf{Q} \equiv Q_1, Q_2, \dots, Q_k$  ... (III.1) correspond to the nuclear coordinates.  $\Theta$  and  $\chi$  represent electronic and vibrational wavefunctions. The potential surfaces in the two electronic states will be denoted by  $E_s(Q)$  and  $E_1(Q)$  while the energies of the vibronic components will be represented by  $E_{sa}$  and  $E_{1\beta}$ , respectively.

As is well known, the BO representation is diagonal within a single

electronic manifold while (hopefully small) matrix elements connect different electronic states. These off diagonal matrix elements are given in the general form:

$$v_{sa,lb} = \frac{1}{2} \sum_k \int d\mathbf{Q} \chi_{sa}(\mathbf{Q}) \left\langle \Theta_s(\mathbf{q}, \mathbf{Q}) \left| \frac{\partial^2}{\partial Q_k^2} \right| \Theta_l(\mathbf{q}, \mathbf{Q}) \right\rangle \chi_{lb}(\mathbf{Q}) \\ - \sum_k \int d\mathbf{Q} \chi_{sa}(\mathbf{Q}) \left\langle \Theta_s(\mathbf{q}, \mathbf{Q}) \left| \frac{\partial}{\partial Q_k} \right| \Theta_l(\mathbf{q}, \mathbf{Q}) \frac{\partial}{\partial Q_k} \chi_{lb}(\mathbf{Q}) \right\rangle \quad (\text{III.2})$$

The electronic matrix elements appearing in (III.2) can be expressed in the exact form:

$$J_{sl}^k = \left\langle \Theta_s(\mathbf{q}, \mathbf{Q}) \left| \frac{\partial}{\partial Q_k} \right| \Theta_l(\mathbf{q}, \mathbf{Q}) \right\rangle \quad (\text{III.3a})$$

$$= \frac{\langle \Theta_s(\mathbf{q}, \mathbf{Q}) | \partial U(\mathbf{q}, \mathbf{Q}) / \partial Q_k | \Theta_l(\mathbf{q}, \mathbf{Q}) \rangle}{E_s(\mathbf{Q}) - E_l(\mathbf{Q})} \quad (\text{III.3b})$$

where  $U(\mathbf{q}, \mathbf{Q})$  corresponds to the molecular potential energy term.

The breakdown of the BO approximation will be encountered under the following circumstances:

(a) Strong interaction between degenerate or quasidegenerate electronic origins. This situation corresponds to the Jahn-Teller and Renner coupling in molecules.

(b) Intersection of potential surfaces: the electronic matrix element (III.3) is a rapidly varying function of the nuclear coordinates, whereupon near the intersection (where  $E_s(\mathbf{Q}) - E_l(\mathbf{Q}) = 0$ ) a new representation of the vibronic wave functions has to be found in a manner analogous to the treatment of the Jahn-Teller problem. Such situations which involve a large configurational change between two electronic states will be encountered in the field of organic photochemistry.

(c) Case of near degeneracy. Now we encounter small configurational change between two electronic states. The electronic integral  $J_{sl}^k$  is a slowly varying function of  $\mathbf{Q}$  and we expect that  $J_{sl}^k \propto \Delta E^{-1}$ , where  $\Delta E = E_{s0} - E_{l0}$  corresponding to the electronic energy gap between the origins of the two electronic states.  $\Delta E$  is appreciable and the  $v_{sa,lb}$  terms are small not only in view of the energy denominator but rather as they involve extremely small<sup>6, 23-26</sup> Franck-Condon vibrational overlap terms. However the smallness of the  $v$  terms does not insure the validity of the BO approximation. The adiabatic approximation is expected to hold only provided the energy difference between the zero order vibronic states is large relative to the coupling matrix element (III.2) so that

$$|E_{sa} - E_{lb}| \gg |v_{sa,lb}| \quad (\text{III.4})$$

When a situation of near degeneracy is encountered we expect the BO approximation to break down even provided that the  $v$  terms are small.

Let us now consider the behaviour of the excited electronic levels of a complex molecule. The zero order vibronic level  $\phi_s$  of a higher excited state

## RADIATIONLESS TRANSITIONS

is quasidegenerate with a manifold  $\{\phi_i\}$  of vibronic levels which correspond the lower excited electronic states and to the ground state. The density of vibronic states of these lower configurations is determined by two factors:

(a) The number of vibrational degrees of freedom.

(b) The energy gap between the zeroth vibronic levels of the two electronic states.

The density of vibronic states at energy  $\Delta E$  above the origin of an electronic state can be approximated by the semiclassical expression in the harmonic approximation<sup>27</sup>:

$$\rho = \frac{\Delta E^{n-1}}{(n-1)!} \prod_{i=1}^n (hv_i)^{-1} \left( 1 + \frac{h}{2} \sum_i v_i / \Delta E \right)^{-1} \quad (\text{III.5})$$

where  $n$  is the number of the vibrational degrees of freedom, characterized by the frequencies  $v_i$ . To obtain some feeling for the order of magnitude of the density of these background states we have displayed in *Table 1* estimates

*Table 1.* Density of vibrational states in a series of hypothetical polyatomic molecules where all  $v_i = 1000 \text{ cm}^{-1}$  and  $\Delta E = 1 \text{ eV}$ .

No. of atoms	$\rho$ cm
3	0.06
4	4
5	50
6	400
10	$4 \times 10^5$

of the vibrational density of levels in a hypothetical polyatomic molecules, characterized by an energy gap of 1 eV, while in *Table 2* we have assembled

*Table 2.* Densities of vibronic states in some aromatic hydrocarbons.

System	lower state	upper state	$\Delta E$ $\text{cm}^{-1}$	$\rho$ $\text{cm}$
Anthracene	$^3B_{2u}$	$^1B_{2u}$	12000	$5 \times 10^{10}$
Naphthalene	$^1B_{3u}$	$^1B_{2u}$	3400	$2 \times 10^3$
Naphthalene	$^1A_{1g}$	$^3B_{2u}$	20000	$8 \times 10^{15}$
Azulene	$^1A_1$	$^1B_1$	14000	$10^{11}$
Benzene	$^3B_{1u}$	$^1B_{2u}$	8400	$8 \times 10^4$

some data for real physical systems. Obviously in view of the overwhelmingly large densities of vibronic states encountered in large molecules we expect that even small coupling matrix elements (equation III.2) will lead to appreciable level mixing. Under these common circumstances, when a discrete zero order level is quasidegenerate with a background manifold of vibronic states, the Born–Oppenheimer separability conditions break down.

Thus in general the excited electronic states of large molecules cannot be considered as 'pure' BO states.

One has to distinguish very carefully between the consequences of intramolecular coupling and intramolecular relaxation. In particular, it should be borne in mind that coupling can be exhibited while relaxation does not occur. We shall, therefore, attack the problem in two steps which will be analogous to the general problem of relaxation already considered.

- (a) The molecular eigenstates of the system will be constructed<sup>28-30, 2a, 15</sup>.
- (b) The conditions for irreversible decay will be then established<sup>30-32, 15</sup>.

#### IV. MOLECULAR EIGENSTATES

A proper representation of the molecular eigenstates  $\psi_n$ , can be obtained from a superposition of zero order Born–Oppenheimer states.

$$\psi_n = a_s^n \phi_s + \sum_l b_l^n \phi_l \quad (\text{IV.1})$$

The Hamiltonian is given by

$$H_{el} = H_{BO} + H_V \quad (\text{IV.2})$$

where  $H_{BO}$  corresponds to the Born–Oppenheimer Hamiltonian while  $H_V$  contains the nuclear kinetic energy, spin–orbit coupling etc.  $\phi_s$  and  $\{\phi_l\}$  are eigenstates of  $H_{BO}$ . Notice how the near degeneracy of levels in a large molecule resembles the situation encountered in the treatment of the pseudo Jahn–Teller effect. However, in the present case the coupling between many quasidegenerate zero order states must be considered rather than that between only a few states. The configuration interaction scheme<sup>15, 28</sup> employed herein is similar to the treatments employed many years ago by Rice<sup>17</sup> in the study of predissociation, and by Fano<sup>16</sup> in the study of autoionization. However, it should be stressed that unlike the cases of autoionization and predissociation, in the present case the dense manifold of states is discrete.

The model I would like to discuss is grossly oversimplified but transparent. First we assume that the levels in the  $\{\phi_l\}$  manifold are equally spaced with spacing  $\rho^{-1}$ . This is not too bad. However the second assumption is rather serious. We shall assume that all the coupling terms are equal and set  $v_{sl} = \langle \phi_s | H_{el} | \phi_l \rangle = v$ . This immediately leads to a simple eigenvalue problem:

$$\begin{pmatrix} E_s - E & v & v \dots & \\ v & E_1 - E & 0 \dots & \\ v & 0 & E_2 - E \dots & \\ \vdots & \vdots & \vdots & \end{pmatrix} \begin{pmatrix} a_s \\ b_1 \\ b_2 \\ \vdots \end{pmatrix} = 0 \quad (\text{IV.3})$$

The solutions for the energies  $E_n$  of the molecular eigenstates (III.1) can be obtained from the equation:

$$E_s - E_n - \pi v^2 \rho \operatorname{Cotan}[\pi \rho(E_s - E_n)] = 0 \quad (\text{IV.4})$$

which can be solved numerically. The expansion coefficients representing

## RADIATIONLESS TRANSITIONS

the weights of the zero order states  $\phi_s$  in the molecular eigenstate  $\psi_n$  are given by :

$$|a_s^n|^2 = \frac{v^2}{(E_n - E_s)^2 + v^2 + (\pi v^2 \rho)^2} \quad (IV.5)$$

Two points have to be made at this stage :

(a) The choice of the BO basis set to describe the molecular eigenstates is arbitrary but extremely useful. In principle all the eigenstates of  $H_0$  have to be included in (IV.1). In the BO representation the admixture of higher excited states (whose electronic origin is located above  $\phi_s$ ) will be very small. On the other hand if we had chosen a poor zero order representation which involves electronic wavefunctions at a fixed nuclear configuration (the 'crude adiabatic approximation')<sup>34</sup> the admixture of these higher states which are not quasidegenerate with  $\phi_s$  would have become important.

(b) The zero-order BO state  $\phi_s$  plays a special role as this state carries oscillator strength from the ground state while the manifold  $\{\phi_l\}$  is devoid of oscillator strength. Thus the intensity distribution in absorption will be determined by  $|a_s^n|^2$ .

The following comments should be made at this point concerning the square of the expansion coefficient (IV.5):

- (a) The distribution is Lorentzian.
- (b) The width  $\Delta$  of the distribution is given by the dominant term in the denominator which is either  $v^2$  or  $(\pi v^2 \rho)^2$ .
- (c) The condition for strong interstate coupling is

$$v\rho \gg 1 \quad (IV.6)$$

This condition implies, of course, that  $\Delta$  is determined by  $v^2 \rho$  rather than by  $v$  itself. Equation (IV.6) will be valid provided that one of the following situations is realized :

- (c1) Strong interaction with a sparse manifold or, alternatively,
- (c2) Relatively weak coupling with a dense manifold. Conditions (c1) or (c2) imply that the width of the distribution will be determined by the simple relation

$$\Delta = \pi v^2 \rho \quad (IV.7)$$

- (d) The criterion (IV.7) for strong mixing is just equivalent to the breakdown of the BO approximation (equation III.4).

When the strong electronic coupling condition applies, the intensity (in absorption) of the zero order states  $\phi_s$  is distributed among a manifold of molecular eigenstates. Two cases have to be considered :

- (1) *Coarsely spaced molecular eigenstates.* The levels are well separated relative to their radiative and inhomogenous widths<sup>2e</sup>. The individual transition moments will be given by :

$$|\langle \phi_0 | \mu | \psi_M \rangle|^2 = |a_s^n|^2 |\langle \phi_0 | \mu | \phi_s \rangle|^2 \quad (IV.8)$$

Thus the intensity is distributed over a coarsely spaced well resolved manifold of states.

- (2) *The statistical limit.* The molecular eigenstates are densely spaced relative to their radiative widths and equation (IV.6) is valid. Now, we cannot

expect to resolve individual levels in the optical spectrum. The following implications are evident:

(2a) The line shape in absorption is:

$$A(E) \propto \rho |a_s^n|^2 = \frac{v^2 \rho}{(E - E_s)^2 + (\pi v^2 \rho)^2} \quad (\text{IV.9})$$

(2b) The absorption line shape is Lorentzian, the half line width being given by (VI.7).

(2c) The Lorentzian line shape is due to the fact that the background continuum does not carry oscillator strength.

(2d) The situation in this case is completely analogous to the Lorentzian distribution of amplitudes and the line shape obtained for a single resonance which results from the interaction with a 'real' continuum (see section II). Thus the dense quasicontinuum acts as an effective continuum.

This situation will be referred to as *The Statistical Limit*.

To conclude this discussion it is interesting to point out that the description, presented herein, of the strong interstate coupling in molecules bears a close resemblance to the problem of intermediate structure in nuclear reactions<sup>35</sup>. In the latter case compound states of the nucleus are constructed as a superposition of a single excitation and more complex excitations in a manner completely analogous to equation (IV.1). The single excitation which can be reached via the incident channel is referred to as a 'doorway state' and is formally analogous to the BO state  $\phi_s$  in the molecular case.

## V. DIFFUSENESS AND INTERFERENCE EFFECTS IN THE ELECTRONIC SPECTRA OF LARGE MOLECULES

We shall now consider the implications of the effects of intramolecular interstate coupling in molecules for the understanding of the intensity distribution in absorption.

(a) *Strongly coupled sparse manifold*. Singlet excited states of small molecules such as SO<sub>2</sub>, NO<sub>2</sub> or CS<sub>2</sub> are quasidegenerate with a relatively low density of vibronic states belonging to the lower triplet state and the ground state. However, because of favourable Franck-Condon vibrational overlap factors (due to changes in the molecular geometry in the excited states) the vibronic coupling terms are quite large. Thus, we expect that  $v\rho > 1$ . The occurrence of vibronic coupling in moderately small molecules implies the redistribution of the intensity of the zero order component  $\phi_s$ , and this redistribution induces the appearance of many new lines (corresponding to all the molecular eigenstates  $\psi_n$ ) into the spectrum. A situation of this type probably explains the high resolution spectrum of NO<sub>2</sub>, where a large number of irregularly spaced lines is observed. The general conclusions cited concur with those of Douglas<sup>36</sup>.

(b) *The statistical limit*: The breakdown of the BO approximation in the statistical limit results in line broadening which arises from a differential distribution of intensity among a large number of closely spaced molecular eigenstates. This 'diffuseness' of the spectral lines occurs as an intramolecular phenomenon.

What are the experimental implications of this result for spectroscopic studies of large molecules?

## RADIATIONLESS TRANSITIONS

(a) *Intravalance excitations.* Intramolecular coupling with a dense vibronic manifold leads to broadening of higher excited states arising from intravalance excitations in large molecules. To assess the role of intramolecular coupling on the line broadening 'trivial' broadening effects have to be eliminated. In the elegant work of Ross *et al.*<sup>37</sup> the following 'irrelevant' broadening mechanisms in the gas phase spectra of large molecules were considered:

- (i) Doppler width
- (ii) Rotational broadening
- (iii) Spectral congestion
- (iv) Photo dissociation
- (v) Non-radiative decompositions (autoionization and predissociation).

In solid-state spectra of molecules trapped in low temperature matrices effects (i), (ii) and (iii) are missing; however the following additional sources of broadening have to be taken into account:

- (vi) Phonon broadening, which can be eliminated by utilization of Spolski matrices for the observation of zero phonon lines.
- (vii) Vibrational relaxation of higher vibronic components.
- (viii) Site splittings.

Ross *et al.*<sup>23-25, 38</sup> have systematically demonstrated that no trivial mechanism can explain the diffuseness of higher intravalance excitations in the gas phase.

(b) *Extravalance excitations.* The situation with respect to line broadening is radically different when extravalance excitations, such as transitions to molecular Rydberg states in large molecules are considered. In the gas phase, these absorption lines corresponding to the Rydberg levels are quite sharp<sup>39</sup>. Thus, for example, the line widths of the 3R Rydberg states of benzene are of the order of a few  $\text{cm}^{-1}$ , i.e. about one or two orders of magnitude lower than the line widths of the  $\pi \rightarrow \pi^* {}^1A_{1g} \rightarrow {}^1E_{1u}$  transition. The situation is reminiscent of relatively weak vibronic coupling in these Rydberg states. This observation can be easily rationalized by noting that the vibronic coupling terms involve one electron operator of the form  $\sum_k \partial V / \partial Q_k$  where  $V$  is the molecular coulomb potential energy while  $\{Q_k\}$  correspond to the nuclear coordinates (see Section IV). Hence the coupling between the large radius Rydberg orbital and the ground state orbital via the  $\partial V / \partial Q_k$  terms is expected to be relatively weak.

(c) *Interference between resonances.* Even when the background quasi-continuum does not carry intensity interesting effects are expected to be encountered when the widths of several Lorentzians (e.g. several vibrational components in a given electronic state) exceed their spacings. Under these circumstances, we cannot limit ourselves to a single resonance as interference effects between resonances are expected to be encountered<sup>31</sup>. No definite experimental evidence for this effect in molecular spectra is at present available.

(d) *Intermediate structure:* Electronic states of large molecules which are characterized by a small electronic energy gap reveal some interesting structure in the optical absorption. Thus the second singlet excited state of the naphthalene molecule which is separated by about  $3000 \text{ cm}^{-1}$  from the

first singlet exhibits some relatively sharp lines superimposed on a diffuse background<sup>40</sup>. This fine-structure is sensitive to the nature of the host crystal (which affects the energy gap) and to the isotopic composition of the molecule. Now, it is obvious that in real life not all the states in the  $\{\phi_l\}$  manifold couple to the  $\phi_s$  with the same strength. In the statistical limit this problem is of minor importance; however in the present intermediate case these strongly coupled levels will borrow most of the oscillator strength and will be resolved in the spectrum.

(e) *Interference with background absorption.* Up to this point we have considered only an isolated resonance. In this case, the 'background' states  $\{\phi_l\}$  do not carry out oscillator strength so that no Fano-type interference effects are expected to be revealed in the optical spectrum. An interesting relevant situation is encountered when Rydberg levels overlap an inhomogeneously broadened  $\pi \rightarrow \pi^*$  transition. Such a situation prevails for the  $2R$  Rydberg state of benzene which in the gas phase is quasidegenerate with the  ${}^1A_{1g} \rightarrow {}^1E_{1u}\pi \rightarrow \pi^*$  transition<sup>41</sup>. In the case of the naphthalene molecule, the  $n = 5$  to  $n = 13$  Rydberg levels overlap a medium intensity ( $f \sim 0.1$ ) transition located near  $62000 \text{ cm}^{-1}$ . The gas phase optical spectrum of naphthalene, as reported recently by Angus, Christ and Morris<sup>41</sup>, reveals several sharp antiresonances. Morris and Jortner<sup>42</sup> discussed the nature of the interference effects which give rise to this unique behaviour in the optical spectrum of an isolated large molecule<sup>42</sup> between resonance and potential scattering.

## VI. INTRAMOLECULAR NON-RADIATIVE DECAY

We now study some of the consequences of statistical mixing, and consider the time development of coherently excited states. The molecule in the ground state is subjected to a radiative perturbation, which in the dipole approximation is

$$H'(t) = \mu \cdot \epsilon \delta(t) \quad (\text{VI.1})$$

where  $\epsilon$  is the electric field acting on the molecule. For simplicity we have used a delta function excitation. The excited state at time  $t = 0$  can be described in terms of a superposition of molecular eigenstates:

$$\Psi(t=0) = \sum_n \mu_{0n} \psi_n \quad (\text{VI.2})$$

where  $\mu_{0n}$  is the transition dipole moment to the molecular eigenstate  $\psi_n$ , which can be displayed in the form

$$\mu_{0n} = a_s^n \mu_{s0} \quad (\text{VI.3})$$

The wave function at time  $t$  is given by

$$\Psi(t) = \sum_n \mu_{0n} \psi_n \exp(-iE_n t / \hbar) \quad (\text{VI.4})$$

Consider now the time development of the amplitude of the zero order state  $\phi_s$  in the excited state which is given by

$$P(t) = |\langle \phi_s | \Psi(t) \rangle|^2 = \frac{\mu_{0s}^2}{\hbar^2} |s(t)|^2 \quad (\text{VI.5})$$

## RADIATIONLESS TRANSITIONS

In the kernel  $S(t)$  is :

$$S(t) = \sum_n |a_s^n|^2 \exp(-iE_n t/\hbar) \quad (\text{VI.6})$$

so that the relaxation rate will be determined by the Fourier transform of the line shape function  $|a_s^n|^2$ . Under the limiting conditions

$$v\rho \gg 1 \quad (\text{VI.7})$$

$$t \ll \hbar\rho \quad (\text{VI.8})$$

The relaxation process is exponential

$$P(t) \propto \exp(-t/\tau_{nr}) \quad (\text{VI.9})$$

where the non-radiative decay time is given by the Fermi Golden Rule :

$$\tau_{nr} = \hbar/2\pi v^2 \rho \quad (\text{VI.10})$$

Up to this point we have considered the relaxation process within the framework of a simple model system. A more general treatment can be easily performed which, as in the case of the absorption coefficient (section V), will lead to a more general criterion for the validity of the statistical limit. Consider again the alternative representation of  $\Psi(t)$  in terms of the BO basis set. Making use of the orthonormality properties of the expansion coefficients  $a_s^n$  and  $b_i^n$  in equation (IV.1), the initial state (VI.2) can then be represented in the form :

$$\Psi(t=0) = \mu_{0s}\phi_s \quad (\text{VI.11})$$

The time evolution of the excited state can now be displayed as the time dependent superposition

$$\Psi(t) = A(t)\phi_s + \sum_l B_l(t)\phi_l \quad (\text{VI.12})$$

Making use of conventional time dependent perturbation theory results in the equation of motion for the amplitude  $A(t)$ :

$$\begin{aligned} \hbar^2 \dot{A}(t) &= - \int_0^t dt' A(t') \sum_l |v_{sl}|^2 \exp\left[\frac{i(E_l - E_s)(t - t')}{\hbar}\right] \\ &= - 2\pi \iint dE dt' A(t') \sum_l |v_{sl}|^2 \exp\left[\frac{i(E - E_s)(t - t')}{\hbar}\right] \delta(E - E_l) \\ &= - \iint dE dt' A(t') \Delta(E) \exp\left[\frac{i(E - E_s)(t - t')}{\hbar}\right] \end{aligned} \quad (\text{VI.13})$$

where

$$\Delta(E) = 2\pi \sum_l |v_{sl}|^2 \delta(E - E_l) \quad (\text{VI.14})$$

In the statistical limit  $\Delta(E)$  is the slowly varying function of the energy<sup>33, 43</sup> and thus we set it to be a constant  $\Delta = \Delta(E)$ . The expression for  $\Delta(E)$  in the

statistical limit is just the half line width (IV.7). One now immediately obtains the exponential decay law :

$$|A(t)|^2 = |A(0)|^2 \exp(-t/\tau_{nr}) \quad (\text{VI.15})$$

## VII. IRREVERSIBLE INTRAMOLECULAR DECAY IN THE STATISTICAL LIMIT

When the background density of vibronic states in a large molecule is extremely high this manifold is expected to act as an effective continuum with respect to line broadening and to intramolecular relaxation. The general criteria obtained for the statistical limit can be summarized as follows:

$$v\rho \gg 1 \quad (\text{VII.1})$$

$$t \ll \hbar\rho \quad (\text{VII.2})$$

$$\Delta(E) = 2\pi \sum_l |v_{sl}|^2 \delta(E - E_l) \quad (\text{VII.3})$$

is smooth.

It should be borne in mind that while conditions (VII.1) and (VII.2) were obtained for a simple model system, equation (VII.3) is general and model independent. The simple model calculations provide us with physical insight concerning the general features of the non-radiative decay process which can be summarized as follows:

(a) Equation (VII.1) provides a necessary condition for line broadening and for the occurrence of intramolecular non-radiative decay: however, this energetic condition is by no means sufficient.

(b) The relation (VII.2) establishes the time scale for the occurrence of the non-radiative decay. In fact  $t_R = \hbar\rho$  corresponds to the recurrence time for the decay of the zero order level  $\phi_s$  into the quasicontinuum. For times longer than  $t_R$ , the amplitude of  $\phi_s$  in  $\Psi(t)$  will increase towards its initial value. However, for large molecules these recurrence times considerably exceed the time scale of any experiment.

(c) The definition of the recurrence time introduces the notion of irreversibility of the intramolecular radiationless process. This recurrence time introduces a Poincare cycle for the irreversible process. An intramolecular radiationless process in the limit of a sufficiently large density of vibronic levels corresponds to an irreversible process on a time scale which is shorter than  $t_R$ .

(d) Electronic relaxation in large molecules (see *Table 3*) obeys the restrictions (VII.1) and (VII.2). Thus these can be considered as legitimate intramolecular relaxation phenomena.

Obviously the simple relations (VII.1) and (VII.2) are gross oversimplifications based on a 'coarse graining' procedure. Let us consider now a real physical system where the necessary and sufficient condition for irreversible non-radiative decay is given by the 'smoothness' of  $\Delta(E)$  (equation VII.3). This restriction is more general and enables us to ascertain the salient features of the intramolecular decay in a large molecule. We note that a 'hidden assumption' involved in the simple model calculations implies that the zero states  $\{\phi_{l0}\}$  have zero widths. If these levels are characterized by

## RADIATIONLESS TRANSITIONS

*Table 3.* Parameters descriptive of radiationless transitions in large molecules.

System	$\tau_{nr}$ sec	$v$ $\text{cm}^{-1}$	$\rho$ $\text{cm}$	$v\rho$	$\hbar\rho$ sec
Anthracene $^1B_{2u} - ^3B_{2u}$ $E = 12000 \text{ cm}^{-1}$	$5 \times 10^{-9}$	$6 \times 10^{-7}$	$5 \times 10^{10}$	$3 \times 10^{10}$	0.25
Naphthalene $^3B_{2u} - ^1A_{1g}$ $E = 20000 \text{ cm}^{-1}$	2	$10^{-14}$	$8 \times 10^{15}$	80	$4 \times 10^4$
Azulene $^1B_1 - ^1A_1$ $E = 14000 \text{ cm}^{-1}$		$6 \times 10^{-11}$	$2 \times 10^{-5}$	$10^{11}$	$2 \times 10^6$
Benzene $^1B_{2u} - ^3B_{1u}$	$10^{-6}$	$1.5 \times 10^{-5}$	$8 \times 10^4$	1.5	$4 \times 10^{-7}$

finite widths  $\{\Gamma_l\}$  then the resonance width should be altered by replacing each delta function in the sum (VII.3) by a Lorentzian<sup>33, 43</sup>:

$$\Delta(E) = \sum_l \frac{(\Gamma_l/2)|v_{sl}|^2}{(E - E_l)^2 + (\Gamma_l/2)^2} = I_m \sum_l \frac{|v_{sl}|^2}{(E - E_l) + i\Gamma_l/2}$$

Obviously when  $\Gamma_l \rightarrow 0^+$  we regenerate equation (VII.3). In order to consider an upper limit  $t_m$  for the decay process, Freed<sup>43</sup> adds an imaginary part  $i\hbar/t_m$  to the energy  $E$  so that

$$E \rightarrow E + \frac{\hbar}{t_m} \quad (\text{VII.4})$$

Such a trick is common in scattering theory and amounts to describing the decay process in terms of a (complex) Green's function  $G(E + i\hbar/t_m)$ . Usually one sets  $\hbar/t_m \rightarrow 0^+$ ; however as pointed out by Freed<sup>43</sup>, this is not really necessary, as the inclusion of the imaginary factor introduces a term of the form  $\exp(-t/t_m)$  in the decay process and thus erases all the behaviour of the system for long times, e.g.  $t \gg t_m$ .

The general form of the resonance width is then

$$\Delta(E) = \sum_l \frac{|v_{sl}|^2 \left( \frac{\Gamma_l}{2} + \frac{\hbar}{t_m} \right)}{(E - E_l)^2 + \left( \frac{\Gamma_l}{2} + \frac{\hbar}{t_m} \right)^2} \quad (\text{VII.5})$$

This result exhibits a superposition of generalized Lorentzians, each characterized by the strength  $|v_{sl}|^2$  and by the width

$$\frac{\Gamma_l}{2} + \frac{\hbar}{t_m} .$$

A general condition for the smoothness of  $\Delta(E)$  is that the widths of successive Lorentzians considerably exceed their spacings. Stated mathematically

$$\frac{\Gamma_l}{2} + \hbar/t_m \gg E_{l+1} - E_l \sim \hbar/\rho \quad (\text{VII.6})$$

Hence the general condition for irreversibility will be displayed in the form:

$$\rho^{-1} \ll \hbar/t_m + \Gamma_l/2 \quad (\text{VII.7})$$

The following cases should now be considered:

(a) Intersystem crossing in the lowest triplet in an isolated molecule. In this case the line widths  $\Gamma_l$  are negligibly small, as the levels  $\{\phi_l\}$  do not carry oscillator strength to the ground state or to any of its vibronic components. Setting  $\Gamma_l \rightarrow 0^+$  one immediately obtains the simple relation (VII.2).

(b) Internal conversion in an isolated molecule. Now the dense manifold  $\{\phi_l\}$  is connected by nonvanishing radiative coupling terms to high vibronic levels of the ground state. This is, of course, the reason for the observation of fluorescence radiation from the second (and any higher) singlet to high vibrational levels of the ground state. Hence  $\Gamma_l > 0$ . Two pertinent cases have to be considered:

(a2) A large energy gap between two excited states of the same multiplicity. Thus for example the first ( ${}^1B_{2u}$ ) and the second ( ${}^1B_{3u}^+$ ) singlet excited states of anthracene are separated by  $\Delta E = 15000 \text{ cm}^{-1}$ . In this case we expect that

$$\Gamma_l \gg \rho^{-1} \quad (\text{VII.8})$$

and the function  $\Delta(E)$  is smooth on any time scale as we can set  $t_m \rightarrow \infty$ .

(b2) A small energy gap between two states of the same multiplicity. A good example in this category involves the  ${}^1B_{2u}$  and the  ${}^1B_{3u}$  excited states of the naphthalene molecule where the energy gap is  $\Delta E = 3400 \text{ cm}^{-1}$ . In this case  $\rho^{-1} \sim 10^{-3} \text{ cm}^{-1}$ . Now  $\rho^{-1} \gg \Gamma_l$  and again the condition  $t_m \ll \hbar\rho$  has to be applied for the decay of the  ${}^1B_{2u}$  state.

(c) Internal conversion and intersystem crossing in a condensed medium. Getting away from the isolated molecule and considering for a moment the medium effects at low temperatures, we note that now  $\Gamma_l$  has a substantial contribution ( $10^{-2}$ – $10^{-1} \text{ cm}^{-1}$ ) due to vibrational relaxation. Hence the condition  $\Gamma_l \gg \rho^{-1}$  is usually satisfied. We can neglect  $t_m^{-1}$  with respect to  $\Gamma_l$  and the decay process is irreversible for long times. Obviously, states which correspond to intermediate cases for the molecule in the low pressure gas phase will reveal irreversible decay when the molecule is embedded in a medium.

To summarize this discussion, the following relations are of interest:

(a) For the case of intersystem crossing

$$\tau_{rad}(l) \gg \hbar\rho \gg t_m \gg \tau_{rad}(s)$$

(b1) For internal conversion (large energy gap):

$$\infty \leftarrow t_m \gg \hbar\rho \gg \tau_{rad}(l) \sim \tau_{rad}(s).$$

(b2) For internal conversion (small energy gap):

$$\tau_{rad}(s) \sim \tau_{rad}(l) \gg \hbar\rho \gg t_m$$

(c) For a molecule in a dense medium:

$$\infty \leftarrow t_m \gg \hbar\rho \gg \tau_{rad}(s) \geq \tau_{v,r}(l)$$

## RADIATIONLESS TRANSITIONS

where  $\tau_{rad}$  and  $\tau_{v,r}$  correspond to lifetimes due to radiative decay and to vibrational relaxation, respectively.

### VIII. THE COUPLING BETWEEN RADIATIVE AND NON RADIATIVE PROCESSES IN LARGE MOLECULES

A large bulk of physical information now available concerning intramolecular coupling and electronic relaxation in polyatomic molecules comes from lifetimes of molecular luminescence. Clearly, a complete theoretical description of the radiationless transition process should emerge from the description of the radiative decay. It should be recalled that we are now considering a phenomenon associated with the decay of a manifold of a large number of closely spaced levels<sup>44-53</sup> (e.g. the molecular eigenstates).

We shall now consider a simplified version of the theory of the radiative decay of polyatomic molecules<sup>29-33</sup>. One pedantic comment should be made at this point concerning the molecular eigenstates representation. When radiative decay processes are considered the molecular eigenstates are no longer proper eigenstates of the Hamiltonian

$$H = H_{el} + H_n + H_{in+} \quad (\text{VIII.1})$$

As before, the molecular Hamiltonian,  $H_{el}$ , consists of the BO term  $H_{BO}$  and an intramolecular perturbation  $H_v$  (vibronic, spin-orbit, etc.).  $H_r$  is the Hamiltonian corresponding to the free radiation field while  $H_{int}$  is the radiation-matter interaction term. The time evolution of a nonstationary state of the system can be described either in terms of the eigenstates of  $H_{BO}$  (the BO basis set) or of  $H_{el}$  (the molecular eigenstates basis). Obviously, the choice of the basis set is merely a matter of convenience and thus does not affect any observable quantities. The questions that have to be answered by a complete study of the radiative decay of a polyatomic molecule are as follows:

- (a) Are simple kinetic schemes, as applied for years by the experimentalist, adequate?
- (b) When will interference effects be observed in the radiative decay?
- (c) How can details of the decay process (e.g. quantum yields and experimental radiative lifetimes) be elucidated?

In order to handle the radiative decay of a large molecule, consider the initial excited state at time  $t = 0$  which is a nonstationary state of  $H$ , and no photons are present. The initial excited molecular state  $\Psi_m(0)$  can always be expressed as a superposition of either the molecular eigenstates  $\{\psi_m\}$  or the BO states  $\phi_s, \{\phi_l\}$ . The initial state of the system is:

$$\begin{aligned} \Psi(0) = \Psi_m(0)|vac\rangle &= \sum_n a_n(0)|\psi_n; vac\rangle = b_s(0)|\phi_s; vac\rangle \\ &\quad + \sum_{l \neq s} b_l(0)|\phi_l; vac\rangle \end{aligned} \quad (\text{VIII.2})$$

where  $|vac\rangle$  is the zero photon state. In many cases of physical interest the initial excited state of the system can be visualized as being prepared by a coherent excitation, by a short light pulse or by a chaotic broad band source whereupon:

$$\begin{aligned} a_n(0) &= \langle \phi_s | \psi_n \rangle \\ b_l(0) &= \delta_{ls} \end{aligned} \quad (\text{VIII.3})$$

Obviously, the completeness of the molecular eigenstates basis and the fact that  $\phi_s$  is the only state which carries oscillator strength immediately imply that in this case:

$$\Psi(0) = \sum_n \langle \phi_s | \psi_n \rangle |\psi_n; vac\rangle \equiv |\phi_s; vac\rangle \quad (\text{VIII.4})$$

We now proceed to provide a simple description of the decay process. A more elaborate treatment was recently provided by Freed and Jortner. The final states of the system consist of one photon ground state  $\phi_{k,e} = |\phi_0; k, e\rangle$  where  $\phi_0$  is the ground electronic state while  $k$  and  $e$  correspond to the wave vector and the polarization vector of the emitted photon. The time dependent state of the system is given by:

$$\begin{aligned} \Psi(t) = & \sum_n a_n(t) |\psi_n; vac\rangle + \sum_k \sum_e c_{ke}(t) |\phi_0; k, e\rangle \equiv b_s(t) |\phi_s; vac\rangle \\ & + \sum_{l \neq s} b_l(t) |\phi_l; vac\rangle + \sum_k \sum_e d_{ke}(t) |\phi_0; k, e\rangle \end{aligned} \quad (\text{VIII.5})$$

with the initial conditions given by equation (VIII.3) and  $c_{k,e}(0) = d_{k,e}(0) = 0$  for all  $k$  and  $e$ . The probability  $A_s(t)$  for the decay of the system is given by:

$$A_s(t) = |\langle \Psi(0) | \Psi(t) \rangle|^2 \quad (\text{VIII.6})$$

Making use of the initial conditions (VIII.3) we get for the decay rate of the excited state, which corresponds to the total number of photons emitted per unit time:

$$\dot{Q}(t) = \frac{\Gamma_s}{\hbar} |A_s(t)|^2 = \frac{\Gamma_s}{\hbar} \left| \sum_n a_n(t) a_n(0) \right|^2 \equiv \frac{\Gamma_s}{\hbar} |b_s(t)|^2 \quad (\text{VIII.7})$$

where  $\Gamma_s$  is the radiative width of the zero order state  $\phi_s$ , equation (VIII.7) reveals the following features of the decay process:

(a) When the BO basis set is employed we have to focus our attention on the decay channels of the zero order state  $\phi_s$ .

(b) When the molecular eigenstates basis is used the decay rate contains a contribution from interference effects between closely spaced levels.

Equation (VIII.5) provides us with a proper description of the time dependent compound state of the system which is presented as a superposition of time independent zero order states. In order to elucidate the features of the decay process we have to establish the equations of motion for the coefficients  $\{a_n(t)\}$  or  $\{b_s(t), b_l(t)\}$ . This can be accomplished by the following methods:

(a) A self-consistent extension of the Wigner-Weisskopf method<sup>54</sup> to account for the decay of a large number of levels<sup>30</sup>.

(b) The ‘unitary relations’ method employed in the field of elementary particles physics<sup>56, 57</sup> which is based on general conservation rules<sup>30</sup>.

(c) The Fano configuration interaction method<sup>16</sup> whereupon the radiation field provides a dissipative continuum<sup>30, 31</sup>.

(d) The Green’s function method adopted to the decay of a large number of metastable levels<sup>33</sup>.

## RADIATIONLESS TRANSITIONS

All these methods lead to the following result: let the time dependent compound state be given in the general form

$$\Psi(t) = \sum_j \alpha_j(t) |\chi_j; vac\rangle + \sum_k \sum_e \beta_{k,e}(t) |\phi_{k,e}\rangle \quad (\text{VIII.8})$$

where the set  $\chi_j$  is any general complete set (molecular eigenstates, BO basis or other). If we define the row vector

$$\alpha(t) = \begin{pmatrix} \alpha_1(t) \\ \alpha_2(t) \\ \vdots \end{pmatrix} \quad (\text{VIII.9})$$

the equation of motion is <sup>30,55</sup>

$$i \frac{d}{dt} \alpha(t) = H_{eff} \alpha(t) \quad (\text{VIII.10})$$

$$H_{eff} = H_{el} - \frac{1}{2} \Gamma \quad (\text{VIII.11})$$

where  $\Gamma$  corresponds to the damping matrix. In discussing phenomena of radiative decay it is customary to introduce the radiative lifetime of states. The damping matrix  $\Gamma$  is defined for some (arbitrary) set of zero photon excited states in the form:

$$\Gamma_{jj'} = (2\pi/\hbar) \sum_k \int d\Omega_k \langle \chi_j; vac | H_{int} | \phi_{k,e} \rangle \langle \phi_{k,e} | H_{int} | \chi_{j'}; vac \rangle \rho_k \quad (\text{VIII.12})$$

where  $\sum_k \int d\Omega_k$  corresponds to the integration overall propagation direction in the  $k$  space and summation over all polarization directions of the emitted photon.  $\rho_k$  is the density of photon states. Thus equations (VIII.10) and (VIII.12) provide us with the general decay law for a manifold of closely spaced levels. The following comments are now in order:

- (a) The damping matrix provides a generalization of the Fermi 'Golden Rule' transition rates.
- (b) The damping matrix  $\Gamma$  is in general non-diagonal.
- (c) The matrix  $H_{eff}$  which determines the decay is non-hermitian (or rather antihermitian). This observation can be rationalized by noting that equation (VIII.10) factors out only a finite number of (zero photon) states of the system instead of considering the infinite number of states which characterize the Hamiltonian (VIII.1).
- (d) When a non-diagonal representation of  $H_{eff}$  is employed (which is usually the case) the states  $|\chi_j; vac\rangle$  do not decay independently, e.g. they cannot be characterized by simple exponential decays. This is the case provided that the off diagonal terms of the damping matrix are large, so that

$$\Gamma_{jj'} \gtrsim |E_j - E_{j'} - \frac{i}{2}(\Gamma_{jj} - \Gamma_{j'j'})| \quad (\text{VIII.13})$$

This effect is known in level crossing, where the decaying states are indistinguishable (e.g. characterized by the same symmetry).

- (e) In principle, one can find a set of zero photon states characterized by

exponential decay, provided that  $\mathbf{H}_{eff}$  is diagonalized by a complex orthogonal matrix  $\mathbf{S}$ , so that

$$\mathbf{S}\mathbf{H}_{eff}\mathbf{S}^{-1} = \mathbf{A} \quad (\text{VIII.14})$$

The real and imaginary parts of the diagonal matrix  $\mathbf{A}$  provide us with the energies and lifetimes respectively of the states for which  $\mathbf{H}_{eff}$  is diagonal.

(f) In the BO basis  $\{\phi_s, \phi_i\}$  the effective Hamiltonian is:

$$\begin{pmatrix} \left(E_s - \frac{i\Gamma_s}{2}\right) & v_{s1} & v_{s2} & \dots \\ v_{s1} & E_1 & 0 & \dots \\ v_{s2} & 0 & E_2 & \dots \\ \vdots & \vdots & \vdots & \ddots \end{pmatrix} \quad (\text{VIII.15})$$

so that  $\mathbf{H}_d$  is off diagonal while the damping matrix is diagonal.

(g) For the molecular eigenstate  $\{\psi_n\}$  basis the effective Hamiltonian is given in the form:

$$\begin{pmatrix} E_1 - \frac{i\Gamma_{11}}{2} & -\frac{i\Gamma_{12}}{2} & \dots \\ -\frac{i\Gamma_{21}}{2} & E_2 - \frac{i\Gamma_{22}}{2} & \dots \\ \vdots & \vdots & \ddots \end{pmatrix} \quad (\text{VIII.16})$$

Now  $\mathbf{H}_d$  is diagonalized; however, we pay the price by having the damping matrix in a non-diagonal representation.

This general formalism can be immediately applied for the following cases:

Table 4. Long radiative lifetimes of small molecules.

Molecule	Transition	$\tau(\text{expt.})$ sec	$\tau(\text{integrated } f)$ sec
$\text{NO}_2$	$^1B_2 - ^1A_1$ $4300 \text{\AA}$	$44 \times 10^{-6}$	$0.3 \times 10^{-6}$
$\text{SO}_2$	$3000 \text{\AA}$ $^1B_1 - ^1A_1$	$42 \times 10^{-6}$	$0.2 \times 10^{-6}$
$\text{CS}_2$	$3200 \text{\AA}$ $^1\Sigma - ^1\Sigma$ $^1\pi - ^1\Sigma$	$15 \times 10^{-6}$	$3 \times 10^{-6}$

(i) Long radiative lifetimes of triatomic molecules (see Table 4). Under these circumstances the levels in the  $\{\phi_i\}$  manifold are coarsely spaced, considerably exceeding the radiative widths of the molecular eigenstates. Application of the molecular eigenstates basis implies that for the off diagonal elements of the damping matrix

$$\Gamma_{nn'} \ll |E_n - E_{n'} - \frac{i}{2}(\Gamma_{nn} - \Gamma_{n'n'})| \quad (\text{VIII.17})$$

## RADIATIONLESS TRANSITIONS

so that these off diagonal terms are negligible. Thus in this limit we get:

$$(\mathbf{H}_{eff})_{nn'} = (E_n - \frac{i}{2}\Gamma_n)\delta_{nn'} \quad (\text{VIII.18})$$

where  $\Gamma_n$  is the radiative width of the molecular eigenstate  $\psi_n$  so that:

$$\Gamma_n \equiv \Gamma_{nn} = \Gamma_s |\langle \psi_n | \phi_s \rangle|^2 = \Gamma_n |a_s^n|^2 \quad (\text{VIII.19})$$

where the coefficient  $a_s^n$  is given by equation (IV.1).

The decay law is given by a sum of exponentials

$$\dot{Q}(t) = \sum_n |a_n(0)|^2 \exp(-\Gamma_n t/\hbar) \quad (\text{VIII.20})$$

Since  $|a_s^n|^2 < 1$  we have from equation (VIII.19)

$$\Gamma_n < \Gamma_s \quad \text{for all } n \quad (\text{VIII.21})$$

We thus have the explanation for the anomalously long radiative lifetimes of small molecules<sup>30</sup>. The occurrence of vibronic coupling in triatomic molecules implies the redistribution of intensity of the zero order component  $\phi_s$  and the 'dilution' of the decay times of the molecular eigenstates each of which now decays independently.

(ii) Short radiative lifetimes of large molecules.

In the statistical limit the decay law is

$$\dot{Q}(t) = (\Gamma_s/\hbar) \exp(-\{\Gamma_s + \Delta/\hbar\}t) \quad (\text{VIII.22})$$

Thus the radiative decay in the statistical limit is exponential and the experimental radiative decay time consists of independent contributions from non-radiative and radiative components.

The quantum yield determined on a time scale appreciably shorter than the recurrence time is given in the form:

$$Y = \Gamma_s / (\Gamma_s + \Delta) \quad (\text{VIII.23})$$

This does not imply that the large molecule acts as a photon trap, but rather that only a fraction  $Y$  of photons will be emitted on the time scale  $t \ll \hbar\rho$ , or stated more generally, on the time scale  $t \ll t_m$  (see section VII).

To conclude this discussion of the statistical limit we should notice that two legitimate complementary descriptions of the decay of an excited state of a large molecule can be given:

(1) Interference effects between a large number of closely spaced zero order levels (e.g. the molecular eigenstates) give rise to the shortening of the radiative lifetime.

(2) The excited state corresponds to a resonance which is coupled to two different continua. Just as the photon continuum allows for irreversible radiative decay, the  $\{\phi_i\}$  manifold acts as a second dissipative channel.

To conclude this discussion we shall briefly consider the general features of radiative decay of polyatomic molecules.

Intramolecular coupling, intramolecular relaxation and no observable radiative interference effects are expected in the following cases:

(a) *Intramolecular radiationless decomposition*. In the well understood cases of predissociation and autoionization we encounter a conventional

relaxation phenomenon. Line broadening is observed and the branching ratio for fluorescence is lower than unity. Obviously, the reduction of emission is a much more sensitive criterion for radiationless decomposition than line broadening.

(b) *The statistical limit.* In large molecules the dense quasi-continuum can be considered for all practical purposes as an effective decay channel. Line broadening and intramolecular relaxation effects are exhibited in this limit.

Intramolecular coupling will be exhibited while no intramolecular relaxation and no radiative interference effects will be observed in the following cases:

(c) *Accidental degeneracy* of two levels corresponding to different electronic terms in a diatomic molecule. A small molecule may exhibit the effects of strong vibronic perturbations between pairs of accidentally degenerate levels. These perturbations considerably exceed the radiative width. A complex spectrum results which is sensitive to external fields; however no radiative interference effects will be exhibited. A typical example involves  $^2\Sigma - ^2\Pi$  mixing in the CN molecule<sup>58</sup>.

(d) *Sparse intermediate case.* The density of vibronic states in the  $\{\phi_i\}$  manifold is rather small ( $\rho \sim 1 \text{ cm}^{-1}$ ); however the coupling matrix elements are large. The situation corresponds to the coarse strongly coupled distribution discussed in section IV. These small molecules will exhibit long radiative lifetime<sup>35</sup>.

Finally we have to consider the circumstances whereupon radiative interference effects will (or may) be observed:

(e) *The resonance limit.* A pair of levels which split by intrinsic or external perturbations and which are spaced within their radiative widths will exhibit quantum beats in the radiative decay.

(f) *The dense intermediate case.* A small electronic energy gap in a large molecule (e.g. the second excited singlet state of naphthalene and pyrene which are separated by  $3000 \text{ cm}^{-1}$  from the first singlet). In this case one has to consider separately the weakly and strongly coupled levels in the vibronic manifold  $\{\phi_i\}$ . Under these circumstances the width of the zero order state is shared between several closely spaced resonances. Several interesting effects can now be encountered for the radiative decay resulting from inter-system crossing in the isolated molecule which corresponds to this situation. Emission will take place from the highly excited vibronic component of the lowest singlet to high vibronic components of the ground state.

The following effects may be observable<sup>33</sup>:

(1) 'Lengthening' of the radiative lifetime of some strongly coupled components.

(2) A possible observation of quantum beats due to interference between a small number of closely spaced levels.

(3) Non-exponential decay due to 'smearing out' of the interference effects, when the number of the strongly coupled levels is too large (but insufficient for the validity of the statistical limit).

(4) Effects of external fields on the level mixing and the decay characteristics.

(5) All these phenomena will be erased when the molecule is embedded in a dense medium in view of external vibrational relaxation effects.

## RADIATIONLESS TRANSITIONS

In summary, we have presented in *Table 5* the experimental phenomena related to intramolecular coupling and intramolecular relaxation while *Table 6* presents some of the characteristic features of the radiative decay of small, medium sized and large molecules.

*Table 5.* Experimental phenomena related to intramolecular coupling and relaxation in molecules

Classification	Radiationless decomposition predissociation autoionization (a)	Sparse level distribution (b)	Dense intermediate case (c)	Statistical limit (d)
System	Small and large molecules	(a) $^2\pi-^2\Sigma$ coupling in CN (b) $\text{SO}_2, \text{NO}_2, \text{CS}_2$	Small gap in large molecules	Large gap in large molecules case (c) in solution
Experimental methods	(1), 2, (3), 6	1, 2, 3, 4, 5	1, 2, 3, 4 (5)	1, 2, 3, 4, 6
Intramolecular interstate coupling	+	+	+	+
Radiative interference	-	-	(+?)	-
Intramolecular relaxation	+	-	(+?)	+

- Experimental methods:
- (1) Decay times
  - (2) Line shapes or intensity distribution in absorption
  - (3) Fluorescence yields
  - (4) Fluorescence spectra
  - (5) External yields
  - (6) Population of final state

## IX. THE NON-RADIATIVE DECAY PROBABILITY AND THE ENERGY GAP LAW IN THE STATISTICAL LIMIT

The theory outlined in the preceding sections provides a unified formal description of electronic relaxation processes in large molecules. However, this formalism will be viewed with suspicion by the experimentalist as it does not provide predictions of the non-radiative decay probability. Furthermore, we have been concerned up to this point with electronic relaxation processes and have paid no attention to photochemical rearrangement reactions. Recently, a general theory of non-radiative processes was considered in the statistical limit by Lin and Bersohn<sup>26</sup> and by Englman and Jortner<sup>59a</sup>, and by Freed and Jortner<sup>59b</sup>; this is based on the following assumptions:

(a) A two electronic-level system was considered, consisting of a small number of levels  $\phi_{s1}, \phi_{s2} \dots$  etc. (the dynamic part) and the dissipative channel  $\{\phi_{lj}\}$ . The second index labels the vibrational states. The general form of the BO functions is

$$\phi_{\alpha\beta}(r, Q^{(\alpha)}) = \Theta_\alpha(r, Q^{(\alpha)}) \chi_{\alpha\beta}(Q^{(\alpha)}) \quad (\text{IX.1})$$

where  $r$  represents the electronic coordinates,  $Q^{(\alpha)}$  labels the nuclear normal coordinates in the electronic state  $\alpha$ , while  $\Theta_\alpha$ , and  $\chi_{\alpha\beta}$  represent electronic and vibrational wave functions.

Table 6. General features of the decay of molecular levels.

Physical Property	Resonance Limit	Sparse Case	Dense Case	Statistical Limit
Number of states $N = (\Delta/2\varepsilon) = \pi V^2 \rho^2$	---	$N > 1$	$N \sim 1$	$N \gg 1$
Level separation relative to radiation width	$\varepsilon \sim \Gamma_s$	$\rho^{-1} \gg \Gamma_s$	$\rho^{-1} \sim \Gamma_s$	$\rho^{-1} \ll \Gamma_s$
Line shape	Natural radiative + conventional broadening	Intensity distribution, well separated lines	Intermediate structure	Lorentzian line shape
Time scale $t$ relative to recurrence time	$t \sim \hbar/\varepsilon$	$t \gg \hbar\rho$	$t \sim \hbar\rho$	$\Delta = \pi V^2 \rho$
Mode of decay	Beat spectrum	Sum of (slowly varying) exponentials (?)	Oscillatory (beats)	Exponential
Mean radiative decay time	---	$\tau_e \sim (N\hbar/\Gamma_s)^(1/2)$	$\tau_e \sim \hbar/\Gamma_s(?)$	$\tau_e = (\hbar/\Delta + \Gamma_s)$
Experimental fluorescence quantum yield	$Y = 1$	$Y = 1$	$Y = 1$	$Y = (\Gamma_s/\Gamma_s + \Delta)$
Features of relaxation	External	External	External	Intramolecular
Examples	Level crossing SO <sub>2</sub> , NO <sub>2</sub> , CS <sub>2</sub>	Level anticrossing ?	?	$\tau_{NR} = \hbar/\Delta$ Anthracene Tetracene

## RADIATIONLESS TRANSITIONS

(b) Interference effects between the compound states constructed from each of the components of the dynamic part are disregarded. Hence, the non-radiative decay probability is displayed in the form:

$$\tau_{nr}^{-1} = \frac{2\pi}{\hbar} \sum_i \sum_j |V_{si, l_j}|^2 p(si) \delta(E_{si} - E_{l_j}) \quad (\text{IX.2})$$

where  $p(si)$  is the population of the initial state  $|si\rangle$  and the coupling matrix elements are

$$V_{si, l_j} = \langle \phi_{si} | H_v | \phi_{l_j} \rangle \quad (\text{IX.3})$$

(c) It was assumed that the normal modes and their frequencies are the same in the two electronic states except for displacements in the origin.

Let the normal coordinates be denoted by  $Q_j (j = 1 \dots N)$  with the effective masses  $M_j$  and frequencies  $\omega_j$ . The equilibrium configuration of the electronic state  $s$  is characterized by the configuration  $Q_j^{0(s)} (j = 1 \dots N)$ . Let  $\Delta Q_j^{(0)} = Q_j^{0(l)} - Q_j^{0(s)}$  correspond to the displacement of the  $Q_j$  normal coordinate in the equilibrium configuration of the electronic state  $l$  relative to the electronic state  $s$ . It will be also useful to define a set of dimensionless coordinates and displacements:

$$q_j = (M_j \omega_j / \hbar)^{\frac{1}{2}} (Q_j - Q_j^{0(s)}) \quad (\text{IX.4})$$

$$\Delta_j = (M_j \omega_j / \hbar)^{\frac{1}{2}} \Delta Q_j^{(0)} \quad (\text{IX.5})$$

(d) The molecular vibrations are harmonic and anharmonicity effects were disregarded. The adiabatic potentials  $W_s$  and  $W_l$  for the two electronic states are then given in the form:

$$W_s = \frac{1}{2} \sum_j \hbar \omega_j q_j^2 \quad (\text{IX.6})$$

$$W_l = \frac{1}{2} \sum_j \hbar \omega_j (q_j - \Delta_j)^2 - \Delta E = W_s - \sum_j \gamma_j q_j - \Delta E + E_M \quad (\text{IX.7})$$

The most important energy parameter introduced at this point is the *energy gap* between the lowest vibronic components of the two electronic states:

$$\Delta E = E_{s0} - E_{l0} \quad (\text{IX.8})$$

$\gamma_j = \hbar \omega_j \Delta_j$  corresponds to the linear coupling term for the  $j$ th mode. The energy term

$$E_M = \frac{1}{2} \sum_j \hbar \omega_j \Delta_j^2 \quad (\text{IX.9})$$

represents the molecular nuclear relaxation energy, or rather half the Stokes shift, due to the reduced displacement  $\Delta_j$ .

These assumptions seem to be rather pedestrian and were in fact used before. In spite of considerable activity in the field conventional computa-

tional methods as employed before cannot be expected to yield reliable information for a large molecule which is characterized by a large number,  $N$ , of vibrational degrees of freedom. In view of the complexity of the problem encountered in the calculation of  $\tau_{nr}^{-1}$  in the statistical limit, conventional 'quantum chemistry' type methods seem to be inadequate. General problems related to the calculation of expressions of the form of equation (IX.2) were encountered in solid state physics. Such a task was considered by Lamb<sup>60</sup> and by others<sup>61, 62</sup> for the Mössbauer effect. The nuclear recoil problem for the displacements in the momentum space requires the same treatment as a harmonic lattice. Indeed, analogous problems were encountered in the theory of line shapes and zero phonon lines in the absorption spectra of impurity centres in solids<sup>63, 64</sup>. Finally, similar methods were introduced<sup>65, 66</sup> for the study of radiationless transitions (e.g. thermal ionization) in solids. Englman, Freed and Jortner attempted to consider the problem of radiationless transitions in a large molecule from the point of view of multiphonon processes. Indeed, for a large molecule when  $N \gg 1$  it seems a logical step to transfer the problem from the field of molecular physics to the realm of solid state physics and to consider the problem of 'phonons in large molecules'.

Two physically interesting cases have to be considered at this point.

(a) When the molecule is inserted into an inert medium which acts as a heat bath, thermal equilibrium among the  $si$  levels can be assumed. Provided that the vibrational relaxation (and excitation) rates considerably exceed the non-radiative decay times we can set:

$$p(si) = \exp(-\beta E_{si}) / \sum_i \exp(-\beta E_{si}) \quad (\text{IX.10})$$

where  $\beta = (k_B T)^{-1}$ , so that when thermal equilibrium prevails, one has

$$\tau_{nr}^{-1} = 2\pi/\hbar \sum_i \sum_j \exp(-\beta E_{si}) |V_{si, t_j}|^2 \delta(E_{si} - E_{t_j}) / \sum_i \exp(-\beta E_{si}) \quad (\text{IX.11})$$

(b) For the case of an isolated molecule (in vacuum or, even better, in outer space) we can consider a coherent excitation of a single vibronic state  $\phi_{si}$ , whereupon  $p(si) = \delta_{i,i'}$ . When this zero order vibronic level  $si'$  corresponds to  $si$  the transition probability is given by (IX.11) in the zero temperature limit (or rather for  $\beta \rightarrow \infty$ ).

Now, the approximate expressions for the non-radiative transition derived above are completely analogous to the formal expressions for the line shape in optical absorption in solids. Indeed, in this approximation the *non-radiative process can be formally regarded as a (symmetry forbidden) optical emission process in the limit of zero energy*. Equation (IX.11) can be handled by the application of the generating function method. The main advantage of this technique is that it handles the generalized density of states function of the form (IX.11) (e.g. the density of states weighted by an arbitrary operator) without the necessity of factoring out these expressions into products of matrix elements and the vibronic density of states.

The non-radiative transition probability can be recast in the form of a Fourier transform:

$$\tau_{nr}^{-1} = C^2/\hbar^2 \exp(-G) \int_{-\infty}^{\infty} dt \exp[(-i\Delta Et/\hbar) + G_+(t) + G_-(t)] \quad (\text{X.12})$$

## RADIATIONLESS TRANSITIONS

where  $C$  is the non-adiabatic coupling matrix element<sup>58, 59</sup> and the functions  $G_{\pm}(t)$  are given by

$$G_+(t) = \frac{1}{2} \sum_j \Delta_j^2 (\bar{n}_j + 1) \exp(i\omega_j t)$$

$$G_-(t) = \frac{1}{2} \sum_j \Delta_j^2 \bar{n}_j \exp(-i\omega_j t) \quad (\text{IX.13})$$

and

$$\bar{n}_j = [\exp(\beta\hbar\omega_j) - 1]^{-1} \quad (\text{IX.14})$$

$\bar{n}_j$  is the number of excited vibrations with frequency  $\omega_j$  at thermal equilibrium. The dimensionless quantity  $G$  is defined in the form

$$G = G_+(0) + G_-(0) = \frac{1}{2} \sum_j \Delta_j^2 (2\bar{n}_j + 1) \quad (\text{XI.15})$$

which corresponds to the change in the number of vibrational quanta in the radiationless transition. This quantity is referred to as the *coupling strength*. The general result derived herein can be recast in a more transparent form for certain limiting cases, which are determined by the magnitude of the coupling strength  $G$  (equation (XI.15)). In order to obtain an approximate estimate for the coupling strength we make use of equation (IX.9) and write the approximate relation

$$G \approx E_M/\hbar\langle\omega\rangle \cot h(\beta\hbar\langle\omega\rangle/2) \quad (\text{IX.16})$$

where  $\langle\omega\rangle = N^{-1} \sum_j \omega_j$  is the mean vibrational frequency. The low and high temperature limits are :

$$G = E_M/\hbar\langle\omega\rangle; \quad \beta\hbar\langle\omega\rangle \gg 1 \quad (\text{IX.17})$$

$$G = 2E_M/\beta(\hbar\langle\omega\rangle)^2; \quad \beta\hbar\langle\omega\rangle \ll 1 \quad (\text{IX.18})$$

The various coupling limits can be defined as follows :

(a) On the strong coupling limit  $G \gg 1$  or alternatively,

$$G \gg \hbar\langle\omega\rangle \coth(\beta\hbar\langle\omega\rangle/2).$$

At low temperatures the strong coupling limit will be encountered where-upon  $E_M$  exceeds the mean vibrational frequency so that the relative displacement of the potential energy surfaces are large, and the Stokes shift will considerably exceed the vibrational frequency. Under these circumstances it is possible for the energy surfaces of the two electronic states to cross or to intersect in the vicinity of the minimum of the upper surface. Such a situation was examined thirty years ago by Teller<sup>67</sup>.

(b) The weak coupling limit is encountered when  $G \ll 1$  or (at low temperatures)  $E_M \ll \hbar\langle\omega\rangle$ . Thus the relative displacement for each normal mode is relatively small.

In the strong coupling limit the general expression can be reduced to a closed form :

$$\tau_{nr} = \frac{C^2(2\pi)^{\frac{1}{2}} \exp[-(\Delta E - E_M)^2/4E_M k_B T^*]}{\hbar(2E_M k_B T^*)^{\frac{1}{2}}} \quad (\text{IX.20})$$

where the effective temperature is defined in the form :

$$k_B T^* = \frac{1}{2} \hbar \langle \omega \rangle \coth(\beta \hbar \langle \omega \rangle / 2) \quad (\text{IX.21})$$

The Gaussian dependence on the energy parameter ( $\Delta E - E_M$ ) in the strong coupling limit is of course analogous to the Gaussian line shape (near the band maximum) devoid of phonon structure for impurity centres. However, equation (IX.20) contains some further interesting information. Inspection of equations (IX.6) and (IX.7) reveals that the potential surfaces  $W_s$  and  $W_1$  intersect on the hypercurve (actually on the  $(N-1)$ -dimensional surface). The intersection point of minimum energy  $E_A$  measured from the energy origin  $E_{s0} = 0$  is

$$E_A = (\Delta E - E_M)^2 / 4E_M \quad (\text{IX.22})$$

The following result is finally obtained in the strong coupling limit

$$\tau_{nr}^{-1} = \frac{C^2(2\pi)^{\frac{1}{2}}}{\hbar(E_M k_B T^*)^{\frac{1}{2}}} \exp(-E_A/k_B T^*) \quad (\text{IX.23})$$

This equation has the general appearance of a conventional rate equation where the energy  $E_A$  plays the role of the activation energy as might have been guessed by the intelligent chemist on intuitive grounds. It is important to stress that the concept of the 'activated complex' does not enter in any way into this treatment. The rate equation results from quantum mechanical transition between greatly displayed potential surfaces.

In the weak coupling limit the integral (IX.12) can be evaluated by the method of steepest descent. The low temperature result is to the lowest order<sup>58, 59</sup>

$$\begin{aligned} \tau_{nr}^{-1} &= \frac{C^2(2\pi)^{\frac{1}{2}}}{\hbar(\hbar\omega_M \Delta E)^{\frac{1}{2}}} \exp(-\gamma \Delta E / \hbar\omega_M) \\ \gamma &= \log\left(\frac{\Delta E}{d e_M}\right) - 1 \end{aligned} \quad (\text{IX.24})$$

where  $\omega_M$  and  $\Delta_M$  are the frequencies and the reduced displacement of the modes of maximum frequency (e.g. the C—H or C—D modes) and

$$d l_M = \frac{1}{2} \sum_{M=1}^d \hbar\omega_M \Delta_M^2.$$

This equation immediately exhibits :

- (a) The energy gap law.
- (b) The isotope effect in the weak coupling limit.

The main accomplishments of this treatment can be summarized as follows :

(a) From the general structure of the theoretical formulae we can ascertain the relative displacement of the two potential energy surfaces expressed in terms of the coupling parameter  $G$  determines whether the molecular system corresponds to the strong or to the weak coupling limit. This classification provides a link between the Teller picture<sup>67</sup> and the conventional tunnelling model for radiationless transitions. In the statistical limit, as it is well-established, the weak (and possibly sometimes the intermediate) coupling

## RADIATIONLESS TRANSITIONS

scheme is appropriate for the description of a large number of radiationless transitions (e.g. electronic relaxation) in aromatic molecules.

(b) In the strong coupling limit the transition probability is determined by the mean molecular frequency, provided, of course, that the  $\Delta_i$  values for a substantial number of different frequencies are non-vanishing. On the other hand, in the weak coupling case the non-radiative transition probability is dominated by the highest molecular frequency  $\omega_M$ .

(c) In the strong coupling limit the transition probability is determined by the energy  $E_A$  corresponding to the point of minimum intersection energy located above the origin of the higher electronic state. In the weak coupling limit the transition probability is essentially determined by the energy gap  $\Delta E$ .

(d) A proper theoretical interpretation of the 'energy gap law' for radiationless transitions in the weak coupling limit is provided. This general energy-difference dependent behaviour is characteristic of many molecular relaxation processes, such as vibrational relaxation.

(e) Following the considerations presented in (b), some features of the intramolecular isotope effect on radiationless transitions can be elucidated. A pronounced isotope effect can be encountered only in the weak coupling limit.

(f) Medium effects resulting from coupling to an inert medium are now elucidated<sup>59</sup>.

(g) From the chemist's point of view the different features of the isotope effects, the energy gap law and the temperature dependence encountered in the weak and strong coupling limits can be summarized as follows: the weak coupling limit corresponds to a tunnelling mechanism between zero order vibronic levels which correspond to different electronic configurations, while in the strong coupling limit we encounter the situation in which adiabatic potential surfaces cross or intersect. It is gratifying that both limits results as particular cases of the same general formalism.

Although conventional radiationless transitions in large aromatic molecules correspond to the weak coupling situation, the strong coupling limit is of considerable physical interest for the interpretation of many reactions encountered in the field of organic photochemistry.

## REFERENCES

- <sup>1</sup> For a review, see G. Herzberg. *Spectra of Diatomic Molecules* (Van Nostrand and Co., 1954), Vol. II, p. 406.
- <sup>2</sup> For reviews, see:
  - (a) M. Kasha. *Discussions Faraday Soc.* **9**, 14 (1950).
  - (b) M. Kasha. *Radiation Res. Suppl.* **2**, 243 (1960).
  - (c) P. Seybold and M. Gouterman. *Chem. Rev.* **65**, 413 (1965).
  - (d) B. R. Henry and M. Kasha. *Ann. Rev. Phys. Chem.* **19**, 161 (1968).
  - (e) J. Jortner, S. A. Rice and R. M. Hochstrasser. *Advan. Photochem.* In press (1971).
- <sup>3</sup> A. Wiedeman. *Ann. Phys.* **34**, 446 (1888).
- <sup>4</sup> A. Jablanski. *Nature* **131**, 839 (1933).
- <sup>5</sup> G. N. Lewis and M. Kasha. *J. Am. Chem. Soc.* **66**, 2100 (1944); **67**, 994 (1945).
- <sup>6</sup> G. W. Robinson and R. P. Frosch. *J. Chem. Phys.* **37**, 1962 (1962); **38**, 1187 (1963).
- <sup>7</sup> (a) C. A. Hutchinson Jr and B. W. Magum. *J. Chem. Phys.* **32**, 1261 (1960).  
(b) M. S. de Groot and J. H. Van der Waals. *Mol. Phys.* **4**, 189 (1961).
- <sup>8</sup> M. Gouterman. *J. Chem. Phys.* **36**, 2846 (1962).

JOSHUA JORTNER

- <sup>9</sup> R. J. Watts and S. J. Strickler. *J. Chem. Phys.* **44**, 2423 (1966).
- <sup>10</sup> R. Williams and G. J. Goldsmith. *J. Chem. Phys.* **39**, 2008 (1963).
- <sup>11</sup> W. R. Ware and P. T. Cunningham. *J. Chem. Phys.* **44**, 4364 (1966).
- <sup>12</sup> A. B. Zahlan, S. Z. Weisz, R. C. Jarmagin and M. Silver. *J. Chem. Phys.* **42**, 4244 (1965).
- <sup>13</sup> (a) G. B. Kistiakowski and C. S. Parmeter. *J. Chem. Phys.* **42**, 2942 (1965).  
 (b) E. M. Anderson and G. B. Kistiakowsky. *J. Chem. Phys.* **48**, 4787 (1968).  
 (c) A. E. Douglas and W. Mathews. *J. Chem. Phys.* **48**, 4788 (1968).
- <sup>14</sup> G. W. Robinson. *J. Chem. Phys.* **47**, 1967 (1967).
- <sup>15</sup> M. Bixon and J. Jortner. *J. Chem. Phys.* **48**, 715 (1968).
- <sup>16</sup> U. Fano. *Phys. Rev.* **124**, 1866 (1961).
- <sup>17</sup> O. K. Rice. *Phys. Rev.* **33**, 478 (1929).
- <sup>18</sup> C. A. Coulson and K. Zalewski. *Proc. Roy. Soc. (London)* **A268**, 437 (1962).
- <sup>19</sup> R. A. Harris. *J. Chem. Phys.* **39**, 978 (1963).
- <sup>20</sup> G. Herzberg. *Electronic Spectra of Polyatomic Molecules* (Van Nostrand & Co., Princeton, N.J., 1966).
- <sup>21</sup> J. Franck and H. Sponer. *Göttingen Nachr.* (1928), p. 241.
- <sup>22</sup> R. Kubo. *Phys. Rev.* **86**, 929 (1952).
- <sup>23</sup> E. F. McCoy and I. G. Ross. *Australian J. Chem.* **15**, 573 (1962).
- <sup>24</sup> G. R. Hunt, E. F. McCoy and I. G. Ross. *Australian J. Chem.* **15**, 591 (1962).
- <sup>25</sup> J. P. Byrne, E. F. McCoy and I. G. Ross. *Australian J. Chem.* **18**, 1589 (1965).
- <sup>26</sup> S. H. Lin. *J. Chem. Phys.* **44**, 3759 (1966).
- <sup>27</sup> P. C. Haarhoff. *Mol. Phys.* **7**, 101 (1963).
- <sup>28</sup> J. Jortner and R. S. Berry. *J. Chem. Phys.* **48**, 2757 (1968).
- <sup>29</sup> D. Chock, J. Jortner and S. A. Rice. *J. Chem. Phys.* **49**, 610 (1968).
- <sup>30</sup> M. Bixon, J. Jortner and Y. Dothan. *Mol. Phys.* **17**, 109 (1969).
- <sup>31</sup> M. Bixon and J. Jortner. *J. Chem. Phys.* **50**, 4061 (1969).
- <sup>32</sup> M. Bixon and J. Jortner. *J. Chem. Phys.* **50**, 3284 (1969).
- <sup>33</sup> K. F. Freed and J. Jortner. *J. Chem. Phys.* **50**, 2916 (1968).
- <sup>34</sup> H. C. Longuet-Higgins. *Advan. Spectr.* **2**, 429 (1961).
- <sup>35</sup> H. Feshbach, A. K. Kerman and R. H. Lemmer. *Ann. Phys. (N.Y.)* **41**, 230 (1967).
- <sup>36</sup> A. E. Douglas. *J. Chem. Phys.* **45**, 1007 (1966); A. E. Douglas and K. P. Huben. *Can. J. Phys.* **43**, 74 (1965).
- <sup>37</sup> J. P. Byrne and I. G. Ross. *Can. J. Chem.* **43**, 3253 (1965).
- <sup>38</sup> G. R. Hunt and I. G. Ross. *J. Mol. Spect.* **9**, 50 (1962).
- <sup>39</sup> P. G. Wilkinson. *Can. J. Phys.* **34**, 596 (1956).
- <sup>40</sup> D. S. McClure. *J. Chem. Phys.* **22**, 1968 (1954).
- <sup>41</sup> J. G. Angus, B. J. Christ and G. C. Morris. *Australian J. Chem.* In press.
- <sup>42</sup> J. Jortner and G. C. Morris. *J. Chem. Phys.* **51**, 3689 (1969).
- <sup>43</sup> K. Freed. *J. Chem. Phys.* **51**, (1970).
- <sup>44</sup> W. Hanle. *Z. Physik* **30**, 93 (1924).
- <sup>45</sup> G. Breit. *Rev. Mod. Phys.* **5**, 91 (1933).
- <sup>46</sup> P. A. Franken. *Phys. Rev.* **121**, 508 (1961).
- <sup>47</sup> M. E. Rose and R. L. Corovillano. *Phys. Rev.* **122**, 1185 (1961).
- <sup>48</sup> T. G. Eck. *Physica* **33**, 157 (1967).
- <sup>49</sup> H. Wieder and T. G. Eck. *Phys. Rev.* **153**, 103 (1967).
- <sup>50</sup> R. L. Kelly. *Phys. Rev.* **147**, 376 (1966).
- <sup>51</sup> J. N. Dod, R. D. Kaul and D. M. Warrington. *Proc. Phys. Soc. (London)* **84**, 176 (1964).
- <sup>52</sup> E. B. Alexandrov. *Optics and Spectroscopy* **17**, 957 (1967).
- <sup>53</sup> J. N. Dodd, W. J. Sandle and D. Zisserman. *Proc. Phys. Soc. (London)* **92**, 797 (1967).
- <sup>54</sup> W. Weisskopf and W. Wigner. *Z. Physik* **63**, 54 (1930).
- <sup>55</sup> K. E. Lassila. *Phys. Rev.* **135A**, 1218 (1964).
- <sup>56</sup> R. P. Feynman, R. B. Leighton and M. Sands. *The Feynman Lectures on Physics* (Addison Wesley, 1965), Vol. 3, Chapter 11-5.
- <sup>57</sup> J. S. Bell and J. Steinberger. *Proceedings of the Oxford International Conference on Elementary Particles* (1965), p. 195.
- <sup>58</sup> H. E. Radford and H. P. Broida. *J. Chem. Phys.* **38**, 644 (1963); *Phys. Rev.* **128**, 231 (1963).
- <sup>59</sup> (a) R. Englman and J. Jortner. *Mol. Phys.* **18**, 145 (1970).  
 (b) K. Freed and J. Jortner. *J. Chem. Phys.* **52**, 6272 (1970).
- <sup>60</sup> W. E. Lamb. *Phys. Rev.* **55**, 190 (1938).

## RADIATIONLESS TRANSITIONS

- <sup>61</sup> W. H. Visscher. *Ann. Phys.* **9**, 194 (1960).
- <sup>62</sup> K. S. Singwi and A. Sjölander. *Phys. Rev.* **120**, 1093 (1960).
- <sup>63</sup> K. Huang and A. Rhys. *Proc. Phys. Soc. (London)* **A204**, 413 (1951).
- <sup>64</sup> M. Lax. *J. Chem. Phys.* **20**, 1752 (1952).
- <sup>65</sup> R. C. O'Rourke. *Phys. Rev.* **91**, 265 (1953).
- <sup>66</sup> R. Kubo. *Phys. Rev.* **86**, 929 (1952).
- <sup>67</sup> E. Teller. *J. Phys. Chem.* **41**, 109 (1937).

# INTERACTION OF CHROMOPHORES IN MONOLAYER ASSEMBLIES

HANS KUHN

*Max-Planck-Institut für Biophysikalische Chemie, Karl-Friedrich-Bonhoeffer-Institut, D 3400 Göttingen, Germany*

## ABSTRACT

The techniques of producing monolayer assemblies are discussed. In the present context these assemblies are of interest because of the interactions between chromophores included in the monolayers—particularly those interactions which lead to energy transfer between the chromophores. Fluorescence effects resulting from this transfer can be utilized to monitor the manipulation of the monolayers and to elucidate the architecture of various types of the assemblies, including those in which there are included protein monolayers.

The fact that it is possible to control the interchromophore distance in the assemblies enables quantitative determination of the distance-dependence of the energy transfer process: by comparison with theory it is then possible to elucidate the multipole nature of the spectroscopic transitions involved. The energy transfer results in changes in lifetimes which can be interpreted quantitatively. A new effect in luminescence is discussed and demonstrated by the monolayer assembling technique (the dependence of the lifetime of an excited molecule surrounded by a non-absorbing dielectric on details in its broad environment).

Application is also made to molecular aggregates i.e. structures in which the chromophores are in direct contact. In the case of sandwich-pairs the shift in absorption peak is in quantitative agreement with that calculated from the electron-gas model. Consideration of the shifts in Scheibe-type aggregates leads to the development of a new structural model—the ‘brick stonework’ model—for these aggregates.

This model has enabled assembling monolayer structures which show the Scheibe-type effect. Dipole moment and polarizability of the excited state of the aggregate are calculated and measured using a new type of electrochromism, obtained by sandwiching a single monolayer of the aggregated dye between fatty acid layers and semitransmitting metal electrodes.

---

The spectroscopic study of chromophore interactions in monolayer assemblies has two aspects:

Investigating monolayers and investigating the nature of interactions.

In this paper we discuss recently investigated examples concerning the first aspect (section 1) and the second aspect (sections 2-3).

## 1. ENERGY-TRANSFER MONITORED MANIPULATION OF MONOLAYERS

### (a) Separation and re-assembling monolayers

The energy transfer between a sensitizer dye in a monolayer and an

acceptor dye in a monolayer deposited on to the first may be easily investigated by studying the fluorescence quenching of the sensitizer or the sensitized fluorescence of the acceptor<sup>1,2</sup>. It should be easy then, by energy transfer, to study the separation and reassembling of monolayers. The exciting problem of a controlled manipulation of objects in the range of molecular dimensions may thus be attacked. An energy-transfer monitored separation of monolayers may be realized in the following way<sup>3,†</sup>:

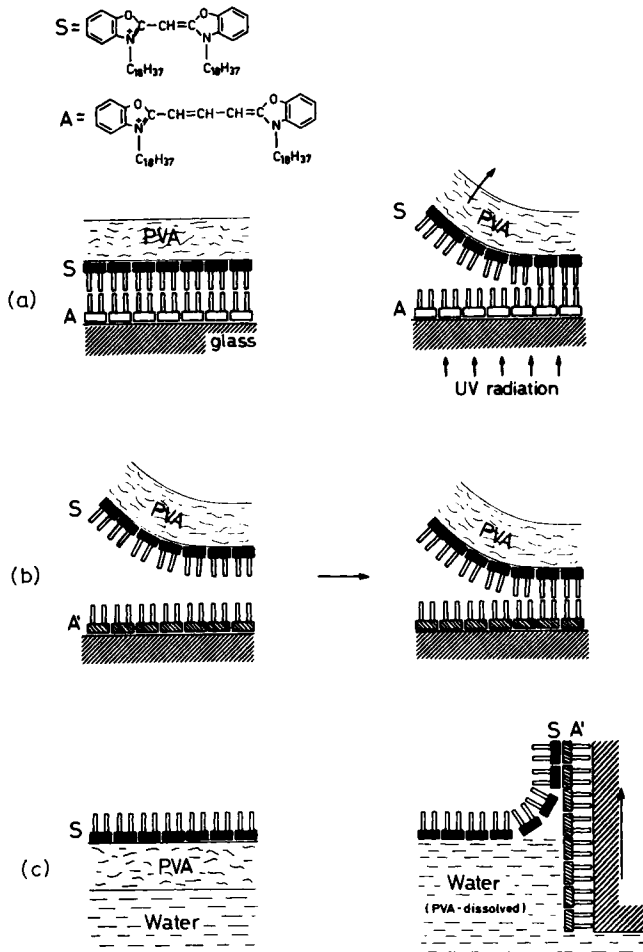


Figure 1. (a) Separation of monolayer S (sensitizer) and A (acceptor); (b) contacting monolayer S (side with hydrocarbon chain ends) with monolayer A'; (c) contacting monolayer S (side with chromophores) with monolayer A'. The monolayers (mixed monolayers of stearylsubstituted dye and arachidic acid, in molar mixing ratio 1:10) are represented schematically, omitting arachidic acid molecules. The chains of the fatty acid molecules and the hydrocarbon substituents of the dye molecules are tightly packed in the layer and oriented parallel to each other and perpendicular to the layer plane.

† Rothen<sup>4</sup> reported a separation of monolayers to occur within molecular accuracy in systems of proteins and lipids, when using a Scotch Tape stripping technique ('molecular microtome').

## CHROMOPHORES IN MONOLAYER ASSEMBLIES

Mixed monolayers of dyes S and A (*Figure 1*) and arachidic acid, which have a well defined and compact structure<sup>2</sup>, are deposited on a glass plate according to *Figure 1* and a polyvinylalcohol film superposed. The film is stripped off as shown in *Figure 1a* and it may be demonstrated that the separation occurs between the two layers:

In the part to the right the two layers are in contact on the plate. When irradiating with UV light, which is absorbed by S, the blue fluorescence of S is largely quenched and the yellow fluorescence of A is observed. In the part on the left the sensitizer layer is stripped off. The film shows the strong blue fluorescence of S, demonstrating the S-layer to be stripped off with the film. The glass plate with layer A appears black since A does not absorb the incident radiation and thus does not fluoresce. However, when we excite with light absorbed by A a uniform yellow fluorescence of the glass plate in both parts is observed showing that a layer is present on the glass plate where the S-layer is stripped off<sup>3</sup>.

By setting the stripped film back onto the plate a reassembling of the dye monolayers in the molecular scale is possible (*Figure 1b*): the fluorescence of S is quenched and the sensitized fluorescence of A is observed at the touching parts, which appear like the part where the polymer film has not been stripped off, demonstrating a molecular contact of the layers. The layer fixed at the polymer film may be brought into contact with any other monolayer A' on a support. Again the molecular contact is indicated by the appearance of the sensitized fluorescence. In this example the neighbour molecules on one side of the monolayer of dye S were changed.

It is also possible to change, in a controlled way, the molecules attaching to the second side of the same monolayer. The polymer film is dissolved according to *Figure 1c* and then the second side of the polymer is brought into contact with an appropriate acceptor. Again a fluorescence quenching

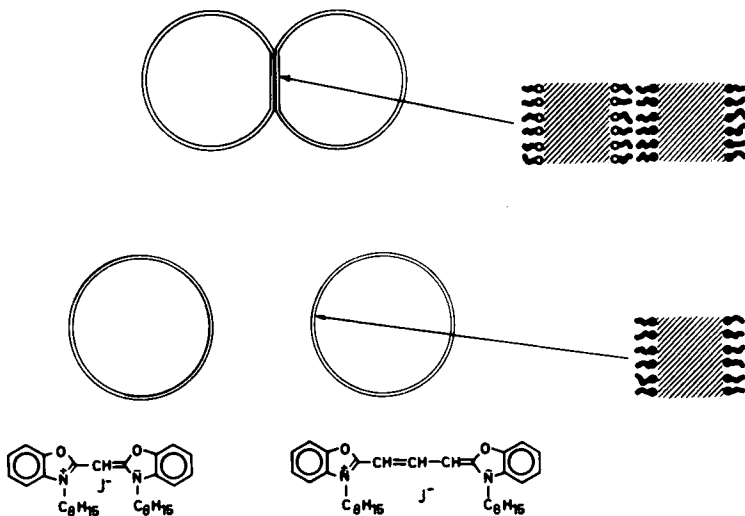


*Figure 2.* Contacting and separation of soap bubbles. Justification of assumed membrane architecture in contact area by using surface active fluorescing dyes.

HANS KUHN

of S and a sensitized fluorescence of A is observed showing that a molecular contact at this second side of the monolayer of S can also be achieved<sup>3</sup>.

These experiments demonstrate how easily monolayers can be manipulated. The possibility of constructing monolayer assemblies of any complicated architecture on a glass plate, of bringing it onto a water surface and of transferring it to any appropriate substrate may be useful in building organized systems by assembling prefabricated elements.

The controlled joining and removal of monolayers may also be achieved by bringing soap bubbles into contact and subsequently separating them (*Figure 2*)<sup>5</sup>. Surface active fluorescent dyes incorporated in the surface layers of the bubbles are not transferred from one bubble to the other showing that the monolayers, when brought into contact, do not rearrange and that the dye molecules are not exchanged between the touching monolayers. In this way a new possibility of forming bimolecular lipid membranes is obtained. Unlike the membranes obtained by the known techniques<sup>6</sup> these membranes may be made asymmetric.

**(b) Protein Monolayers**

In the case of protein monolayers the manipulation and construction of organized assemblies is of particular interest regarding their implications for a synthetic molecular biology. Several proteins have been adsorbed in an enzymatically active form at a monolayer film of arachidic-acid or methylstearate<sup>7</sup>. In this way compact layers of the proteins are obtained. This is best seen from the electron micrograph of the iron rich protein ferritin

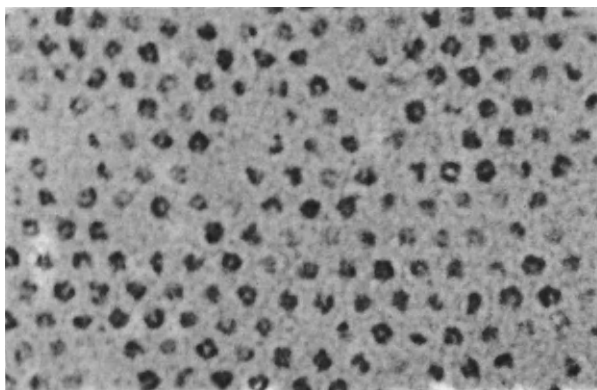


*Figure 3.* Electron micrograph of protein ferritine adsorbed on a monolayer of methylstearate and trimethyldodecylammonium bromide. Protein molecules form monolayer with long range order<sup>7</sup>.

(*Figure 3*). These films, handled like fatty acid films, may be used as components of organized assemblies of monolayers. We discuss a possibility for proving the architecture of an assembly by studying energy transfer from a dye to a chromophoric group in the protein<sup>7</sup>. An assembly with the architecture shown in *Figure 4a* may be easily obtained following the usual

## CHROMOPHORES IN MONOLAYER ASSEMBLIES

procedure. The haem-groups of the protein act as acceptors for the excitation energy of dye S and quench its fluorescence. The fluorescence being a measure of the distance between sensitizer and acceptor, the architecture of the system may be proved. The fluorescence intensity is plotted against an

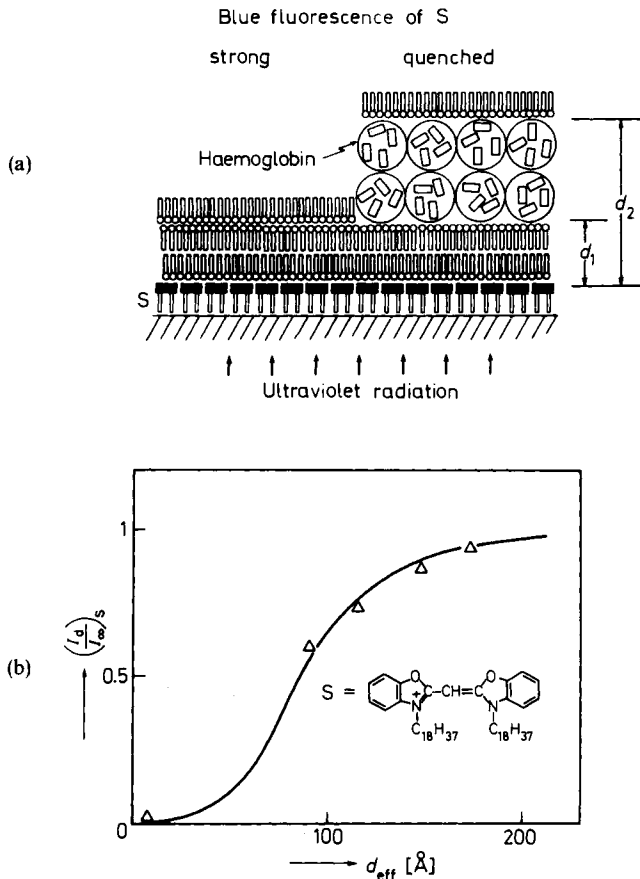


Figure 4. Energy transfer from fluorescing dye S to haemoglobin. (a) Cross section of arrangement. (b) Intensity of fluorescence of S against  $d_{\text{eff}}$ , where  $1/d_{\text{eff}}^4 = (\frac{1}{3})(d_1^{-3} - d_2^{-3})/(d_2 - d_1)$ ; experimental points and theoretical curve.

appropriately defined effective distance  $d_{\text{eff}}$  (Figure 4b). The experimental points lie on the theoretical curve. A monolayer of plasma-albumin was interposed between sensitizer dye and acceptor haemoglobin<sup>7</sup>. The pronounced increase in fluorescence intensity is a measure of the thickness of this additional interlayer. Its value agrees with expectation. This demonstrates the possibility of assembling complicated arrangements containing different proteins.

## 2. NATURE OF DEACTIVATION PROCESSES

### (a) Multipole nature of phosphorescence of dyes

It is well known that the fluorescence of a molecule corresponds to a dipole emission, but little is known about the multipole nature of a forbidden transition such as phosphorescence<sup>8</sup>. There a molecule might act as an electric quadrupole, magnetic dipole or electric dipole emitter. In all three cases a long range energy transfer must be expected, the distance-dependence being different in each case<sup>9</sup>. Thus, by comparing the experimental distance-dependence of energy transfer with the theoretical dependence found for each case, the multipole nature of the phosphorescence may be determined. Since it was assumed before that an energy transfer over a large range is only possible for dipole-dipole interaction, this point shall be discussed in more detail.

For describing the luminescence and the energy transfer it is advantageous to use the classical approach. The results, very easily obtained and translated into quantum mechanical language, agree with those obtained by a more strict treatment<sup>9</sup>.

The molecule is described as a classical antenna. The emission power  $L_e$  is obtained from the classical electromagnetic theory and is given in *Table 1*

*Table 1.* Power emitted and absorbed for various multipole radiations  $\mu_0$ ,  $m_0$ ,  $Q_0$ , amplitude of electric dipole, magnetic dipole and electric quadrupole respectively;  $c$  the velocity of light,  $\omega = 2\pi\nu_s$ ,  $\sigma$  number of molecules per unit area,  $\alpha$  a numerical factor discussed following equation (4)

Emitter	Magnetic dipole	Electric dipole	electric quadrupole
$L_e$ emitted power	$(1/48\pi^2 c) m_0^2 \omega^4$	$(1/3c^3) \mu_0^2 \omega^4$	$(1/60c^5) Q_0^2 \omega^6$
$L_a$ power absorbed by acceptor layer at distance $d$	$\text{const.} \times \omega^2 \times m_0^2 a\sigma \times \frac{1}{d^2}$	$\text{const.} \times \mu_0^2 a\sigma \times \frac{1}{d^4}$	$\text{const.} \times Q_0^2 a\sigma \times \frac{1}{d^6}$
	$\text{const.} = \frac{2\pi}{3} \alpha^2$	$\text{const.} = \frac{128\pi^5}{3} \alpha^4$	$\text{const.} = \frac{128\pi^7}{15} \alpha^6$

for the three cases. The probability of an excited molecule emitting a quantum of light (energy  $h\nu_s$ ), in the time interval  $dt$ , is  $dP_e$  and is given by

$$\frac{dP_e}{dt} = \frac{L_e}{h\nu_s} \quad (1)$$

Now let us put an acceptor molecule at a point near the emitting antenna. In the classical picture the emitting molecule produces a certain alternating electromagnetic field, and  $F_0$  shall be the amplitude of the electric field strength. The power absorbed by the acceptor molecule is

$$L'_a = aF_0^2 \quad (2)$$

where constant  $a$  depends on the nature of the acceptor molecule and is related to the extinction coefficient of the molecule for light of frequency  $\nu_s$ .

The field  $F_0$  in the environment of an oscillating multipole is given by Hertz's solution of the Maxwell equations and in the proximity field region

## CHROMOPHORES IN MONOLAYER ASSEMBLIES

(at a distance small compared to the wavelength of the luminescent light  $\lambda_s$ ),  $F_0$  is simply given by Coulomb's law and the induction laws for electric and magnetic multipoles respectively (*Figure 5*). The power absorbed by a layer

The diagram illustrates the calculation of the amplitude of the electric field ( $F_0$ ) at a distance  $r$  from three types of dipoles:

- Electric Dipole:** Represented by two vertical arrows pointing in opposite directions. The formula is  $\downarrow F_0 = \frac{\mu_0}{r^3}$ .
- Magnetic Dipole:** Represented by a rectangle with a vertical arrow inside. The formula is  $\bullet F_0 = \frac{m_0 \omega}{r^2}$ .
- Electric Quadrupole:** Represented by two pairs of vertical arrows pointing in opposite directions. The formula is  $\longrightarrow F_0 = \frac{3Q_0}{r^4}$ .

Figure 5. Amplitude of electric field ( $F_0$ ) in proximity of oscillating electric dipole (amplitude  $\mu_0$ ), magnetic dipole (amplitude  $m_0$ ), electric quadrupole (amplitude  $Q_0$ ).

of acceptor molecules,  $L_a$ , is obtained by summing over the contributions  $aF_0^2$  of each single molecule (*Table 1*).

Energy transfer and emission being competitive processes, the lifetime of the excited state is shortened by increasing the amount of energy transfer, and thus the decay time of the phosphorescence is shortened. The decay time  $\tau_d$  for a distance  $d$  between sensitizer and acceptor layer is related to  $L_a$ ,  $L_e$  and  $L_t$  ( $L_t$  is the power loss by non-radiative processes, other than the process of energy transfer to acceptor A):

$$\tau_d/\tau_\infty = (L_e + L_t)/(L_e + L_t + L_a).$$

The quantum yield of the luminescence,  $q_s$ , is related to  $L_e$  and  $L_t$  by  $q_s = L_e/(L_e + L_t)$ . [When A is absent,  $q_s$  is the probability of a molecule in the luminescent excited state emitting a photon.  $q_s$  must be distinguished from  $q'_s$  (number of emitted quanta/number of absorbed quanta)]. With the data in *Table 1* the equation

$$\frac{\tau_d}{\tau_\infty} = [1 + (d_0/d)^p]^{-1} \quad (3)$$

$$d_0 = \alpha(\lambda_s/n)(A_s q_s)^{1/p} \quad (4)$$

is obtained with  $p = 2, 4$  and  $6$  for magnetic dipole, electric dipole, and electric quadrupole, respectively<sup>10</sup>.  $n$  is the refractive index of the medium. The value of the numerical factor  $\alpha$  depends on the orientation of emitter and acceptor. Under usual experimental conditions the transition moments of the acceptor molecules are statistically oriented in the plane of the layer. Then  $\alpha = 3^4/8\pi$  for a magnetic dipole and for an electric dipole  $\alpha$  ranges between the values  $0.098$  and  $0.12$ , for an electric quadrupole between the values  $0.14$  and  $0.21$ . In the case of a sufficiently narrow luminescence band

$A_s$  is the absorption (1-transmission) of the acceptor layer. In the general case,  $A_s$  is defined by the expression

$$A_s = \int A(v) f_s(v) (v_s/v)^4 dv \quad (5)$$

with  $f_s(v)$  being the normalized quanta distribution function, and  $v_s$  the frequency of the maximum of the fluorescence band of the sensitizer;  $A(v)$  is the absorption of  $A$  at frequency  $v$ . The value of the quantum yield,  $q_s$ , must lie between 1 and 0.06 since the measured overall quantum yield  $q'_s$  (number of emitted quanta/number of absorbed quanta) is 0.06. By inserting the lower limit of  $q_s$  and  $\alpha$  and the upper limit of  $q_s$  and  $\alpha$  in equation (4) we find the results given in Figure 6. The experimental points are given in the figure. The experimental value  $d_0 = 100 \text{ \AA}$  rules out an electric quadrupole or a magnetic dipole but not an electric dipole radiation. With equation (4) we

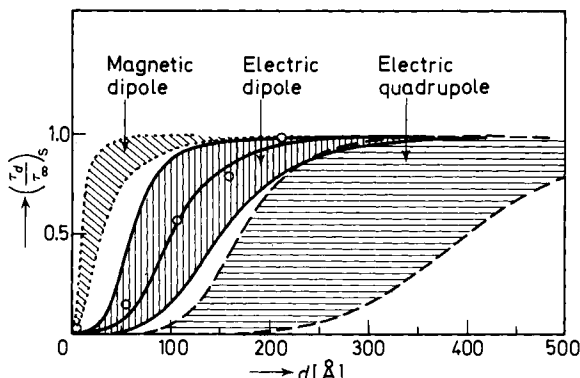
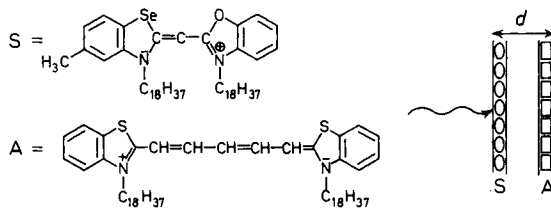


Figure 6. Multipole nature of phosphorescence of dye S. Decay time of phosphorescence ( $\tau_p$ ) versus distance  $d$  between S and layer of acceptor A. Theoretical range for magnetic dipole, electric dipole and electric quadrupole radiations. Experimental points on theoretical curve for electric dipoles with appropriate value  $q_s$ .

calculate that the quantum yield for an electric dipole radiation lies between the values 0.42 (dipole oscillating parallel to the layer plane) and 0.21 (dipole oscillating perpendicular to the layer plane). Thus the quantum yield  $q_s$  is distinctly higher than the measured overall quantum yield of the phosphorescence,  $q'_s = 0.06$ .

The results may be checked by another method (not discussed here) based on the monolayer assembling technique: measuring the directional pattern

## CHROMOPHORES IN MONOLAYER ASSEMBLIES

of the phosphorescence as a function of the distance between the emitting molecule and a metal mirror<sup>2, 10, 11</sup>.

It would be of interest to realize experimentally the quadrupole emitter, since it should result in a considerably larger range of energy transfer than the electric dipole.

### (b) Luminescence lifetime in the proximity of an interface

We have considered the shortening of the lifetime of the excited state by a transfer of energy to an acceptor. A surprising effect may be demonstrated related to energy transfer with the monolayer assembling technique: changing the lifetime of the excited state without changing the luminescence quantum yield<sup>12</sup>. The decay time of the luminescence is found to be dependent on the distance between emitter and the interface of two differently polarizable dielectrics<sup>13</sup>. It may be shortened or lengthened depending on this distance. Thus the average lifetime of the excited state of a molecule or the probability ( $dP_e$ ) of exciting a quantum of light depends on the broad environment of the molecule. The process of emitting the light quantum does not only depend on the excited molecule, but on the total system of molecule plus its environment. The excited molecule, so to say, knows all about its surroundings when it decides to emit a quantum of light. This experiment constitutes an unusual manifestation of the wave-particle duality of light.

For a quantitative consideration it is advantageous to use again the classical picture and equation (1) for translating the result into the quantum mechanical language.

First let us again look at the energy transfer from an excited molecule S described as an oscillating dipole to an acceptor A in the alternating field of

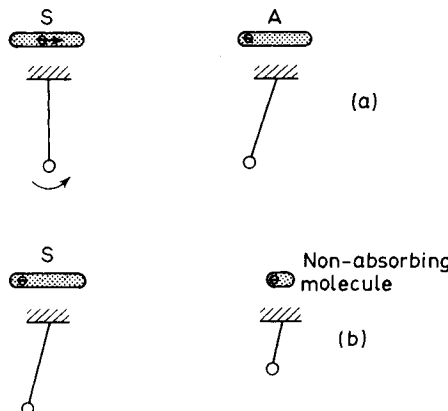


*Figure 7.* Fluorescent molecule S and acceptor molecule A (a) or non-absorbing molecule (b). Classical picture neglecting retardation effect. Phase shift between oscillators S and A in case (a), in-phase oscillation of oscillators in case (b).

S (*Figure 7a*). A may be described as a damped oscillator. It will oscillate with a phase shift relative to S. The field of A damps S and therefore diminishes the decay time of S: energy is transferred from S to A.

$A$  is now substituted for a non-absorbing molecule. It will oscillate in phase with  $S$ , and thus does not damp  $S$  (*Figure 7b*). However, this statement is not completely correct, since the electromagnetic field needs some time to reach the non-absorbing molecule and the echo field to reach  $S$ . This echo field has an accelerating or retarding effect on  $S$  depending on this phase shift between echo field and elongation of  $S$ . Thus the molecule, even when not absorbing energy, influences the decay time of  $S$ .

In the case of an absorbing molecule  $A$ , its influence on the emission power  $L_e$  is negligible and the decrease of the decay time is determined by the absorbed power  $L_a$ . For a non-absorbing molecule,  $L_a = 0$ , but the

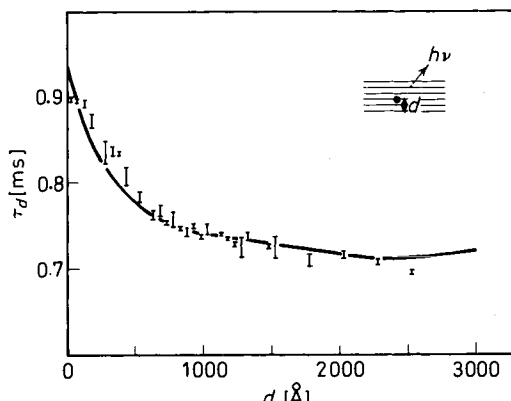


*Figure 8.* Red luminescent europium complex at distance  $d$  from fatty acid/air interface. Lifetime of luminescence ( $\tau_d$ ) as a function of  $d$ . Theoretical curve and experimental points. The quantum yield of the luminescence being constant and equal to 1,  $\tau_d$  is markedly dependent on  $d$ . This effect is caused by the time the electromagnetic radiation needs to travel from the emitter to the neighbouring polarizable molecules and the echo by these molecules to travel to the emitter, i.e. a time of the order of  $(3 \times 10^{-6} \text{ cm})/(3 \times 10^{10} \text{ cm/sec}) = 10^{-16} \text{ sec}$ .

influence of this molecule on the radiative decay process of  $S$  is important. This process then must be considered as being due to the system of both molecules.

In the case of many non-absorbing molecules, a dielectric extending over the shaded part in *Figure 8*, we have to sum up over the echoes of each molecule and, for a particular case, the curve in *Figure 8* is obtained for the decay time ( $\tau_d$ ) as a function of the distance between emitter and interface ( $d$ )<sup>13</sup>. The experimental points correspond to the measured decay times of samples obtained by depositing a monolayer of a strongly luminescent europium complex on a glass plate and superposing on it fatty acid monolayers (fatty acid and glass have almost the same refractive index).

The theoretical curve is obtained by assuming a quantum yield  $q_s = 1$  (this value was obtained by energy transfer experiments<sup>2</sup>) and the good agreement between theory and experiment substantiates the value. The resulting theoretical curve depends strongly on  $q_s$  and thus this type of experiment is useful as a method for determining  $q_s$ , which is otherwise

## CHROMOPHORES IN MONOLAYER ASSEMBLIES

difficult to determine. Similar experiments with a metal surface as interface have been described elsewhere<sup>9, 12</sup>

### 3. LIGHT ABSORPTION OF AGGREGATES OF DYES IN MONOLAYER ASSEMBLIES

#### (a) Absorption by sandwich-pair aggregates

In the foregoing part we studied the weak interaction of molecules at relatively large separations. In the following we consider molecules in direct contact. Using the monolayer assembling technique, sandwich-pair arrangements of identical or different dye molecules may be studied<sup>14</sup>. The experimental band shifts and changes in oscillator strength were found to be in quantitative agreement with the values calculated using a refined one-dimensional electron gas model<sup>15</sup>. *Table 2* gives, for some cases, the theo-

*Table 2.* Shifts (nm) of some Scheibe-type aggregates ( $\lambda_P$ ) and dimers ( $\lambda_D$ ) with respect to the corresponding monomers ( $\lambda_M$ )

	$\lambda_P - \lambda_M$ theor.	$\lambda_P - \lambda_M$ exp.	$\lambda_D - \lambda_M$ theor.	$\lambda_D - \lambda_M$ exp.
	+ 54	+ 40	- 30	- 40
	+ 23	+ 25	- 18	- 25
	+ 23	+ 19	- 18	- 16

retical and observed shifts  $\lambda_D - \lambda_M$  between the absorption peak of the dimer ( $\lambda_D$ ) and of the monomer ( $\lambda_M$ ). Based on this approach is the following assumption which highly facilitates calculation:

The  $\sigma$ -electrons of the dye molecule and of the surrounding solvent molecules are treated as an infinite medium of dielectric constant 2.5 and the  $\pi$ -electrons are considered as being in this medium and as moving along the zigzag lines in *Figure 9*, i.e. along the lines of highest  $\pi$ -electron density.

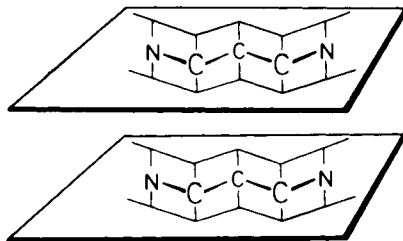


Figure 9. Model used to calculate molecular aggregate spectra shown for simplest cyanine in sandwich arrangement.

### (b) Absorption by Scheibe-dye aggregates

This model may be applied to the Scheibe-dye aggregates (J-aggregates)<sup>16</sup> characterized by a very narrow and high absorption peak corresponding to an in-phase oscillation of the oscillators substituting each dye molecule<sup>17</sup>. In the well known case of pseudo-isocyanine (*Figure 10*) this peak has a bathochromic shift of 53 nm relative to the monomer peak.

The aggregate structures shown in *Figures 10a* and *b* have been proposed

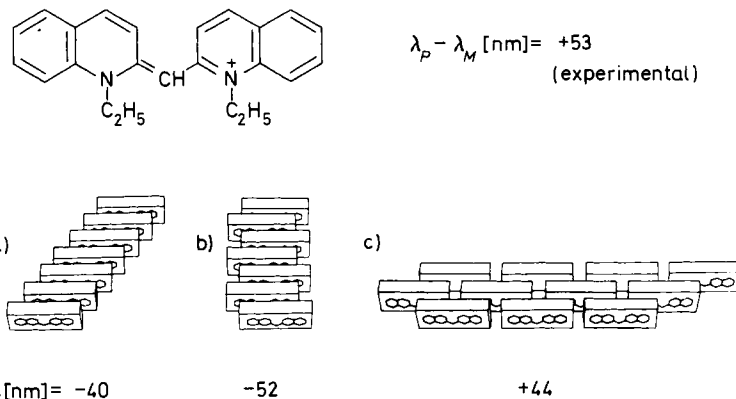


Figure 10. Scheibe-aggregate forming dye pseudoisocyanine. Experimental and theoretical values for aggregate to monomer band shift  $\lambda_p - \lambda_m$ . (a) staircase arrangement; (b) ladder arrangement; (c) brick-stonework arrangement.

in the past<sup>16</sup>. Assuming these structures, the electron gas model calculation gives hypsochromic instead of bathochromic shifts<sup>18</sup>. However, when the structure shown in *Figure 10c* (a brick-stonework-like arrangement of the dye molecules) is assumed the model calculation gives a bathochromic shift of 44 nm, which is in approximate agreement with experiment. It is a well known fact that the formation of Scheibe-dye aggregates is facilitated by bulky meso-substituents. This fact is explained by the brick-stonework model, which allows a tight packing of the molecules.

Keeping in mind this new structural concept, let us try to find a way to get Scheibe-aggregates of dyes by appropriately arranging the molecules in

## CHROMOPHORES IN MONOLAYER ASSEMBLIES

the monolayer<sup>19</sup>. We consider stearyl substituted cyanine dyes, not known as aggregate forming, such as dye S in *Figure 1*. The chromophore may be viewed schematically as a rectangular block with the dimensions given in *Figure 11a*, and the two hydrocarbon substituents as cylinders of diameter 5 Å. According to *Figure 11b* a close packing of the chromophores is only possible for a brick-stonework-like arrangement, with the chromophore

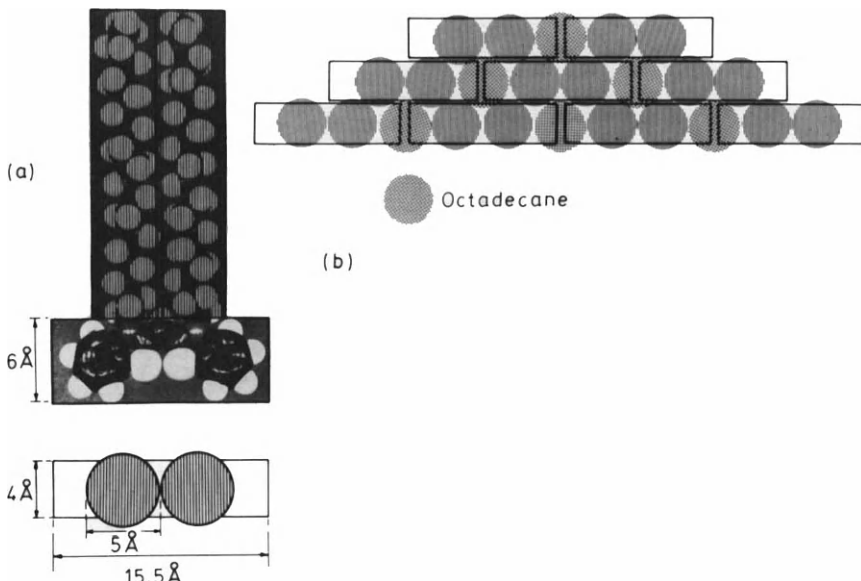


*Figure 11.* Scheibe-dye-aggregate formation in monolayer. (a) Dye molecule in broad side view and bird's-eye view. Chromophores approximated by rectangular block, stearyl groups by cylinders. (b) Brick-stonework arrangement of chromophores, octadecane chains fitting in the cylindrical holes left over by the stearyl substituents of the dye.

planes perpendicular to the monolayer plane, and the chromophore long axes parallel. This arrangement should lead to a stable layer, if closest packing of the hydrocarbon chains is also achieved. This condition is met by putting a hydrocarbon chain into each hole of the structure left over by the stearyl substituents of the dye molecules, i.e. by spreading a 1:1 mixture of this dye and a hydrocarbon such as octadecane (*Figure 11b*). The brick-stonework aggregates are forced to be formed by this trick and are really observed<sup>19</sup>: the typical narrow absorption band and the almost coinciding fluorescence band occur (*Figure 12*). The band, as explained by the model, appears only within a small range of the dye to hydrocarbon mixing ratio. For mixed dye monolayers, with a mixing component having a polar head group, the Scheibe-dye aggregate peak is not observed (*Figure 12b*): the polar head group of the mixing component breaks a hole in the structure.

In pure dye monolayers no compact structure is possible and no Scheibe-aggregates are observed. *Table 2* shows, for some cases, the theoretical and

experimental shift  $\lambda_p - \lambda_M$  of the peak of the Scheibe-dye-aggregates ( $\lambda_p$ ) with respect to that of the monomer ( $\lambda_M$ ).

In the case of carbocyanine dyes, which have two additional methine groups in the chain, a closely packed structure of mixed monolayers of dye

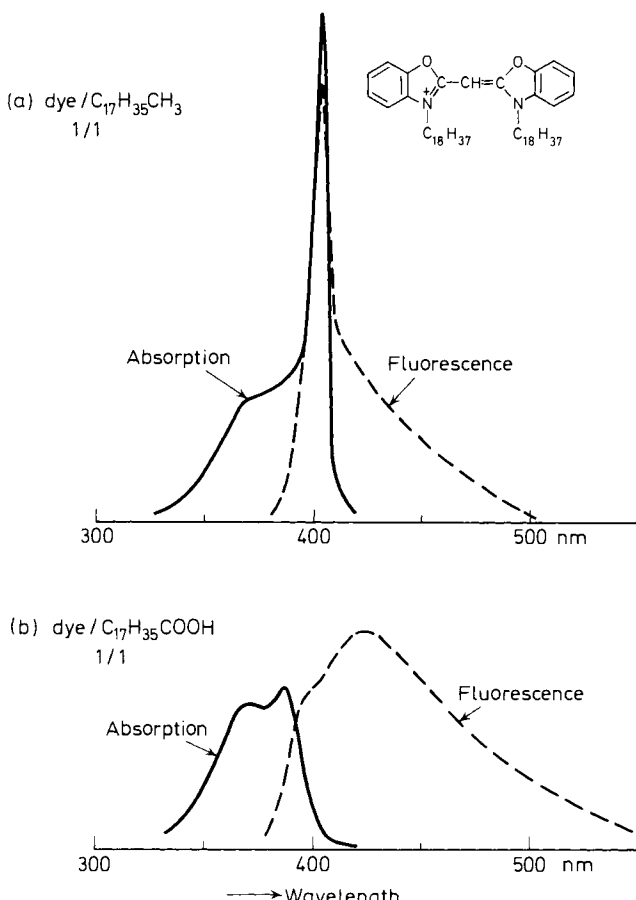


Figure 12. Spectra of cyanine dye and octadecane (a) and arachidic acid (b) in mixing ratio 1:1.

and octadecane is not possible and we may conclude that these dyes, contrary to the dyes considered above, should form no Scheibe-aggregates under similar conditions, and no such aggregates have been observed.

### (c) Electrochromism of Scheibe-dye aggregates

A brick-stonework aggregate monolayer may be sandwiched between arachidic acid monolayers and semitransmitting aluminium layers (Figure 13a)<sup>20</sup>. By applying voltages of a few volts, electric fields up to  $5 \times 10^6$  V/cm may be applied to the dye molecules. The excitation energy of the dye is changed in such fields and shifts of the absorption band are observed.

## CHROMOPHORES IN MONOLAYER ASSEMBLIES

A shift proportional to the applied field and a contribution proportional to the square of the field may be distinguished. The first contribution measures the difference between the dipole moment of the excited state and the ground state of the molecule, the second the change in polarizability.

The band shift is obtained by measuring the absorption change as a function of the frequency of the incident light (*Figure 14*). (In order to ensure a simple situation it is necessary to keep the distance between the aluminium electrodes such that the system has the property of an interference filter). In the example of *Figure 14* the values  $\Delta\mu_y = 0.07$  Debye and  $\Delta\alpha_{yy} = 1.5 \text{ \AA}^3$  are obtained from the linear and quadratic contributions, respectively.

In the known methods for obtaining information on these quantities, in contrast to the present method, the molecules are oriented in an electric field<sup>21</sup>. Then both polarizability and dipole moment changes produce band

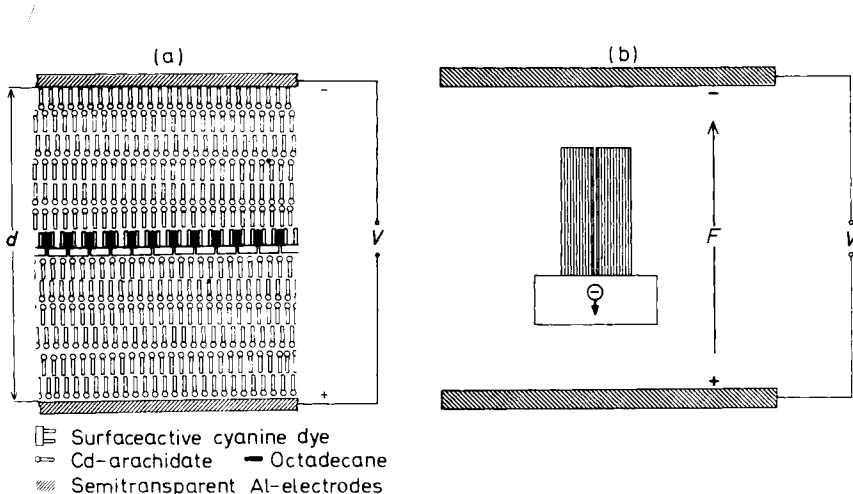


*Figure 13.* (a) Cross section through capacitor for measuring electrochromism. A single monolayer of Scheibe-dye-aggregate forming cyanine sandwiched between monolayers of cadmium arachidate and semitransparent electrodes. (b) Dye molecule in electric field. When light is absorbed negative charge moves in direction of arrow.

shifts proportional to the square of the field. For this reason it is not possible to measure polarizability changes by these methods.

Theoretical values for  $\Delta\mu_y$  and  $\Delta\alpha_{yy}$  of the dye in *Figure 14*, obtained by an electron gas model calculation ( $\Delta\mu_y = 0.2$  Debye,  $\Delta\alpha_{yy} = 3 \text{ \AA}^3$ ), have the same sign and similar absolute values as the above experimental data.

In the case of the linear contribution the essentials of the calculation are seen by considering the electron clouds given by the electron gas model in its simplest form, neglecting the branching of the  $\pi$ -electron system. The chromophore system then extends over the shaded area in *Figure 15*. The wave function of the highest occupied state has a wave with three antinodes, the next state four antinodes. By inspecting the electron clouds in both states it is immediately seen that the centre of gravity of the cloud, when exciting the chromophore, is shifted in the direction of the arrow in *Figure 13b*.

In the presence of an electric field, with a direction as indicated in *Figure 13b*, the excitation energy  $\Delta E$  is decreased, since the excitation of the molecule moves negative charge towards the positive electrode. Thus the absorption band of each single molecule is shifted to the red when applying the voltage. This causes a corresponding shift of the aggregate band: in the

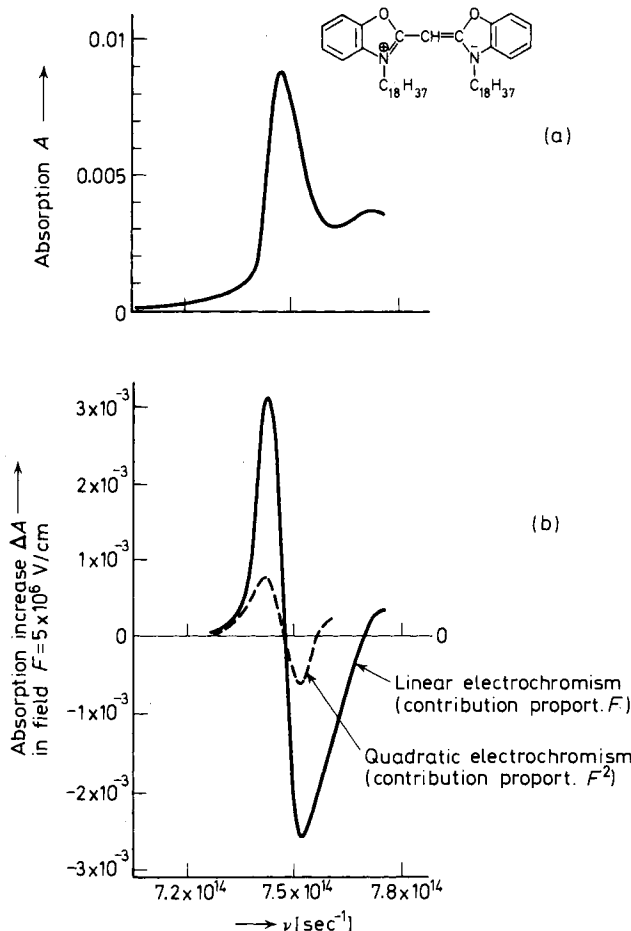
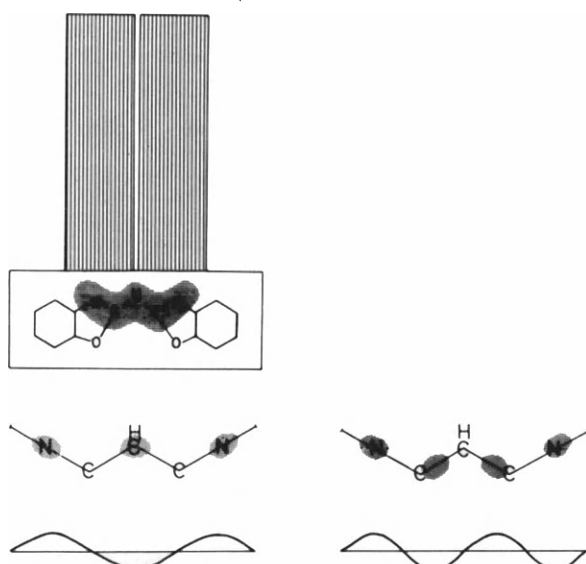


Figure 14. Electrochromism of cyanine dye. (a) Absorption  $A(v)$  of monolayer on a glass plate; (b) Monolayer in condenser of Figure 13. Absorption change  $\Delta A(v)$  induced in electric field of  $5 \times 10^6$  V/cm. Contribution proportional to  $F$  (full curve); contribution proportional to  $F^2$  (dashed curve).

classical picture the dipole substituting the dye oscillates slower and, consequently, the frequency of the coupled in-phase oscillation corresponding to the aggregate band is slower. When the polarizability of the applied voltage is reversed, the excitation energy is increased.

## CHROMOPHORES IN MONOLAYER ASSEMBLIES



*Figure 15.* Dye in *Figure 14*. Portion of chromophore taken into account in model calculation (shaded area). Proceeding from highest occupied orbital (three antinodes) to next orbital (four antinodes), the centre of gravity of electron cloud moves in direction from top to bottom.

## REFERENCES

- <sup>1</sup> M. M. Zwick and H. Kuhn. *Z. Naturforsch.* **17a**, 411 (1962); K. H. Drexhage, M. M. Zwick and H. Kuhn. *Ber. Bunsenges. Phys. Chem.* **67**, 62 (1963).
- <sup>2</sup> H. Bücher, K. H. Drexhage, M. Fleck, H. Kuhn, D. Möbius, F. P. Schäfer, J. Sondermann, W. Sperling, P. Tillmann and J. Wiegand. *Mol. Cryst. L* **2**, 199 (1967).
- H. Bücher, H. Kuhn, B. Mann, D. Möbius, L. v. Szentpály and P. Tillmann. *Photogr. Sci. Engng.* **11**, 233 (1967); Equation (8) should read  $E = K\Delta(\ln 10)^{-1}$  and in the equation following (8), instead of  $\alpha = (3/4\pi)[(\ln \lambda)/24]^{1/2} = 0.133$ , read  $\alpha = (3/4\pi)[(\ln 10)36]^{1/2} = 0.120$ .
- H. Bücher, O. v. Elsner, D. Möbius, P. Tillmann and J. Wiegand. *Z. Physik. Chem. N. F.* **65**, 152 (1969).
- <sup>3</sup> O. Inacker, D. Möbius and H. Kuhn. In print.
- <sup>4</sup> A. Rothen. *J. Phys. Chem.* **63**, 1929 (1959); *Biochim. Biophys. Acta* **88**, 606 (1964); *Physical Techniques in Biological Research* D. H. Moore, Ed., Vol. II, Part A, 2nd ed., Academic Press, New York and London, 1968, p. 217.
- <sup>5</sup> W. Mormann and H. Kuhn. *Z. Naturforsch.* **24b**, 1340 (1969).
- <sup>6</sup> P. Mueller, D. O. Rudin, H. T. Tien and W. C. Wescott in *Recent Progress in Surface Science* Vol. I. Academic Press, New York, London 1964, Ch. II.
- <sup>7</sup> P. Fromherz. *FEBS Letters*, **11**, 205 (1970); *Nature, Lond.* **231**, 267 (1971); *Biochim. Biophys. Acta*, **225**, 382 (1971).
- <sup>8</sup> S. Freed and S. I. Weissmann. *Phys. Rev.* **60**, 440 (1941); S. I. Weissmann and D. Lipkin. *J. Am. Chem. Soc.* **64**, 1916 (1942).
- <sup>9</sup> H. Kuhn. *J. Chem. Phys.* **53**, 101 (1970).
- <sup>10</sup> O. Inacker, H. Kuhn, H. Bücher, H. Meyer and K. H. Tews. *Chem. Phys. Lett.* **7**, 213 (1970). Instead of  $q_s = 0.14$  in first line of left row on page 215, read  $q_s = 0.41$ .
- <sup>11</sup> M. Fleck. Thesis, University of Marburg, 1968; K. H. Drexhage, M. Fleck and H. Kuhn. *Ber. Bunsenges. Phys. Chem.* **71**, 915 (1967).
- <sup>12</sup> K. H. Drexhage, M. Fleck, H. Kuhn, F. P. Schäfer and W. Sperling. *Ber. Bunsenges. Phys. Chem.* **70**, 1179 (1966); K. H. Drexhage, H. Kuhn, F. P. Schäfer. *Ber. Bunsenges. Phys. Chem.* **72**, 329 (1968).

HANS KUHN

- <sup>13</sup> K. H. Tews, O. Inacker and H. Kuhn. *Nature* **909**, 276 (1970). Equation (5) contains a printing error. Instead of  $x(\sin(x) - \pi/2)$  read:  $x(Si(x) - \pi/2)$ ; instead of 'ref. 5' in the third paragraph read 'ref. 6'.
- <sup>14</sup> H. Kuhn. *Naturwissenschaften* **54**, 429 (1967).
- <sup>15</sup> V. Czikkely, G. Dreizler, H. D. Försterling, H. Kuhn, J. Sondermann, P. Tillmann and J. Wiegand. *Z. Naturforsch.* **24a**, 1821 (1969).
- <sup>16</sup> G. Scheibe. *Angew. Chem.* **52**, 633 (1939); O. Wörz and G. Scheibe. *Z. Naturforsch.* **24b**, 381 (1969).
- <sup>17</sup> Th. Förster. *Naturwissenschaften* **33**, 166 (1946); E. G. McRae and M. Kasha. *J. Chem. Phys.* **28**, 721 (1958).
- <sup>18</sup> V. Czikkely, H. D. Försterling and H. Kuhn. *Chem. Phys. Lett.* **6**, 11 (1970).
- <sup>19</sup> H. Bücher and H. Kuhn. *Chem. Phys. Lett.* **6**, 183 (1970).
- <sup>20</sup> H. Bücher and H. Kuhn. *Z. Naturforsch.* **25b**, 1323 (1970).
- <sup>21</sup> See e.g. W. Liptay. *Angew. Chem.* **81**, 195 (1969); K. Siebold, H. Navangul and H. Labhardt. *Chem. Phys. Lett.* **3**, 275 (1969).

# ENERGY TRAPPING PROCESSES IN AROMATIC CRYSTALS

H. C. WOLF and K. W. BENZ

3 Physikalisches Institut der Universität Stuttgart,  
7 Stuttgart 1, Azenbergstrasse 12, Germany

## ABSTRACT

Excitons in ideal aromatic crystals are delocalized. So far no experimental evidence for self trapping of excitons is known. Trapping of energy is possible in mixed crystals or in crystals containing defects. Disturbed exciton states due to the presence of foreign molecules or due to structural defects (the so-called X-traps) are the most characteristic type of defects in aromatic crystals. Some spectroscopic experimental data on X-traps are collected and discussed. The most sensitive method for detecting traps is that of sensitized delayed fluorescence. The kinetics of sensitized delayed fluorescence is discussed and compared with that of prompt fluorescence. Trap concentrations as low as  $10^{-10}$  mol/mol can be detected using delayed fluorescence.

## I. THE IDEAL CRYSTAL

The *energy levels* of an ideal aromatic crystal, like naphthalene or anthracene, lie in bands: valence bands, exciton bands and conduction bands. Energy is completely delocalized in the ideal crystal.

The time scale for *transitions* is determined by the electronic structure of these bands, and by the transition matrix elements. Transitions between these crystal states are:

*Absorption* from the ground state  $S_0$  to excited states  $S_i$ .

*Fluorescence* from the lowest excited singlet state  $S_1$  to  $S_0$ . The lifetime of  $S_1$  is typically between 5 and 500 nsec.

*Internal conversion* between different excited S states or triplet (T) states. These processes occur in less than 0.1 nsec.

*Intersystem crossing* between the singlet and the triplet manifold. The typical time constants are 100–1000 nsec.

*Phosphorescence* from the lowest excited triplet state  $T_1$  to the ground state  $S_0$ . The lifetime of  $T_1$  is typically between 1 and  $10^4$  msec and is determined by radiationless processes.

*Energy storage* for times longer than 0.5  $\mu$ sec is possible only in the  $T_1$  band. Energy relaxation between the energy bands (internal conversion) is due to exciton-phonon interaction. Trapping processes, which are able to localize energy at specific sites in the perfect crystal are unknown so far. There is no experimental evidence for the self trapped exciton, which was first discussed by Frenkel<sup>1</sup>, and later by Sidman<sup>2</sup>.

*Self trapping* of an exciton is a process in which the exciton induces a lattice relaxation, which should be responsible for some energy loss, for a Stokes-shift between absorption and emission and, perhaps, for some kind of localization of the exciton. Among the well investigated crystals only in anthracene is there a Stokes-shift between the maxima of  $S_0-S_1$  absorption and  $S_1-S_0$  emission, even after exclusion of other traps (Figure 1)<sup>3,4</sup>.

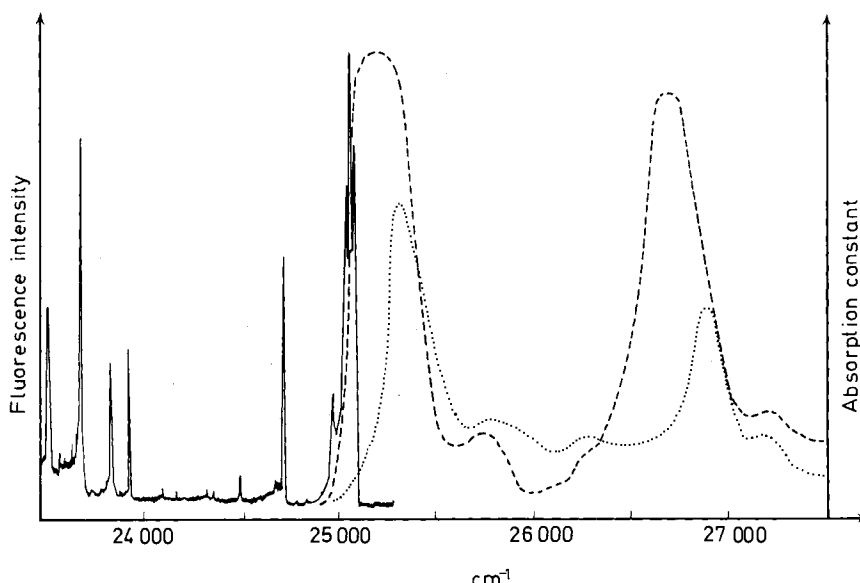


Figure 1. Absorption (right) and fluorescence (left) spectrum of crystalline anthracene near 0.0 of the lowest singlet transition. After references 3 and 4. 4.2°K. The absorption spectrum is given parallel to axes  $b$  (—) and  $a$  (....). The 0.0 line in emission at  $25\,097\text{ cm}^{-1}$  is not visible due to reabsorption. The first strong emission line is the 0.0 line of the  $X_1$ -series<sup>4</sup>

But this Stokes-shift gives no evidence for exciton self trapping. The shift has been explained by the specific exciton band structure in anthracene<sup>4</sup> and the  $k$ -selection rule. An alternative explanation makes use of special surface states<sup>5</sup>.

In conclusion, the problem of traps and trapping is a problem of the real, imperfect crystal.

## II. THE REAL CRYSTAL

For the spectroscopist, the main difference between the ideal and the real crystal is the existence of traps in the latter. Very often emission spectra are, more or less, only trap spectra because of the high sensitivity of the sensitized fluorescence.

*Exciton traps* are sites capable of holding energy that, otherwise, propagates through the lattice. Traps are localized, non-periodic states in the crystal. Their time scale is determined by the specific electronic structure of the trap.

## ENERGY TRAPPING PROCESSES IN AROMATIC CRYSTALS

Traps change the spectral energy distribution in spectra, especially in fluorescence. Traps change the time dependence of electronic population and depopulation processes in the crystal.

Traps are interesting:

as probes for measuring intrinsic properties of the host crystal, for instance the phonon structure of the host crystal from the phonon wings, which accompany guest fluorescence lines in mixed crystals<sup>6</sup>.

in themselves, because they are responsible for electronic and optical properties of the mixed or real crystal, which are different from those of the pure or ideal host crystal.

In the following two specific topics are discussed in detail: the so called X-traps, and the kinetics of trap-induced delayed fluorescence.

### III. DIFFERENT KINDS OF TRAPS

In organic crystals, three types of traps have been observed and discussed so far:

1. *Guest molecules*, like the oldest example, tetracene in anthracene. The guest molecule can be identified by its spectral properties, which are different from those of the host crystal. Guest molecules are traps, if their  $S_1$  state is lower than the host crystal  $S_1$  exciton band. If these guest molecules are deep traps ( $\Delta E \gg kT$ ), sensitized fluorescence is observed.

2. *Self trapping*. This process has been discussed in section I.

3. *Disturbed exciton states in the crystal, X-traps*. These X-traps are very characteristic defects in organic crystals. The name X-series has been coined for vibronic series in the luminescence spectra of crystals which are identical with the intrinsic host emission, but red shifted by a certain amount of energy<sup>7</sup>. This is the emission from disturbed regions of the crystal.

The perturbation can be due to the presence of *foreign molecules* (impurities

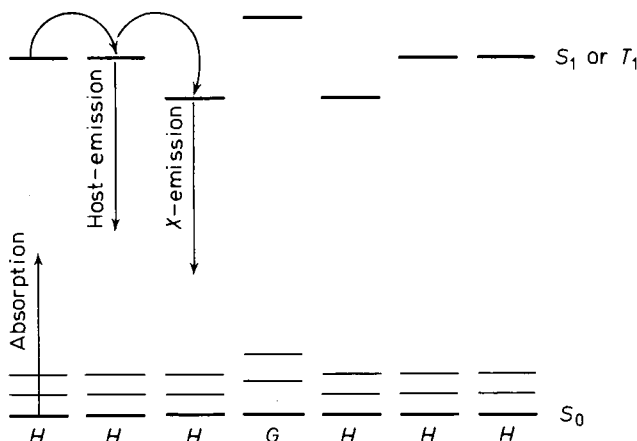


Figure 2. Energy level scheme of a host (H) crystal with guest (G) molecules, which induce X-traps. For simplification, the host exciton band is approximated by the individual molecule energy levels

or guest molecules) in the matrix, which cannot act as traps themselves, because the energy of their lowest  $S_1$  state is higher than the bottom of the host  $S_1$  band. But host molecules around these impurities are shifted in energy and can act as energy traps. A schematic energy level diagram for  $X$ -traps is shown in *Figure 2*. These impurity-induced  $X$ -traps can be removed partially or completely by crystal purification.

The second possible reason for  $X$ -series can be *structural defects* or dislocations in the lattice. These  $X$ -traps are insensitive towards purification processes, but they can be removed by annealing.

It is impossible to understand most of the spectroscopic solid-state properties of organic crystals without taking into account these  $X$ -traps. They are the analogues of the so called  $\alpha$  and  $\beta$ -bands in alkali halides<sup>8</sup>, which have been well known for nearly forty years.

It is important to notice that the  $X$ -traps, which have been found so far, are always relatively shallow traps. At room temperature they are more or less ineffective.

#### IV. EXAMPLES OF X-TRAPS IN OPTICAL SPECTRA

In this section are collected some experimental data on  $X$ -traps in different crystals, and identified by different methods.

In the fluorescence spectrum of naphthalene crystals of high purity, 4 main series of lines have been identified<sup>7</sup>: one of them, with 0.0 at  $31474\text{ cm}^{-1}$ , is the emission originating from the exciton band  $S_1$ . The other three, with 0.0 at 31444, 31418 and 31395, are emission series originating from naphthalene molecules with an  $S_1$ -level  $\Delta E = 30, 56$  and  $79\text{ cm}^{-1}$ , respectively, below the bottom of the naphthalene exciton band.

The perturber which induces the  $30\text{ cm}^{-1}$   $X$ -trap has been identified as thionaphthene. The other perturbers are impurities  $X$ , unidentified so far. This is the reason for the name  $X$ -trap. All the  $X$ -series have the vibronic progressions characteristic of the naphthalene molecule. The  $X$ -series are identical in energy with the naphthalene series, but shifted to lower energy by  $\Delta E$ . The lines of the  $X$ -series are much sharper than the lines in the host series.

In contrast to these impurity-induced  $X$ -traps,  $\beta$ -methyl-naphthalene in naphthalene is a real trap, with 0.0 at  $31059\text{ cm}^{-1}$  and a vibronic structure of the fluorescence spectrum characteristic of the  $\beta$ -methyl-naphthalene molecule.

One can create additional  $X$ -traps by introducing *structural imperfections* into the crystal. In naphthalene this has been investigated using plastic deformation<sup>9</sup>. In the fluorescence spectrum of plastically deformed naphthalene crystals, one observes three different characteristic structures:

1. One sharp  $X$ -series, shifted  $165\text{ cm}^{-1}$  to lower energies (0.0 at  $31309\text{ cm}^{-1}$ ).
2. A continuous background (called subnaphthalene series in reference 9).
3. Emission typical of excimers with the maximum at about  $24000\text{ cm}^{-1}$ .

These three types of spectra can be reduced in intensity by annealing. In some cases, annealing is improved by simultaneous excitation with light<sup>9</sup>. The relative intensity of the different spectra is a function of temperature, corresponding to the different trap depth.

## ENERGY TRAPPING PROCESSES IN AROMATIC CRYSTALS

The fluorescence spectrum of extremely pure anthracene crystals also contains many lines which are due to *X*-traps. In addition to the intrinsic fluorescence, originating at  $25097\text{ cm}^{-1}$ , *X*-series are observed<sup>10</sup> with 0.0 at 25074, 25030, 24850 and  $24823\text{ cm}^{-1}$ . Similar observations are reported by other authors<sup>11, 12</sup>.

*X*-traps are present also in the triplet state  $T_1$ . It is much easier to observe them via delayed fluorescence than directly by phosphorescence spectra. In naphthalene, the following triplet state *X*-traps have been identified<sup>13</sup>: thionaphthalene introduces an *X*-trap with  $\Delta E = 45\text{ cm}^{-1}$ , durene one at  $60\text{ cm}^{-1}$ , and other *X*-traps are present which have not been identified so far<sup>14</sup>. As in the singlet state,  $\beta$ -methyl-naphthalene is a guest molecule, not an *X*-trap, with  $\Delta E = 240\text{ cm}^{-1}$ . In anthracene crystals, the trap<sup>10</sup>  $X_4$  which is  $274\text{ cm}^{-1}$  below the  $S_1$  exciton band is also an *X*-trap in the triplet state, with<sup>15</sup>  $\Delta E = 24\text{ cm}^{-1}$ .

In addition to the unperturbed exciton emission of the host and *X*-series, the spectrum of delayed fluorescence in anthracene and naphthalene crystals contains a continuous background, which is due to a continuous energy distribution of traps<sup>14, 15</sup>. All types of trap spectra are much more pro-

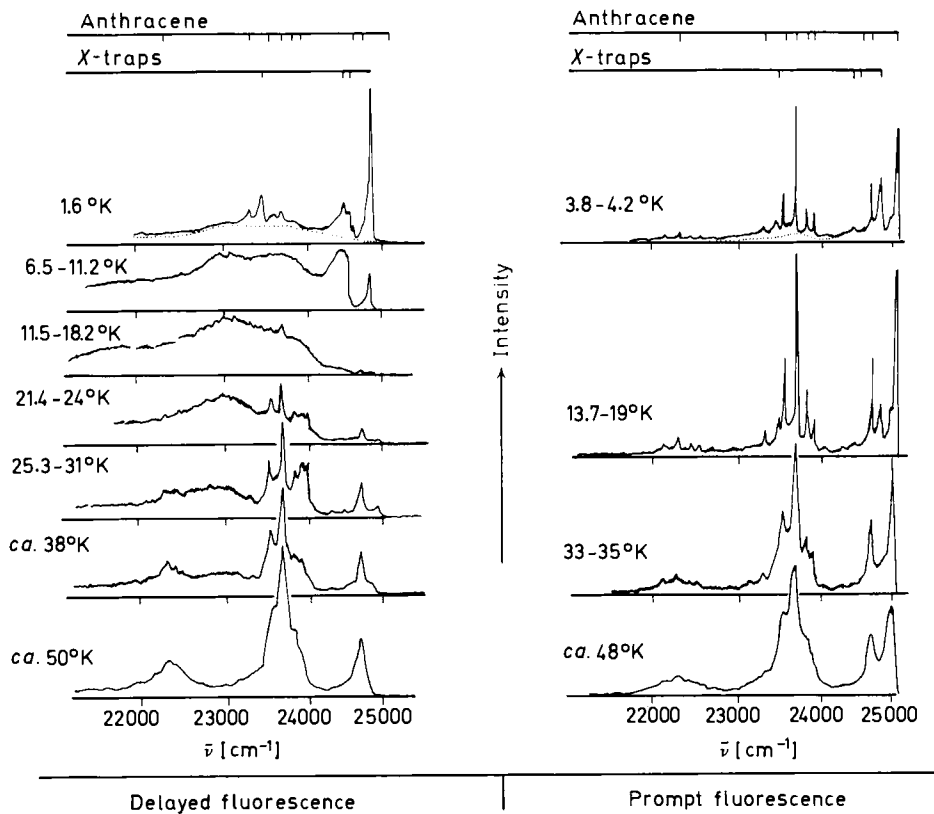


Figure 3. Spectrum of delayed and prompt fluorescence of very pure anthracene crystals between 1.6 and  $50^\circ\text{K}$ . From reference 15

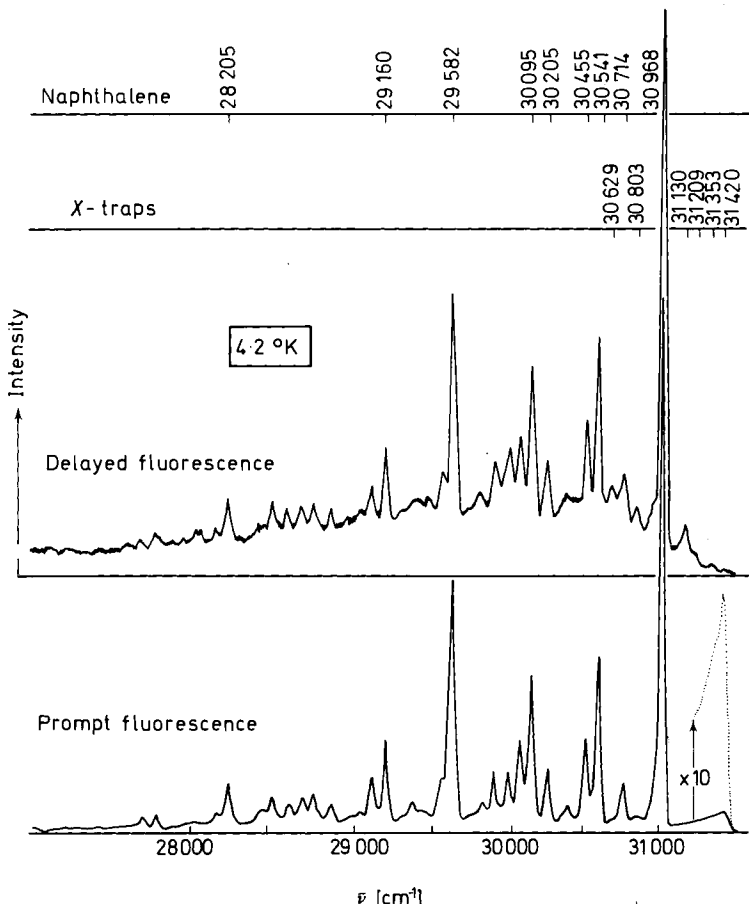


Figure 4. Spectrum of delayed and prompt fluorescence of a very pure naphthalene crystal at 4.2°K. From reference 15

nounced in delayed fluorescence than in prompt fluorescence—an observation which will be discussed in section VI. The trap spectra disappear with increasing temperature when the traps are thermally depopulated. Figure 3 shows the temperature dependence of delayed and prompt fluorescence in pure anthracene crystals. In delayed fluorescence the trap emission is much more pronounced than in prompt fluorescence. A plot of the *X*-trap emission relative to the continuous background versus temperature (Figure 5) can be used to determine the trap depth  $\Delta E$ .

*X*-traps are also observable in phosphorescence. In pyrazine crystals at 4.2°K two *X*-series have been observed<sup>16</sup>. Azumi called them impurity induced resonance defects.

#### V. X-TRAPS IN ESR SPECTRA

*X*-traps can be identified and are important also in ESR spectra of the metastable triplet state  $T_1$  at low temperature. A good example is quinoxaline

## ENERGY TRAPPING PROCESSES IN AROMATIC CRYSTALS

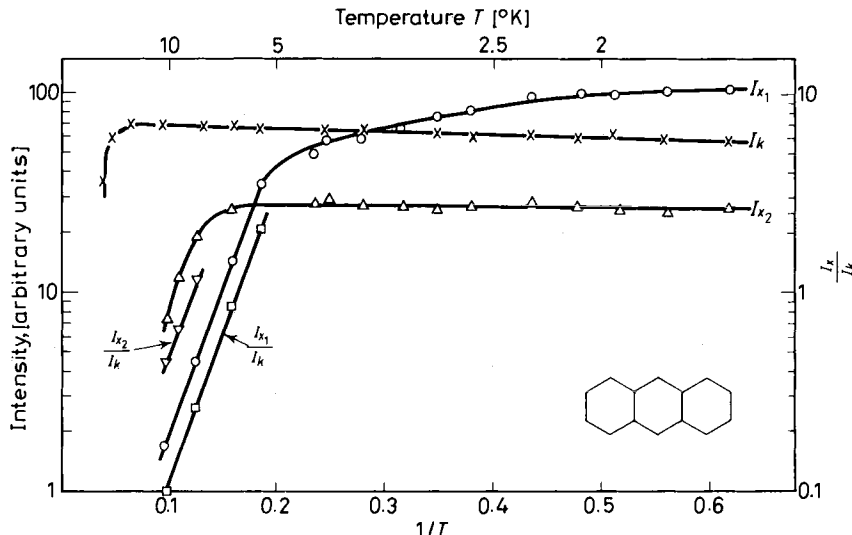


Figure 5. Temperature dependence of the intensity  $I$  of the series  $X_1$ ,  $X_2$  and the continuum  $K$  in the delayed fluorescence spectrum of anthracene crystals between 1.6 and 20°K. Determination of the trap depth  $\Delta E$ . From reference 15

in a naphthalene matrix<sup>17</sup>. In a matrix of normal naphthalene ( $N-h_8$ ), quinoxaline introduces an  $X$ -trap with  $\Delta E = 60 \text{ cm}^{-1}$ . The ESR spectrum observed at low temperature ( $< 4.2^\circ\text{K}$ ) (Figure 6) is therefore due to naphthalene molecules. This is demonstrated by the hyperfine structure of the ESR spectrum. The hyperfine structure is due to the four equivalent  $\alpha$  protons in the naphthalene molecule. The hyperfine structure due to the  $\beta$ -protons cannot be resolved. According to the angular dependence of the ESR-spectrum, the misorientation of the  $X$ -trap naphthalene molecule is less than  $2^\circ$ . In addition, the ESR spectrum shows no indication of any delocalization of the triplet energy. This means that the  $X$ -trap is probably only *one* very slightly disturbed naphthalene molecule in the vicinity of the quinoxaline molecule. With increasing temperature the ESR signal vanishes due to thermal detrapping (Figure 7).

In contrast to  $N-h_8$ , quinoxaline in perdeutero-naphthalene is a real trap. The ESR spectrum of  $N-d_8$  crystals doped with quinoxaline is therefore a quinoxaline spectrum. The hyperfine structure is typical of two equivalent  $\alpha$  protons and four equivalent  $\beta$ -protons (Figure 6).

ESR and ENDOR spectroscopy is a powerful method for getting very detailed information on the structure of  $X$ -traps. Other  $X$ -traps which have been identified, using ESR-spectroscopy, are due to quinazoline and thionaphthene in naphthalene and dibenzothiophene and carbazole in fluorene<sup>18</sup>.

Theoretical calculations on the electronic structure of disturbed exciton states were first published by Merrifield<sup>19</sup>. A very detailed comprehensive review is given by Rice and Jortner<sup>20</sup>. Many new experimental data have been collected in the meantime. It seems worthwhile to use these data as a

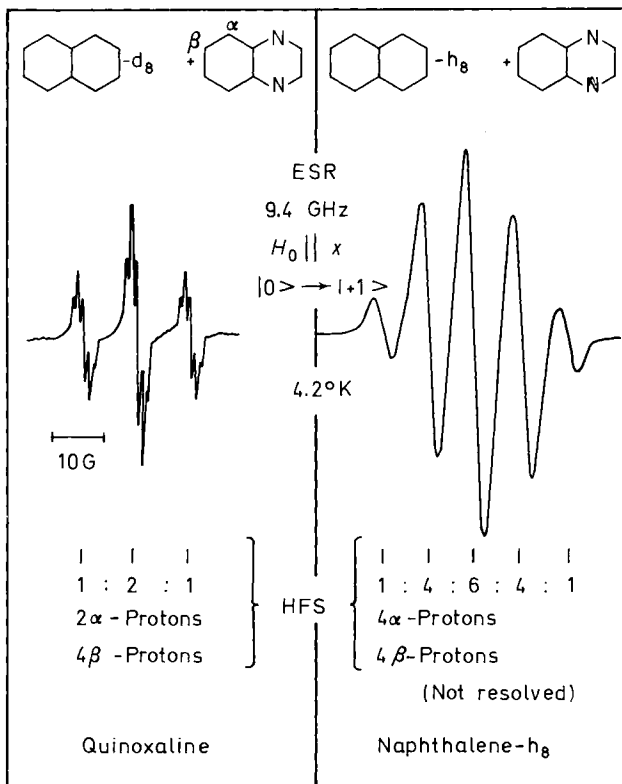


Figure 6. Hyperfine structure of one ESR-line ( $\Delta m = 1$  transition) in the ESR spectrum of the triplet state of quinoxaline in perdeutero-naphthalene (left), and of the  $X$ -trap which is induced by quinoxaline in naphthalene (right). The quinoxaline concentration was the same in both crystals. The hyperfine structure is characteristic of quinoxaline (left) and of naphthalene (right). (This figure was kindly supplied by M. Schwoerer)

basis for more detailed theoretical work, which could help us to get a better understanding of the nature of these defects in molecular crystals. In semiconducting materials, like silicon and germanium, similar disturbed exciton states are known. An empirical rule has been proposed<sup>21</sup>, which correlates the trap depth and the physical nature of the perturber.

In a series of recent papers, Jortner *et al.*<sup>22</sup> have treated the  $X$ -trap problem theoretically in a very detailed manner. They have shown that  $X$ -trapping is due to the solvent shift terms. An  $X$ -trap host molecule is just a host molecule in a different environment. It seems worthwhile to apply these calculations to the experimental data collected above.

In Table 1 experimental data on  $X$ -traps in naphthalene and anthracene crystals are collected.

## VI. KINETICS OF TRAPPING PROCESSES

Trapping processes are responsible for the well known phenomenon of

## ENERGY TRAPPING PROCESSES IN AROMATIC CRYSTALS

 Table 1. Some X-traps in naphthalene and anthracene and their trap depths,  $\Delta E$ , in the singlet and in the triplet state

Matrix	Perturber	$\Delta E$ in $S_1$ $\text{cm}^{-1}$	$\Delta E$ in $T_1$ $\text{cm}^{-1}$	References
<b>Naphthalene</b>				
	thionaphthene	30	45	7, 13
	unknown impurity	56		7
	unknown impurity	79		7
	structural defect	165		9
	continuum	continuous		9
	durene		60	13
	quinoxaline		ca. 60	17
	unknown	144		14
	unknown	268	23	14
	unknown	346	32	14
<b>Anthracene</b>				
	unknown defects or impurities	23 67 247 274		10 10 10 24
	continuum	continuous		10, 15

sensitized fluorescence, where low concentrations of impurity molecules are able to convert the host fluorescence into guest (impurity) emission. The delayed fluorescence is even more sensitive towards impurities, because of the effectiveness of energy transfer, and sensitized delayed fluorescence is a method for detecting impurities or traps in concentrations a hundred times lower than is sensitized prompt fluorescence.

This is demonstrated by Figures 8 and 9. Figure 8 shows the fluorescence spectrum of a mixed crystal naphthalene with  $2 \times 10^{-7}$  parts of anthracene. Whereas in prompt fluorescence the anthracene concentration is too low to convert much of the naphthalene emission into anthracene fluorescence and anthracene emission is almost absent, in delayed fluorescence the anthracene emission is more intense than that of naphthalene. Energy transfer can be measured quantitatively by determining the quantum ratio  $Q_G/Q_H$  (guest quanta divided by host quanta) as a function of guest concentration. This quantum ratio is, according to Figure 9, 100 times higher in delayed fluorescence than in prompt fluorescence. Also Figures 3 and 4 demonstrate the much higher sensitivity of delayed fluorescence than of prompt fluorescence towards impurities and traps.

In this section, the effectiveness of delayed sensitized fluorescence is calculated and compared with that of sensitized prompt fluorescence.

The kinetics of population and depopulation of traps, which can be guest molecules or X-traps, is described in the following general scheme (Figure 10):

1. Excitons are created by absorption of light of intensity  $I$  with absorption coefficient  $\alpha_S$  or  $\alpha_T$ . Exciton bands  $S_1$  or  $T_1$  are populated by internal conversion and intersystem crossing.
2. Excitons can decay with emission of a photon, radiatively, into the ground state  $S_0$  with a rate constant  $k_H^*$  for singlets and  $\beta_H^*$  for triplets.

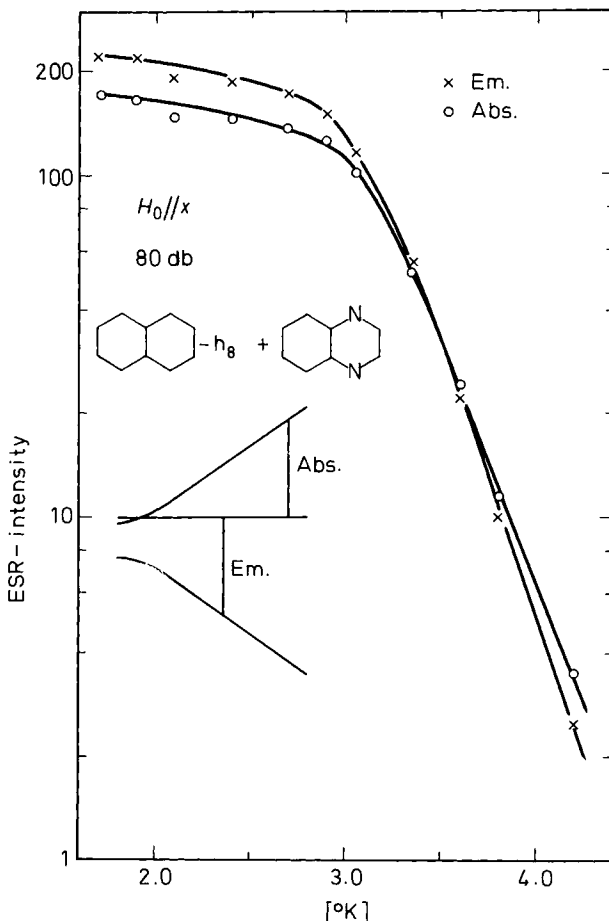


Figure 7. Temperature dependence of the intensity of the two ESR lines of the  $X$ -trap induced in naphthalene by quinoxaline. One of the two lines is emissive due to optical spin polarization.  
(This figure was kindly supplied by M. Schwoerer)

3. Radiationless processes are competitive, with rate constants  $k'_H$  and  $\beta'_H$ ;  $k = k' + k^*$ ,  $\beta = \beta' + \beta^*$ .
4. Excitons can relax into traps, which are  $\Delta E$  lower in energy with a rate constant  $k_{HG}$  and  $\beta_{HG}$ .
5. Traps can be thermally depopulated back into the exciton band, if the temperature is high enough.
6. Traps can be depopulated by emission of a photon radiatively into the ground state  $S_0$ , rate constant  $k'_G$ .
7. Traps can be depopulated nonradiatively  $k''_G$ .
8. Triplet traps can be depopulated by triplet-triplet annihilation, annihilation coefficient  $\gamma_G$ .
9. Triplet annihilation is also effective in the  $T_1$  exciton band, without traps, annihilation coefficient  $\gamma$ .

ENERGY TRAPPING PROCESSES IN AROMATIC CRYSTALS

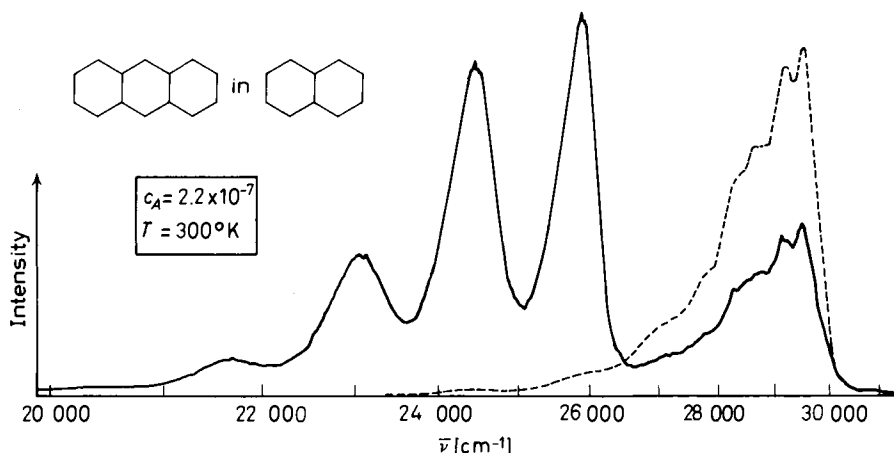


Figure 8. Spectrum of prompt (broken line) and delayed (full line) fluorescence in a naphthalene crystal containing  $2.2 \times 10^{-7}$  parts of anthracene, at room temperature. Anthracene emission is below  $26500\text{ cm}^{-1}$ . From reference 15

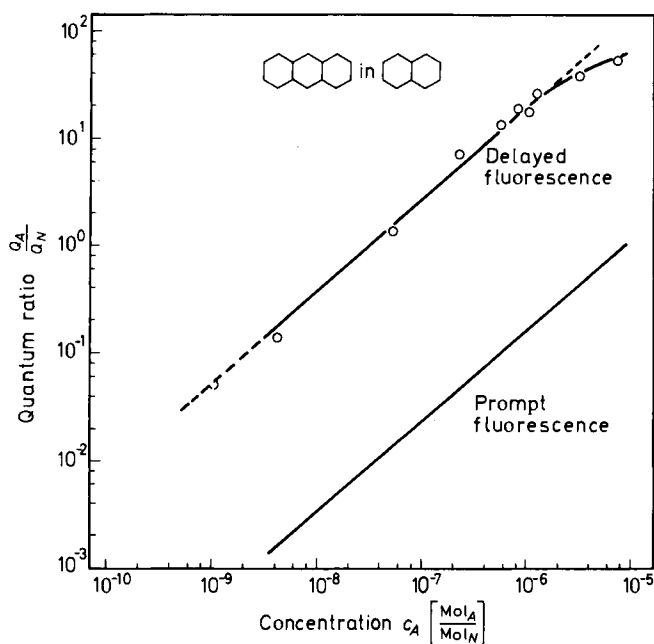


Figure 9. Quantum ratio  $Q_A/Q_N$  in naphthalene crystals with different anthracene concentrations, delayed and prompt fluorescence. The concentration was measured by absorption. From references 14 and 15

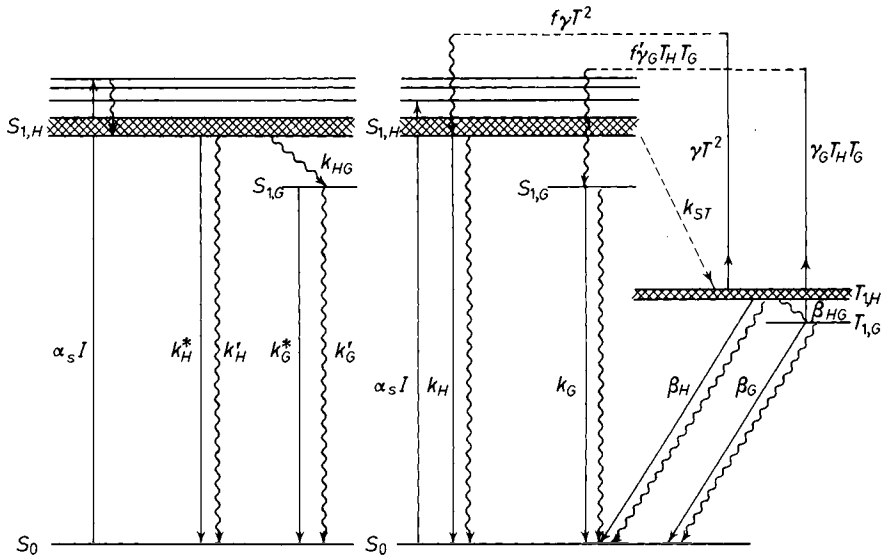


Figure 10. Kinetics of sensitized prompt fluorescence (left) and sensitized delayed fluorescence (right) for a host-guest system

The process which determines the effectiveness of traps is mainly process 4, the exciton capture by traps. During their lifetimes excitons scan the crystal for traps. The concentration of traps, the exciton lifetime and the diffusion rate of the exciton determine, therefore, the capture probability.

Many different models for exciton motion have been discussed in the past. It seems that the very simple hopping model is a quite adequate description<sup>23</sup>, at least as long as energy transfer is concerned. In this model the exciton jumps statistically from molecule to molecule in the lattice with a characteristic hopping time  $t_h$ . This time is related to the diffusion coefficient  $D$  by an expression of the form<sup>23</sup>  $t_h = \pi D R N_H$ ;  $R$  = defect radius,  $N_H$  = number of host molecules per cm<sup>3</sup>. The number of lattice sites visited during the lifetime is given by the quotient lifetime divided by hopping time (if one neglects the probability of visiting the same site more than once)<sup>24</sup>. This model has been discussed in great detail by Suna recently<sup>25</sup>. In prompt fluorescence one measures the singlet traps which are populated by the scanning exciton, in delayed fluorescence the triplet traps.

The quantum ratio of guest to host emission is calculated in the following way (Figure 10):

#### A. Prompt fluorescence

The rate equations for host and guest singlet excitons  $S_H$  and  $S_G$  (number of excited states per volume) are in the deep trap limit ( $\Delta E \gg kT$ ), neglecting intersystem crossing into the triplet state,

$$\frac{dS_H}{dt} = \alpha_s I - k_H S_H - k_{HG} S_H \quad (1)$$

$$\frac{dS_G}{dt} = k_{HG}S_H - k_G S_G \quad (2)$$

The quantum flux  $Q_H, Q_G$  (number of quanta per volume and sec) is given by

$$Q_H = k_H^* S_H \quad (3)$$

$$Q_G = k_G^* S_G \quad (4)$$

In the stationary case,  $dS/dt = 0$ , one gets from (2)

$$\frac{S_G}{S_H} = \frac{k_{HG}}{k_G} \quad (2a)$$

and finally the quantum ratio

$$\left(\frac{Q_G}{Q_H}\right)_{\text{prompt fluorescence}} = \frac{k_G^*}{k_H^*} \times \frac{k_{HG}}{k_G} \quad (5)$$

(5) can also be written in the form

$$\left(\frac{Q_G}{Q_H}\right)_{PF} = \eta_G \frac{k_{HG}}{k_H^*} \quad (5a)$$

$\eta_G$  = quantum yield of the guest fluorescence

In the hopping model, the simplest assumption for the transfer rate constant  $k_{HG}$  is

$$k_{HG} = \frac{c_G}{t_{h, \text{ singlet}}} \quad (6)$$

$c_G$  = guest concentration in mol/mol

$t_h$  = hopping time

With (5) and (6) one gets as quantum ratio

$$\left(\frac{Q_G}{Q_H}\right)_{\text{prompt fluorescence}} = \frac{\eta_G c_G}{k_H^* t_{h, \text{ singlet}}} = K_{\text{singlet}} \times c_G \quad (7)$$

$K$  = transfer constant as defined in reference 23.

Equation (6) is based on the following simplifications:

1. It is assumed that transfer of excitation is by hopping from molecule to the nearest neighbour molecule, and that the capture cross section is the same for host and guest molecules. The validity of this assumption is questioned by new experiments of Baessler *et al.*<sup>32</sup>.

2. It is assumed that the probability for the hopping exciton to meet a guest molecule is proportional to the guest concentration. Due to the possibility that the excitation is able to visit one lattice site more than once, this assumption is valid only at low concentrations<sup>24</sup>.

Equation (7) has been derived and verified in the system anthracene/tetracene<sup>26</sup>. In this system, the measured transfer constant  $K_{\text{singlet}}$  in the equation  $Q_G/Q_H = K \times c_G^p$ , is  $(6 \pm 3) \times 10^4$ , with the exponent  $p = 0.8 \pm 0.2$ .  $K$ -values in other systems have the same order of magnitude<sup>23</sup>. At a guest concentration of  $c_G = 10^{-7}$ , the quantum ratio is 0.01. Therefore it is possible to detect traps and impurities using sensitized fluorescence at concentrations down to  $10^{-7} - 10^{-8}$ .

Using equation (7), the hopping time  $t_h$  can be calculated. For the system anthracene in naphthalene, the following value has been measured:

$$K_{\text{singlet}} = 10^5 \text{ (Figure 9)}$$

Taking  $\eta_G$  (anthracene in naphthalene) = 1 and  $k_H^*$  (naphthalene, room temperature) =  $2 \times 10^6 \text{ sec}^{-1}$ , one gets for naphthalene

$$t_{h,\text{singlet}} = 5 \times 10^{-12} \text{ sec} (\pm 50\%)$$

Equations (1)-(7) are valid for a two component system, host and guest. If there are other traps present with a trap depth comparable to  $kT$ , then the apparent quantum ratio is a function of temperature<sup>23, 26</sup>. By this freezing of energy transfer one can measure trap concentrations down to approximately  $10^{-7}$ .

### B. Delayed fluorescence

Again we discuss only a two component system (guest and host), and we assume homogeneous excitation. If one excites into the singlet state, the following rate equations describe the time dependence of concentration of triplet excitons,  $T_H$  and  $T_G$  (Figure 10):

$$\frac{dT_H}{dt} = \eta_{ST}\alpha_S I - \beta_H T_H - \beta_{HG} T_H - \gamma_G T_H T_G - \gamma T_H^2 \quad (11)$$

$\eta_{ST}$  = quantum yield for intersystem crossing

$$\frac{dT_G}{dt} = \beta_{HG} T_H - \beta_G T_G - \gamma_G T_H T_G \quad (12)$$

If one excites directly into the triplet state, one has to replace the expression  $\eta_{ST}\alpha_S I$  in (11) by  $\alpha_T I$ .

At low concentration, delayed host fluorescence is entirely due to host/host annihilation, and delayed guest fluorescence entirely due to host/guest annihilation. Therefore the rate equations for singlet excitons created by triplet-triplet annihilation are:

$$\frac{dS_H}{dt} = \frac{1}{2}f\gamma T_H^2 - k_H S_H \quad (13)$$

$$\frac{dS_G}{dt} = \frac{1}{2}f'\gamma_G T_H T_G - k_G S_G \quad (14)$$

$f$  and  $f'$  are the fraction of triplet-triplet annihilation processes which result in singlet states  $S_1$ .  $f$  and  $f'$  are near<sup>27</sup> 0.4.

ENERGY TRAPPING PROCESSES IN AROMATIC CRYSTALS

In the stationary case,

$$\frac{dT_H}{dt} = \frac{dT_G}{dt} = \frac{dS_H}{dt} = \frac{dS_G}{dt} = 0.$$

Saturation of traps is neglected. Using equations (3), (4), (13) and (14), one gets the quantum ratio :

$$\left(\frac{Q_G}{Q_H}\right)_{\text{Delayed fluorescence}} = \frac{\eta_G}{\eta_H} \times \frac{f' \gamma_G}{f \gamma} \times \frac{T_G}{T_H} \quad (15)$$

The triplet concentrations  $T_G$  and  $T_H$  are a function of the intensity  $I$  of the exciting light. At low excitation intensities (or low stationary triplet concentrations), the triplet lifetime is determined by monomolecular decay, at high excitation intensities by bimolecular annihilation. The two limiting cases have to be discussed separately.

*a. Weak excitation,  $\beta_G T_G \gg \gamma T_G T_H$*

Equation (12) transforms into

$$\frac{T_G}{T_H} = \frac{\beta_{HG}}{\beta_G} \quad (12a)$$

Equation (12a) is completely analogous to the singlet state equation (2a), and the quantum ratio is independent of  $I$ :

$$\frac{Q_G}{Q_H} = \frac{\eta_G f' \gamma_G}{\eta_H f \gamma} \frac{\beta_{HG}}{\beta_G} \quad (15a)$$

In the hopping model, the transfer rate is given by

$$\beta_{HG} = \frac{c_G}{t_{h, \text{ triplet}}} \quad (16)$$

and finally one gets the quantum ratio

$$\begin{aligned} \left(\frac{Q_G}{Q_H}\right)_{\substack{\text{Delayed fluorescence}, \\ \text{weak excitation}}} &= \frac{\eta_G f' \gamma_G}{\eta_H f \gamma} \frac{c_G}{\beta_G t_{h, \text{ triplet}}} \\ &= K_{\text{triplet}} \times c_G \end{aligned} \quad (17)$$

Comparing equations (7) and (17) one realises immediately that the ratio of the transfer constants  $K_{\text{triplet}}/K_{\text{singlet}}$  is determined by the ratio

$$\frac{k_H^* t_{h, \text{ singlet}}}{\beta_G t_{h, \text{ triplet}}}$$

Now the experimental results (*Figure 9*) are compared with equation (17). In the system anthracene in naphthalene, the experimentally determined transfer constant is roughly

$$K_{\text{triplet}} = 3 \times 10^7 \text{ (Figure 9)}$$

We use the following approximate numerical values:

$\eta_G = 1^{28}$ ,  $\eta_H = 0.2^{28}$ ,  $f = 0.4^{27}$ ,  $\gamma = 3.5 \times 10^{-12} \text{ cm}^3 \text{ sec}^{-1}$ <sup>14</sup>, and we assume without experimental proof that  $f = f'$  and  $\gamma = \gamma_G$ ;  $\beta_G = 300 \text{ sec}^{-1}$ <sup>14</sup>. So we get the triplet hopping time  $t_h$ :

$$t_h = 5 \times 10^{-11} \text{ sec} (\pm 50\%)$$

This value is consistent with results from ESR<sup>29</sup> and NMR<sup>30</sup> measurements.

Now we are able to discuss the *limiting sensitivity* of sensitized delayed fluorescence for detecting impurities. Since the transfer constant  $K = 3 \times 10^7$ , the quantum ratio equation (17) is 0.01 at  $c_G = 3 \times 10^{-10}$ . Consequently, using delayed fluorescence, one is able to detect anthracene in naphthalene at concentrations as low as  $10^{-10}$ , more than two orders of magnitude lower than using prompt fluorescence. This is mainly due to the long lifetime of the triplet traps,  $\beta_G$  in equation (17), since the hopping time  $t_h$  is 10 times longer for triplet excitons than for singlets. Similar conclusions have been derived for the mixed system anthracene in phenanthrene<sup>31</sup>.

### $\beta$ . Strong excitation, $\beta_G T_G \ll \gamma_G T_G T_H$

From equation (12) one gets

$$T_G = \frac{\beta_{HG}}{\gamma_G} \quad (12b)$$

and from (15)

$$\left( \frac{Q_G}{Q_H} \right)_{\substack{\text{Delayed fluorescence} \\ \text{strong excitation}}} = \frac{\eta_G f' \beta_{HG}}{\eta_H f \gamma T_H} \quad (15b)$$

In this case, the quantum ratio is dependent on the intensity of excitation  $I$ . In the limiting case of high intensity and low guest concentration,  $T_H \simeq (\alpha I / \gamma)^{\frac{1}{2}}$ . Therefore the quantum ratio is proportional to  $I^{-\frac{1}{2}}$ . This is demonstrated in *Figure 11*.

In *multi-component* systems the intensity relations are much more complex because there is competition between different traps. The extremely high sensitivity of sensitized delayed fluorescence is valid apparently only at not too low temperatures, where the  $X$ -traps and all kinds of shallow traps are no longer effective. In the system naphthalene +  $\beta$ -methyl-naphthalene, the quantum ratios for prompt and for delayed fluorescence at 4.2°K are nearly equal<sup>14</sup>. This is due to the presence of  $X$ -traps in naphthalene, and to the introduction of additional shallow traps when doping naphthalene with  $\beta$ -methylnaphthalene. These shallow traps are responsible for the very strong temperature dependence of delayed fluorescence intensity below 100°K (*Figure 12*).

Since  $X$ -traps are always present even in pure crystals, and since trapping processes can be so tremendously effective, it seems justified to say that one can hardly overestimate the importance of traps and trapping processes in organic molecular crystals.

ENERGY TRAPPING PROCESSES IN AROMATIC CRYSTALS

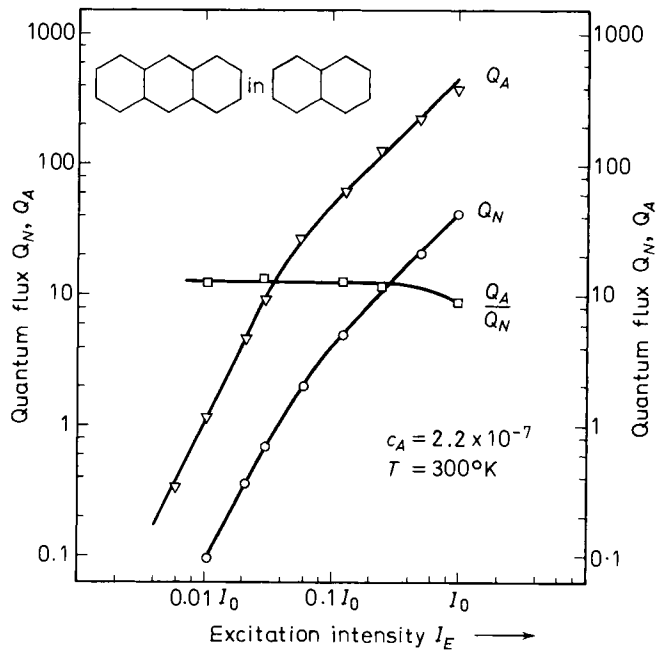


Figure 11. Quantum flux  $Q_A$  and  $Q_N$  and quantum ratio  $Q_A/Q_N$  of delayed fluorescence in naphthalene crystals containing  $2.2 \times 10^{-7}$  parts of anthracene, as a function of excitation intensity  $I$ , room temperature. From reference 14

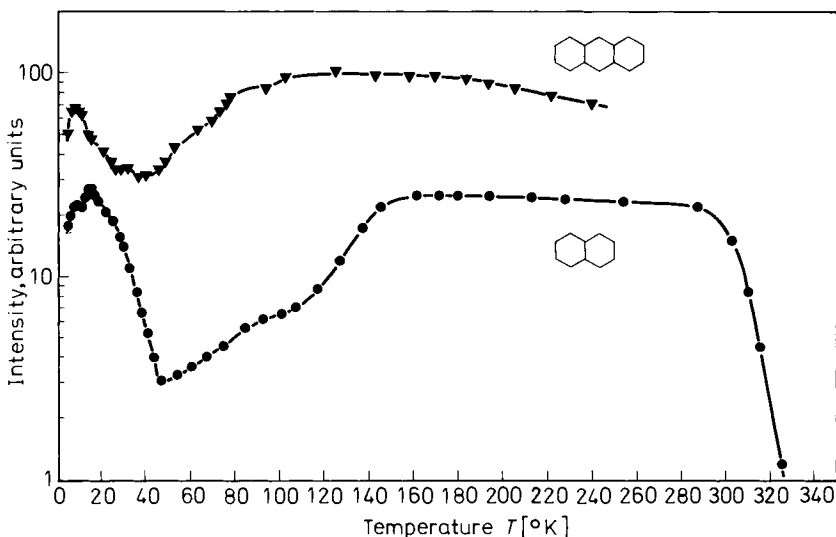


Figure 12. Integral intensity of delayed fluorescence in typical very pure anthracene and naphthalene crystals as a function of temperature. From reference 15

H. C. WOLF AND K. W. BENZ

### ACKNOWLEDGEMENT

Figures 3, 4, 5, 8, 9 and 12 have appeared previously in *Die Zeitschrift für Naturforschung* and permission to reproduce them here is gratefully acknowledged.

### REFERENCES

- <sup>1</sup> Y. I. Frenkel, *Phys. Rev.* **37**, 17, 1276 (1931).
- <sup>2</sup> J. W. Sidman, *Phys. Rev.* **102**, 96 (1956).
- <sup>3</sup> H. L. Jetter and H. C. Wolf, *Phys. Stat. Sol.* **22**, K39 (1967).
- <sup>4</sup> E. Glockner and H. C. Wolf, *Z. Naturforsch.* **24a**, 943 (1969).
- <sup>5</sup> S. A. Rice, G. C. Morris and W. L. Greer, *J. Chem. Phys.* **52**, 4279 (1970).
- <sup>6</sup> R. Ostertag and H. C. Wolf, *Phys. Stat. Sol.* **31**, 139 (1969).
- <sup>7</sup> A. Pröpstl and H. C. Wolf, *Z. Naturforsch.* **18a**, 724 (1963).
- <sup>8</sup> See, for instance, *Physics of Color Centers* Ed. W. B. Fowler, Academic Press, New York (1968).
- <sup>9</sup> R. Schnaithmann and H. C. Wolf, *Z. Naturforsch.* **20a**, 76 (1965).
- <sup>10</sup> E. Glockner and H. C. Wolf, *Z. Naturforsch.* **24a**, 943 (1969).
- <sup>11</sup> G. C. Morris et al. Fifth Molecular Crystal Symposium, Philadelphia (1970).
- <sup>12</sup> L. E. Lyons and L. J. Warren, Fifth Molecular Crystal Symposium, Philadelphia (1970).
- <sup>13</sup> H. Port and H. C. Wolf, *Z. Naturforsch.* **23a**, 315 (1968).
- <sup>14</sup> K. W. Benz, Dissertation, Stuttgart (1970).
- <sup>15</sup> K. W. Benz, W. Häcker and H. C. Wolf, *Z. Naturforsch.* **25a**, 657 (1970).
- <sup>16</sup> T. Azumi and Y. Nakano, *J. Chem. Phys.* **51**, 2515 (1969).
- <sup>17</sup> M. Schwoerer and H. Sixl, *Chem. Phys. Lett.* **2**, 14 (1968) and **6**, 21 (1970).
- <sup>18</sup> H. Sixl and M. Schwoerer, *Z. Naturforsch.* **25a**, 1383 (1970).
- <sup>19</sup> R. E. Merrifield, *J. Chem. Phys.* **38**, 920 (1963).
- <sup>20</sup> S. A. Rice and J. Jortner, in *Physics and Chemistry of the Organic Solid State* Ed. Fox, Labes and Weissberger, Vol. 3, Interscience, New York (1967).
- <sup>21</sup> J. R. Haynes, M. Lax and W. F. Flood, *J. Phys. Chem. Solids* **8**, 392 (1959).
- <sup>22</sup> B. S. Sommer and J. Jortner, *J. Chem. Phys.* **50**, 187, 822, 839 (1969).
- <sup>23</sup> H. C. Wolf, in *Advances in Atomic and Molecular Physics* Ed. Bates and Estermann. Vol. 3, Academic Press, New York 1967.
- <sup>24</sup> W. Häcker, Diplomarbeit, Stuttgart (1969).
- <sup>25</sup> A. Suna, *Phys. Rev.* **B1**, 1716 (1970).
- <sup>26</sup> K. W. Benz and H. C. Wolf, *Z. Naturforsch.* **19a**, 177 (1964).
- <sup>27</sup> R. P. Groff, R. E. Merrifield and P. Avakian, *Chem. Phys. Lett.* **5**, 168 (1970).
- <sup>28</sup> A. Hammer, Dissertation, Stuttgart (1968).
- <sup>29</sup> D. Haarer and H. C. Wolf, *Mol. Cryst.* **10**, 359 (1970).
- <sup>30</sup> H. Kolb and H. C. Wolf, Colloque Ampere Bukarest (1970).
- <sup>31</sup> E. M. Yee and M. A. El Sayed, *J. Chem. Phys.* **52**, 3075 (1970).
- <sup>32</sup> H. Baessler, G. Vaubel and H. Kallmann, *J. Chem. Phys.* **53**, 370 (1970).

# ELECTRONIC SPECTRA OF ORGANIC SOLID SOLUTIONS: EFFECTS OF LATTICE DISORDER ON SPECTRAL LINE WIDTHS AND MULTIPLICITIES

SYDNEY LEACH

*Laboratoire de Photophysique Moléculaire†, Bâtiment 213,  
Faculté des Sciences, 91—Orsay, France*

## ABSTRACT

Line widths and multiplicities observed in solute electronic spectra of dilute organic solid solutions depend to a great extent on lattice disorder and solute site inhomogeneities. A definition of the structure of different types of organic solids is followed by a discussion on defects in these solids and of some of their photophysical consequences. The formation of organic solid solutions and the effect of various thermal treatments are considered in the light of the previous discussion. The influence of lattice phonon structure on spectral line widths is discussed for near-perfect and increasingly disordered solid solutions, in terms of the optical analogue of the Mössbauer effect. At low temperature effect is less important than static and dynamic solute site inhomogeneities in determining observed spectral line widths. The latter should be narrowest for substitutional solutions. The formation of such solutions depends on a number of parameters amongst which are the solute and solvent molecular geometries and volumes. The effect of these two parameters on solute spectral line widths has been studied. Multiplet structure in the electronic spectra of crystalline organic solutions is discussed. The origin of solute site plurality is considered in terms of the mechanism of crystal growth.

## I. INTRODUCTION

The electronic and geometrical structures and the vibrational dynamics of organic molecules can be determined by detailed analysis of the electronic spectra of these species in the gas phase at low pressures. In the solid phase, molecular spectra will be perturbed to an extent that depends on the nature and the degree of intermolecular coupling. The electronic spectra of organic solid solutions have been used to characterize the spectroscopic and structural properties of solute molecules, in particular under experimental conditions where the solute molecules are essentially isolated in suitable matrices at low temperatures. These conditions are particularly favourable for the study of the optical transitions of trapped free radicals and the phosphorescence from triplet states of aromatic stable molecules. Furthermore, in

---

† Groupe de recherche du C.N.R.S. associé à la Faculté des Sciences d'Orsay.

## SYDNEY LEACH

matrices ate low temperatures, hot bands are generally suppressed thus facilitating vibronic analysis<sup>1, 2</sup>.

The perturbation of the solid solution spectra with respect to the gas phase can be used to study certain structural and dynamic properties of the matrix and also to determine the state of dispersion and aggregation of the solute<sup>1, 3</sup>.

Among other applications of electronic spectroscopy of organic solutions, particularly pertinent to the present symposium, are the study of energy transfer<sup>4</sup> and photochemistry in the solid state<sup>5</sup>.

Most of the earlier spectroscopic work on organic solid solutions, from 1910 to 1960, was done in glassy matrices at low temperatures. Particular mention should be made to the pioneer work of von Kowalski<sup>6</sup>, on stable molecule solutes, and to the studies of Lewis and his co-workers<sup>7</sup> and Porter and his co-workers<sup>8</sup> on the absorption spectra of aromatic radicals trapped in rigid organic glasses. Fluorescence spectra of trapped radicals have also been studied in rigid glass solutions<sup>5a, 9</sup>.

In 1954 McClure<sup>10</sup> introduced the 'oriented gas' type of study in which the solute is presumed to be in a substitutional site in an aromatic crystalline matrix. Two years earlier, Shpol'skii<sup>11</sup> observed narrow line fluorescence spectra of aromatic solutes in crystalline linear paraffin matrices and has since created a very active school which has made a considerable number of spectroscopic studies using the 'Shpol'skii effect'<sup>12</sup>.

However, much of the published work on the electronic spectra of organic solid solutions is difficult to interpret without ambiguity since many insufficiently studied parameters govern their structure. These parameters include: (a) modification of the intrinsic electronic and structural properties of the solute molecule with respect to the gas phase; (b) the state of dispersion of the solute molecules; (c) the nature and configuration of the solute site; (d) solute-solute interactions; (e) solute-matrix interactions. Furthermore, these parameters are often sensitive to a number of experimental variables, not always well controlled or indicated in earlier publications, such as the method of preparation of the solid solutions and their thermal history.

A systematic discussion has recently been made concerning some of the above parameters<sup>1, 3</sup>. The present paper can be considered as a development of certain aspects of references 1 and 3. In it will be discussed problems concerning spectroscopic line widths and multiplet structure which were only briefly mentioned in the previous study or which were considered from a different viewpoint. Their treatment here requires an initial discussion, which is given in the next section, of the basic physics of organic solids and solutions relevant to electronic spectroscopy.

## II. THE STRUCTURE OF ORGANIC SOLIDS

### II. 1. Crystals and amorphous solids

Spectroscopists and photochemists studying organic solids usually classify them as belonging to one of three categories: monocrystals, polycrystalline material and glasses. In molecular solids composed of organic molecules the electrostatic and dispersive intermolecular attractive forces are of the

## ELECTRONIC SPECTRA OF ORGANIC SOLID SOLUTIONS

order of a few kcal/mole. The particular molecular arrangement in such solids will be determined essentially by a true or a metastable minimum of free energy.

For organic crystals the criterion of minimum free energy will usually result in a tendency to form a close packed structure<sup>13</sup> whose particular configuration will depend mainly on the repulsive forces between the peripheral atoms of neighbouring molecules<sup>14, 15</sup>.

If several close packed structures of similar energies are possible, there will be a tendency for the crystal to assume the structure having the highest number of symmetry elements<sup>14</sup>.

*Monocrystals* are characterized by a lattice structure in which the constituent molecules are related by periodic translations. Long range order exists over a large, virtually infinite number of lattice cells in an ideal monocrystal. A single crystal is an individual monocrystal.

*Polycrystalline* material is composed of a mosaic of monocrystals having a variety of relative spatial orientations. In the ideal case, long range order for each monocrystal ceases at the mosaic limits. The existence of manifold crystal boundaries gives rise to high scattering of visible light and an opaque quality as compared to the low light scattering and, in appropriate spectral regions, the transparency of single crystals.

The existence of long range order is testified by x-ray and electron diffraction studies of single crystals and polycrystals. When the regions of organized structure are non-existent or small (for example, periodicity no greater than 50–100 Å) and the grain boundaries are very extensive, then the solid can be said to have an *amorphous* structure and is highly opaque. A *glass* is another form of amorphous structure in which periodicity does not exist or only over a very small region, but for which there is apparently no granular structure so that the glass is transparent.

Very little is known about the structure of amorphous solids and glasses composed of organic materials except for polymers<sup>16</sup>.

### II. 2. Defects in organic solids

Spectroscopic, photochemical and energy transfer properties of perfect organic solids will be modified in the presence of intrinsic or extrinsic (impurity) defects.

Thermodynamic considerations show that defects will always be present in solids. Consider, for example, the formation of a vacancy in a crystal. It should first be remarked that the molecular diffusion concomitant with vacancy creation is theoretically possible at any temperature since the crystal always contains internal vibrational energy. Vacancy creation will increase the crystal energy since energy has to be expended in overcoming the forces which tend to keep a molecule in its initial position in the lattice. However, at the same time there will also be an increase in the entropy of the system since some configurational order is destroyed in the crystal. A theoretical equilibrium concentration of vacancies, greater than zero, will therefore exist at each temperature. The value of this equilibrium concentration will depend on the compromise between the principles of minimum energy and maximum entropy. A similar discussion can be developed for other types of defects<sup>17</sup>.

## SYDNEY LEACH

Although experimental investigations of defects have been extensive for many types of solids, it is only within recent years that such studies have been undertaken for organic solids<sup>18</sup>. Data on organic solids are still rather limited, so that part of the following discussion is based on information obtained on other systems.

In organic crystals, the intrinsic point defects will be, in general, lattice vacancies. Interstitial defects are not likely in closed packed structures. Another type of point defect can arise from the presence of disoriented molecules in the lattice. Linear dislocations of the edge and spiral types, and planar dislocations of the grain boundary and twinning types also occur. The planar dislocations can be considered as creating internal surfaces in crystals. Another type of internal boundary occurs when crystal grains of different crystallographic order or of different chemical composition exist juxtaposed.

Radiotracer and other studies of self-diffusion (point defect migration) have been made in organic crystals<sup>18</sup>. Rates of self-diffusion along dislocations and sub-grain boundaries are higher than for self-diffusion through the lattice. Intrinsic self-diffusion rates are  $10^4$  times greater for plastic crystals, such as the high temperature form of cyclohexane, than for linear condensed aromatic crystals. For benzene, the point defect diffusion rate is about  $10^2$  times lower than for cyclohexane. The large differences in defect mobilities in different systems will be significant in determining the defect concentration in organic solid solutions.

Another important factor concerns dislocation glides in which there is a slip of adjacent crystal planes in the neighbourhood of a dislocation. As far as a particular slip system is concerned, these glides may be different for pure crystals and for crystals containing impurity molecules.

It should be noted that impurity molecules can be substitutional defects or, if they are of sufficiently small dimensions, they can occupy interstitial positions. When the impurity molecule has a much larger volume than the matrix molecules, more than one matrix molecule can be displaced or replaced.

One can also envisage a number of defect complexes<sup>17</sup>: impurity molecule-vacancy pairs; vacancy clusters (although these should be rare in annealed close packed molecular solids); dislocation-vacancy interactions; dislocation-impurity molecule complexes.

In addition, impurity-impurity complexes, leading eventually to solute aggregation can occur in many systems and can be detected spectroscopically<sup>1, 3</sup>. In the discussion in this paper we will leave aside the problem of solute aggregation which has been dealt with elsewhere<sup>1, 3</sup>.

Defects and defect complexes will have specific spectroscopic, photophysical and photochemical consequences. For organic crystals, they will tend to act as traps limiting or modifying exciton and phonon propagation in the matrix. The trapping properties will depend on the interaction between the defect electronic or vibrational states and these quasi-particles. The extent of exciton or phonon trapping will be temperature dependent. Critical defect concentrations and temperatures for these effects will depend not only on the type of defect or defect complex but also on the particular exciton—for example, singlet or triplet—or phonon wave packet. It is

## ELECTRONIC SPECTRA OF ORGANIC SOLID SOLUTIONS

therefore to be expected that in organic solid solutions, the luminescence spectra (quantum yield<sup>19</sup> and spectral structure<sup>20</sup>) of the matrix and of the solute and the yield of matrix → solute energy transfer will be functions of the nature and concentration of defects as well as of the temperature<sup>21</sup>.

### II. 3. The formation of organic solid solutions

Spectroscopic studies on organic solid solutions have been done mainly on solid solutions prepared from the melt or liquid phase and subjected to different types of cooling procedures.

#### (a) Glasses

Glass preparation is usually done by low temperature quenching of the glass forming liquid. Little data exist on the physics of the formation of organic glasses. However, from information on polymer and inorganic glasses it is reasonable to suppose that in glass-forming organic compounds the high viscosity ( $\sim 10^{12}$  poise) at the liquidus temperature prevents ordered alignment of the constituent molecules. A high degree of configurational order will therefore not occur on freezing.

The arrangement of the constituent molecules in the glass will be similar to the 'instantaneous' structure of the liquid. Local ordering may or may not occur, according to the presence or absence of ordered cybotactic groups in the liquid phase. Such cybotactic groups could not be of large extent in glass-forming materials otherwise it would be difficult to account for the high viscosity and diffusion properties in the region of the liquidus temperature. Furthermore, if order is present in local domains in the glass its configuration does not necessarily correspond to that of a crystalline variety of the same substance. The existence of so-called short-range order in liquids or glasses as determined by diffraction or scattering techniques usually gives little information as to the existence of any true periodic structure since the correlation functions obtained by these methods often simply reflect a statistical distribution of intermolecular distances and are so hardly informative about true local order.

Many different types of solvent and solvent mixtures have been used to form organic glasses<sup>22</sup> for electronic spectroscopy and organic solid-state photochemistry. Organic glasses will tend to form if the constituent molecules are associated in the liquid through hydrogen bonding, which therefore opposes certain forms of ordered alignment, or if the solvent molecules contain a multiplicity of side chains and so possess many quasi-independent degrees of local movement.

#### (b) Crystalline solid solutions

Rapid quenching, slow cooling, and rapid quenching followed by annealing at a fixed temperature, are the three thermal treatments usually employed in forming crystalline solid solutions from the liquid phase. These different techniques can give rise to samples having substantially different spectroscopic and photochemical properties since the crystallographic structure is sometimes, and the defect structure and concentration are always, dependent on the thermal history of the sample<sup>4, 23</sup>. Furthermore, the presence of occluded gases can have important perturbing effects on the structure of the solid formed<sup>4</sup>.

The following model is proposed concerning the structure of the matrix in the case of *quenching*. The liquid phase may contain cybotactic or paracrystalline domains, or these may be absent. On rapid freezing there will be dissipation of heat from the solvent, this dissipation generally being anisotropic in quenching experiments. Nucleation rapidly takes place leading to an incipient microcrystal which could have a faulted structure initially of lower free energy than a non-faulted structure (see section V). Rapid growth of the microcrystal will occur, leading to the introduction of a large number of defects. However, the continual lowering of the temperature tends to build up high strain energy since the barrier to self-diffusion will increase as thermal energy is reduced. Strain relief will occur by cleavage and by the introduction of dislocations. The fact that organic crystals have high thermal expansivities also contributes to the formation of lattice strain. The sample will therefore tend to consist of a mass of small crystallites of high defect content.

Occluded gases will tend to be trapped and act as extrinsic defects further perturbing the regularity of the polycrystal lattices and leading to dislocation and microcrystal formation. It is to be emphasized that the defect concentration at the quench temperature  $T_q$  will be very much greater than the equilibrium concentration would have been at  $T_q$ .

The solute molecules (neglecting solute aggregation) will tend to be fixed in a variety of defect and defect-complex situations. This will lead to spectral line broadening or multiplet structure according to the statistical distribution of solute-matrix interactions, as will later be discussed in detail.

In the case of *slow cooling* (and leaving aside the question of the possibility of considerable supercooling) there will exist at the freezing point  $T_f$  a certain defect structure in the nucleated growing crystal whose concentration will correspond approximately to that of the equilibrium concentration at  $T_f$ . Let us assume extremely slow cooling. As the temperature is very gradually lowered there will be a decrease in the equilibrium number of intrinsic point defects. Here too, there will be a tendency for lattice strain energy due to excess point defects to be relieved by their migration (at a rate depending on the self-diffusion rate) to form dislocations, and eventually by cleavage. However, slow cooling should lead to a smaller dislocation content and to larger single crystals than rapid cooling since a process of continuous annealing will tend to occur in the former case.

Nevertheless, on practical time scales for laboratory crystal growth, the true concentration of defects will in general be greater, and often considerably greater, than the equilibrium concentration since at very low temperatures the diffusion rate will be extremely slow. It is important to note the importance of the remark made in the previous section, that plastic crystals, e.g. the high temperature form of cyclohexane, have much higher self-diffusion rates than 'brittle' crystals such as the linear condensed aromatic molecules. One might therefore expect plastic crystals to have a much smaller defect concentration than the 'brittle' crystals. This could lead to a much smaller statistical width of solute-matrix interactions in the case of plastic crystal matrices and could so give rise to narrower spectral line widths than for 'brittle' crystal matrices (although as we shall see, the relative size of the solute and solvent molecules is also a capital factor).

## ELECTRONIC SPECTRA OF ORGANIC SOLID SOLUTIONS

In some experiments in our laboratory, solid crystalline solutions have been formed by annealing rapidly quenched samples, the annealing being carried out at a temperature just below the freezing point or close to a crystallographic phase transition temperature. J. Kahane-Paillois and C. Pfister have observed that the spectra of coronene solutions in *n*-heptane, are identical after slow cooling and after annealing if the latter is carried out for 2 or 3 days<sup>25</sup>. In our laboratory, C. Michel found for the anthracene-*n*-heptane system that 20 hours annealing just below the freezing point sufficed to obtain the same spectral behaviour as a slowly cooled solution (one hour from 300°K to 80°K)<sup>26</sup>.

One further point should be noted. Molecular solids, in particular plastic crystals, usually possess several crystallographic forms and thus exhibit crystallographic phase transitions at certain temperatures. The plastic is often a high temperature form that goes over to a 'brittle' form at a phase transition temperature thus creating new stresses and giving rise to cleavage of a monocrystal initially in the plastic form. This makes it difficult to prepare monocrystals for spectroscopic studies in the stable low temperature crystallographic forms of crystals of molecules such as cyclohexane.

### III. SPECTROSCOPIC LINE WIDTHS IN ORGANIC SOLID SOLUTIONS: INFLUENCE OF THE PHONON STRUCTURE

Molecular rotation is virtually quenched in low temperature solids and so does not contribute to vibronic band widths. The principal factors governing widths of solute vibronic bands of an organic solid solution at a particular temperature are the phonon structure of the lattice and the site inhomogeneity of the solute. The influence of the phonon structure will first be examined. Interpretations of the narrow line widths observed in organic crystalline solid solutions (Shpolskii effect) have been made in recent years in terms of an optical analogue of the Mössbauer effect and are therefore based essentially on the phonon structure and phonon relaxation phenomena in the solid<sup>27</sup>.

Let us consider the phonon structure of an ideal organic crystal and its relation to the width of solute vibronic bands and then examine the effects of imperfections and disordered structure on the band widths.

It will first be assumed that solute concentration is sufficiently low, and the solute molecules sufficiently well dispersed, for solute-solute interactions to be negligible<sup>1, 3</sup>. Furthermore it is assumed, throughout this paper, that the energy of the electronic excited state in the solute optical transition under consideration is more than 1 eV below the lowest exciton level of the matrix, so that mixing of solute and matrix excited states will be unimportant in determining solute spectral line widths<sup>3</sup>.

#### III. 1. Nearly perfect crystals

The atomic displacements in the crystal can be resolved into lattice waves at any instant. The lattice waves will be a superposition of normal modes of the lattice, the energy content of each mode being time variant. In the nearly perfect crystal, each lattice wave will be composed chiefly of one

particular lattice vibration mode. Interchange among modes, i.e. the variation of energy content among the superposed normal modes, will be slow and exists, on the harmonic model, only because of deviations from crystal perfection.

The presence of a solute molecule, i.e. an extrinsic impurity centre, will modify the strict periodicity in the equilibrium spatial positions of the molecular motifs in the crystal. The solute molecules, and a neighbouring region of matrix molecules where lattice translational symmetry is effectively lost, will constitute a perturbed local region with particular properties concerning dynamic processes in the crystal in particular lattice vibration relaxation processes.

Three types of vibrations are of importance for electronic spectroscopy of the solute molecule:

(1) Solute intramolecular vibrations which in general will be only weakly coupled to the matrix lattice since the interatomic forces within the molecule are of two orders of magnitude greater than intermolecular forces. Intramolecular vibrational modes will therefore manifest themselves in the electronic spectra virtually as if the solute molecule were isolated (i.e. similar to low pressure gas phase conditions)<sup>1,3</sup>.

(2) Localized vibrations of the solute which will essentially be librational and translational oscillations of the solute molecule in an apparent fixed cage of the matrix<sup>3</sup>.

(3) Nonlocalized vibrations which correspond to vibrations of the crystal

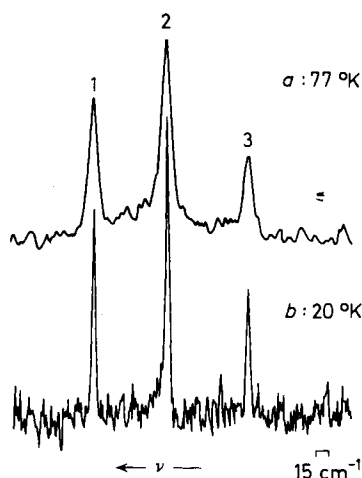


Figure 1. Part of the fluorescence spectrum  $^1B_{2g} \rightarrow A_{1g}$  of benzene in annealed solid solution in cyclohexane (concentration  $10^{-3}$  M/l). (a) 77°K; (b) 20°K.  
Vibronic transitions<sup>52,53</sup>: 1 = 0, 0- 991 ( $a_{1g}$ ) (36722  $\text{cm}^{-1}$ )  
2 = 0, 0- 675 ( $a_{2u}$ ) - 402 ( $e_{2u}$ ) (36636  $\text{cm}^{-1}$ )  
3 = 0, 0- 1173 ( $e_{2g}$ ) (36540  $\text{cm}^{-1}$ )

Spectrum a has been displaced relative to spectrum b to eliminate a temperature dependent shift of the spectral origin.

## ELECTRONIC SPECTRA OF ORGANIC SOLID SOLUTIONS

lattice as a whole and which are essentially identical to the lattice vibrations of the matrix in the absence of solute inclusions<sup>3, 28</sup>.

One might expect that vibronic transitions of the solute should show a fairly broad structure corresponding to lattice phonon creation or annihilation associated with the vibronic transition. However, Trifonov, Rebane and others<sup>27</sup> have shown that there is an optical analogue to the Mössbauer effect in which the  $\gamma$ -ray recoil kinetic energy is replaced by the excess potential energy created by the difference in intermolecular interactions in the ground and excited states. In similar fashion to the Mössbauer case there is a high probability for transitions to occur in which no phonons are created or destroyed (i.e.  $\Delta n = 0$  transitions, where  $n$  is a quantum number associated with nonlocalized lattice vibrations). These are the so called zero-phonon transitions. In the approximation of harmonic vibrations and identical oscillators in the excited and unexcited lattice, the no-phonon transitions corresponding to a particular vibronic band will coalesce to give a spectral line whose width should be of the order of  $10^{-3} \text{ cm}^{-1}$  for an allowed transition and even smaller for a forbidden transition. At the same time there will exist a background or wing corresponding to the creation and annihilation of phonons, i.e. transitions where  $\Delta n > 0$ , whose shape will therefore also depend on the phonon population of the initial state at a given temperature. It is the spectral background, continuous because of the high density of phonon states, which manifests the relaxation, among the normal lattice modes, of the excess potential energy created by the optical transition.

On this model, an increase in temperature should not lead to a change in the zero-phonon line width but only to a modification of the relative intensity of the zero-phonon line and the associated continuum.

In a more refined treatment, dealt with at length in the recent book of Rebane<sup>27</sup>, the consideration of anharmonicity, displaced oscillators and distorted oscillators, leads to an increase in zero-phonon line width due to thermal broadening, or, more precisely to a splitting of the  $\Delta n$  transitions which at practical spectral resolution will be unresolved and give rise to a broadened line envelope. However, the line width, although increased by one or two orders of magnitude above the harmonic undisplaced oscillator case, will still be much smaller, on this refined model, than experimental line widths at low temperatures which are of the order of  $1 \text{ cm}^{-1}$  and greater for the zero-phonon lines<sup>1, 24, 27, 29</sup>.

Although at low temperatures observed electronic spectra have broader lines than is expected only on the basis of the optical analogue of the Mössbauer effect, their shape and temperature behaviour show general qualitative agreement with the distorted and/or displaced oscillator model of this effect.

Figure 1 shows the widths of three typical bands of the fluorescence spectrum of benzene in cyclohexane ( $10^{-3} \text{ M/l}$ ) at  $20^\circ\text{K}$  and at  $77^\circ\text{K}$ . A background or wing due to phonon creation or annihilation processes is not very extensive in these spectra. The effect of increasing the temperature between  $20^\circ\text{K}$  and  $77^\circ\text{K}$  is mainly to broaden the line widths.

In Figure 2 is shown a part of the reflection spectrum of benzene in cyclohexane at temperatures between  $80^\circ\text{K}$  and  $163^\circ\text{K}$ . At  $80^\circ\text{K}$ , the 0,0 and the 0,0 + 521 bands both exhibit a zero-phonon line and an extensive

phonon wing which is mainly to higher energies. The intensity variation observed within these wings indicate peaked phonon distributions, the maxima probably corresponding to localized vibrations.

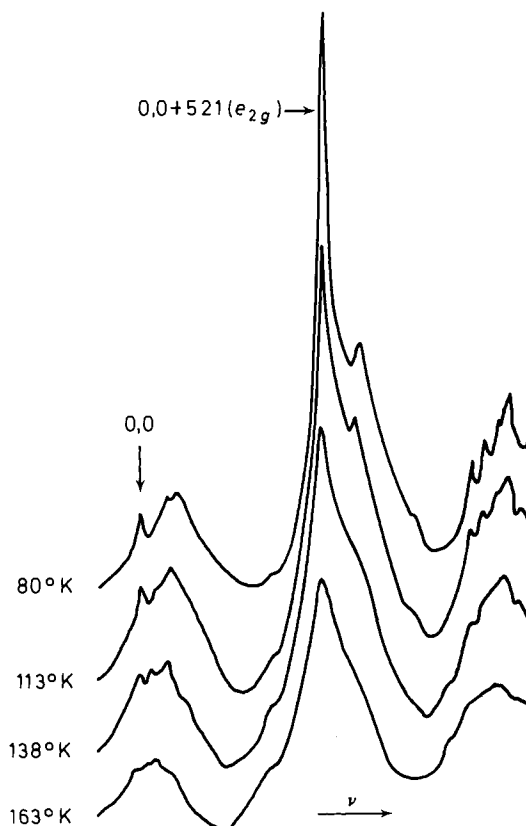


Figure 2. Part of the reflection spectrum  $^1B_{2u} - ^1A_{1g}$  of benzene in solid solution in cyclohexane (concentration  $10^{-3}$  M/l) as a function of temperature. The temperature dependent shift of the spectral origin has been eliminated by relative displacement of the spectra.

As the temperature increases the zero-phonon lines progressively broaden and their maxima decrease in height. There is a concurrent increase in the integrated intensity of the phonon wings whilst the subsidiary maxima shift to lower energies.

It is to be remarked that the phonon wing associated with the 0,0 transition is more important than that associated with transitions involving excitation of intramolecular vibrations. This is probably related to the fact that the pure electronic transition is forbidden for the  $^1B_{2u} - ^1A_{1g}$  transition of a  $D_{6h}$  benzene. Since the observed 0,0 band arises because of interactions with the crystal field, it will only appear weakly, but phonon assisted 0,0 transitions could become formally allowed through coupling of the pure electronic transition with lattice vibrations of appropriate symmetry and so give a relatively intense wing with respect to the zero-phonon 0,0 line.

## ELECTRONIC SPECTRA OF ORGANIC SOLID SOLUTIONS

We have observed that phonon assisted transitions are generally more evident in absorption or reflection spectra than in fluorescence spectra. Since in the former spectra the phonon wing is essentially to higher energies with respect to the zero-phonon line, this result indicates that phonon creation has a greater probability in absorption to an excited electronic state than in fluorescence to the ground electronic state. In this connection it should be noted that the solute in its excited state will, in general, be located within a strained, electronically unrelaxed, solvent cage (see section III. 3). The propensity for creation of phonons associated with the optical transition may thus be enhanced in the absorption/reflection spectra as compared with the fluorescence transition: in fluorescence, the relaxation of the solute-solvent cage complex can be effected, if necessary completely, through electronic redistribution in the solute molecule in going from the excited to the ground electronic state.

### III. 2. Disordered solids

The above discussion has been concerned with the phonon structure in the case of an assumed near perfect crystal, in which implicitly the solute molecules occupy substitutional sites in the lattice. We will now examine the effect of increasing disorder on the phonon structure in the solid. This disorder will be considered to be of two types, inhomogeneity in the sites of the solute molecules and intrinsic defect structures in the matrix. The most disordered structure will be that of an amorphous solid or a glass, as discussed in section II.

Although as disorder increases in the solid the periodic properties are progressively lost, it must be remembered that each molecular unit has an equilibrium site and vibrates about that site. Even an amorphous solid will have, in principle, normal modes of vibration. The solute intramolecular vibrations will hardly be modified by the increasing disorder in a molecular solid since their coupling with the matrix will in general remain weak. As far as the matrix is concerned the nonlocalized vibrations will have a frequency spectrum of normal modes which differs little from that of the lattice waves of the perfect crystal except in the high frequency region which describes the relative motion of neighbouring molecular units. Indeed the normal modes of low frequency will be similar in character to the waves in a homogeneous isotropic elastic continuum, for in the limit of long waves the atomic structure is unimportant.

As disorder increases, the phonon relaxation time will decrease, i.e. the rate of interchange of energy among the normal modes will become more rapid. As the limit of an amorphous solid is approached the interchange of energy will become so rapid that it becomes meaningless to talk of lattice waves, since each component of instantaneous displacement will have changed shape while propagating through a distance of one wavelength<sup>30</sup>.

We will now extend the optical analogue of the Mössbauer effect to the case of increasing structural disorder.

For each particular solute molecule one would expect that the zero-phonon line should exist under all circumstances, but the background of transitions in which phonons are created or annihilated will tend to be reduced in width since the higher frequency part of the phonon spectrum separates out

as localized vibrations as lattice periodicity is increasingly lost. In the limit of the amorphous solid each vibronic band of a particular solute molecule will consist only of a zero-phonon line and a few associated local vibrations of the solute molecule in the matrix cage. However the observed vibronic band widths for a disordered solid solution will not be those narrow band widths associated with an individual solute molecule since there will be a wide statistical distribution of solute-matrix interactions. For each vibronic band there will be a statistical spectrum of zero-phonon lines and of localized vibrations. The width of the vibronic band envelope will therefore depend on the variety of solute-matrix interaction configurations and the population of such configurations.

Experimentally one often observes a decrease in line widths on annealing a solid solution, in agreement with the above discussion, since such thermal treatment will give rise to a reduction in the number of intrinsic lattice defects, leading to increased periodicity of the lattice, and a concomitant greater homogeneity of solute molecule sites. The statistical plurality of solute-matrix interactions in a defect solid therefore has an effect on vibronic band widths that much more than counteracts any reduction in the high frequency part of the phonon spectrum of the matrix due to loss of lattice periodicity.

In organic vitreous solutions, the vibronic band widths are of the order of  $100\text{ cm}^{-1}$ , or greater, which illustrates the great range of solute-matrix interactions in this case. It should be stressed that vibronic analyses based on bands of such width are to be considered with much caution, since such band envelopes may mask unresolved vibronic structure. An example of this is given in *Figure 3* which compares broad bands of the fluorescence spectrum of benzene in E.P.A. glassy solution at  $77^\circ\text{K}$  with the well resolved structure of benzene fluorescence in crystalline cyclohexane solution at  $77^\circ\text{K}$ .

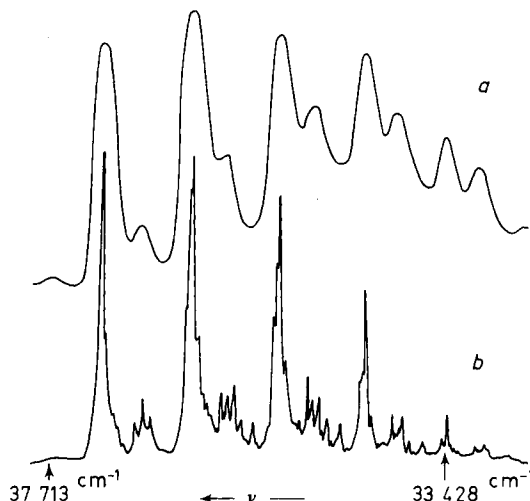


*Figure 3.* Fluorescence spectra of benzene in solid solution (concentration  $10^{-3}\text{ M/l}$ ) at  $77^\circ\text{K}$ . (a) E.P.A. matrix. (b) Annealed cyclohexane matrix. The origin of spectrum *a* has been shifted relative to spectrum *b* to eliminate the difference in solvent shifts. The broad bands in spectrum *a* are the envelopes of the peaks in spectrum *b* each of which corresponds to an individual vibronic transition<sup>52,53</sup>.

### III. 3. The dynamic variation of solute-matrix interactions

The previous discussion has shown that the width and shape of a vibronic band will depend on the range of solute-matrix interactions. In the present section will be discussed the role of the dynamic variation of solute-matrix interactions which results from thermal vibrations of the matrix.

It is convenient to begin with the case of a completely disordered solid, to which a glass is a good approximation. This discussion will lead, *inter alia*, to an explanation of the apparent paradox that excitation of a glassy solution by *monochromatic* light gives rise to broad band fluorescence spectra.

In general, the solute molecule dimensions and interaction with its surrounding solvent cage will differ in the excited electronic state as compared with the ground state. Relaxation of the solvent cage, i.e. change of the *equilibrium positions* of the cage molecules, will in general not occur in low temperature solid solutions in times shorter than the fluorescent state lifetime which is of the order of  $10^{-8}$  s. (Relaxation could generally occur in times shorter than the phosphorescent lifetime, which can be of the order of one second for aromatic hydrocarbon solutes.) However, oscillations of the matrix molecules about their equilibrium positions have periods as short as  $10^{-11}$ – $10^{-12}$  s. The vast majority of excited state molecules will therefore have been able to dissipate to the matrix any excess intramolecular vibrational energy before optical emission occurs. Fluorescence and phosphorescence emission in low temperature solid solutions will, in general, occur from the zero intramolecular vibrational state of the electronically excited solute. This will be true not only for glassy solutions but also for mixed crystals.

In a glass, the matrix consists of a set of coupled oscillators whose coupling constants have a wide statistical distribution. In durations of the order of  $10^{-8}$  s, because of the lack of translational invariance in the disordered medium, vibrations of the matrix due to thermal energy will cause the position of each matrix molecule (solute and solvent) to undergo a kind of local Brownian movement. The variation of the relative positions of the solvent cage molecules with respect to the solute molecule will create a time dependent modification of solute-solvent interactions. This can be considered as causing local, random, time dependent variations of the average dielectric constant of the medium.

*Absorption* spectra are obtained using a continuous light source or by sweeping the spectrum continuously. For each photon absorbed, the time involved ( $\sim 10^{-15}$  s), in the interaction between the electromagnetic field and the absorbing molecule, will be much shorter than vibrational periods of the matrix so that the geometrical configuration of the solvent cage surrounding a particular absorbing solute molecule will be effectively 'frozen in' during the optical transition (Franck-Condon principle). If the absorption source were of picosecond duration, the resulting solute absorption spectrum would reflect the instantaneous spatial distribution of solute-solvent interactions range since the transition energy of a particular vibronic transition (zero phonon line plus local vibrations) would differ for each spatially different solute-solvent configuration.

However, the exposure times necessary for obtaining absorption spectra have hitherto been much greater than picoseconds (although the advent of high intensity mode-locked lasers makes picosecond absorption experiments

possible<sup>31</sup>), so that in practice the absorption spectrum will correspond to an exploration of the time dependent variation of solute-solvent interactions among all possible solute sites. Since the range and relative 'population' of solute-solvent interactions will not vary with time, taking the solid solution as a whole, the range of solute-solvent interactions explored spatially by a picosecond source should be the same as that explored in normal sources over times which allow dynamic variation of solute-solvent interaction to take place.

Let us now consider the process of *fluorescence* excited by *monochromatic* radiation. Each absorbed monochromatic photon will *select* those solute-solvent cage local complexes which 'instantaneously' have energy levels in resonance with the incoming photon frequency. Since monochromatic excitation of picosecond duration is physically impossible because of the energy spread in such a short train of light waves, monochromatic excitation will, in practice, occur over durations permitting dynamic variation of solute-solvent interactions. The molecules excited by the incident monochromatic radiation in normal sources will therefore be those selected by temporal exploration of the dynamic variation of solute-solvent interactions. The excited molecules, as we have discussed above, will lose excess intramolecular (and local intermolecular) vibrational energy before emission. Furthermore, the relatively long radiative lifetime as compared with the matrix vibrational periods implies that, in general, the solute-matrix interaction for an individual solute molecule will be different at the time of emission as compared with that of absorption. The result is that, even with monochromatic excitation, the vibronic band widths for a glassy solution will be broad and reflect the full range and relative populations of solute-solvent configurations in the matrix. This discussion shows that the apparent paradox of narrow band excitation giving rise to broad band emission is a consequence of the dynamic vibrational properties of the glassy matrix and not of a static distribution of inhomogeneous equilibrium solute sites.

In more ordered solid solutions, the displacements of the lattice sites will generally have a smaller range than for disordered solids since, under a total potential energy of similar order of magnitude, the translational invariance in the former imposes concerted motion of the individual sites as compared with the Brownian motion type of displacement in the latter case. Therefore, the more perfect the solid, the narrower will be the range of dynamic variation of solute-matrix interactions and the sharper will be the vibronic band widths.

#### IV. SPECTROSCOPIC LINE WIDTHS IN ORGANIC SOLID SOLUTIONS: INFLUENCE OF SOLUTE SITE INHOMOGENEITY

We have seen, in section III, that solute site inhomogeneities are undoubtedly an important factor determining vibronic band widths of the solute. For spectroscopic analysis it is required that line widths should be as narrow as possible so that vibronic band resolution is a maximum. The range of solute-matrix interactions and their dynamic variations must therefore be reduced to a minimum. This would be fulfilled for annealed true substitutional solid solutions.

Previous articles have discussed the physical conditions for the formation

## ELECTRONIC SPECTRA OF ORGANIC SOLID SOLUTIONS

of substitutional organic solid solutions<sup>1,3</sup>. It was emphasized that for formation of substitutional organic mixed crystals, the solute and matrix molecules should have, ideally, the same molecular geometry and molecular volumes and that the interaction forces between solute and solvent molecules should be very similar in nature and strength to the forces operative in crystals of each species considered separately. Furthermore, for the formation of continuous solid solutions, the crystallographic system of solute should, in general (but with some specific exemptions), be identical with that of the solvent<sup>3,13</sup>.

It should be noted that these conditions are fulfilled exactly for isotopic mixed crystals, but in such cases there would be a strong interaction between the excited states of solute and solvent since they lie close to each other. As we have mentioned earlier, interest here is exclusively in cases where the solute and solvent excited states are sufficiently well apart in energy for interaction to be negligible, at least to first order<sup>3</sup>.

For such cases, the principal parameters investigated in spectral line width studies have been those of molecular geometry and molecular volume. Bolotnikova<sup>32</sup> has studied the influence of the solvent on fluorescence line widths of naphthalene, anthracene and naphthacene in solid solutions at 77°K. The matrices used were *n*-hexane, *n*-heptane, *n*-octane and *n*-nonane. She observed that the matrix giving the narrowest solute line width was that in which the length of the long axis of the fluorescent molecule was approximately the same as the length of the linear paraffin solvent molecule: naphthalene 7.2 Å, *n*-pentane 7.36 Å; anthracene 10 Å, *n*-heptane 10.0 Å; naphthacene 12.8 Å, *n*-nonane 12.8 Å.

It is probable that the solute molecule replaces a solvent molecule to form a substitutional solid solution in the most favoured cases or possibly, in the case of linear paraffin solvents, a kind of inclusion compound<sup>12</sup>. However it is not impossible that some of the solutions studied by Bolotnikova are in fact interstitial in nature<sup>26</sup>.

If the solute molecular volume is much bigger than the solvent molecule then defect structures or solute aggregation occurs. This has been found in our laboratory using cyclohexane as a solvent. Benzene, toluene, benzyl radical and fluorobenzene have molecular volumes which are less than or of the same order as that of cyclohexane ( $\sim 100 \text{ \AA}^3$ ), so that lattice substitution in the matrix does not present steric problems. The vibronic band widths are less than  $5 \text{ cm}^{-1}$  for these solutes in annealed cyclohexane<sup>3</sup> at 77°K. However, polysubstituted benzene derivatives, whose molecular volumes are greater than that of cyclohexane, do not form substitutional solid solutions with this solvent. We have found that solute aggregation, and partial interstitial solution formation, occur at solute concentrations of  $5 \times 10^{-2} \text{ M/l}$  or  $10^{-3} \text{ M/l}$  for *o*-xylene<sup>33</sup>, *m*-xylene<sup>33</sup>, *p*-xylene<sup>33</sup>, mesitylene<sup>34</sup>, durene<sup>35</sup>, pentamethylbenzene<sup>36</sup> and hexamethylbenzene<sup>37</sup>.

The electronic spectra of durene<sup>35</sup>, pentamethylbenzene<sup>36</sup> and hexamethylbenzene<sup>37</sup> in *n*-pentane, *n*-hexane and *n*-heptane solid solutions at 77°K, at concentrations between  $10^{-2} \text{ M/l}$  and  $10^{-4} \text{ M/l}$ , were found to be characteristic of the formation of interstitial solutions. Solute aggregation also occurred but to a decreasing extent in the more dilute solutions.

For the three solutes studied it was found that the band widths of the

interstitial type solute spectra were most narrow in the *n*-hexane solid solutions. The range of solute-matrix interactions would therefore appear to be smallest in *n*-hexane solid solutions for these solutes.

On the basis of the results for naphthalene obtained by Bolotnikova<sup>32</sup>, durene, which resembles naphthalene in molecular size and in having  $D_{2h}$  symmetry, might have been expected to behave like naphthalene for which *n*-pentane is the best solvent. The fact that *n*-hexane is the best solvent for durene shows that a different parameter must be involved than in the case of naphthalene-*n*-pentane solid solutions. The long axis of durene is no greater than 7 Å in length, according to the crystallographic data of Robertson<sup>38</sup>, whereas the *n*-hexane has a length of 8.57 Å<sup>13</sup>. However, the diagonal axis formed by two opposed C—CH<sub>3</sub> bonds in durene is about 8.5 Å in length. This axis, in the absence of mutual repulsion of neighbouring methyl groups, would be at an angle of 30° with respect to the major axis of the aromatic molecule.

It was therefore suggested<sup>35</sup> that for steric reasons durene molecules cannot fit into linear paraffin matrices in similar fashion to nonsubstituted linear aromatic hydrocarbons. The potential energy minimum for solute-solvent interaction is suggested to occur in *n*-hexane not when the long axis of the durene molecule is parallel to the *c*-axis of the matrix crystal (in the direction of which the solvent molecules are aligned), but when the solute molecule has rotated by 30° about the C<sub>2</sub> axis perpendicular to its molecular plane. Durene molecules will therefore tend to orient themselves in this fashion. The large band width observed, even in *n*-hexane, indicates that in interstitial solutions of this type, the matrix cages are highly irregular. A similar interpretation was given to account for *n*-hexane being the best solvent for pentamethylbenzene<sup>36</sup> and hexamethylbenzene<sup>37</sup>.

Two more cases will be discussed in this section. The first concerns the observation of narrow line electronic spectra when the solute molecule is very much bigger than solvent molecules. Numerous examples have been studied by Shpolskii and his co-workers; indeed one of the earliest observations of narrow line spectra was for coronene in *n*-heptane. A striking case<sup>39</sup> is that of phthalocyanine C<sub>32</sub>H<sub>18</sub>N<sub>8</sub> which gives sharp line fluorescence and absorption spectra in *n*-octane, *n*-nonane and *n*-decane at 77°K. A solute molecule of this size must replace at least two solvent molecules and is probably trapped between layers of the paraffin molecules. Coupling with the matrix is evidenced by the fact that the coronene vibrational frequencies are solvent sensitive, varying by 1 to 2 per cent among the three paraffin solvents.

Narrow line spectra of phthalocyanine could be accounted for by considerations based on section III. 3. The presence of a solute of mass and size much greater than the matrix molecules could give rise to local vibrations where displacements of neighbouring oscillating lattice sites relative to the heavy solute are reduced as compared with their displacements in impurity-free regions of the paraffin crystal. The resulting narrow range of dynamic variation of solute-solvent interactions would give rise to narrow vibronic bands. Furthermore, the large number of matrix molecules in the solvent cage would tend to give a more smoothed out time dependent solute-solvent interaction. This interpretation is consistent with the fact that sharp line

## ELECTRONIC SPECTRA OF ORGANIC SOLID SOLUTIONS

electronic spectra are observed for coronene in three solvents of different linear dimensions<sup>13</sup>: *n*-octane 11.0 Å, *n*-nonane 12.8 Å, and *n*-decane 13.4 Å.

The other case of interest arises from the observation of broad vibronic bands in some substitutional solid solutions for which, on the contrary, one might expect narrow line spectra. An example is the fluorescence spectrum of *m*-xylyl radicals which have been formed by  $\lambda$  2537 Å photolysis of *m*-xylene molecules in a *m*-xylene crystal<sup>33</sup>. The vibronic band widths are of the order of 300 cm<sup>-1</sup> (*Figure 4*). The *m*-xylyl radicals may be formed by trapping of the *m*-xylene exciton at defect site complexes or, by analogy with observations on duryl formation in durene crystals<sup>40</sup>, via a single photon photosensitized reaction involving aromatic aldehyde impurities. In both cases *m*-xylene molecules atypically situated in the crystal lattice will be favoured sites for

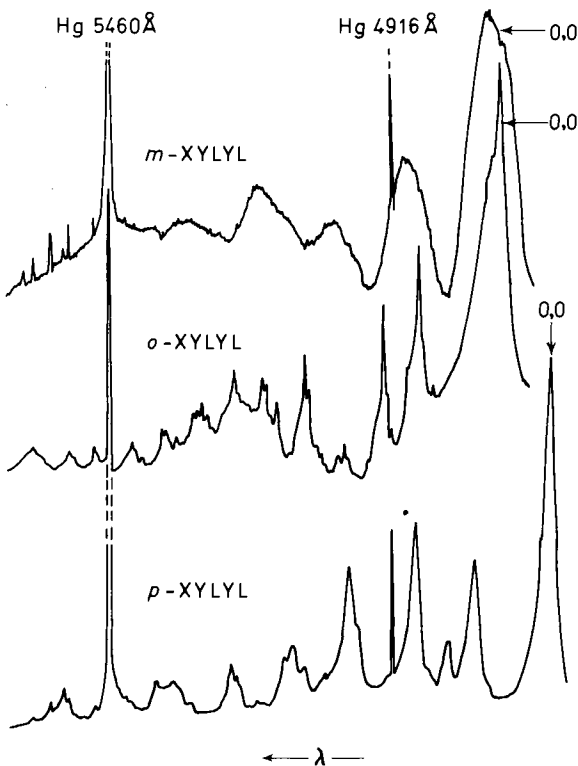


*Figure 4.* Fluorescence spectra at 77°K: *m*-xylyl in polycrystalline *m*-xylene; *o*-xylyl in polycrystalline *o*-xylene; *p*-xylyl in polycrystalline *p*-xylene.

radical formation. A similar situation exists for formation of *o*-xylyl in *o*-xylene crystals and *p*-xylyl in *p*-xylene crystals. However, their vibronic line widths are much narrower, as can be seen in *Figure 4*.

The broadened bands of *m*-xylyl are not due to an intramolecular phenomenon since this radical, as well as *o*-xylyl and *p*-xylyl, give well resolved gas phase emission spectra both at low<sup>41</sup> and at high<sup>34</sup> spectral

#### SYDNEY LEACH

resolution. Furthermore, *m*-xylyl is known to give narrow line spectra in photolysed solutions of *m*-xylene in crystalline methylcyclopentane solid solutions<sup>42</sup> at 88°K. The width of *m*-xylyl fluorescence bands in *m*-xylene must therefore be due to a large range of radical sites, related to the range of sites of the photolysed parent molecules. It is possible that this larger range of radical sites as compared with *o*-xylyl and *p*-xylyl arises from the lesser hindrance to rotation of the methyl groups in *m*-xylene, leading to a greater and more varied number of defect sites being frozen in at low temperatures and an enhanced dynamic variation of radical-matrix interactions. The potential barrier to methyl rotation is 270 cal/mol for *m*-xylene, 1100 cal/mol for *p*-xylene and 2200 cal/mol for *o*-xylene<sup>43</sup>; it is interesting to note that this order is also that of decreasing line width for the fluorescence vibronic bands of these radicals.

#### V. MULTIPLE SITES

Absorption and fluorescence spectra of organic solid solutions often exhibit a multiplet structure i.e. each vibronic band of a spectrum has several components which repeat throughout the spectrum. Several years ago<sup>44</sup> we enumerated the variety of possible causes for this multiplet structure: multiple solute sites, lattice vibrations, matrix polymorphism, solute aggregates. Emphasis will be placed here on multiple solute sites and matrix polymorphism.

The work of Bowen and Brocklehurst<sup>45</sup> and of Shpol'skii and his associates<sup>11, 12</sup> on the electronic spectra of coronene in linear paraffin solid solutions drew initial attention to the presence of line multiplets and their evolution with thermal treatment and purification of the solvent. The number of multiplets varies with the solvent<sup>12</sup>. These results and the more recent work of Kahane-Paillous and Pfister<sup>46, 47</sup> have shown clearly the existence of different solute sites in coronene-linear paraffin solutions. The nature of these sites is difficult to interpret but the geometrical factors involved have recently been discussed by Pfister<sup>47</sup>. Earlier it was suggested by Shpol'skii and Klimova<sup>12</sup> that frozen-in rotational isomers of the linear paraffins give rise to different solute sites.

The existence of frozen-in metastable forms of the matrix was demonstrated for quenched solutions of benzene in cyclohexane by Leach, Lopez-Delgado and Grajcar<sup>23</sup>. When the solutions were annealed the multiplet structure disappeared and only single vibronic lines were observed.

The fluorescence spectra of a 10<sup>-3</sup> M/l solute of benzene in cyclohexane are shown, as a function of temperature, in Figure 5. For the solution initially quenched to 80°K from room temperature each vibronic band shows two components, HTT and BT, separated by 80 cm<sup>-1</sup>. The relative intensity of the HTT components decrease as the temperature is increased; the HTT components disappear completely at 175°K leaving only the BT components.

Cyclohexane undergoes a crystallographic phase transition at 186°K from the stable low temperature (BT) form II (whose structure is uncertain<sup>3</sup>) to the cubic structure, form I, stable at higher temperatures (HT).

It can be seen in Figure 5 that the HT spectrum above 186°K has broadened considerably and has shifted by about 100 cm<sup>-1</sup> to higher energies with

## ELECTRONIC SPECTRA OF ORGANIC SOLID SOLUTIONS

respect to that observed at 175°K. Reduction of the temperature below 186°K brings about a reverse change from the HT to the BT spectrum but the HTT components do not appear again. The HTT spectrum is therefore related to a metastable crystallographic form III of the cyclohexane matrix

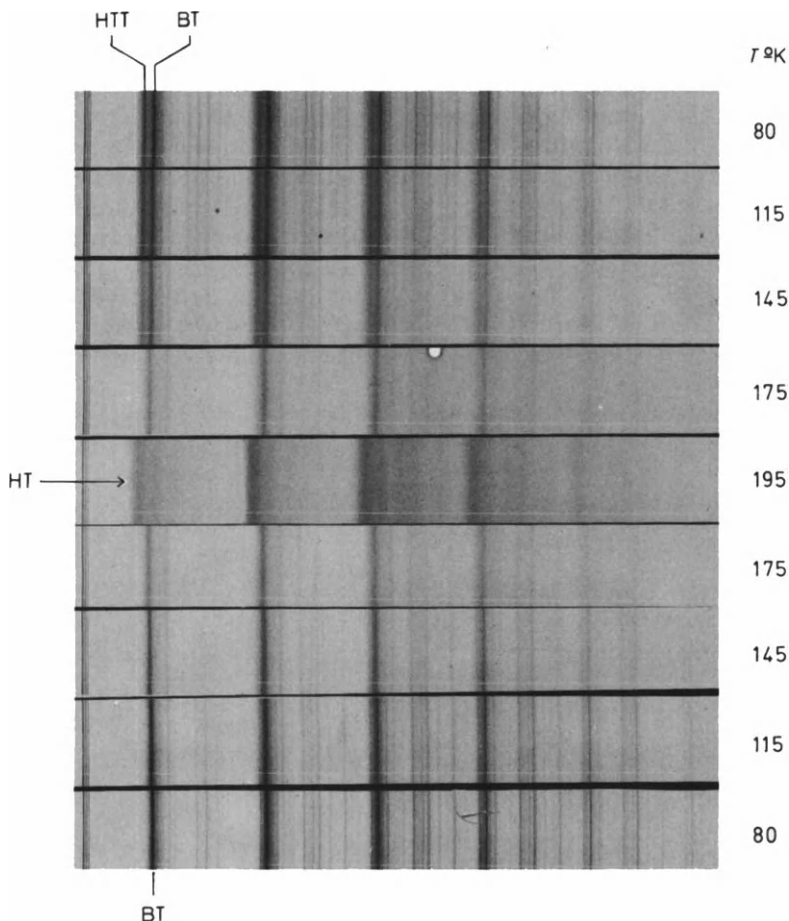


*Figure 5.* Effect of temperature cycle on the fluorescence spectrum of benzene in cyclohexane solid solution ( $10^{-3}$  M/l).

whose formation is induced by the quenching operation. The BT and HT spectra are associated with forms II and I of solid cyclohexane respectively. Form I shows considerable rotational disorder<sup>48</sup> and this could account for the broader vibronic bands above 186°K.

The identification of solute sites can be carried out not only by thermal treatment experiments but also through the photo-excitation spectra of the fluorescence of solute molecules trapped at separate sites.

From the discussion in section III. 3 one can draw an important conclusion regarding such experiments. If solute-matrix configurations cannot be

transformed into each other *via* vibrations of the matrix in times smaller than experimental times, then they will have separate excitation spectra. Such spectra have been observed for sites in the quenched cyclohexane solutions of benzene<sup>23</sup> discussed above, in which each type of solute site, at 80°K, is associated with individual microcrystals of different crystallographic structure, cyclohexane forms III and II, and which must be separated by grain boundaries hindering dynamic coupling between them.

Different excitation spectra of two components of the coronene fluorescence spectrum in *n*-hexane and *n*-heptane solid solutions were observed by Svishchyov<sup>49</sup>. As mentioned above, the nature of these sites is still uncertain.

In recent experiments in our laboratory, Michel<sup>26</sup> has studied the excitation spectra of the first three groups of multiplets of the fluorescence spectrum, at 3757 Å ( $\alpha$ ), 3788 Å ( $\beta$ ) and 3808 Å ( $\gamma$ ), of anthracene in *n*-heptane solution at 77°K. The separation between  $\alpha$  and  $\gamma$  is about 390 cm<sup>-1</sup> which is of the order of a 395 cm<sup>-1</sup> low frequency vibration of anthracene. This led Bolotnikova *et al.*<sup>50</sup> to attribute the  $\gamma$  multiplet band to the 0,0 transition and the  $\alpha$  band to 0,0 + 390 cm<sup>-1</sup>, in which an upper state vibration is excited.

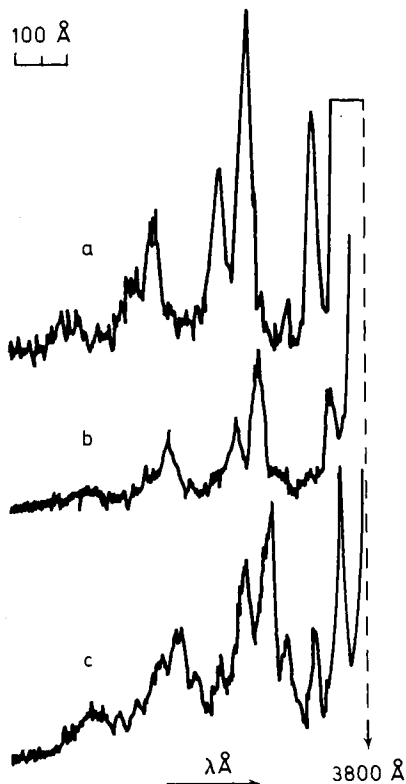


Figure 6. Excitation spectra of  $\alpha$ ,  $\beta$  and  $\gamma$  components of the 0,0 region of the fluorescence spectrum of anthracene in quenched solid solution in *n*-heptane ( $10^{-3}$  M/l) at 77°K: (a)  $\alpha$  component at 3757 Å; (b)  $\beta$  component at 3788 Å; (c)  $\gamma$  component at 3808 Å.

## ELECTRONIC SPECTRA OF ORGANIC SOLID SOLUTIONS

Such an interpretation implies that vibrational relaxation is incomplete in the excited electronic state. However *Figure 6* shows clearly that the  $\alpha$ ,  $\beta$  and  $\gamma$  bands have different excitation spectra, of similar allure but displaced about 25 Å from each other, so that they must be attributed to 0,0 transitions associated with anthracene molecules in three different sites in the *n*-heptane matrix. Upper state vibrational relaxation is therefore normally effected in the *n*-heptane solution at 77°K. Comparison of band intensities in absorption and fluorescence spectra showed however that the  $\gamma$  band is a superposition of the  $\gamma$  site 0,0 band and the 0,0–395 cm<sup>-1</sup> band of the  $\alpha$  site, the latter band involving a vibration excited in the ground state. This work will be reported more fully elsewhere.

In conclusion we wish to make a few remarks concerning the origin of multiple sites in terms of the mechanism of mixed crystal growth.

It is reasonable to suppose that for molecular solids, in which intermolecular forces are weak and generally non-directional, the presence of extrinsic impurities, whether they be the chosen solute molecules or accidental extraneous impurities, can induce particular and varied forms of short range or long range order in the surrounding matrix. In other words, in the presence of extrinsic impurities, the balance between minimum energy and maximum entropy determining the packing structure of the matrix around the solute can lead to a number of metastable minima of free energy and so to the co-existence of a number of different local structures in the polycrystalline medium. In some cases, the different structures may simply reflect the existence of misoriented solute or solvent molecules. The removal of impurities<sup>45</sup> or the annealing of the solid<sup>46,47</sup> would modify the number relative populations of these structures and so give rise to variations in the number of multiplets and their relative intensities. The persistence of multiple sites after thorough annealing of the solid solution indicates either that the potential barrier to the conversion of the different structures into the most stable one is very high or that the various minima of free energy have substantially the same value.

Finally it should be pointed out that the size of the microcrystals can be an important factor in determining the stable or metastable crystallographic form and the defect content. It is possible that in the initial nucleation stage a particular structural configuration of the incipient microcrystal could have a lower free energy than an equal volume of the equilibrium infinite crystal<sup>51</sup>. When growth has occurred beyond a certain critical size, the free energy will equal and then exceed that of an equal volume of the infinite crystal. The consequent strain energy will then be released by cleavage or by the introduction of dislocations and a crystallographic microphase transition to the new equilibrium structure. The growth to the final equilibrium infinite crystal could indeed take place *via* a series of different structural configurations having successively the lowest free energy of any possible configuration for that particular size of crystallite. It is therefore possible that in polycrystalline matrices, such as the linear paraffins, especially for quenched samples, the polycrystal could be composed of crystallites of different size having different structural configurations and different defect contents. This should be taken into account in interpreting the spectral observations of multiplet structure in solid solutions in linear paraffins.

SYDNEY LEACH  
ACKNOWLEDGMENTS

The author is indebted to many of his students and co-workers whose results are quoted here. Particular acknowledgment is due to Antonio Lopez-Campillo for helpful discussions during the preparation of this paper.

### References

- <sup>1</sup> S. Leach. *J. de Physique* **28**, C3-134 (1967).
- <sup>2</sup> S. Leach. *Int. Conf. Spectroscopy*, Bombay 1967, ICSU publication, (1968) p. 155.
- <sup>3</sup> S. Leach. *10th European Congress on Molecular Spectroscopy*, Liège 1969. *Mem. Soc. Roy. Sci. Liège*, 5<sup>e</sup> sér., **20**, 179 (1970).
- <sup>4</sup> S. Leach, A. Lopez-Campillo, R. Lopez-Delgado and C. Tomas-Magos. *C.R. Acad. Sci. (Paris)* **263B**, 1230 (1966).
- <sup>5</sup> (a) S. Leach and L. Grajcar. *Fifth Int. Symp. Free Radicals*, Uppsala, 1961, Almqvist and Wiksell, Stockholm (1961), paper 36;  
 (b) E. Migirdicyan and S. Leach. *Bull. Soc. Chim. Belges* **71**, 845 (1962).
- <sup>6</sup> J. von Kowalski. *Phys. Z.* **12**, 956 (1911); *Verh. deutsch. Phys. Ges.* **13**, 952 (1911).
- <sup>7</sup> G. N. Lewis and D. Lipkin. *J. Am. Chem. Soc.* **64**, 2801 (1942).
- <sup>8</sup> I. Norman and G. Porter. *Proc. Roy. Soc. (London)* **A230**, 399 (1955).
- <sup>9</sup> S. Leach. *Luminescence of organic and inorganic materials* Ed. Kallmann and Spruch, Wiley, N.Y. (1962) p. 176.
- <sup>10</sup> D. S. McClure. *J. Chem. Phys.* **22**, 1668 (1954); *ibid.* **24**, 1 (1956).
- <sup>11</sup> E. V. Shpol'skii, A. A. Il'ina and L. A. Klimova. *Dokl. Akad. Nauk S.S.R.* **87**, 935 (1952).
- <sup>12</sup> E. V. Shpol'skii. *Soviet Phys. Usp.* **3**, 372 (1960); *ibid.* **5**, 522 (1962); *ibid.* **6**, 411 (1963).
- <sup>13</sup> A. I. Kitaigorodskii. *Organic Chemical Crystallography*, Consultants Bureau, N.Y. (1961).
- <sup>14</sup> A. I. Kitaigorodskii. *Acta Cryst.* **18**, 585 (1965).
- <sup>15</sup> D. P. Craig, R. Mason, P. Pauling and D. P. Santry. *Proc. Roy. Soc. (London)* **A286**, 98 (1965).
- <sup>16</sup> J. D. Ferry. *Viscoelastic properties of polymers* Wiley, N.Y. (1961).
- <sup>17</sup> R. A. Swalin. *Thermodynamics of solids* Wiley, N.Y. (1962).
- <sup>18</sup> J. Sherwood. *Organic solid state chemistry* Ed. G. Adler, Gordon and Breach, N.Y. (1969) p. 37.
- <sup>19</sup> A. Bree and R. Zwarich. *Mol. Crystals and Liquid Crystals* **5**, 369 (1969).
- <sup>20</sup> W. Helfrich and F. R. Lipsett. *J. Chem. Phys.* **43**, 4368 (1965);  
 F. R. Lipsett and G. MacPherson. *Can. J. Phys.* **44**, 1485 (1966).
- <sup>21</sup> S. Leach and E. Migirdicyan. *Fluorescence à longue durée de vie de composés organiques*, 9<sup>e</sup> série, Actions chimiques et biologiques des radiations. Ed. M. Haissinsky, Masson, Paris (1966) p. 117.
- <sup>22</sup> D. R. Scott and J. B. Allison. *J. Phys. Chem.* **66**, 561 (1962).
- <sup>23</sup> S. Leach, R. Lopez-Delgado and L. Grajcar. *J. Chim. Phys.* **63**, 194 (1966).
- <sup>24</sup> R. Ostertag and H. C. Wolf. *Phys. Stat. Sol.* **31**, 139 (1969).
- <sup>25</sup> C. Pfister. Private communication.
- <sup>26</sup> C. Michel. Thèse 3<sup>e</sup> cycle, Orsay 1970.
- <sup>27</sup> K. K. Rebane. *Impurity spectra of solids* Plenum Press, N.Y. (1970).
- <sup>28</sup> S. Leach and R. Lopez-Delgado. *J. de Physique Colloque N° 2*, 139 (1966).
- <sup>29</sup> S. Leach and R. Lopez-Delgado. *J. de Physique* **28**, C3-150 (1967).
- <sup>30</sup> P. G. Klemens, in *Non-Crystalline Solids*. Ed. V. D. Fréchette, Wiley, N.Y. (1960) p. 508.
- <sup>31</sup> P. M. Rentzepis. *Photochem. Photobiol.* **8**, 579 (1968).
- <sup>32</sup> T. N. Bolotnikova. *Opt. Spectr.* **7**, 138 (1959).
- <sup>33</sup> S. Leach, A. Lopez-Campillo, R. Lopez-Delgado and M. C. Tomas-Magos. *J. de Physique*, **28**, C3-147 (1967).
- <sup>34</sup> M. C. Cossart-Magos. Unpublished work in this laboratory.
- <sup>35</sup> G. Durocher and S. Leach. *J. Chim. Phys.* **66**, 628 (1969).
- <sup>36</sup> G. Durocher. *J. Chim. Phys.* **66**, 985 (1969).
- <sup>37</sup> G. Durocher. *J. Chim. Phys.* **66**, 637 (1969).
- <sup>38</sup> J. M. Robertson. *Proc. Roy. Soc. (London)* **A141**, 594 (1933); *ibid.* **A142**, 659 (1933).
- <sup>39</sup> F. F. Litvin and R. I. Personov. *Sov. Phys. Doklady* **6**, 134 (1961);  
 R. I. Personov. *Opt. Spectr.* **15**, 30 (1963).
- <sup>40</sup> E. Migirdicyan. In press, *J. Chem. Phys.* **55** (15 August 1971).
- <sup>41</sup> T. F. Bindley, A. T. Watts and S. Walker. *Trans. Faraday Soc.* **58**, 849 (1962).

## ELECTRONIC SPECTRA OF ORGANIC SOLID SOLUTIONS

- <sup>42</sup> A. Pellois. Thèse 3e cycle, Rennes (1969);  
A. Pellois and J. Ripoche. *Spectrochim. Acta* **26A**, 1051 (1970).
- <sup>43</sup> J. Haupt and W. Muller-Warmuth. *Z. Naturforsch.* **23a**, 208 (1968).
- <sup>44</sup> S. Leach. *J. Chim. Phys.* **61**, 1629 (1964).
- <sup>45</sup> E. J. Bowen and B. Brocklehurst. *J. Chem. Soc.* p. 3875 (1954); *ibid.* p. 4320 (1955).
- <sup>46</sup> C. Pfister and J. Kahane-Paillous. *J. Chim. Phys.* **65**, 876 (1968).
- <sup>47</sup> C. Pfister. *J. Chim. Phys.* **67**, 418 (1970).
- <sup>48</sup> M. Renaud and R. Fourme. *J. Chim. Phys.* **63**, 27 (1966).
- <sup>49</sup> G. V. Svishchyov. *Izv. Akad. Nauk S.S.R.* **27**, 696 (1963); *Opt. Spectr.* **18**, 350 (1965).
- <sup>50</sup> T. N. Bolotnikova, L. A. Klimova, G. N. Neresesova and L. F. Utkina. *Opt. Spectr.* **21**, 237 (1966).
- <sup>51</sup> B. G. Bagley. *J. Cryst. Growth* **6**, 323 (1970).
- <sup>52</sup> S. Leach and R. Lopez-Delgado. *J. Chim. Phys.* **61**, 1636 (1964).
- <sup>53</sup> R. Lopez-Delgado. Thèse d'Etat, Paris 1969 (C.N.R.S. n° 3880).

# MAGNETIC EFFECTS ON TRIPLET EXCITON INTERACTIONS

R. E. MERRIFIELD

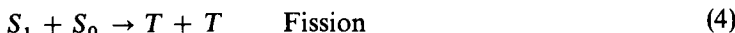
*Central Research Department, E. I. du Pont de Nemours and Company,  
Wilmington, Delaware 19898, USA*

## ABSTRACT

The rates of many bimolecular reactions involving triplet excitons are magnetic field dependent at room temperature and for modest field strengths. The specific interactions discussed are the fusion of a pair of triplet excitons to yield either a single or triplet exciton, the interaction between a triplet exciton and a trapped triplet, the fission of a singlet exciton into a pair of triplets and the triplet exciton-free radical interaction. The magnetic field effects result from the influence of the field on the spin wavefunctions of the triplet exciton together with the existence of spin selection rules for the interactions. A simple theory of these effects is presented. Application of the theory to the experimental field dependence results yields new information about the mechanisms of these interactions.

## I. INTRODUCTION

. Some of the most interesting properties of triplet excitons are consequences of the fact that they are triplets—that is, that they consist of three closely spaced levels whose energies and wavefunctions can be modified by the application of a magnetic field. Since triplet excitons in organic crystals typically have diffusion lengths of the order of 30 microns, they explore a large volume of the crystal during their lifetimes and have an opportunity to undergo a variety of interactions with any other objects which may be simultaneously present in the crystal<sup>1</sup>. Some of these interactions which have been experimentally demonstrated are summarized by the following ‘chemistry’:



where  $S_0$  and  $S_1$  represent molecules of the crystal in their ground and first excited singlet states, respectively,  $T$  represents the lowest triplet state, and  $D$  represents a doublet-state species (e.g. a free radical). The states designated

by lower case letters represent analogous states localized at an impurity molecule in the crystal. It turns out that the rates of the reactions listed above are in many cases magnetic field dependent at room temperature and for modest field strengths—conditions under which spin polarization of the triplet exciton is completely negligible. It is the purpose of this review: first, to summarize the experimental findings on the magnetic field dependence of these reactions; second, to show that the field dependence can be understood quantitatively on the basis of a simple model of triplet exciton interactions; and finally, to show how application of the theory to the experimental results can provide a powerful tool for illuminating some rather subtle details of these interactions.

## II. SPIN STATES OF A TRIPLET EXCITON IN A FIELD

Before turning to triplet-exciton interactions, it will be useful to review the effects of a magnetic field on the spin states of an individual triplet exciton since these spin states are intimately involved in determining the rates of the interaction processes.

It is well known that the spin states of a triplet exciton are described by the following spin Hamiltonian<sup>2</sup>:

$$\mathcal{H} = g\beta\mathbf{H} \cdot \mathbf{S} + DS_z^2 + E(S_x^2 - S_y^2) \quad (6)$$

where the first term describes the Zeeman interaction and the remaining terms represent the fine structure which results from the interaction between the magnetic dipoles of the two unpaired electrons which comprise the triplet state.

The fact that this spin Hamiltonian describes a triplet exciton rather than the triplet state of an isolated molecule appears only implicitly in the expression. The exciton Hamiltonian differs from the molecular one in two respects: first, the hyperfine structure term, which would be present in the molecular Hamiltonian as a result of the interaction between electron and nuclear spins, is averaged to zero by the rapid motion of the exciton; and second, the fine-structure tensor for the exciton is an average over the various inequivalent molecules in the crystal structure. This is also a consequence of the rapid motion of the exciton.

Turning next to the energies and wavefunctions of the triplet in a magnetic field, let us look first at the zero-field limit. One of the consequences of the presence of the fine-structure terms is to lift the degeneracy of the three triplet sublevels which would otherwise exist at zero field. The zero-field eigenstates are<sup>3</sup>:

$$\begin{aligned} |x\rangle &= 2^{-\frac{1}{2}}(|-1\rangle - |+1\rangle) \\ |y\rangle &= i2^{-\frac{1}{2}}(|-1\rangle + |+1\rangle) \\ |z\rangle &= |0\rangle \end{aligned} \quad (7)$$

whose energies are  $D - E$ ,  $D + E$ , and  $0$ , respectively. The spin states on the right-hand side are quantized with respect to the  $z$ -axis of the fine-structure tensor.

## MAGNETIC EFFECTS ON TRIPLET EXCITON INTERACTIONS

Turning next to the high-field limit, i.e. where the Zeeman energy is large compared to the fine structure splitting, the fine-structure terms can be treated as a first-order perturbation on the Zeeman levels  $|0\rangle$ ,  $|+1\rangle$  and  $| -1\rangle$ , which are quantized with respect to the external field. The result is that the energy levels are anisotropic—that is, they depend on the direction of the magnetic field with respect to the principal axes of the fine structure tensor. This is illustrated in *Figure 1*. Explicitly, the first-order energies are<sup>4</sup>:

$$E_0 = (D - E) \cos^2\alpha + (D + E) \cos^2\beta$$

$$E_{\pm 1} = \pm g\beta H + D - \frac{1}{2}(D - E) \cos^2\alpha - \frac{1}{2}(D + E) \cos^2\beta \quad (8)$$

where  $\alpha$  and  $\beta$  are the angles made by the field with the  $x$  and  $y$  principal axes, respectively, of the fine-structure tensor. However, to first order the spin wavefunctions follow the magnetic field and are not affected by the fine structure terms.

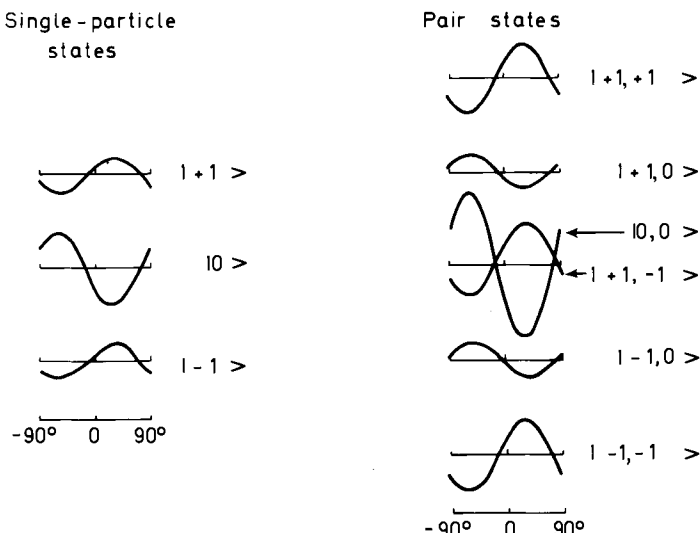


*Figure 1.* Anisotropy of energies in the high-field limit of the magnetic sublevels of a single triplet exciton and a pair of triplets in anthracene. The magnetic field lies in the  $ac$  plane of the crystal and the indicated angles are with respect to the  $a$  axis. The energy scale is arbitrary. (Reproduced by kind permission of the American Chemical Society. *Accounts of Chemical Research*, 1, 129 (1968))

At intermediate fields where the fine structure and Zeeman terms are comparable, both the energy levels and wavefunctions of the triplet are complicated and rapidly varying functions of both the magnitude and direction of the applied field.

## III. TRIPLET EXCITON INTERACTIONS

### A. Homofusion

In many ways the most interesting interaction of a triplet exciton is the interaction with another identical exciton. The possible outcomes of an interaction between a pair of triplets are indicated in *Figure 2* in which it is

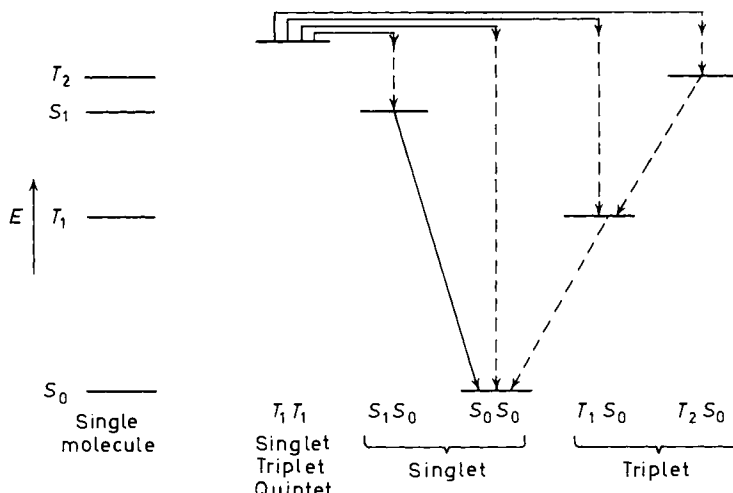


Figure 2. Electronic energy levels of a single molecule (far left) and of a pair of molecules showing the possible outcomes of the interaction of a pair of molecules in their triplet states. All of the indicated transitions are radiationless except that from  $S_1 S_0$  to  $S_0 S_0$ , which is responsible for delayed fluorescence

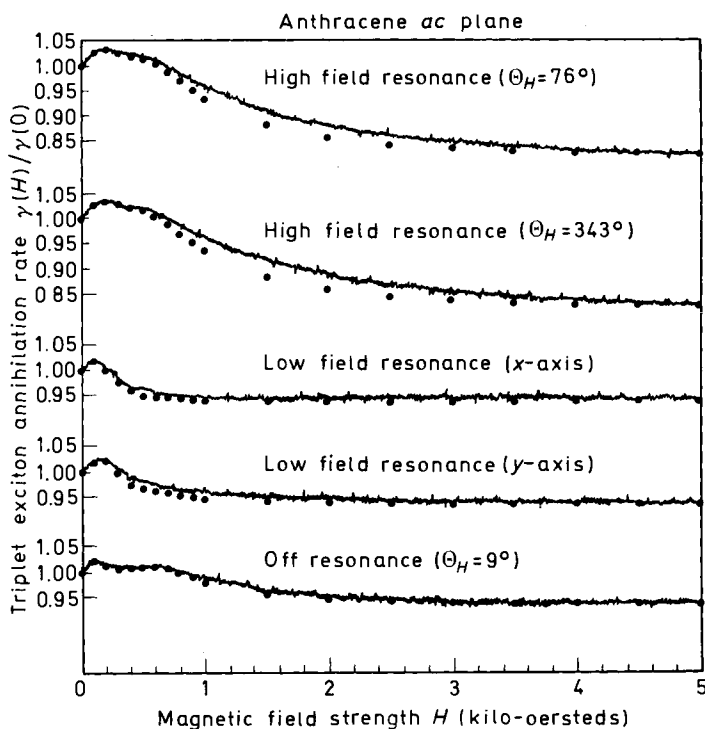


Figure 3. Experimental measurements and theoretical calculations (dots) of the field dependence of the singlet-channel fusion rate,  $\gamma_s$ , for several representative directions  $\Theta_H$  in the  $ac$  plane of anthracene. The  $x$  and  $y$  axes of the dipolar tensor are at  $\Theta_H = 29.5^\circ$  and  $299.5^\circ$ , respectively.

(Reproduced by kind permission of the Physical Review. *Phys. Rev. B* **1**, 896 (1970).)

## MAGNETIC EFFECTS ON TRIPLET EXCITON INTERACTIONS

seen that there are several electronic energy levels of the pair which lie below the  $2T$  state, one of which,  $S_1 + S_0$ , results in the subsequent emission of luminescence (delayed fluorescence). It is an experimental fact that delayed fluorescence resulting from the homofusion of triplet excitons is magnetic field dependent<sup>4,5</sup>. Typical experimental results for an anthracene crystal are shown in Figures 3 and 4.

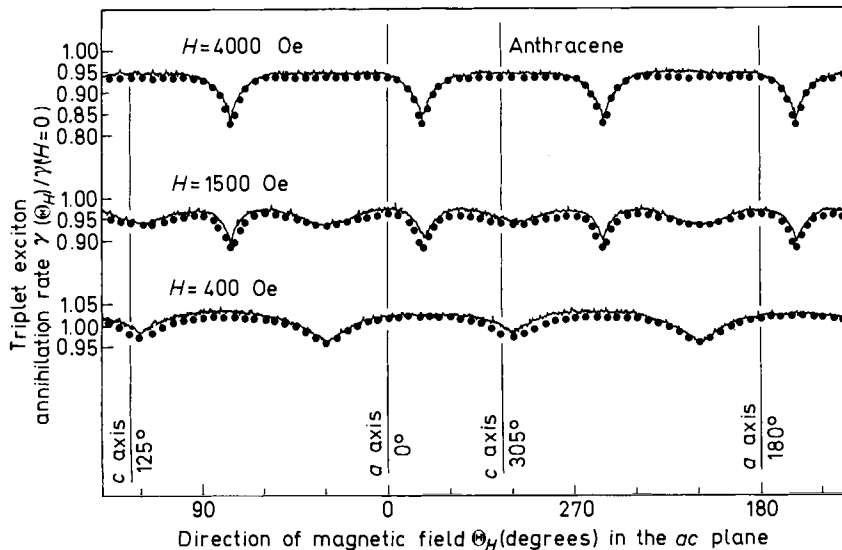


Figure 4. Experimental measurements and theoretical calculations (dots) of the anisotropy of the singlet-channel fusion rate,  $\gamma_s$ , in the  $ac$  plane of anthracene for three magnetic field strengths. The high-field resonances are evident at 4000 Oe and the low-field resonances at 400 Oe. At 1500 Oe the two sets of resonances coexist. The low-field resonance directions coincide with the  $x$  and  $y$  principal axes of the fine-structure tensor. (Reproduced by kind permission of the Physical Review. Phys. Rev. B1, 896 (1970))

In order to describe the interaction of a pair of triplets we require the spin Hamiltonian of a pair. The simplest assumption is that it is simply the sum of two single-particle Hamiltonians, i.e.

$$\mathcal{H} = g\beta\mathbf{H} \cdot (\mathbf{S}_1 + \mathbf{S}_2) + D(S_{z_1}^2 + S_{z_2}^2) + E(S_{x_1}^2 + S_{x_2}^2 - S_{y_1}^2 - S_{y_2}^2) \quad (9)$$

It could be argued that this Hamiltonian is obviously incomplete in that it contains no terms describing the interaction between the two triplets, and in fact such an interaction certainly must exist in order for the fusion process to take place. However, it turns out that this interaction is negligible with respect to its influence on the spin part of the pair wavefunction and the consequent field dependence of the fusion rate. Whether or not such an interaction is included, one of the most important properties of the pair Hamiltonian is the fact that it is invariant under interchange of the two excitons. This has the important consequence that the eigenstates can be classified into those which are even and odd under the interchange operation.

At zero field the pair eigenstates are those shown in Figure 5. It is seen that the interchange symmetry leads to a degeneracy in pair states such as  $|xy\rangle$

R. E. MERRIFIELD

where the two excitons have different single particle states. None of the zero-field pair states corresponds to a definite spin multiplicity. This can be seen by examining the eigenstates of total spin expressed in terms of the zero-field pair wavefunctions. These are:

$$\begin{aligned} \text{Singlet: } & |S\rangle = 3^{-\frac{1}{2}}(|xx\rangle + |yy\rangle + |zz\rangle) \\ \text{Triplets: } & |T_x\rangle = 2^{-\frac{1}{2}}(|yz\rangle - |zy\rangle) \\ \text{Quintets: } & |Q_a\rangle = 2^{-\frac{1}{2}}(|xx\rangle - |yy\rangle) \\ & |Q_b\rangle = 6^{-\frac{1}{2}}(|xx\rangle + |yy\rangle - 2|zz\rangle) \\ & |Q_x\rangle = 2^{-\frac{1}{2}}(|yz\rangle + |zy\rangle) \end{aligned} \quad (10)$$

where the states  $|T_y\rangle$ ,  $|T_z\rangle$  and  $|Q_y\rangle$ ,  $|Q_z\rangle$  are obtained from  $|T_x\rangle$  and  $|Q_x\rangle$  by cyclic permutation of  $x$ ,  $y$  and  $z$ . Note that the singlet and quintet states are even under interchange of the two triplets, while the triplet states are odd. This is a general result regardless of the value of the magnetic field.

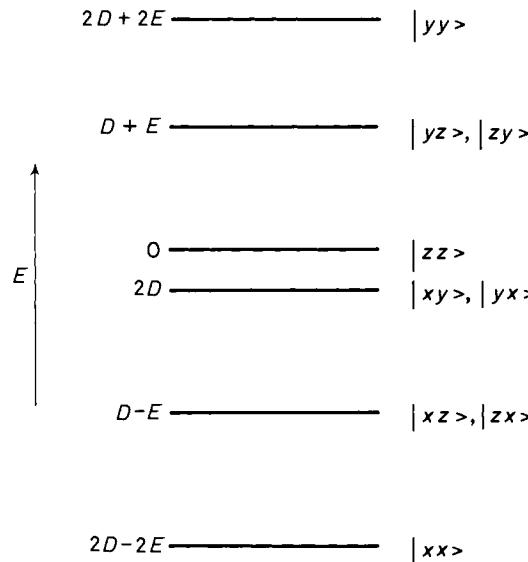


Figure 5. Zero-field spin states and energy levels for a pair of triplet excitons. The states at  $D + E$ ,  $2D$  and  $D - E$  are doubly degenerate

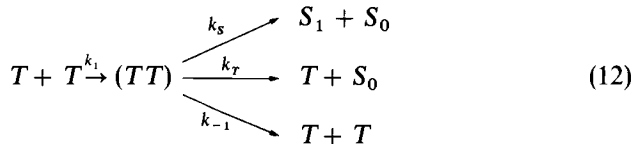
Turning next to the high-field limit, the anisotropies of the energies of the high-field pair states are shown in *Figure 1*. The pure spin states expressed in terms of these high-field, pair eigenstates are:

$$\begin{aligned} |S\rangle &= 3^{-\frac{1}{2}}(|00\rangle - |+-\rangle - |-+\rangle) \\ |T_0\rangle &= 2^{-\frac{1}{2}}(|+-\rangle - |-+\rangle) \\ |Q_0\rangle &= 6^{-\frac{1}{2}}(2|00\rangle + |+-\rangle + |-+\rangle) \\ |T_{\pm 1}\rangle &= 2^{-\frac{1}{2}}(|\pm 0\rangle - |0\pm\rangle) \\ |Q_{\pm 1}\rangle &= 2^{-\frac{1}{2}}(|\pm 0\rangle + |0\pm\rangle) \\ |Q_{\pm 2}\rangle &= |\pm\pm\rangle \end{aligned} \quad (11)$$

## MAGNETIC EFFECTS ON TRIPLET EXCITON INTERACTIONS

Note that, as shown in *Figure 1*, for most field directions the two types of pair eigenstates which have a singlet component have different energies. However, there do exist particular field directions for which these states become degenerate so that at these level crossings a pure singlet eigenstate of the pair is possible<sup>4</sup>.

The next task is to relate the foregoing discussion of the pair spin states to the kinetics of the fusion process. This will be done in terms of the following simple kinetic scheme:



in which triplets come together to form pairs which can react via either a singlet or triplet channel or can scatter without reaction. It is assumed that the probability of fusion from a given one of the nine pair states is proportional to the spin amplitude for the appropriate channel. The kinetic equation for  $P_n$ , the steady state population of the  $n^{\text{th}}$  pair states is<sup>6</sup>:

$$\frac{1}{9}k_1[T]^2 = (k_{-1} + k_S|S_n|^2 + k_T|\mathbf{T}_n|^2)P_n \quad (13)$$

where

$$|S_n|^2 = |\langle S|\psi_n\rangle|^2$$

and

$$|\mathbf{T}_n|^2 = \sum_{m=1}^3 |\langle T_m|\psi_n\rangle|^2$$

are the fractional singlet and triplet character, respectively, of the  $n^{\text{th}}$  pair state, whose spin wavefunction is  $|\psi_n\rangle$ . Under steady-state conditions the total rates of fusion for the singlet and triplet channels become

$$\gamma_S[T]^2 = \sum_n k_S|S_n|^2 P_n = \frac{k_1[T]^2}{9} \sum_n \frac{k_S|S_n|^2}{k_{-1} + k_S|S_n|^2 + k_T|\mathbf{T}_n|^2} \quad (14)$$

$$\gamma_T[T]^2 = \sum_n k_T|\mathbf{T}_n|^2 P_n = \frac{k_1[T]^2}{9} \sum_n \frac{k_T|\mathbf{T}_n|^2}{k_{-1} + k_S|S_n|^2 + k_T|\mathbf{T}_n|^2} \quad (15)$$

where  $\gamma_S$  and  $\gamma_T$  are the overall rate constants for the reactions



This simple kinetic scheme is not really complete as a result of the degeneracies which can occur among the pair spin states. In the presence of a degeneracy the particular linear combinations of the degenerate pair of states which are to be used in calculating the spin amplitudes are ambiguous, and the value calculated for  $\gamma_S$  and  $\gamma_T$  will depend on what choice is made. A more

complete treatment of the dynamics of the interaction involving consideration of the density matrix of the pair spin states has been developed<sup>4</sup> which resolves this ambiguity. Rather than giving the details of this treatment, we shall merely state the salient result, which is that in the presence of a degeneracy, that linear combination of the degenerate states is to be taken which comes closest to diagonalizing the total spin of the pair. Thus in the case of the degeneracy resulting from the interchange symmetry, even and odd combinations are to be used, the odd combination being in all cases a pure triplet. Similarly, at the high-field level-crossing pure singlet and quintet combinations are the appropriate pair states.

As a result of the considerations outlined in the preceding paragraph, it follows that the singlet and triplet channels for fusion are independent in the sense that no one pair state will simultaneously have both singlet and triplet character. Thus  $\gamma_T$  is field independent (since  $|T_n|^2 = 1$  for a pure triplet, regardless of the triplet basis states<sup>7</sup>) and the expression for  $\gamma_S$  becomes

$$\gamma_S = \frac{k_1}{9} \sum_n \frac{k_S |S_n|^2}{k_{-1} + k_S |S_n|^2} \quad (17)$$

The singlet amplitudes are constrained by the sum rule  $\sum_n |S_n|^2 = 1$  and the value of  $\gamma_S$  depends on the manner in which this unit of singlet character is distributed over the pair states. This can be seen by considering the simple situation in which  $N$  of the pair states have equal singlet character, i.e.  $|S_n|^2 = 1/N$  for  $N$  states and is zero for the rest. In this case

$$\gamma_S(N) = \frac{k_1}{9} \times \frac{k_S}{k_{-1} + (k_S/N)} \quad (18)$$

which is a monotonically increasing function of  $N$ . This illustrates the salient characteristic of equation (17), namely, that  $\gamma_S$  increases as the singlet character becomes spread over more of the pair states and has its minimum value if one pair state is a pure singlet.

The magnetic field dependence of the fusion rate is thus described by equation (17), together with the field dependence of the pair spin wavefunctions and consequent field dependence of the  $S_n$ . The principal qualitative features of the magnetic field dependence of  $\gamma_S$  shown in *Figures 3 and 4* can now be accounted for. At zero field there are, from equation (10), three pair states which have singlet character, i.e.  $|xx\rangle$ ,  $|yy\rangle$  and  $|zz\rangle$ . At high fields it is seen from equation (11) that there are in general two such states, i.e.  $|00\rangle$  and  $2^{-\frac{1}{2}}(|+-\rangle + |-+\rangle)$ , so that  $\gamma_S$  will be less than at zero field. At the particular field orientations for which these two states are degenerate, the pure singlet state becomes an eigenstate and  $\gamma_S$  will decrease further (a level-crossing resonance). At intermediate fields the singlet character will be distributed over all of the even pair states and  $\gamma_S$  will be larger than the zero-field value. This is illustrated in *Figure 6* which shows how the magnetic field dependence of  $\gamma_S$  is related to the field dependence of the energy levels and the distribution of singlet character over the six even states of the triplet pair. It is seen that the region of rapid variation of  $\gamma_S$  with field occurs, as

## MAGNETIC EFFECTS ON TRIPLET EXCITON INTERACTIONS

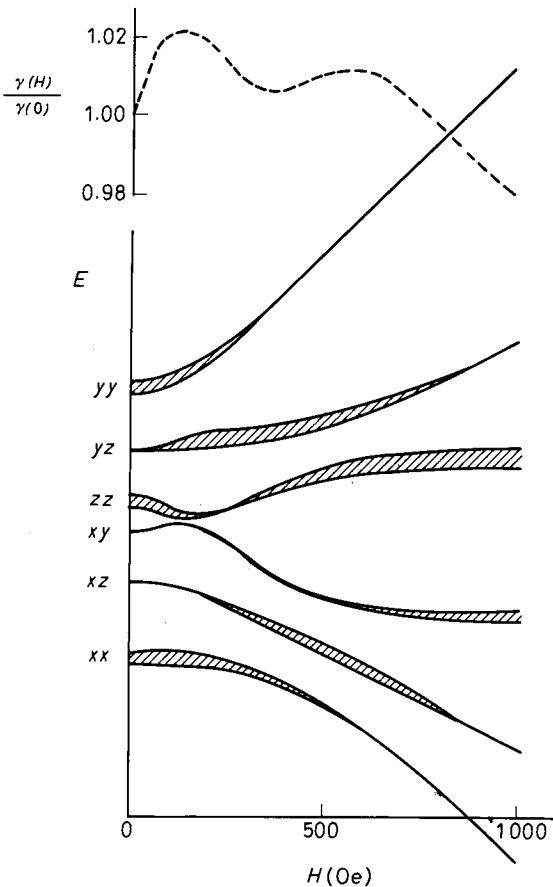


Figure 6. Typical calculated variation at low fields of the pair spin energy levels (lower solid curves) and singlet-channel fusion rate (upper dashed curve). The heights of the cross hatched areas are proportional to the fractional singlet characters of the pair states. The parameters employed in the calculation are:  $D = -56$  Oe,  $E = 350$  Oe and  $k_s/k_{-1} = 0.4$

expected, in the region where the Zeeman energy and zero-field splitting are comparable.

The only case so far in which detailed experimental data exist and have been quantitatively compared with calculations based on this model is that of the anthracene crystal<sup>4</sup>. Typical experimental results along with the calculated points are shown in Figures 3 and 4. The parameter values which give the best fit to the experimental data are the following:

$$\begin{aligned}
 k_{-1} &= (2.8 \pm 0.3) \times 10^9 \text{ sec}^{-1} \\
 k_s &= (1.1 \pm 0.1) \times 10^9 \text{ sec}^{-1} \\
 D &= -56 \pm 10 \text{ Oe} \\
 E &= 350 \pm 30 \text{ Oe}
 \end{aligned} \tag{19}$$

For comparison, the values of  $D$  and  $E$  measured directly by ESR<sup>8</sup> are  $-62 \pm 15$  Oe and  $350 \pm 20$  Oe, respectively.

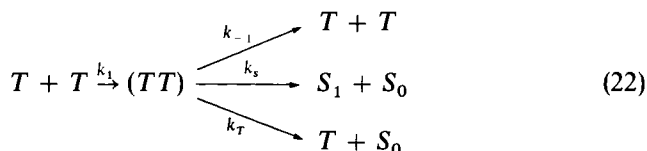
This does not yet yield a complete picture of the fusion process. Information is still lacking on the importance of the triplet channel as a consequence of its magnetic field independence and the fact that it does not lead to delayed fluorescence. However, the field independence of  $\gamma_T$  can be exploited in a slightly modified experimental situation to give the desired information<sup>7</sup>. The basic idea is to examine the field dependence of delayed fluorescence under conditions of high exciton density in which the fusion channel becomes important in determining the steady-state exciton concentration so that one can examine the competition between the singlet and triplet channels. In the high-density limit where the bimolecular decay of triplets dominates the monomolecular decay, the steady-state triplet concentration,  $[T]$ , is determined by

$$\alpha = (2\gamma_s + \gamma_T)[T]^2 \quad (20)$$

where  $\alpha$  is the rate of triplet generation and the coefficients of  $\gamma_s$  and  $\gamma_T$  reflect the fact that a singlet-channel fusion event removes twice as many triplets as a triplet-channel event. The delayed fluorescence intensity,  $\phi$ , is proportional to

$$\gamma_s[T]^2 = \frac{\gamma_s}{2\gamma_s + \gamma_T} \alpha \quad (21)$$

It can be seen that measurement of the field dependence of  $\phi$  under these conditions will yield information on the relative magnitudes and field dependences of  $\gamma_s$  and  $\gamma_T$ . Thus, if these two quantities should have the same field dependence, the delayed fluorescence would become field independent in the high-density limit. However, if, as expected theoretically,  $\gamma_T$  is a constant, then the field dependence of  $\phi$  will be reduced in amplitude from the low-density results and the amount of this reduction in amplitude will yield the ratio  $\gamma_T/\gamma_s$ . Groff, *et al.*<sup>7</sup>, have carried out such high-density experiments which confirm that  $\gamma_T$  is indeed field independent and yield  $\gamma_T/\gamma_s(0) = 3.5 \pm 0.2$ . Combining this result with the previous ones, we arrive at the following picture of the triplet fusion process:



$$k_{-1} = (2.8 \pm 0.3) \times 10^9 \text{ sec}^{-1}$$

$$k_s = (1.1 \pm 0.1) \times 10^9 \text{ sec}^{-1}$$

$$k_T = (1.7 \pm 0.2) \times 10^9 \text{ sec}^{-1}$$

From these values of the rate constants, together with equation (17), it can be concluded that of the encounters of two triplet excitons 4 per cent lead to fusion via the singlet channel, 13 per cent to triplet-channel fusion and the remaining 83 per cent scatter without reaction. This example

## MAGNETIC EFFECTS ON TRIPLET EXCITON INTERACTIONS

illustrates the power of the magnetic field experiments in illuminating many of the details of triplet-exciton interactions which are not accessible by any other means.

The homofusion of triplet excitons has been observed in many other organic crystals and in most cases exhibits a magnetic field dependence qualitatively similar to that seen in anthracene, although anthracene remains the only case in which really detailed results exist at present. One crystal in which qualitatively different behaviour is found is 9,10-diphenylanthracene. The field dependence of delayed fluorescence from this crystal is shown in *Figure 7*. The behaviour at low fields is similar to that of anthracene, but three additional peaks are found at 5.5, 11 and 22 kOe. The reason for the existence of this additional structure at high fields is not really understood,

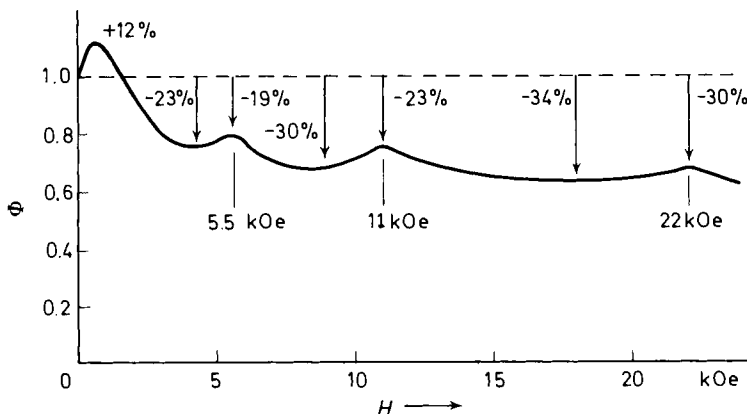


*Figure 7.* Magnetic field dependence of delayed fluorescence intensity from a 9,10-diphenylanthracene crystal of unknown orientation

but it can be partially accounted for on the assumption that for some unknown reason there exist two kinds of triplet excitons in the crystal which differ in energy by about  $1\text{ cm}^{-1}$ . The high-field energy levels in such a situation are shown in *Figure 8*. It is seen that the singlet-containing ( $M_S=0$ ) levels of the pair are crossed at three different fields (in the ratio of 1:2:4) by levels which have no singlet character ( $M_S = \pm 1, \pm 2$ ). This is in contrast to the type of level crossing discussed earlier for anthracene in which two levels, both of which have singlet character, cross with a resulting decrease in fusion rate. This type of level crossing, i.e. a singlet and a pure nonsinglet, would be expected to lead to an increase in fusion rate as observed experimentally. Whether or not this picture bears any relation to the true explanation, it is clear that additional information about triplet excitons in this crystal is contained in the high-field structure.

Another type of triplet homofusion process is the reaction between triplet states of molecules in solution<sup>9</sup>. This process, too, is magnetic field dependent<sup>10,11</sup> as illustrated in *Figure 9* for delayed fluorescence resulting from fusion of triplet-state anthracene molecules in ethanol solution. The observed field dependence is accounted for on the basis of a model similar to that outlined above for crystals<sup>11</sup>. However, it is considerably more

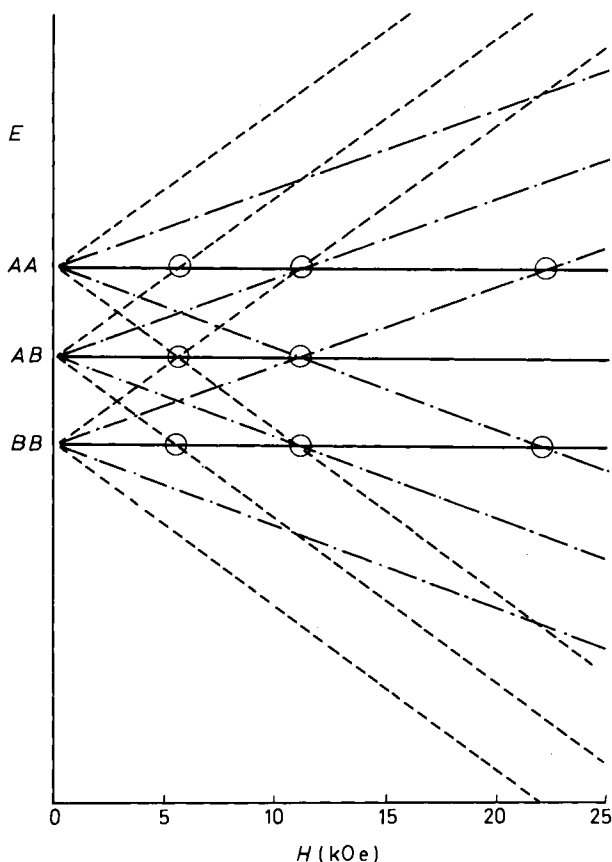


Figure 8. Hypothetical energy level scheme suggested by experimental results on 9,10-diphenylanthracene. There are two types of triplet excitons, denoted *A* and *B*, giving rise to three types of pairs. The Zeeman levels are  $M_S = 0$  (solid lines),  $M_S = \pm 1$  (dot-dash) and  $M_S = \pm 2$  (dashes). Level crossings involving the  $M_S = 0$  levels are indicated by circles

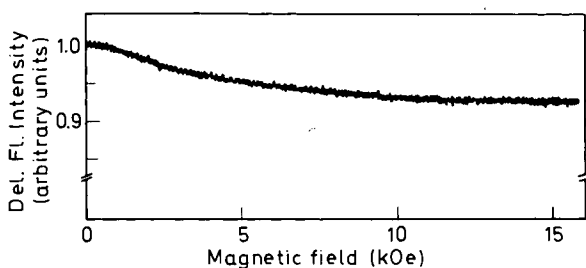


Figure 9. Dependence of delayed fluorescence intensity on magnetic field strength for a  $10^{-4}$  M solution of anthracene in ethanol at  $25^\circ\text{C}$ . (Reproduced by kind permission of Academic Press, New York. *Proceedings of the International Conference on Organic Scintillators and Liquid Scintillation Counting*, San Francisco, July 1970)

## MAGNETIC EFFECTS ON TRIPLET EXCITON INTERACTIONS

complicated in detail because of the necessity for averaging over all the possible molecular orientations which can occur in solution. Analysis of the experimental field dependence curve yields  $k_s/k_{-1} \approx 12$  for the solution experiment of *Figure 9*, compared to the value of 0.4 for this ratio in the anthracene crystal. Thus, in contrast to the situation in the crystal, triplet fusion in solution is diffusion limited.

### B. Heterofusion

In the discussion of the preceding section it is clear that the symmetry of the pair spin Hamiltonian plays a dominant role in determining the magnetic field dependence of the homofusion rate constant. It is therefore of interest to examine the consequences of removing this symmetry. This can be done by looking at delayed fluorescence resulting from the fusion of a triplet exciton with a triplet state of an impurity molecule incorporated in the crystal<sup>12</sup> (a localized exciton), i.e. heterofusion, the process of equation (3). Since the interchange symmetry is destroyed in this situation, the separation of the triplet pair states from the singlets and quintets is no longer obtained. One of the consequences of this broken symmetry is that we must now use the expression (14) rather than equation (17) for the fusion rate constant since now a given pair state may have both singlet and triplet character simultaneously. At zero field the following relation between singlet and triplet amplitudes can be shown to hold<sup>12</sup>:

$$|\mathbf{T}_n|^2 = \frac{1}{2} - \frac{3}{2} |\mathbf{S}_n|^2 \quad (23)$$

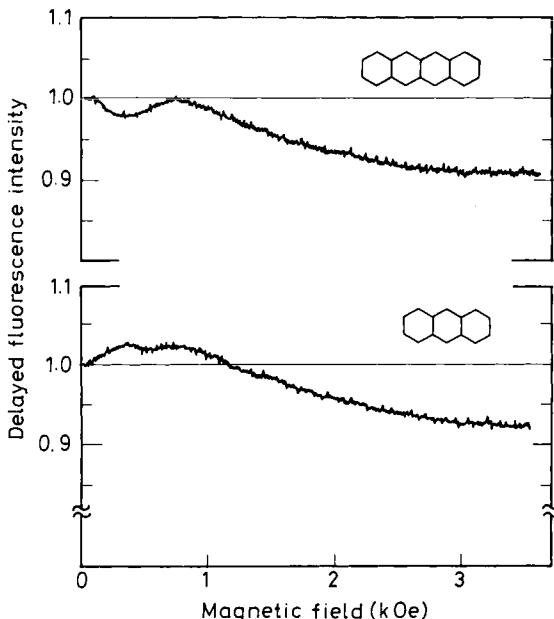


*Figure 10.* Field dependence of delayed emission from tetracene (heterofusion, top curve) and from anthracene (homofusion, bottom curve) in an anthracene crystal doped with 0.01 ppm tetracene. The field is oriented along the *a* axis. (Reproduced by kind permission of the Physical Review. *Phys. Rev. Letters* **25**, 105 (1970))

If this relation is used to eliminate the triplet amplitudes from equation (14), the result is

$$\gamma_s = \frac{k_1}{9} \sum \frac{k_s |S_n|^2}{(k_{-1} + \frac{1}{2}k_T) + (k_s - \frac{3}{2}k_T)|S_n|^2} \quad (24)$$

This has the same form as equation (17) for homofusion, but with the important difference that the coefficient of  $|S_n|^2$  in the denominator need not be positive. If this coefficient is negative, i.e. if  $k_s < \frac{3}{2}k_T$ , then the dependence of  $\gamma_s$  on the way in which the singlet character is distributed over the pair states will be the inverse of that for homofusion. In particular, the initial field dependence would be a *decrease* in  $\gamma_s$  rather than an increase.

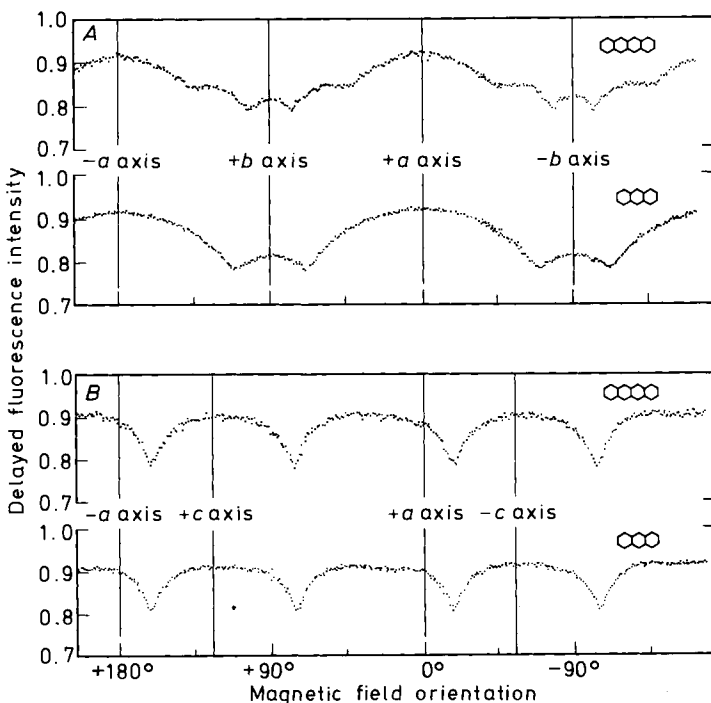
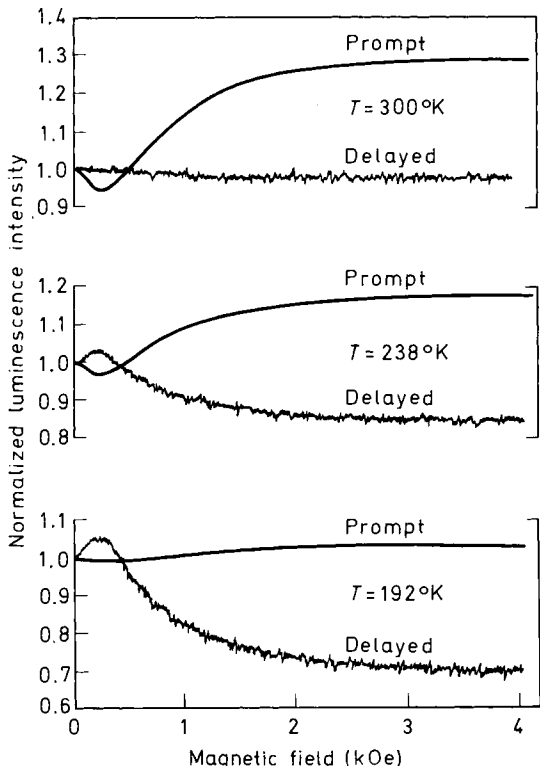


Figure 11. Dependence of tetracene and anthracene components of delayed fluorescence emission on the orientation of a 4 kOe magnetic field in the *ab* (top) and *ac* (bottom) planes of an anthracene crystal doped with 0.01 ppm tetracene. (Reproduced by kind permission of the Physical Review. *Phys. Rev. Letters* **25**, 105 (1970))

Figure 10 shows the field dependence of the heterofusion rate in a crystal of anthracene doped with ca. 0.01 ppm tetracene<sup>12</sup>. In this case the initial field dependence is indeed a decrease, thus confirming the qualitatively different nature of the heterofusion process. Following the initial decrease, at higher fields the field dependence resembles that for homofusion. This is presumably a result of the increasing importance of the (symmetric) Zeeman term in the pair spin Hamiltonian *vis-à-vis* the (unsymmetrical) fine-structure terms although explicit calculations of the theoretical field dependence do not

## MAGNETIC EFFECTS ON TRIPLET EXCITON INTERACTIONS

yet exist. The high-field anisotropy shown in *Figure 11* shows another interesting qualitative difference from homofusion. The additional structure apparent in the figure is a result of the fact that heterofusion events involving a free exciton and triplets trapped on tetracene molecules at either of the two possible substitutional sites in the anthracene crystal structure<sup>13</sup> can be



*Figure 12.* Magnetic field dependence of prompt and delayed fluorescence intensities in a tetracene crystal. The field is oriented at  $-20^\circ$  with respect to the *b* axis in the *ab* plane of the crystal.  
(Reproduced by kind permission of the Physical Review. *Phys. Rev. B1*, 815 (1970))

distinguished. The observed anisotropy is thus a superposition of two sets of level-crossing resonances. Analysis of the angular position of the high-field resonances shows that the tetracene molecule enters the anthracene lattice approximately substitutionally.

### C. Exciton Fission

Equation (4), the reverse of the triplet fusion reaction, is not observed in the vast majority of molecular crystals since it is too highly endothermic (*ca.*  $4000\text{ cm}^{-1}$  for anthracene). However, in the case of the tetracene crystal, the  $2T$  level lies only about<sup>14</sup>  $1200\text{ cm}^{-1}$  above  $S_1$  so that fission of a singlet exciton into a pair of triplets is energetically feasible. The occurrence of this process was first suggested by Swenberg and Stacy<sup>15</sup> to account for the

anomalously low fluorescence quantum yield of tetracene crystals. The correctness of this suggestion has been verified by experimental demonstration that the prompt fluorescence quantum yield of tetracene is magnetic field dependent<sup>16,17</sup> (in contrast to fluorescence of other organic crystals) and that this field dependence is the inverse of that of triplet exciton fusion in the same crystal<sup>14</sup>. This is illustrated in Figures 12 and 13.

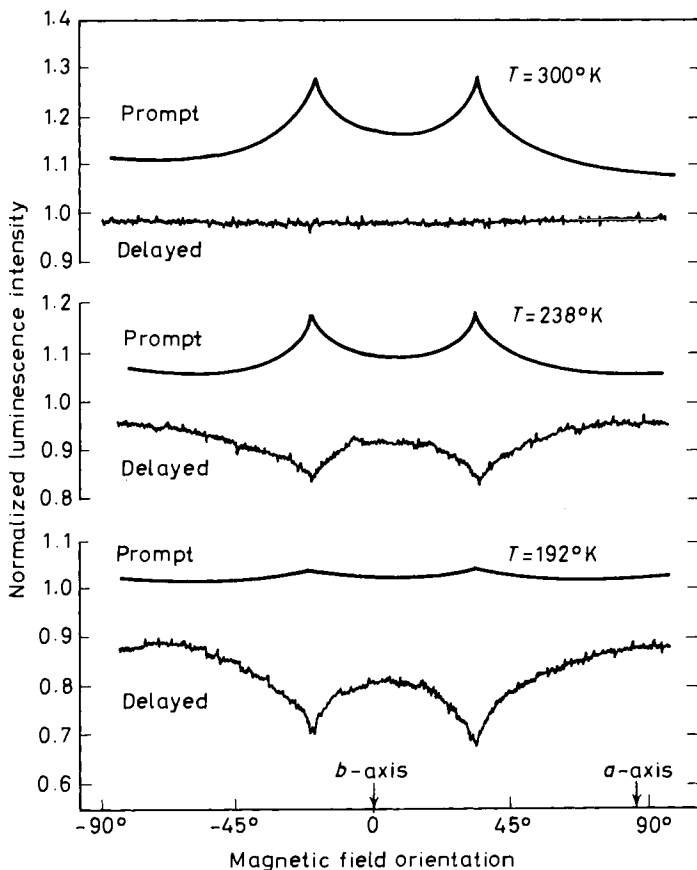


Figure 13. Dependence of prompt and delayed fluorescence intensity on the orientation of a 4 kOe magnetic field in the *ab* plane of a tetracene crystal. (Reproduced by kind permission of the Physical Review. *Phys. Rev.* **B1**, 815 (1970))

At room temperature most singlet excitons produced in the crystal decay via fission, so that the field dependence of the prompt fluorescence intensity is the inverse of the field dependence of the fission rate constant. On the other hand, the delayed fluorescence, in which singlets are being produced by the fusion reaction, shows virtually no field dependence since the singlet production and decay rates have the same field dependence. Since the fission reaction is endothermic, the situation is reversed at low temperatures where most singlets decay radiatively. These effects show clearly in Figures 12 and 13.

## MAGNETIC EFFECTS ON TRIPLET EXCITON INTERACTIONS

### D. Triplet-Radical Interaction

It is well known that the lifetimes of triplet excitons are shortened in the presence of paramagnetic impurities in the crystal<sup>18</sup>. Presumably the radicals act as catalysts for intersystem crossing from  $T$  to  $S_0$  by allowing the process of equation (5) to take place without violating spin selection rules. The six spin states of a triplet exciton-doublet radical pair can be analyzed in a manner very similar to that employed for a pair of triplets<sup>19</sup>. The overall spin states will be doublet-quartet mixtures whose field dependence will be

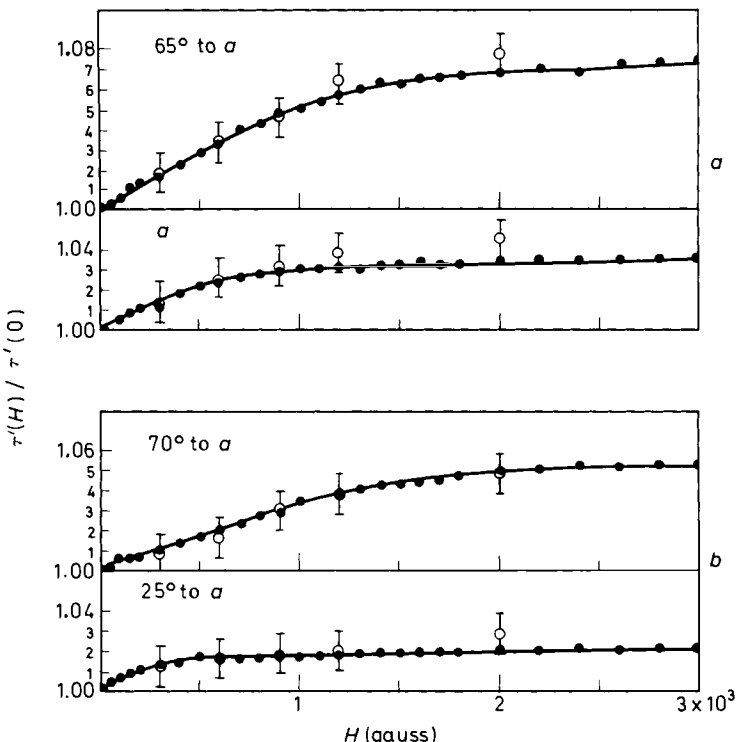


**Figure 14.** Magnetic field dependence of triplet exciton lifetime in x-irradiated anthracene. (a) dose  $4 \times 10^3$  R,  $\tau(0) = 1.55$  msec.  $H$  in  $ab$  plane in directions at  $65^\circ$  (resonance) and  $0^\circ$  with respect to the  $a$  axis. (b) dose  $1 \times 10^3$  R,  $\tau(0) = 4.95$  msec.  $H$  in  $ac$  plane along  $70^\circ$  (resonance) and  $25^\circ$  to  $a$  directions. Open circles: direct measurements. Curves drawn from steady-state delayed fluorescence intensity ratios. (Reproduced by kind permission of the Physical Review. *Phys. Rev. Letters* 21, 609 (1968))

reflected in a corresponding field dependence of the rate of triplet quenching, which is proportional to the doublet character of the combined spin state since the final state in equation (5) is a pure doublet. In this case the model predicts a monotonic decrease of quenching rate with increasing magnetic field, as well as the existence of a set of high-field level-crossing resonances which will occur at the same positions as the resonances observed in triplet-triplet fusion. Experimental results on the quenching of triplet excitons in an anthracene crystal by radicals introduced by x-irradiation are shown in Figure 14<sup>19</sup>. The qualitative predictions of the model are well confirmed by

the experimental results, although from these results it is not possible to decide whether the radical simply catalyses intersystem crossing in the host crystal or whether there is energy transfer to the radical.

#### IV. SUMMARY

The principal conclusions, which emerge from the work which has been reviewed here, are that the rate of any triplet exciton process which is subject to a spin selection rule is expected to be magnetic field dependent and that analysis of this field dependence can lead to considerable information regarding the details of triplet-exciton interactions. It is perhaps worth emphasizing that the magnetic field effects discussed here do *not* result from spin polarization or partial alignment of the triplet exciton magnetic moment by the field; the magnetic energies involved in these experiments are entirely negligible compared to thermal energies. Rather, the magnetic field exerts its influence through its effects on the spin wavefunctions of the triplet excitons.

The examples given in the foregoing do not exhaust the potential catalogue of triplet-exciton interactions which could be expected to be affected by a magnetic field. For example, it is known<sup>20</sup> that triplet excitons interact with free and trapped electrons and holes in organic crystals. Some of the details of this interaction should be amenable to study by magnetic-field effects. Another example is the interaction between triplet states and molecular oxygen<sup>21</sup>. The mechanism by which oxygen quenches triplets could perhaps be clarified by magnetic-field experiments.

#### REFERENCES

- <sup>1</sup> P. Avakian and R. E. Merrifield. *Mol. Cryst.* **5**, 37 (1968).
- <sup>2</sup> H. Sternlicht and H. M. McConnell. *J. Chem. Phys.* **35**, 1793 (1961).
- <sup>3</sup> J. H. van der Waals and M. S. de Groot. *Mol. Phys.* **2**, 333 (1959).
- <sup>4</sup> R. C. Johnson and R. E. Merrifield. *Phys. Rev.* **B1**, 896 (1970).
- <sup>5</sup> R. C. Johnson, R. E. Merrifield, P. Avakian and R. B. Flippin. *Phys. Rev. Letters* **19**, 285 (1967).
- <sup>6</sup> R. E. Merrifield. *J. Chem. Phys.* **48**, 4318 (1968);  
A. Suna, *Phys. Rev.* **B1**, 1716 (1970).
- <sup>7</sup> R. P. Groff, R. E. Merrifield and P. Avakian. *Chem. Phys. Lett.* **5**, 168 (1970).
- <sup>8</sup> D. Haarer, D. Schmid and H. C. Wolf. *Phys. Status Solidi* **23**, 633 (1967).
- <sup>9</sup> C. A. Parker. *Photoluminescence of Solutions*. Elsevier Publishing Company, Amsterdam (1968).
- <sup>10</sup> L. R. Faulkner and A. F. Bard. *J. Am. Chem. Soc.* **91**, 6495 (1969).
- <sup>11</sup> P. Avakian, R. P. Groff, R. E. Kellogg, R. E. Merrifield and A. Suna. *Proceedings of the International Conference on Organic Scintillators and Liquid Scintillation Counting, San Francisco, July 1970* (Academic Press, to be published).
- <sup>12</sup> R. P. Groff, R. E. Merrifield, P. Avakian and Y. Tomkiewicz. *Phys. Rev. Letters* **25**, 105 (1970).
- <sup>13</sup> A. M. Mathieson, J. M. Robertson and V. C. Sinclair. *Acta Cryst.* **3**, 245 (1950).
- <sup>14</sup> R. P. Groff, P. Avakian and R. E. Merrifield. *Phys. Rev.* **B1**, 815 (1970).
- <sup>15</sup> C. E. Swenberg and W. T. Stacey. *Chem. Phys. Lett.* **2**, 329 (1968).
- <sup>16</sup> N. Geacintov, M. Pope and F. Vogel. *Phys. Rev. Letters* **22**, 593 (1969).
- <sup>17</sup> R. E. Merrifield, P. Avakian and R. P. Groff. *Chem. Phys. Lett.* **3**, 155 (1969).
- <sup>18</sup> S. Z. Weisz, P. Richardson, A. Cobas and R. C. Jarnagin. *Mol. Cryst.* **3**, 168 (1967).
- <sup>19</sup> V. Ern and R. E. Merrifield. *Phys. Rev. Letters* **21**, 609 (1968).
- <sup>20</sup> W. Helfrich. *Phys. Rev. Letters* **16**, 401 (1966).
- <sup>21</sup> S. P. McGlynn, T. Azumi and M. Kinoshita. *Molecular Spectroscopy of the Triplet State* (Prentice-Hall, Englewood Cliffs, New Jersey, 1969), pp. 284-293.

# CHARGE-CARRIER INJECTION INTO HOMO-MOLECULAR CRYSTALS

W. MEHL

*Orbisphere Corporation, 91 Route de la Capite, 1223 Cologny/Geneva,  
Switzerland*

## ABSTRACT

The properties of the interface between homomolecular crystals and electrolytes or metals is reviewed. Correlations between various experimental measurements and controllable parameters are predicted. The theoretical analysis is based on the assumption that the equilibrium potential difference at the contact interface is located within the solid and that the interaction is entirely electrostatic. Exceptions to this model are noted and tentative explanations are given.

## PROPERTIES OF THE INTERFACE BETWEEN A MOLECULAR CRYSTAL AND AN ELECTROLYTE

Equilibrium at the interface between a semiconductor and an electrolyte is characterized by the equality of the electrochemical potential of electrons (the Fermi level) on the two sides of the boundary plane which is established by a redistribution of charge resulting in the formation of an electrical double layer, an electronic charge in the solid being compensated by an excess of ionic charge in the electrolyte. In most molecular crystals so far investigated the concentration of intrinsic carriers seems to be very small indeed so that, upon contact with an electrolyte, equilibrium can be established only by modifying the carrier distribution in valence or conduction band to display accumulation of electrons in the former and of holes in the latter.

Recent work on the investigation of the carrier injection into anthracene crystals from metals and electrolytes<sup>1</sup> has shown that the electrostatic potential difference  $\Delta\Phi$ , at the interface, is in most cases determined by the difference of the Fermi levels for the two phases before contact, i.e. the interaction is entirely electrostatic and specific chemical interactions can be neglected:

$$\Delta\Phi = F_c - F_s \quad (1)$$

$F_c$  and  $F_s$  denote the Fermi levels of the molecular crystal and of the electrolyte before contact, the sign of  $\Delta\Phi$  denoting the sign of the charge on the semiconductor surface using the electrolyte as reference. All potentials refer to the charge free bulk of semiconductor and electrolyte, i.e. for electron injection  $\Phi > 0$  in the semiconductor surface and  $\Phi < 0$  in the electrolyte, while for

hole injection  $\Phi < 0$  in the semiconductor surface and  $\Phi > 0$  in the electrolyte.

The differential equations describing the space charge variations of the electrostatic field  $E$  and the electrostatic potential at equilibrium are

$$\frac{dE}{dx} = 4\pi qe_0 n(x)/\kappa_M \quad (2)$$

$$\frac{d\Phi}{dx} = -E \quad (3)$$

$$\frac{dn}{dx} = \mu n E / qD \quad (4)$$

For simplicity a one-dimensional system was chosen.  $n(x)$  is the density of carriers at the point  $x$ ,  $e_0$  is the magnitude of the electronic charge,  $qe_0$  is the actual charge on each carrier and  $\kappa_M$  is the permittivity of the crystal. The first equation is Poisson's equation in which the volume charge is due to injected carriers following the assumption that these are in large excess over the thermally generated carriers. Equation (3) expresses the field as a gradient of potential and equation (4) states that in the equilibrium case the diffusion of electrons away from the interface is balanced by the drift of electrons towards the contact. Solutions to the system of differential equations (2) to (4) with various boundary conditions have been given by several authors who may be consulted for details of the calculations<sup>2, 3</sup>.

Lohmann<sup>4</sup> has given a solution for the case of an infinite solid with zero field at infinity on which a discussion of the potential distribution at the interface molecular crystal/electrolyte may be based. The interfacial potential distribution may be represented to a good approximation by the sum of three contributions

$$\Delta\Phi_T = \Delta\Phi_C + \Delta\Phi_H + \Delta\Phi_e \quad (5)$$

where  $\Delta\Phi_c$  represents the space charge inside the semiconductor,  $\Delta\Phi_H$  the potential difference across the inner Helmholtz layer, the region between the solid and the electrolyte into which ions do not penetrate unless there are specific chemisorption forces and  $\Delta\Phi_e$ , the potential difference across the diffuse double layer, the ionic space charge in the electrolyte formed by counter ions. Neglecting specific adsorption the potential gradient in the Helmholtz layer will be approximately constant, i.e. the potential difference  $\Delta\Phi_H$  across the layer is determined by the field  $E_H$  multiplied by the thickness of this layer.

Because of the continuity of the normal component of the displacement at the interface between crystal and electrolyte

$$\kappa_c \left( \frac{d\Phi}{dx} \right)_{x=0} = \kappa_H \left( \frac{d\Phi}{dx} \right)_{x_H > x > 0} \quad (6)$$

and the potential drop across the Helmholtz layer being thus

$$\Delta\Phi_H = \left( \frac{\kappa_c}{\kappa_H} \right) x_H \left( \frac{d\Phi}{dx} \right)_{x=0} \quad (7)$$

Lohmann<sup>4</sup> has derived from the system of differential equations (2) to (4) with the boundary condition  $E \rightarrow 0$  for  $x \rightarrow \infty$ :

$$\left( \frac{d\Phi}{dx} \right)_{x=0} = (L_D^0)^{-1} \exp\left( -\frac{\bar{\Delta}_{n,p}}{2kT} \right) \quad (8)$$

where  $L_D^0$  is a formal Debye length which would be observed for an insulator when all electrons in the valence band are released to the conduction band, assuming the density of states in both bands to be equal.  $\bar{\Delta}_{n,p}$  represents the distance between carrier band and Fermi level at the crystal surface. From (7) and (8):

$$\Delta\Phi_H = \left( \frac{\kappa_c}{\kappa_H} \right) \left( \frac{qx_H}{L_D^0} \right) \exp\left( -\frac{\bar{\Delta}_{n,p}}{2kT} \right) \quad (9)$$

From (9) the potential drop across the Helmholtz layer has been calculated as a function of the distance between Fermi level and carrier band at the insulator surface at equilibrium (*Figure 1*) verifying the previously made and

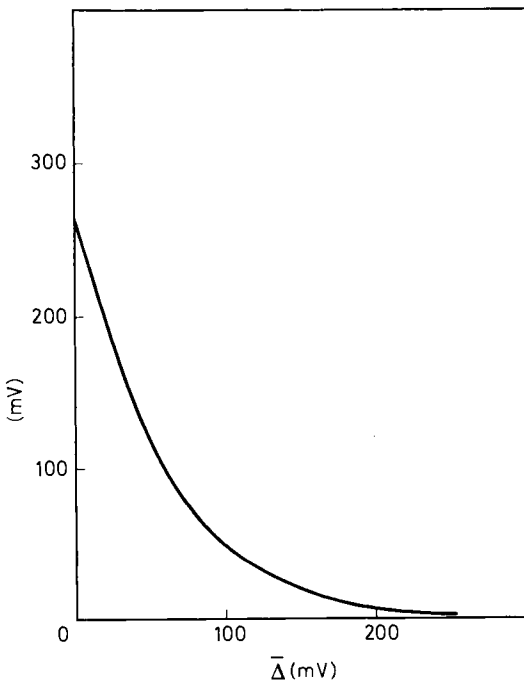


Figure 1. Potential drop across the Helmholtz layer as a function of the distance between Fermi level and carrier band at the crystal surface at equilibrium (Based on reference 4).

experimentally supported assumption that a sizeable potential drop across the Helmholtz layer can be expected only for the degenerate surface.

Unfortunately the direct experimental verification of the results of the preceding discussion is complicated by the extremely small carrier concentration in the bulk of the crystal. It was found that this difficulty can be overcome

when fairly strong oxidizing (or reducing) redox systems and extremely thin insulator films were chosen. The situation can then be realized when the thickness of the crystal is small compared to the Debye lengths of the two space charge layers which thus overlap so that the low intrinsic 'bulk' concentration of carriers does not materialize<sup>6</sup>.

For simplicity we assume the contact at each insulator face to be established by the same redox electrolyte. The electrostatic potential has then a maximum at the centre of the crystal and a single solution to the boundary problem can be given by moving the origin of the coordinate system to the centre<sup>5</sup>.

$$n(x) = n_c \sec^2 \left( \left\{ \frac{2\pi e_0^2 n_c}{kT} \right\}^{\frac{1}{2}} x \right) \quad (10)$$

$$\frac{e_0 \Phi(x)}{kT} = -2 \log \cos \left( \left\{ \frac{2\pi e_0^2 n_c}{kT} \right\}^{\frac{1}{2}} x \right) \quad (11)$$

where  $n_c$  is the carrier density at the centre of the crystal (*Figure 2*).

Equations (10) and (11) describe the general principle only, because for a real crystal the free carrier density is, due to trapping effects, smaller than

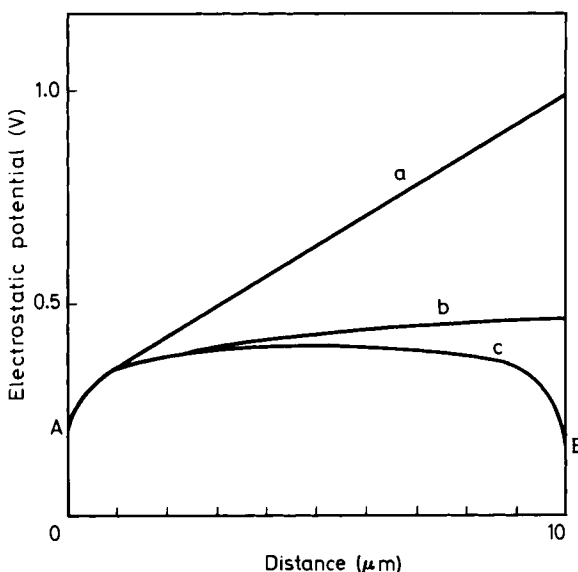


*Figure 2.* Variation of the electrostatic potential through a 10  $\mu\text{m}$  thick insulator film sandwiched between two electrolytic contacts. At interface A the potential step is 0.1eV. At interface B the potential step is: 1eV for curve a (monotonic case), 0.472eV for curve b (intermediate case), 0.1eV for curve c (symmetrical case) (Based on reference 5).

equation (10) would suggest. Nevertheless it has been possible to measure reversible redox potentials at very thin anthracene membranes<sup>6</sup>.

## CHARGE-CARRIER INJECTION INTO HOMO-MOLECULAR CRYSTALS

### ENERGETIC CONSIDERATIONS ON CARRIER GENERATION

As for molecular solids the lattice forces are of the van der Waals type there will be only small overlap between the orbitals of adjacent molecules. For anthracene e.g. the calculated intermolecular resonance integrals range in value from 5 to  $30 \times 10^{-16}$  erg for nearest-neighbour pairs, depending on orientation<sup>7</sup>. Thus the energetics of carrier formation may be described in terms of localized electrons and holes<sup>8</sup>, although the mobilities are probably best described in terms of the band approximation. Localized electrons and holes can be considered as negative and positive hydrocarbon ions respectively. The properties of these ions have been well investigated in solution<sup>9</sup> and, provided that the molecule is alternant, the spin and charge density distribution, apart from the sign of the latter, are identical for cations and ions. The frequencies of the excited electronic states, and excitation probabilities, are also independent of the sign of the charge. This simplifies the discussion of the properties of these ions.

The energy for formation of a hole or an electron can thus be calculated from either the ionization potential ( $I$ ) of the molecule and the polarization energy  $P_c^+$  or from the electron affinity ( $A$ ) and the polarization energy  $P_c^-$ . As values for  $I$  and  $A$  have been determined experimentally<sup>10</sup> the remaining unknown quantities are the polarization terms.

The analogous polarization energies in liquid solution (differential real potentials) have recently been reported for a series of hydrocarbon positive and negative ions<sup>11</sup>. The solvent used was methyl cyanide. It was found that the polarization energies are identical for positive and negative ions of the same hydrocarbon. This implies that the solvent has the role simply of a dielectric medium for these large ions, and that there are no specific chemical solvation effects. It follows that a very good approximation to the polarization terms for these ions in another medium will be obtained by the use of the Born relationship to correct for the change in dielectric constant. Applying this to the case of ions in hydrocarbon crystals we have

$$P_c^\pm = P_s^\pm \frac{(\epsilon_c - 1) \epsilon_s}{(\epsilon_s - 1) \epsilon_c} \quad (12)$$

where the subscripts  $c$  and  $s$  refer to the crystal and solution respectively, and  $\epsilon$  is the dielectric constant.

In *Table 1*, the ionization potentials, electron affinities and ion polarization energies  $P_s^\pm$  for  $\text{CH}_3\text{CN}$  solution are listed for a series of alternant hydrocarbons. The dielectric constants of the crystals and the corresponding polarization energies  $P_c^\pm$  calculated using equation (12) are also shown. In the last two columns of the table, the crystal ionization potential  $I_c (= I + P_c^\pm)$  and the crystal electron affinity  $A_c (= A - P_c^\pm)$  are recorded. We consider these crystals as intrinsic semiconductors and thus determine the energy of the Fermi level to be

$$F_c = \frac{I_c + A_c}{2} = 4.15 \text{ eV} \quad (12)$$

as the mean value for the hydrocarbons listed in *Table 1*. The constancy of the Fermi level is a consequence of the Pople-Hush rule of the constancy of

Table I. Electrochemical properties<sup>†</sup> of some aromatic hydrocarbons (based on reference 8)

Hydrocarbon	$I^a$	$A^b$	$-P_s^{xc}$	$\epsilon_c^d$	$-P_c^x$	$I_c$	$A_c$	$F_c$
Naphthalene	8.20	0.15			1.28(42)	6.92	1.43	4.18
Anthracene	7.61	0.55	1.94	3.38	1.74(42)	5.86	2.29	
Chrysene					1.41	6.20	1.96	4.08
Pyrene	8.01	0.33	1.83	2.97	1.25	6.76	1.58	4.17
Phenanthrene	7.72	0.39	1.86	3.36	1.35	6.37	1.74	4.06
1,2-Benzanthracene	8.06	0.20	1.76	2.54	1.10	6.96	1.30	4.13
Triphenylene	7.74	0.46	1.86	3.41	1.35	6.39	1.81	4.10
	8.19	0.14	1.84	3.41	1.34	6.85	1.48	4.17

<sup>†</sup> Ionization potentials and electron affinities ( $I, A$ ) of hydrocarbons in the gas phase and in the crystal ( $I_c, A_c$ ).  $P_s^x$  and  $P_c^x$  are the polarization energies of ions in methyl cyanide solution and in the hydrocarbon crystal respectively.  $\epsilon_c$  is the dielectric constant of the crystal.  $F_c$  is the energy of the Fermi level. The data for naphthalene crystal and for the first line for anthracene crystals were taken from reference (40). All energies are in eV.

<sup>a</sup> For sources of data see reference 11.

<sup>b</sup> See reference 12.

<sup>c</sup> See reference 11.

<sup>d</sup> Calculated from molecular polarizabilities using the method of Denbigh, *Trans. Faraday Soc.* **36**, 936 (1940). Crystal densities are calculated from unit cell data of A. I. Kitaigorodskii, 'Organic Chemical Crystallography' (translated from Russian by Consultant Bureau, New York, 1963).

## CHARGE-CARRIER INJECTION INTO HOMO-MOLECULAR CRYSTALS

the sum of electron affinity and ionization energy for alternant hydrocarbons<sup>13</sup>. In *Table 1* an electron in vacuum at infinity has been used as the reference energy state. Conversion between energy levels measured on this reference system and those measured on the electrochemical scale may be achieved through use of energy on the vacuum scale of the origin of the hydrogen electrode scale which has been determined<sup>14</sup> to be

$$E_{H+H_2} = -4.5 \text{ eV}, \text{ so that } E^H = -4.5 - E.$$

## INJECTION OF CARRIERS FROM ELECTROLYTES

### Electrostatic Interaction

The thermally generated intrinsic carrier density in homo-molecular crystals is so small that it is useful to think of these solids as perfect insulators. It is well known that a space charge limited current can be passed through an insulator if one of the contacts is 'ohmic'<sup>2, 15</sup>. In the ideal situation an ohmic contact provides an infinite reservoir of carriers just inside the surface of the solid from which a current can be injected into the bulk of the solid by an applied electric field. The magnitude of the current at any particular field strength will then be determined by the properties of the space charge in the solid which reflects the bulk properties of the crystal.

In real systems the current increases with the applied field until the surface reservoir of carriers is exhausted. With further increase in voltage the magnitude of the current is no longer controlled by the bulk properties of the solid but rather by the surface generation rate. Investigation of the deviation from the space charge limited current behaviour is profitable for the understanding of the surface reaction which leads to carrier injection. Kinetically a dynamic exchange of carriers between the contact and the crystal takes place, the currents in both directions being identical at equilibrium. When the exchange is with an electrolyte solution containing a redox system we may write the surface reaction in the form



The electron or hole donor species in solution  $A^\pm$  transfers a carrier to a molecule in the crystal,  $M$ , generating a carrier in the surface reservoir  $M^\pm$  and an acceptor species  $A$ .

An electrolyte forms an ohmic contact to a crystal if there is a large concentration of carriers in the surface reservoir at equilibrium i.e. if the carrier band is bent in the vicinity of the Fermi level. On application of an electric field the surface reservoir will be emptied very quickly unless it is replenished by a sufficiently fast surface generation process. When the applied voltage is sufficiently high to reduce the surface concentration of carriers to zero the current becomes saturated, provided the applied field does not affect the surface reaction.

The limiting current is determined either by the rate of the charge transfer reaction, equation (13), which can thus be readily determined, or by the limiting diffusion rate of donor species to the solid/solution interface. This view has been confirmed experimentally by using as a model system anthra-

cene platelets which were sandwiched between two electrolyte contacts<sup>1</sup>. The passage of a continuous hole current through the crystal was possible if one of the contacts contained a redox system which was strongly oxidizing i.e. which has a sufficiently positive redox potential (European sign convention) and which has a high rate constant for the electron exchange reaction. Energetic balance is provided by the equality of the electrostatic work of injection and the chemical energy acquired in the donation reaction. Electron injection has also been observed when the analogous requirements, redox systems with sufficiently negative equilibrium potentials and fast exchange rate, were fulfilled<sup>1</sup>. A quantitative treatment of the model outlined above has been derived for the case when the electron transfer reaction is a member of the simplest class of redox reactions, for which the activation processes associated with the charge transfer reaction consist exclusively of rearrangement of the outer coordination sphere, change of the bond lengths in the inner coordination sphere and polarization of the crystal lattice, having only weak interactions between the orbitals of the solid and the species in the solution<sup>1</sup>.

Detailed theoretical studies on such systems have been made by various authors who agree that in the first approximation the cross section through the potential energy surface made by the reaction coordinate is parabolic<sup>16-18</sup>. The reaction coordinate is frequently imagined to be the effective charge, which changes during the electron transfer process from the initial to the final state, on the species in the electrolyte.

Using these theories and the approximation that all of the potential difference in the interface is located within the solid it has been shown that the limiting injection current from redox systems is given by (1):

$$i_{\text{lim}} = ZFN_c [A^{\pm}] \exp \{ -(\lambda/4RT) [1 + \bar{\Delta}/\lambda]^2 \} \quad (14)$$

A formula for  $Z$  has been derived<sup>19</sup>; it is roughly  $10^7 \text{ cm}^4 \text{ mole}^{-1} \text{ sec}^{-1}$ .  $N_c$  is the density of vacant states in the solid ( $\sim 10^{20} \text{ cm}^{-3}$ ),  $[A^{\pm}]$  the concentration of the donor species,  $F$  the Faraday,  $\lambda$  the energy parameter defining the reaction energy parabolas and  $\bar{\Delta}$  the gap between carrier band and Fermi level at the crystal surface. Equation (14) shows that in order for a redox electrolyte to provide an ohmic contact  $\lambda$  and  $\bar{\Delta}$  must be small. The first condition is fulfilled if the homogeneous electron exchange rate for the redox system



is fast. The energy gap at the crystal surface is determined by

$$\bar{\Delta} = \Delta - FV \quad (16)$$

where  $\Delta$  is the gap between carrier band and Fermi level in the bulk of the crystal and  $V$  is the magnitude of the potential difference at equilibrium between the surface and the bulk of the solid.  $V$  is linearly related to the redox potential  $E_0$ :

$$V \approx E_0 - E_{FB} \quad (17)$$

Here  $E_{FB}$  is the so called 'flat band potential' which is the equilibrium poten-

## CHARGE-CARRIER INJECTION INTO HOMO-MOLECULAR CRYSTALS

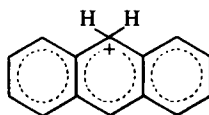
tial of a redox system for which, in contact with the crystal, the situation  $V = 0$  is obtained. A large magnitude for  $V$  requires that  $E_0$  is well separated from  $E_{FB}$  i.e. the redox system has to be either strongly oxidizing or strongly reducing.

### Specific Chemical Interaction between Crystal and Contact

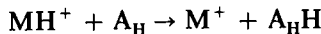
In the preceding discussion it has been shown that charge carriers can be injected into molecular crystals if certain energetic conditions are fulfilled. Experimental evidence has shown that the realization of these conditions is a sufficient but not a necessary criterion for the electrolyte to form an injecting contact. Cases have been found for which electrolytes do not obey the electrostatic conditions discussed above yet permit carrier injection into molecular crystals on application of an electric field.

#### *Hydrogen Atom Transfer*

It has been shown that hydrocarbons can form proton complexes in which the proton is linked to one of the carbon atoms by a covalent bond<sup>20</sup>. The structure of protonated anthracene is probably



In homogeneous solutions protonated hydrocarbon molecules can donate hydrogen atoms to suitable H-acceptors with the formation of radical ions:



In this mechanism the rate of hydrogen atom transfer is proportional to the acidity function of the solvent medium. The identical reaction takes place if the protonated hydrocarbon molecules form the surfaces of the crystal. The radical ions then form a charge reservoir from which carriers can be injected into the bulk of the crystal under the influence of an applied electric field.

Hoffmann has shown<sup>21</sup> that oxygen and anthraquinone are very efficient H-acceptors in contact with an anthracene crystal with a protonated surface. He has found that for low voltages the current was determined by the space charge in transit through the crystal while for sufficiently high voltages a limiting current was observed which was determined by the rate of carrier generation at the crystal/solution interface. In the case of protonated anthracene crystals and oxygen or anthraquinone, carrier generation was limited by the rate of diffusion of these species to the crystal/solution interface. Under suitably chosen experimental conditions it should be possible to determine from the limiting injection current the rate of the hydrogen atom transfer reaction.

#### *Alkali Metal Complexes*

According to the electrostatic model a contact without an energy barrier

can be made to the valence band of a semiconductor for metals whose work function  $\Phi$  is sufficiently large that  $\Phi \geq F + \Delta$ , where  $F$  is the energy of the Fermi level and  $\Delta$  is the separation of Fermi level and valence band in the bulk of the crystal. As  $F \approx -4.17$  eV and  $\Delta \approx -1.9$  eV for metals<sup>22</sup> with  $\Phi > 6$  eV, dark injection of holes can be expected and, following the equivalent argument, for metals with  $\Phi < 2.3$  eV electron injection should be possible.

The latter value can be reached with alkali metals and from contacts consisting of either caesium or a sodium-potassium alloy dark injection in anthracene crystals was indeed observed<sup>35, 41</sup>. The electrostatic argument presented above must, however, be accepted with great reservation only, because electron injection leading to a space charge limited current has also been found for Na-K alloy contacts to naphthalene crystals. For naphthalene  $F = -4.17$  eV and  $\Delta \approx 2.75$  eV, so that  $\Phi \approx \leq 1.6$  eV must be reached according to the electrostatic model before an 'ohmic' contact can be established while for the Na-K alloy the lowest value for  $\Phi$  reported<sup>23</sup> is 2.0 eV.

A much more likely explanation for the injection mechanism of electrons into anthracene and naphthalene is a specific chemical reaction leading to the formation of radical ions. It is known that anthracene and naphthalene form, with alkali metals, compounds of the type  $[(\text{alkali metal})_n(\text{hydrocarbon})]$  with  $1 \leq n \leq 2$ . The properties of these compounds have been investigated by Ubbelohde and co-workers<sup>24</sup>. Their colour is deep blue and from density measurements it was concluded that e.g. for the compound [Na<sub>1.7</sub> Anthracene] the volume containing 1 mole of anthracene is 163.4 cm<sup>3</sup> which compares with 155.0 cm<sup>3</sup> per mole of pure anthracene. Indeed an expansion of the part of an anthracene crystal which was in contact with an Na-K alloy could be observed. Also, both for anthracene and naphthalene, the formation of an intensely blue coloured compound was observed in the contact area and ESR measurements showed the presence of radical ions<sup>25</sup>.

We must thus conclude that the injection of electrons into anthracene and naphthalene crystals from alkali metals is the results of a chemical reaction which results in the formation of hydrocarbon radical ions which represent a reservoir of electrons.

Supporting this view Many<sup>42</sup> demonstrated, in a series of ingenious experiments, that at the interface between anthracene and an alkali or alkaline earth metal a single discrete set of traps is formed. The traps are 0.95 eV deep and are present with a density of about  $10^{13}$  cm<sup>-3</sup>. By optical excitation electrons can be injected from these traps into the conduction band of anthracene. Detrapping occurs by interaction of occupied traps with photons, triplet or singlet excitons. The traps are continuously filled by electron injection from the metal contact.

### Field Assisted Carrier Injection

Solutions of various redox systems have been found from which carriers can be injected in molecular crystals although energetic considerations exclude the 'outer sphere activated' electron transfer mechanism<sup>1, 21</sup>.

The best investigated example is the injection of holes into naphthalene crystals from a solution of ceric sulphate in 15 N sulphuric acid<sup>25</sup>. The standard redox potential for Ce<sup>4+</sup>/Ce<sup>3+</sup> is  $E_0^H = 1.45$  V and the level for the

## CHARGE-CARRIER INJECTION INTO HOMO-MOLECULAR CRYSTALS

naphthalene may be found at  $E_v^H = 2.3\text{--}2.4$  V so that, following equation (14), no hole injection current into naphthalene crystals should be detectable. Nevertheless a significant hole current was measured. The current voltage curves showed several characteristic differences compared to the familiar current-voltage curves measured with the same system on anthracene:

1. No saturation current was observed.
2. The current is smaller than the space charge limited current for the same field strength.
3. The current voltage curve is independent of the crystal thickness.
4. A change in the  $\text{Ce}^{4+}$  concentration affected the total current voltage curve.

In particular, when the concentration of  $\text{Ce}^{4+}$  changed while the applied voltage at the naphthalene crystal was kept constant, the current varied according to  $i \sim c^n$  with  $0.45 \leq n \leq 0.6$ .

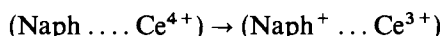
The results prove that the current voltage curve is independent of the bulk properties of naphthalene in the total voltage range investigated. We must thus assume that the applied voltage decays partly across a surface layer which consists of a complex formed by the absorption of ceric ions at the naphthalene surface. The complex may be of the charge transfer type with naphthalene as electron donor and ceric ions as acceptor.

Complex formation between aromatic hydrocarbons and metal ions has been observed in the solid state hitherto for the systems<sup>26</sup> benzene/ $\text{Ag}^+$  and<sup>27</sup> anthracene/ $\text{Ce}^{4+}$ . Measurement of the isotopic hydrogen exchange in the presence of platinum ions also indicates complex formation between aromatic hydrocarbons and platinum (II) ions<sup>28</sup>. Our assumption of complex formation between naphthalene and ceric ions is supported by ESR measurements which showed a signal with  $g = 2.0043$  for a mixture of ceric sulphate and naphthalene. With this model the concentration dependence of the current at constant voltage reflects an adsorption isotherm for ceric ions which has the form of the Ostwald-Freundlich isotherm  $c_{\text{ads}} = \alpha c^n$ ,  $n < 1$ . It is known that for intermediate degrees of coverage adsorption phenomena can frequently be described by an isotherm of this type<sup>29</sup>.

During these experiments the highest applied field strength was  $5 \times 10^5$  V/cm across the sample which may consist of naphthalene coated by a surface layer of the charge transfer complex. The potential difference in the surface layer can be estimated by means of the formula

$$E_s = \frac{\epsilon_B}{\epsilon_s} E_B$$

where  $E_B$  is the field within the bulk of the sample and  $E_s$  is that in the surface film;  $\epsilon_B$  is the dielectric constant of naphthalene and  $\epsilon_s$  is the corresponding quantity for the surface layer. Since  $\epsilon_s \approx \epsilon_B$  the field strength across the surface layer will be roughly the same as that across the sample. From the difference between the  $\text{Ce}^{4+}/\text{Ce}^{3+}$  and Naph/Naph<sup>+</sup> (Naph and Naph<sup>+</sup> are the naphthalene molecule and positive ion) equilibrium potentials we can estimate that the energy for charge separation in a ceric-naphthalene charge transfer complex according to



will be about 1eV. If we assume the distance between the charge centres to be about 5Å, we would need a field strength of  $2 \times 10^7$  V/cm in order to obtain complete charge separation. This crude estimate shows that this effect is not a likely explanation for the current observed. A more complicated model may therefore be necessary.

## PHOTOINJECTION OF CARRIERS

### Electrolyte Contacts

According to the model of Kallmann and Pope<sup>30</sup> photoinjection of carriers into a single crystal of anthracene is caused by excitons which are generated by light absorption, diffuse to the surface and react here with electron donors or acceptors. The charges so generated can migrate through the crystal under the influence of an applied electric field. The maximum current which can pass through the interface is

$$i_{\text{lim}} = Fk_e[M^*] \quad (18)$$

where  $F$  is the Faraday and  $M^*$  is the density of excited molecules at the crystal surface. This has to be treated as a diffusion problem for excited species and a migration problem for carriers through the crystal with the kinetic equation for the interfacial reaction as a common boundary condition.

A solution for this problem has been given in the form<sup>31</sup>

$$\frac{i_{\text{lim}} - i_0}{Fe_0 I_0} = \Phi = f_1 f_2 \quad (19)$$

where

$$f_1 = 1/[1 + 1/(\epsilon\sqrt{Dt})] \quad (20)$$

and

$$f_2 = 1/[1 + 1/(k_e C_A^* \sqrt{\tau/D})] \quad (21)$$

Here  $i_{\text{lim}}$  is the limiting photocurrent which can be observed at high enough applied voltages,  $I_0$  is the light intensity,  $i_0$  is the limiting value for the dark injection current,  $\epsilon$  is the absorption coefficient for the wavelength of the radiation used,  $D$  is the diffusion coefficient and  $\tau$  the mean life-time for excitons.  $\Phi$  is the quantum efficiency for the electrochemical charge injection process which has been factorized into the efficiencies of collection of excitons by the surface,  $f_1$ , and the efficiency of the charge separation  $f_2$ . At small values of  $f_2$ , the measured current is linearly proportional to the concentration  $C_A^*$  of the solution phase species. A quantitative discussion of  $f_2$  is possible if the charge transfer reaction is of the outer sphere type for which we can apply the treatment of Marcus-Hush<sup>16, 17</sup>.

We write the interface reaction in the form:



The standard free energy change of this reaction is given by

$$\Delta F^* = \mu_M^{\circ\pm} + \mu_A^\circ - \mu_{1_{M^*}}^\circ - \mu_A^{\circ\pm} \quad (23)$$

## CHARGE-CARRIER INJECTION INTO HOMO-MOLECULAR CRYSTALS

For the same reaction with groundstate molecules we obtain

$$\Delta F = \mu_M^{\circ\pm} + \mu_A^\circ - \mu_M^\circ - \mu_A^{\circ\pm} \quad (24)$$

which can be expressed as [see equation (16)]

$$\Delta F = \bar{A} \quad (25)$$

Thus

$$\Delta F^* - \Delta F = \mu_{M^*}^\circ - \mu_M^\circ \quad (26)$$

If  $E_x$  is the energy difference between the excited state and the ground state we obtain

$$\Delta F_p = \bar{A} - E_x \quad (27)$$

so that [see reference (31)]

$$k_e = Z \exp \left\{ \frac{-\lambda}{4RT} \left[ 1 + \frac{-E_x}{\lambda} \right]^2 \right\} \quad (28)$$

Detailed experimental investigations of the mechanism of photoinjection into anthracene were made<sup>32</sup> with aqueous solutions of  $\text{Na}_2\text{IrCl}_6$ ,  $\text{TlCl}_3$  and  $\text{FeCl}_3$ . They showed a striking anomaly, namely that the rate of the photoinjection reaction with  $\text{IrCl}_6^{2-}$  was of about the same order of magnitude as  $\text{Tl}^{3+}$  or  $\text{Fe}^{3+}$  while the dark injection reaction with  $\text{IrCl}_6^{2-}$  was more than five orders of magnitude faster than with the other two ions.

It was found that for the hexaquoiron complexes the magnitude of the polarization energy change in solution associated with the charge transfer step was so small that an excited state of the reduced component was preferred as a product of the reaction, while a large polarization energy change for the thallium system rendered the ground state of the product most accessible for the reaction. It was shown that in the case of  $\text{IrCl}_6^{2-}$  virtually all the energy of the excitons is transferred by resonance energy transfer. To prove this, the exciton diffusion problem was solved for simultaneous electron and energy transfer<sup>33</sup>. The result showed an unchanged collection efficiency for excitons while the efficiency of charge separation was now

$$f_2 = \frac{1}{1 + \frac{1}{k_e C_e \sqrt{(\tau/D)}} + \frac{k_Q C_Q}{k_e C_{A^\pm}}} \quad (29)$$

where  $k_Q$  is the rate constant for the energy transfer reaction and  $C_Q$  the concentration of quenching species in solution. In the case of  $\text{IrCl}_6^{2-}$   $C_Q = C_{A^\pm}$ .

The quenching rate constant was determined from (27) and compared with a value derived from the application of Förster's treatment<sup>34</sup> of resonance energy transfer upon quenching at the interface between solid and an electrolyte. For a  $10^{-2}$  molar solution of  $\text{Na}_2\text{IrCl}_6$  in  $\text{InHCl}$  the experimental value was  $k_Q = 2.05 \times 10^8 \text{ cm}^4 \text{ mole}^{-1} \text{ sec}^{-1}$  and the value derived from theory  $k_Q = 3.9 \times 10^7 \text{ cm}^4 \text{ mole}^{-1} \text{ sec}^{-1}$ .

## **Excitation of the Contact**

### *Metallic Contact*

While space charge limited electron currents in anthracene have been reported with alkali metal contacts<sup>35</sup>, hole injection from metallic contact has proven to be difficult. Dark injection has been observed from evaporated gold<sup>35</sup> and selenium<sup>36</sup> contacts, but the exact mechanism is in doubt; it seems to be a poorly reproducible field assisted process.

Williams and Dresner<sup>37</sup> have shown that for metals with  $\Phi < E_v$  hole injection is still possible if the missing energy  $E_v - \Phi$  is supplied by light. The authors irradiated a contact through the anthracene crystal with light of variable wavelength and measured the photocurrent passing through the crystal under an applied electric field. On plotting the photocurrent against the square root of the wavelength a straight line relationship was found from which, by extrapolation, they determined the lower limit  $E_{lim}$  of the light energy for photoinjection of holes. For gold, silver, aluminium, lead and magnesium they found

$$\Phi(\text{metal}) + E_{lim}(\text{metal}) = E_v(\text{anthracene})$$

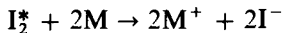
where  $E_v = 5.8 \pm 0.34$  eV which is in good agreement with  $E_v \approx 6$  eV determined from electrochemical data<sup>14</sup>. For the metals mentioned the interaction at the interface metal/anthracene is thus entirely electrostatic i.e. specific chemical interactions could be neglected.

The detailed analysis of the spectral response of the photoinjection current showed a very complex structure which reflected the structure of the valence band. The valence band was shown to be split into many well defined bands, separated from each other by the energy of a vibrational quantum. Interaction between the electron states at the Fermi level of the metal and any level of the valence band is possible.

### *Electrolytic Contact*

Injection from excited species in the electrolyte is difficult to achieve because the lifetime of singlet states is so short that electron transfer cannot compete with transfer to the groundstate and the absorption coefficient for triplet excitation is usually so small that the concentration of excited states is too low to be noticeable. Fortunately there is at least one exception: the visible absorption of the iodine molecule (near 520 m $\mu$ ) arises mostly from transitions between the ground state  $^1\Sigma^+$  and the excited state  $^3\Pi^+$ . The radiative lifetime of the transition  $^3\Pi^+ \rightarrow ^1\Sigma^+$  has recently been determined<sup>38</sup> to be  $(7.2 \pm 1.0) \times 10^{-7}$  sec.

An iodine solution was illuminated through the anthracene crystal and the photocurrent measured<sup>39</sup>. The spectral response of the current closely resembled the absorption spectrum of iodine. The exciton diffusion model, which was used to analyse the case of charge injection through electron transfer reaction with excitons, could be applied to this case. The mean free path of the  $^3\Pi^+$  iodine molecules was thus determined to be  $\sqrt{D\tau} = (3 \pm 2) \times 10^{-6}$  cm. It was concluded that no significant energy transfer between iodine molecules takes place and the photoinjection reaction can be described by



## CHARGE-CARRIER INJECTION INTO HOMO-MOLECULAR CRYSTALS

## REFERENCES

- <sup>1</sup> W. Mehl and J. M. Hale. "Insulator Electrode Reactions", in *Advances in Electrochemistry and Electrochemical Engineering* (Ed. P. Delahay and C. W. Tobias) Vol. 6, pp. 399–458. Interscience, New York (1967) and other references quoted there.
- <sup>2</sup> N. F. Mott and R. W. Gurney. *Electronic Processes in Ionic Crystals*, p. 170. Oxford University Press: London (1940).
- <sup>3</sup> K. Klier. *Coll. Czech. Chem. Commun.* **27**, 920 (1962).
- <sup>4</sup> F. Lohmann. *Surface Science* **14**, 431 (1969).
- <sup>5</sup> R. H. Fowler. *Statistical Mechanics*, p. 364. Cambridge University Press: London (1966).
- <sup>6</sup> W. Mehl, J. M. Hale and M. H. Davies. Publication being prepared.
- <sup>7</sup> O. H. Le Blanc. *J. Chem. Phys.* **35**, 1275 (1961).
- <sup>8</sup> N. S. Hush. Unpublished manuscript.
- <sup>9</sup> P. Balk, S. de Brujin and G. J. Hooijink. *Mol. Phys.* **1**, 151 (1958) and further references quoted there.
- <sup>10</sup> R. S. Becker and E. Chen. *J. Chem. Phys.* **45**, 2403 (1966).
- <sup>11</sup> B. Case, N. S. Hush, R. Parsons and M. E. Peover. *J. Electroanal. Chem.* **10**, 360 (1965).
- <sup>12</sup> W. E. Wentwerth and R. S. Becker. *J. Am. Chem. Soc.* **85**, 2210 (1963).
- <sup>13</sup> N. S. Hush and J. A. Pople. *Trans. Faraday Soc.* **51**, 600 (1955).
- <sup>14</sup> F. Lohmann and W. Mehl. *Ber. Bunsenges. Physik. Chem.* **77**, 493 (1967).
- <sup>15</sup> M. A. Lampert and P. Mark. *Current Injection in Solids*. Academic Press: New York (1970).
- <sup>16</sup> N. S. Hush. *Trans. Faraday Soc.* **57**, 557 (1961).
- <sup>17</sup> R. A. Marcus. *Ann. Rev. Phys. Chem.* **15**, 155 (1964).
- <sup>18</sup> R. R. Dogonadze, A. M. Kuznetsow and Yu. A. Chizmadzhev, *Russ. J. Phys. Chem.* (English Transl.) **38**, 652 (1964).
- <sup>19</sup> R. R. Dogonadze and Yu. A. Chizmadzhev. *Proc. Acad. Sci. USSR, Phys. Chem. Sect. (English Transl.)* **150**, 402 (1963).
- <sup>20</sup> W. Aalbersberg, G. J. Hooijink, E. L. Macker and W. P. Weijland. *J. Chem. Soc.* **3055** (1959).
- <sup>21</sup> A. K. Hoffmann. *Nature* **218**, 1157 (1968).
- <sup>22</sup> N. Geacintov and M. Pope. *J. Chem. Phys.* **45**, 3884 (1966).
- <sup>23</sup> *Landolt-Börnstein* (Ed. K. H. and A. M. Hellwege) Vol. II, Sect. 6, p. 913. Springer: Berlin (1959).
- <sup>24</sup> W. A. Holmes-Walker and A. R. Ubbelohde. *J. Chem. Soc.* 720 (1954).
- <sup>25</sup> F. Lohmann and W. Mehl. *J. Chem. Phys.* **50**, 500 (1969).
- <sup>26</sup> H. G. Smith and R. E. Rundle. *J. Am. Chem. Soc.* **80**, 5075 (1958).
- <sup>27</sup> I. Gränacher. *Solid State Commun.* **2**, 365 (1964).
- <sup>28</sup> J. L. Garnett and R. J. Hedges. *Chem. Commun.* 1220 (1967).
- <sup>29</sup> J. T. Davies and E. K. Rideal. *Interfacial Phenomena*, pp. 184/185. Academic Press: New York (1963).
- <sup>30</sup> H. Kallmann and M. Pope. *J. Chem. Phys.* **32**, 300 (1960).
- <sup>31</sup> J. M. Hale and W. Mehl. *Electrochim. Acta* **13**, 1483 (1968).
- <sup>32</sup> W. Mehl and J. M. Hale. *Discussions Faraday Soc.* **45**, 30 (1968).
- <sup>33</sup> W. Mehl and J. M. Hale. *Ber. Bunsenges. Physik. Chem.* in print.
- <sup>34</sup> Th. Förster. *Ann. Physik* **2**, 55 (1947).
- <sup>35</sup> W. Mehl and B. Funk. *Physics Letters* **25A**, 364 (1967).
- <sup>36</sup> J. Dresner. *Phys. Rev.* **143**, 558 (1966).
- <sup>37</sup> R. Williams and J. Dresner. *J. Chem. Phys.* **46**, 2133 (1967).
- <sup>38</sup> L. Brewer, R. A. Berg, and G. M. Rosenblatt. *J. Chem. Phys.* **38**, 1381 (1963).
- <sup>39</sup> W. Mehl, J. M. Hale and J. S. Drury. *Ber. Bunsenges. Physik. Chem.* **73**, 855 (1969).
- <sup>40</sup> L. E. Lyons and J. C. Mackie. *Proc. Chem. Soc. (London)* **71**, (1962).
- <sup>41</sup> W. Mehl. *Solid State Comm.* **6**, 549 (1968).
- <sup>42</sup> A. Many, J. Levinson and I. Teucher. *Mol. Cryst.* **5**, 121 (1968).

# ELECTRON AND HOLE GENERATION IN ANTHRACENE CRYSTALS†

R. G. KEPLER

*Sandia Laboratories, Albuquerque, New Mexico 87115, USA*

## ABSTRACT

Experimental results regarding electron and hole production in anthracene crystals are reviewed with emphasis on the relevance of these studies to the fundamental question of the nature of the excess electron states in these low mobility crystals. It is pointed out that a number of experiments suggest that above a threshold of about 4 eV in anthracene crystals, electronic transitions involve transitions of an electron from a ground state to a quite broad band rather than to bound states, some of which subsequently autoionize to create carriers, as has been thought to be true in the past. Most of the electrons created in this process apparently immediately recombine with the hole which was simultaneously created because they both have very small mean free paths for energy losing collisions and thus remain trapped in each other's coulomb field. Another experimental test of this hypothesis is proposed. The various types of carrier generation processes which have been observed and which will ultimately be useful in studies of highly excited states in anthracene crystals are reviewed.

## INTRODUCTION

The description of carrier transport in low mobility materials is still an outstanding problem in solid state physics and it appears that organic solids can play a very important role in determining what processes are involved. Generally it has been found that carrier mobility in organic crystals is in the low mobility range and in some ways, primarily experimental, organic crystals are simple, clean systems compared to the inorganic crystals in which low mobility transport has been observed. At least in the case of anthracene, high purity single crystals are relatively easily prepared in which electron and hole lifetimes are in excess of 100  $\mu$ secs and very extensive measurements have been carried out to experimentally characterize both carrier and energy transport processes.

In this paper studies of carrier production in anthracene will be reviewed with primary emphasis on the relevance of these studies to the fundamental question of the nature of the excess electron states. Before reviewing the carrier generation studies, a brief discussion of our present knowledge of carrier transport in anthracene is presented.

---

† This work was supported by the U.S. Atomic Energy Commission.

## CARRIER TRANSPORT

During the past ten years there have been extensive investigations of the drift mobility of both electrons and holes in anthracene crystals. It is well established that both carriers have mobilities of the order of  $1 \text{ cm}^2/\text{V sec}$ , that the mobilities are slightly anisotropic and that they depend weakly on temperature<sup>1</sup>. Theoretical calculations in the early sixties using the tight binding approximation provided very good agreement between theory and experiment<sup>2</sup>. It was assumed that the mean free path or mean free time was isotropic and these quantities were used as adjustable parameters. This theory indicated that the bands were extremely narrow, of the order of  $kT$  or less, but in spite of the bands being very narrow, the theory did satisfy uncertainty principle requirements. Such experimental data as mobility anisotropy and pressure dependence seemed to support the theory and there were numerous improvements added to the initial paper<sup>3</sup>.

In these papers the electron phonon interaction was introduced phenomenologically through the adjustable mean free path or mean free time and no attempt was made to discuss the interaction quantitatively. Subsequently, there have been a number of papers on the electron phonon interaction<sup>4</sup> and, in general, the indications are that the electron phonon interaction is stronger than is consistent with the simple tight binding band calculation and that some form of hopping motion seems to be called for.

A fairly good test of the validity of tight binding band theory was proposed by LeBlanc<sup>5</sup> and Friedman<sup>6</sup>. They pointed out that if the narrow band theory were right an anomalous Hall effect would be observed; the magnitude of the Hall current should indicate a mobility of the order of  $5-10 \text{ cm}^2/\text{V sec}$  and the sign of the current should be reversed. Numerous measurements of a Hall effect have been reported but the results disagree<sup>7</sup>.

It has been shown that both electrons and holes do move in bands which are less than  $kT$  wide. Hoesterey<sup>8</sup>, in a study of trap modulated mobility, showed that quantitative agreement between theory and experiment could be obtained if it was assumed that all the states in the hole band were within  $kT$  of the top. Naphthacene molecules were added in known quantities as an impurity in anthracene crystals and the drift mobility of holes studied as a function of both naphthacene concentration and temperature. The naphthacene molecules act as an electron trap 0.43 eV deep. Similarly, it has been found that carbazole acts as an electron trap 0.26 eV deep and that quantitative agreement between theory and experiment can be obtained by assuming that all the states in the electron band are within  $kT$  of the bottom of the band<sup>9</sup>.

It has also been shown experimentally that both electrons and holes have very short mean free paths, small compared to  $100 \text{ \AA}$ . A number of laboratories have measured the electron-hole recombination coefficient<sup>10,11</sup> and found it to be about  $1 \times 10^{-6} \text{ cm}^3 \text{ sec}^{-1}$ . This large value for the recombination coefficient requires that the mean free path of both electrons and holes be small compared to the dimensions of the coulomb potential well, that is, small compared to the distance at which the potential of one carrier in the electric field produced by the other is equal to  $kT$ , about  $120 \text{ \AA}$  in anthracene. Langevin<sup>12</sup> pointed out that under these conditions the relative drift

## ELECTRON AND HOLE GENERATION IN ANTHRACENE CRYSTALS

velocities  $v_d$  of an electron and a hole when they are a distance  $r$  apart is  $(\mu_h + \mu_e) (e/\epsilon r^2)$  where  $\mu_e$  and  $\mu_h$  are the electron and hole drift mobility, respectively, and  $\epsilon$  is the dielectric constant. Therefore, the rate of influx of electrons into a sphere of arbitrary radius  $r$  drawn around a hole, and thus the recombination rate constant, is

$$\gamma = 4\pi r^2 v_d = \frac{4\pi e}{\epsilon} (\mu_h + \mu_e).$$

By substituting  $1 \text{ cm}^2/\text{volt sec}$  for  $\mu_e$  and  $\mu_h$  and  $\epsilon = 3$ ,  $\gamma$  is found to be  $1.2 \times 10^{-6} \text{ cm}^3 \text{ sec}^{-1}$ , in excellent agreement with the experimental values. Therefore, experimentally it has been shown that the carriers have mean free paths small compared to  $100 \text{ \AA}$ .

Finally, one last experimental observation<sup>13</sup>, which may ultimately be very important in determining which theoretical model is correct, is that apparently the drift mobility of carriers in anthracene is independent of applied fields up to fields of  $10^5 \text{ V/cm}$ . This means that even at drift velocities comparable to what the narrow band theory says is the thermal velocity of the carriers, the drift mobility is still about  $1 \text{ cm}^2/\text{V sec}$ . This observation makes it highly unlikely that the narrow band description is valid.

In summary, it has been shown experimentally that electrons and holes in anthracene have drift mobilities on the order of  $1 \text{ cm}^2/\text{V sec}$  and that the mobilities are weakly temperature dependent and independent of field up to  $10^5 \text{ V/cm}$ . Also, the carriers move in a band of states which is less than  $kT$  wide with a mean free path which is small compared to  $100 \text{ \AA}$ . It seems fairly certain that the tight binding band theory is inadequate to explain these observations and that some form of hopping motion needs to be incorporated in the theory although no theory has yet been developed.

## CARRIER GENERATION

As might be expected the carrier generation processes in these low mobility, short mean free path molecular crystals exhibit some differences from that of the well understood, high mobility materials and it appears that very careful studies of the carrier generation process will provide new insight into carrier transport processes in these low mobility materials. Excitons play a large role in some of the processes and discussions are in progress regarding the role of highly excited molecular states and geminate recombination, i.e. recombination of an electron and hole before they have had a chance to separate from one another. Typically the quantum efficiency for the various carrier generation mechanisms has been found to be extremely low, of the order of  $10^{-4}$ .

The early photoconductivity work on anthracene involved carrier generation by excitons interacting with impurities on the surface or surface states<sup>1</sup>. Strongly absorbed light created excitons very near the crystal surface and these in turn interacted with the surface. Many puzzling phenomena were and still are observed but generally it has been found that the processes involved are too complex to provide any insight into the fundamental properties of the anthracene crystal.

## X-Ray Experiments

Recent work on carrier generation by x-rays in anthracene has provided strong evidence that geminate recombination plays a big role in carrier generation processes<sup>11</sup>. When x-rays interact with semiconductors, it is usually found that the average energy deposited per electron hole pair created is of the order of three times the band gap<sup>14</sup> and in gases, even gases of fairly complex molecules, it is found that of the order of 30 eV are deposited for each ion pair created<sup>15</sup>. In the case of anthracene crystals it was found that on the average 3000 eV were deposited for every electron hole pair created, about one hundred times as much as expected on the basis of the ion yield in gases and more than two hundred times as much as that expected on the basis of experiments conducted on semiconductors. These results, however, have been shown to be consistent with the very large value of the recombination coefficient discussed in the last section<sup>11</sup>.

The large value of the recombination coefficient shows that the mean free paths for energy losing collisions for electrons and holes are small compared to the dimensions of the coulomb potential well, i.e. small compared to the distance  $r_0$ , at which the coulomb potential energy of one carrier in the field of the other is equal to  $kT$ . Therefore, even when an electron is created with sufficient kinetic energy to escape from the coulomb field of the hole left behind, there is a very high probability that it will lose the energy before it has had a chance to escape.

When it is appropriate to describe the motion of a charge carrier with the diffusion equation, that is when the mean free path is small compared to  $r_0$ , Onsager<sup>16</sup> has shown that the probability that a diffusing charge carrier will escape from a coulomb potential well is  $e^{-r_0/r}$  where  $r$  is the distance at which the carrier starts diffusing. He was investigating the creation of ion pairs by high energy radiation in high pressure gases. Onsager also showed that the number of charge carrier pairs created,  $\varphi$ , would depend on the applied field and be  $\varphi = A(T)[1 + (e^3/2\epsilon k^2 T^2)E]$  where  $A(T)$  depends on the initial distribution of diffusing carriers and is a function of temperature but does not depend on the electric field. Higher order terms in  $E$ , the applied electric field, have been neglected.

Hummel and Allen<sup>17</sup> have applied this theory in detail to some experimental studies of carrier generation by high energy radiation in hexane and find excellent agreement between theory and experiment. In order to calculate the yield of carriers it is necessary to know the energy spectrum of the electrons created by the radiation as well as the range energy relation and as a result there is considerable uncertainty in this quantity. However, if the yield of carriers is plotted as a function of the applied field, a straight line should result at relatively low fields, if geminate recombination is occurring, and as Onsager pointed out, the slope of this line divided by the yield of carriers at zero electric field should be equal to  $e^3/2\epsilon k^2 T^2$ , a quantity which contains no adjustable parameters. Therefore, the field dependence of the carrier yield provides an excellent test for this theory. It is interesting to note that in the studies of ion yields in dielectric liquids<sup>18</sup> the yield of ion pairs is very large in the high mobility liquids, almost certainly indicating that the mean free path is becoming comparable to  $r_0$  so that it is no longer

## ELECTRON AND HOLE GENERATION IN ANTHRACENE CRYSTALS

valid to describe the carrier motion on the scale of a coloumb potential well with a diffusion equation.

### Single Photon Experiments

Getting back to anthracene, Batt, Braun and Hornig<sup>19</sup> and Geacintov and Pope<sup>20</sup> have investigated the applicability of geminate recombination to single photon carrier generation processes. It has been shown that single photons of energy greater than 4 eV create free carriers by either a band-to-band transition or a transition to an excited state of the anthracene molecule which can subsequently autoionize. The quantum yield is very low,  $10^{-4}$ , and it was initially thought that this indicated that in an organic molecular crystal like anthracene a direct band-to-band transition was a relatively improbable or forbidden process<sup>21</sup> and that most of the absorbed photons created excitons even when the energy was sufficiently high for a single photon to create a carrier. There have been discussions regarding whether the carriers were created by a weakly allowed band-to-band transition or by autoionization of excitons<sup>22</sup>. The observation of geminate recombination has now added a new dimension to these discussions because it now provides a third possibility.

Batt *et al*<sup>19</sup> and Geacintov and Pope<sup>20</sup> studied the electric field and temperature dependence of carrier generation in the wavelength range where carriers are created by a single photon process. They found fairly good agreement between Onsager's theory and their experimental results, strongly indicating that the carriers are generated in a band-to-band transition and that the low quantum yield arises from geminate recombination. As was pointed out in the discussion of carrier generation by x-rays, the quantum efficiency will depend on the details of where the carriers started diffusing but the electric field dependence, in terms of the slope of a graph of the number of carriers created as a function of electric field divided by the number of carriers created at zero electric field, should have a very specific value. The slope divided by the intercept should be  $e^3/2\epsilon k^2 T^2$  and, therefore,

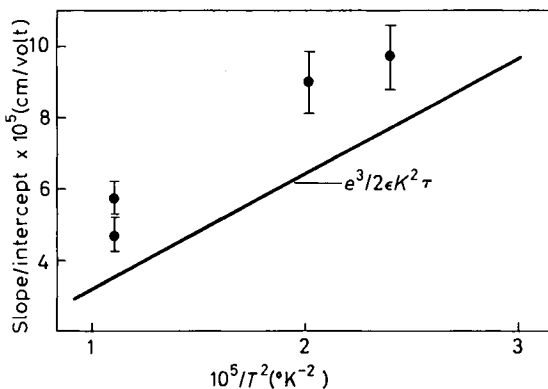


Figure 1. Temperature variation of the carrier generation electric field dependence. The points represent experimental results and the solid line is a theoretical prediction after Batt, Braun and Hornig<sup>19</sup>.

should not only have a very specific value but this value should vary as  $T^{-2}$ . The agreement between theory and experiment obtained by Batt *et al*<sup>19</sup> is shown in *Figure 1*.

It should be relatively easy to determine experimentally whether or not the low quantum efficiency for carrier generation results from geminate recombination by measuring the fluorescence quantum efficiency as a function of exciting light wavelength in the wavelength range near 4 eV. If geminate recombination is responsible for the low quantum efficiency, the fluorescence quantum yield above 4 eV should drop to about one fourth of its value below 4 eV because it seems unlikely that the singlet character of the molecule ground state would be preserved during the photoionization and carrier recombination process. Therefore, three triplet excitons should be created for every singlet, resulting in one fourth the quantum efficiency. Since it is very difficult to eliminate the possibility of surface quenching of singlet excitons, it would probably be a much more definitive experiment to look for an increase in the number of triplet excitons created by measuring the delayed fluorescence after a pulse of light. Apparently neither of these experiments have been carried out to explicitly check this hypotheses.

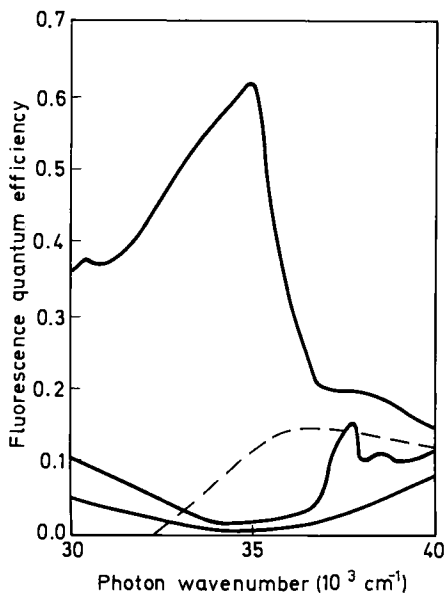


Figure 2. Fluorescence quantum efficiency after Wright<sup>23</sup>, upper solid line; extinction coefficient parallel and perpendicular to the *b* axis in the *ab* plane after Bree and Lyons<sup>24</sup>, two lower solid lines; and carrier yield after Geacintov and Pope<sup>22</sup>, dashed line, versus wavenumber of the incident light.

Wright<sup>23</sup> has measured the fluorescence quantum yield, however, and combining his results with those of Bree and Lyons<sup>24</sup> for the extinction coefficient and Geacintov and Pope<sup>22</sup> for carrier generation as a function of wavelength, results in *Figure 2*. The results are suggestive in the sense that there is a big drop in the quantum efficiency at about the right energy but

## ELECTRON AND HOLE GENERATION IN ANTHRACENE CRYSTALS

not conclusive. Wright interpreted his results on the basis of exciton annihilation at the surface and absorption by a layer of anthraquinone on the crystal surface.

### Exciton Ionization

Experiments on anthracene crystals using photons of energy greater than about 3 eV are very difficult because photons with energy greater than 3 eV are absorbed very near the crystal surface and the excitons interact strongly with the surface. A number of second order processes have been observed however and these processes probably will be used to study carrier generation processes in the future when variable wavelength, high intensity lasers become more generally available.

Exciton-exciton annihilation is one second order process which has been considered for years. The existence of the process was questioned for a time but a fairly recent publication<sup>25</sup> appears to present quite definite proof of its existence. It is, of course, not possible to vary the energy of excitation in this process and thus study the nature of highly excited states, but it has been shown that the yield of carriers per exciton-exciton annihilation is very low. Measurements of the exciton-exciton annihilation rate constant<sup>26</sup> have shown that it is about  $10^{-8} \text{ cm}^3 \text{ sec}^{-1}$  while the rate of carrier generation<sup>25</sup> by the same process is about  $10^{-12} \text{ cm}^3 \text{ sec}^{-1}$ . Thus the quantum efficiency for carrier generation by this process appears to be  $10^{-4}$ , the same as that found for generation by the single photon process.

Another process involving singlet excitons that has been well established is exciton photoionization<sup>27,28</sup>. In studies of carrier generation in anthracene crystals by light from a Q spoiled ruby laser it was found that the number of carriers generated varied as the intensity of the light cubed. It is well known that excitons can be created in anthracene by two photon absorption of ruby laser light and it was hypothesized that carriers were being generated by photons interacting with excitons created by two photon absorption. In order to test this hypothesis an anthracene crystal was irradiated by two pulses of light from a laser separated in time of arrival at the crystal<sup>27</sup> by from 0 to 40 nsec. The two pulses were obtained by sending

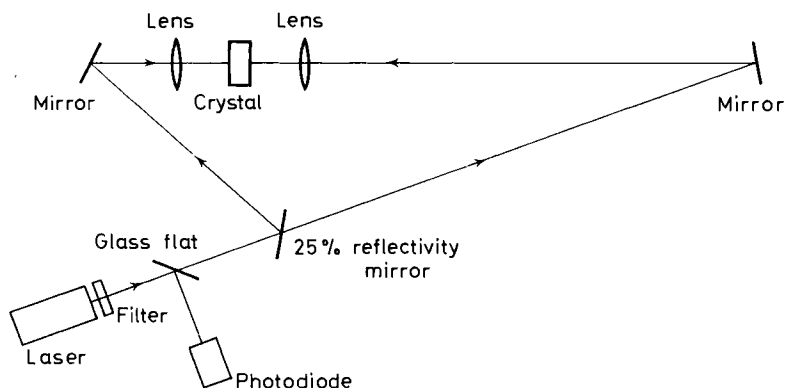
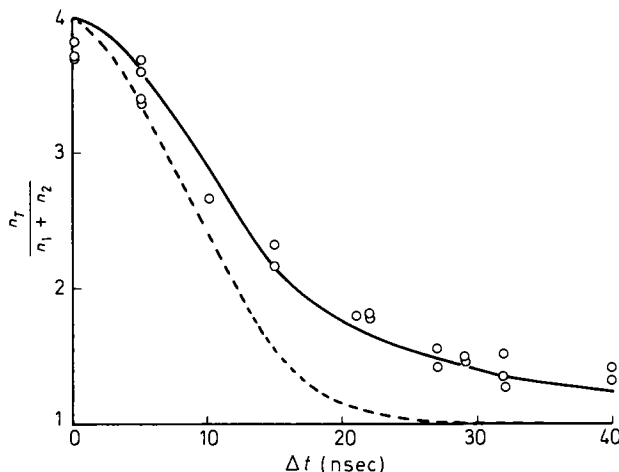


Figure 3. Experimental arrangement used to establish the exciton photoionization process.

the light from the laser through a partially reflecting mirror and the difference in time of arrival was obtained by varying the length of the path one of the pulses took in getting to the crystal. A block diagram of the experimental arrangement is shown in *Figure 3*. The number of carriers created when the two pulses hit the crystal, as well as the number created by each pulse separately, were measured and the experimental results are shown in *Figure 4*.



*Figure 4.* Ratio of the number of carriers, produced by two almost simultaneous light pulses incident on an anthracene crystal, to the sum of the number produced by each pulse independently as a function of the difference in the times of arrival at the crystal of the two pulses. The solid line is the theoretical curve calculated for singlet exciton photoionization and the dashed line is the theoretical curve for three-photon absorption.

The dashed curve indicates the results that would have been expected if no intermediate state were involved, that is if the number of carriers created was just proportional to the integral over time of the intensity of the light cubed. The solid curve was calculated assuming that singlet excitons with a lifetime of 27 nsec were created by two photon absorption and that carriers were created when these excitons were subsequently ionized by another photon. The cross section for exciton photoionization was found to be about  $10^{-19} \text{ cm}^2$ .

It has also been found that photons from a neodymium laser (1.18 eV) can photoionize excitons but the cross section is about two orders of magnitude smaller than the cross section for ruby laser photons<sup>29</sup> (1.8 eV). In order to carry out this experiment excitons were created by 4250 Å light, obtained by passing the light from a xenon flash tube (about a 2 μsec long pulse) through a monochromator, and while the 4250 Å light was irradiating the crystal, a pulse of photons from a Q spoiled neodymium laser was sent through the crystal. Since the 4250 Å light pulse created carriers by itself, it was necessary to measure both the number of carriers created by the 4250 Å light and the number of carriers created when both light pulses were incident on the crystals. It was assumed that the excess carriers created were created

## ELECTRON AND HOLE GENERATION IN ANTHRACENE CRYSTALS

by exciton photoionization. It was possible to fire the neodymium laser at various times during the flash lamp pulse and measure the number of excess carriers created as a function of the 4250 Å intensity at the time the laser was fired. The experimental results are shown in *Figure 5*. The intensity of the 4250 Å light was about  $5 \times 10^{17}$  photons  $\text{cm}^{-2} \text{ sec}^{-1}$  at peak intensity and

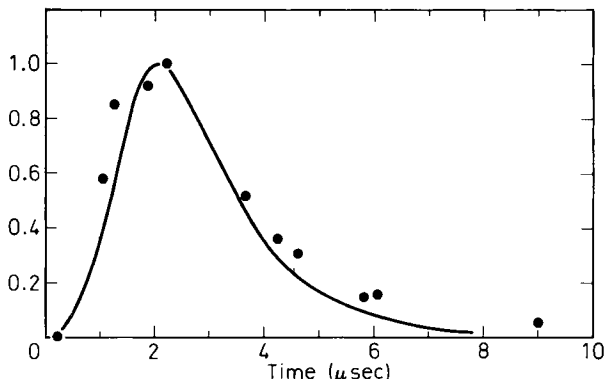


*Figure 5.* The number of additional carriers created by applying a pulse of light from a neodymium laser to an anthracene crystal during excitation of the crystal with a pulse of 4250 Å light from a flash lamp. The solid curve is the intensity of the 4250 Å light versus time and the solid dots are the number of excess carriers created by the laser pulse. The time at which the laser pulse fired is indicated by the time at which the dot is plotted.

there were about  $2 \times 10^{16}$  photons  $\text{cm}^{-2}$  in the laser pulse. From this experiment the cross section for photoionization of singlet excitons by neodymium laser photons was found to be about  $2 \times 10^{-21} \text{ cm}^2$ .

## Two Photon Experiments

Strome<sup>30</sup> has recently shown that carriers can also be generated by direct two photon processes. He studied carrier generation in anthracene crystals with photons with energies of 2.07 eV, 2.16 eV and 2.35 eV. At these energies, both the number of singlet excitons and the number of carriers created by the photon pulse were found to depend on the intensity squared. These data were interpreted as evidence for direct two photon transitions.

Strome used a Q spoiled ruby laser to generate anti-Stokes stimulated Raman lines in liquid nitrogen and liquid oxygen to obtain his light pulses. In our laboratory, similar experiments were carried out using frequency-doubled neodymium light (2.35 eV). The intensity dependence of both the fluorescence and the number of carriers created are shown in *Figure 6*. The generation coefficients for carriers and for excitons found in our experiments were  $1 \times 10^{-31} \text{ cm sec}$  and  $8 \times 10^{-28} \text{ cm sec}$ , respectively, in excellent agreement with those found by Strome for 2.35 eV photons. It should be noted that in this two photon process there again appears to be a quantum efficiency for carrier generation of about  $10^{-4}$ .

This observation led to an unsuccessful attempt to detect absorption by

excitons<sup>31</sup>. The amount of frequency doubled deodymium laser light transmitted by a 2 cm long anthracene crystal was measured as a function of the intensity of the light. Since the number of excitons created by the light could be calculated from the results of the experiment reported in the previous paragraph, the cross section for photon absorption could be calculated if a saturation in the amount of light transmitted by the crystal could be observed.

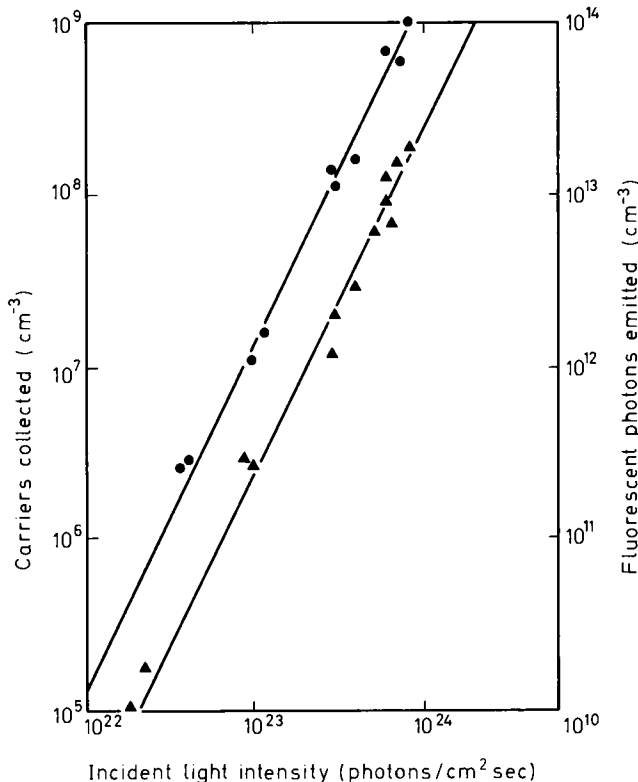


Figure 6. The number of fluorescent photons and the concentration of carriers created in an anthracene crystal by a pulse of frequency doubled neodymium laser light versus the intensity of the light.

Since saturation was not observed, the experimental results, shown in Figure 7, only allowed an upper limit of  $10^{-17} \text{ cm}^2$  to be set on the cross section for exciton absorption at 5300 Å.

## SUMMARY

In anthracene crystals it is known that both holes and electrons have relatively low mobilities, move in a band of states narrow in energy, of the order of  $kT$  at room temperature or less and that they both have short mean free paths, small compared to 100 Å. However, the basic mechanism of transport in these crystals has not been established. Early attempts at tight

## ELECTRON AND HOLE GENERATION IN ANTHRACENE CRYSTALS

binding band calculations have given perhaps the most satisfying answers, but in those calculations electron phono interactions were treated phenomenologically and, as investigations into these interactions continue, it appears less likely that a coherent, band theory type approach is adequate.

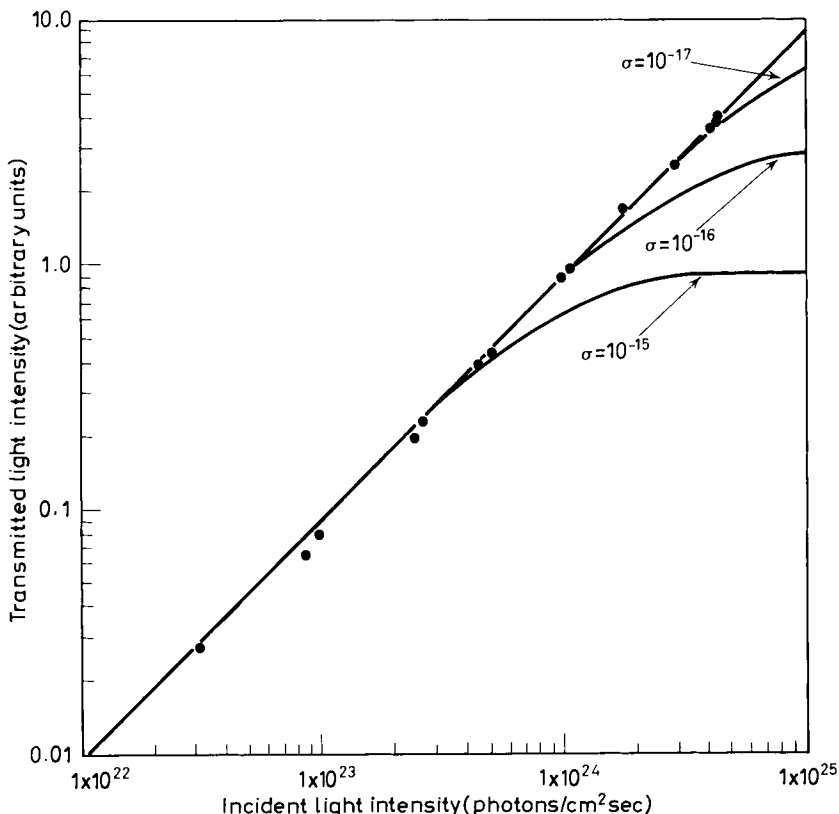


Figure 7. The intensity of light at 5300 Å transmitted by a 2 cm long anthracene crystal as a function of the incident light intensity. The curves labelled  $\sigma = 10^{-15}$ ,  $\sigma = 10^{-16}$ , and  $\sigma = 10^{-17}$  are the theoretical predictions based on the assumption of an exciton absorption cross section of  $10^{-15} \text{ cm}^2$ ,  $10^{-16} \text{ cm}^2$ , and  $10^{-17} \text{ cm}^2$  respectively.

In photoconductivity experiments, band-to-band transitions appear to occur above about 4 eV and no evidence has been found for a narrow band. The quantum efficiency for carrier generation, however, is very low, about  $10^{-4}$ , for all experiments reported for which a quantum efficiency can be determined. There are reasons to believe that this small yield can be explained in terms of geminate recombination, i.e. recombination of an electron with the hole that was created along with the electron before the electron escapes from the coulomb attraction of the hole. In general, the photoconductivity results appear to suggest that above about 4 eV there is something like a wide band of electron states to which transitions can occur.

In anthracene crystals it has been shown that in addition to the standard

## R. G. KEPLER

one photon carrier generation process, carriers can be generated by exciton photoionization and two photon transitions to highly excited states. With the advent of high power, continuously tunable lasers, these processes could provide the means by which the nature of highly excited electron states in organic crystals are elucidated, and thus, ultimately perhaps, the key to the basic transport mechanism.

## REFERENCES

- <sup>1</sup> R. G. Kepler. *Organic Semiconductors* Ed. J. J. Brophy and J. W. Buttrey (Macmillan, New York, 1962) p. 1.
- <sup>2</sup> O. H. LeBlanc Jr. *J. Chem. Phys.* **35**, 1275 (1961).
- <sup>3</sup> J. L. Katz, J. Jortner, S.-I. Choi and S. A. Rice. *J. Chem. Phys.* **39**, 1683 (1963); R. Silbey, J. Jortner, S. A. Rice and M. T. Vala. *J. Chem. Phys.* **42**, 733 (1965); **43**, 2925 (1965); R. M. Glaser and R. S. Berry. *J. Chem. Phys.* **44**, 3797 (1966).
- <sup>4</sup> S. H. Glarum. *J. Phys. Chem. Solids* **24**, 1577 (1963); W. Siebrand. *J. Chem. Phys.* **41**, 3574 (1964); L. Friedman. *Phys. Rev.* **140**, A1649 (1965); P. Gosar and S.-I. Choi. *Phys. Rev.* **150**, 529 (1966); R. W. Munn and W. Siebrand. *J. Chem. Phys.* **52**, 6391 (1970).
- <sup>5</sup> O. H. LeBlanc Jr. *J. Chem. Phys.* **39**, 2395 (1963).
- <sup>6</sup> L. Friedman. *Phys. Rev.* **A133**, 1668 (1964).
- <sup>7</sup> G. C. Smith. *Phys. Rev.* **185**, 1133 (1969).
- <sup>8</sup> D. C. Hoesterey and G. M. Letson. *J. Phys. Chem. Solids* **24**, 1609 (1963).
- <sup>9</sup> R. G. Kepler. Unpublished results.
- <sup>10</sup> W. Helfrich and W. G. Schneider. *Phys. Rev. Letters* **14**, 229 (1965); M. Silver. *Bull. Am. Phys. Soc.* **11**, 269 (1966).
- <sup>11</sup> R. G. Kepler and F. N. Coppage. *Phys. Rev.* **151**, 610 (1966).
- <sup>12</sup> See H. S. W. Massey and E. H. S. Burhop. *Electronic and Ionic Impact Phenomena* (Oxford University Press, New York, 1952) Chapter X.
- <sup>13</sup> D. C. Hoesterey. *Bull. Am. Phys. Soc. Ser. II* **13**, 479 (1968).
- <sup>14</sup> See for example F. E. Emery and T. A. Rabson. *Phys. Rev.* **140**, A2089 (1965).
- <sup>15</sup> H. W. Fulbright. *Handbuch der Physik*, Ed. S. Flügge (Springer-Verlag, Berlin, 1958) Vol. XLV, p. 11.
- <sup>16</sup> L. Onsager. *Phys. Rev.* **54** 554 (1938).
- <sup>17</sup> A. Hummel, A. O. Allen and F. H. Watson Jr. *J. Chem. Phys.* **44**, 3431 (1966); A. Hummel and A. O. Allen. *J. Chem. Phys.* **44**, 3426 (1966).
- <sup>18</sup> W. F. Schmidt and A. O. Allen. *J. Chem. Phys.* **52**, 2345 (1970).
- <sup>19</sup> R. H. Batt, C. L. Braun and J. F. Hornig. *Appl. Opt. Suppl.* **3**, 20 (1969); *J. Chem. Phys.* **49**, 1967 (1968).
- <sup>20</sup> N. E. Geacintov and M. Pope. *Proceedings of the Third International Photoconductivity Conference*, (Pergamon Press, 1969) Ed. E. M. Pell, p. 293.
- <sup>21</sup> M. Silver and R. Sharma. *J. Chem. Phys.* **46**, 692 (1967).
- <sup>22</sup> See for example N. Geacintov and M. Pope. *J. Chem. Phys.* **50**, 814 (1969).
- <sup>23</sup> W. H. Wright. *J. Chem. Phys.* **45**, 874 (1966).
- <sup>24</sup> A. Bree and L. E. Lyons. *J. Chem. Soc.* **1956**, 2662; L. E. Lyons and G. C. Morris, *ibid.* **1959**, 1551.
- <sup>25</sup> C. L. Braun. *Phys. Rev. Letters* **21**, 215 (1968).
- <sup>26</sup> A. Bergman, M. Levine and J. Jortner. *Phys. Rev. Letters* **18**, 593 (1967); N. A. Tolstoi and A. P. Abramov. *Soviet Phys.-Solid State* **9**, 255 (1967).
- <sup>27</sup> R. G. Kepler. *Phys. Rev. Letters* **18**, 951 (1967).
- <sup>28</sup> E. Courtens, A. Bergman and J. Jortner. *Phys. Rev.* **156**, 948 (1967).
- <sup>29</sup> R. G. Kepler. Unpublished results.
- <sup>30</sup> F. C. Strome Jr. *Phys. Rev. Letters* **20**, 3 (1968).
- <sup>31</sup> R. G. Kepler. *Appl. Opt. Suppl.* **3**, 25 (1969).